Fluids at Interfaces:
Casimir Effect, Depletion and Thermo-osmosis

Fluids at Interfaces:

Casimir Effect, Depletion and Thermo-osmosis

A thesis submitted to
Università degli Studi dell'Insubria
in partial fulfilment of the requirements
for the degree of *Philosophiæ Doctor*

by

Pietro Anzini

Supervisor
Alberto Parola
Full Professor of Physics

October 2018

Colimus enim Deum,
et colis nos Deus.

Augustinus Hipponiensis

Contents

1 Introduction

Interfacial phenomena are widespread in nature: Adsorption, wetting, spreading, capillary rise, drop and bubble formation, evaporation, rippling are just some examples of phenomena where interfaces play a key role. Therefore it is not surprising that the singular behaviour exhibited by interfaces already attracted the attention of ancient natural philosophers. Pliny the Elder, born *Gaius Plinius Secundus* in Como (AD 23 - 79), reported in his treatise *Naturalis Historia* [177] that *"everything is smoothed by oil, and that is the reason why divers send out small quantities of it from their mouths, because it smoothes any part which is rough and transmit the light to them"*[1]. Many centuries later, Leonardo da Vinci (1452-1519) described for the first time capillary phenomena[2] and analysed the motion of water in the ground making use of this effect [137] . During the seventeenth and eighteenth century the optical properties of surface films were intriguing for many scientists committed to the observation of the amazing colours in Newton's rings, discovered a short time before [159]. However, the seismic breakthrough in the understanding of interfacial phenomena were the achievements obtained independently by Laplace [131] and Young [252]: The two equations that bear their names successfully predict capillarity rise in narrow tubes, account

[1] *"Omne oleo tranquillari, et ob id urinantes ore spargere, quoniam mitigat naturam asperam lucemque deportet"*, Gaius Plinius Secundus, *Naturalis Historia*, Liber II CVI, *Mirabilia fontium et fluminum.*

[2] As reported in Ref. [137]: *"Enfin, deux observations capitales, celle de l'action capillaire et celle de la diffraction, dont jusqu'à présent on avait méconnu le véritable auteur, sont dues également à ce brillant génie"*. See also *Manuscripts of Leonardo da Vinci*, Vol. N, Sheets 11, 67 and 74.

for the shape of bubbles, describe the interfaces between liquids and solids. Furthermore, right at that time the relevant role of cohesive interactions became clear and new developments in the study of interfaces were put forward mainly by van der Waals [226] and Rayleigh [184], who replaced the too crude approximation of sharp interface, originally put forward by Laplace, with a more physical idea of smooth interface. At the end of the nineteenth century the Marangoni effect was discovered [146] and it was understood the role of interfaces in transport processes. The modern era of the study of interfacial phenomena has been characterised by the tireless work of Boris Derjaguin and his co-workers at the Moscow Academy of Sciences [44]. His research ranges from theory to experiments, from studies on the stability of films to the formalisation of the concept of the disjoining pressure, from the development of the DLVO theory to important insights in surface transport phenomena. More recently, the contributions put forward by Rowlinson, Widom and J. R. Henderson [198], together with the intuitions of de Gennes [40], provided new blood to this field.

Among the plethora of phenomena in soft matter physics strongly affected by the structure of interfaces, three specific examples will be investigated in this Thesis: The critical Casimir effect, the depletion interaction between corrugated particles and thermo-osmosis. The common element characterising these phenomena is the essential role of interfaces: Due to the interaction with surfaces the properties of fluids at contact with them (or confined in thin films) significantly differ from that of the same matter in bulk and give rise to new and unexpected effects. Many observations report that the perturbation in the density profile due to the interface can extend in the fluid up to a distance of several molecular diameters. Also the dynamic properties of fluids, such as the transport coefficients, are expected to be deeply modified in the region near an interfaces. Consequently any proper treatment of surface phenomena must be based on a microscopic statistical mechanical description of inhomogeneous fluids. The three problems presented above will be studied in this spirit: We will make use of microscopic approaches able to account for the peculiar behaviour of fluids near interfaces, where continuum theories necessarily miss the microscopic details on the molecular lengthscale.

The *critical Casimir effect* [72] is the long-range interaction between two planar walls in a critical fluid due to the confinement, achieved by the wall interfaces, of the critical density fluctuations. The force between the walls obeys scaling laws which can be predicted by means of finite-size scaling theories and are evaluated through Monte Carlo simulations [144]. These results are valid only in the long-wavelength limit and a microscopic theory able to describe the Casimir force at all distances is still missing. However, the overall interaction between colloidal particles in critical solvents can be strongly influenced by the behaviour at short distances [144]. In Chapter 2 we provide a microscopic description of the critical Casimir force, introducing a novel density functional approximation coupled to the hierarchical reference theory of fluids, a bulk liquid state theory which proved accurate also near

the critical point [171]. The resulting interaction between the walls is seen to change character on lowering the temperature: The strong oscillations induced by layering of the molecules, typical of the depletion mechanism in hard core systems, are gradually smoothed and, close to the critical point, a long-range attractive tail emerges leading to a scaling form which agrees with the expectations based on scaling approaches.

The *depletion interaction* is an effective attractive force arising between colloidal particles immersed in a solvent: The first prediction of this effect dates back to the seminal work by Asakura and Oosawa [6] and has been obtained assuming that the colloidal particles were perfectly smooth spheres immersed in an ideal gas. Anyway, many natural and synthesised colloidal particles are characterised by surface heterogeneities. Several lines of evidence point out that the interaction potential between corrugated particles strongly deviates from the basic Asakura-Oosawa result [120]. In Chapter 3 we address the study of the interaction potential mediated by an ideal gas between two rough colloidal particles, as a function of the geometry, the dimension and the spatial configuration of the corrugations. The resulting explicit expressions for the potential can be easily computed, without free parameters, resorting to Derjaguin approximation. The comparison with recent numerical simulations [113] shows an encouraging agreement and allows predicting the onset of colloidal aggregation in dilute suspensions of rough particles.

When a thermal gradient is applied to a fluid at contact with a surface a stationary flow develops[3]. This effect, referred to as *thermo-osmosis*, has been discovered in the late nineteenth century [69] but successful theoretical descriptions have been up to now devised only when the fluid is a rarefied gas [209]. Nevertheless, thermo-osmosis turns out to be the driving mechanism of thermophoresis in liquids and, in addition, represents the most elementary out-of-equilibrium problem that we can conceive, because the system is kept in a stationary nonequilibrium state by a constant temperature gradient. Tentative descriptions of thermo-osmosis in liquids have been put forward by Derjaguin on the basis of nonequilibrium irreversible thermodynamics [46]. However, these continuum approaches can only partially account for surface induced effects like thermo-osmosis, because the relevant thermodynamic quantities change over a lengthscale comparable with the range of inter-particle potentials. Chapter 4 presents a microscopic theory of thermo-osmosis based on a generalisation of linear response theory to inhomogeneous and anisotropic environments and to thermal disturbances. The predicted thermo-osmotic flow is fully characterised in terms of two physically different equilibrium properties of the inhomogeneous fluid near the surface. Close similarities to both kinetic theory [209] and irreversible thermodynamics [46] results can be recovered by retaining each of these contributions, showing that the gas and liquid regimes

[3]Here we are assuming that external symmetry breaking fields, e. g. the gravitational field, are not present.

are indeed governed by different physical mechanisms.

The critical Casimir effect, the depletion between corrugated particles and thermo-osmosis will be individually discussed in the following chapters. Each Chapter includes introduction, analysis and final considerations about a single phenomenon.

2

Critical Casimir effect in fluids

Two perfectly conducting plates in vacuum attract themselves according to the celebrated law

$$\frac{F(L)}{\Sigma} = -\frac{\pi^2}{240}\frac{\hbar c}{L^4}, \tag{2.1}$$

where Σ is the surface of the two plates, $L \ll \sqrt{\Sigma}$ their distance, and c the speed of light in vacuum. The conciseness of Eq. (2.1) renders anyone speechless: The interaction does not keep trace of the type of conductor and the only relevant quantities are the distance L and the product $\hbar c$. This amazing and unexpected effect was predicted theoretically by Casimir in 1948 [31] and is due to the confinement, made by the conducting plates, of the zero-point (vacuum) fluctuations of the quantized electromagnetic field. An important feature of the phenomenon, known as *Casimir effect*, is that, even though it is quantum in nature, it predicts a non vanishing force between two macroscopic objects: If we consider two conducting plates of area $1\,\mathrm{cm}^2$, at a distance of $1\,\mu$m, the Casimir force is of the order of 10^{-7} N. Casimir's claim has been experimentally confirmed only in 1997 [127, 128] through high precision measurements of the force between a gold plate and a gold plated sphere.

Casimir effect does not represent an *unicum*: Casimir himself, with the help of his assistant Polder, understood that the physical mechanism behind the interaction between the planar conductors in vacuum (2.1) also leads to the van der Waals and London [141] forces. Actually, the presence of atoms modifies (in a sense, confines) the vacuum fluctuations of the electromagnetic field, giving rise to a net attractive interaction. This microscopic interaction

between atoms is called after them Casimir-Polder effect [32].
However, fluctuations are ubiquitous in nature, and their confinement gives rise to the diverse manifestations of the so called *fluctuation-induced* forces which originate intriguing phenomena also in condensed matter physics [72, 145, 135, 83, 104] and cosmology [157, 238][1]. The effect discovered by Casimir is nothing but the prototype of fluctuation-induced interactions.

In this Chapter our attention will be focused on the so called *critical Casimir interaction* [72], arising from the confinement of the density fluctuations in a critical fluid. The *universal* properties of the critical Casimir force are now well understood by means of techniques specific of finite-size scaling and renormalization group theory [121], whereas a non-universal (i.e. microscopic) analysis of this effect is still lacking. In this Chapter we try to fill this gap providing a *microscopic* theoretical description of the critical Casimir interaction by examining the solvent-mediated forces between two hard walls immersed in a hard core Yukawa fluid. The investigation is performed in the super-critical region in order to exclude wetting phenomena, which deserve a separate analysis. We developed an appropriate theoretical tool for such a study: A Density Functional Theory (DFT), which proved accurate in the description of confined fluids, coupled to the hierarchical reference theory of fluid, a liquid state theory reliable also in the critical region.
The Chapter is organised as follows. The first Section is an introduction to fluctuation-induced interactions, with a focus to the critical Casimir effect. Section 2.2 critically reviews the density functional theory for inhomogeneous fluids, betraying that a specific implementation of DFT accurate in the critical region is still lacking. In Section 2.3 we propose a Weighted Density Approximation (WDA) especially designed for being accurate also near the critical point. This theory is validated against other DFT prescriptions, as well as available numerical simulations, in several non-critical states. In Section 2.4 our approach is applied to a Yukawa fluid in critical conditions: We discuss both the microscopic density profile and solvent-mediated force between two walls. Section 2.5 takes into account the universal properties of the effective interaction. The emergence of scaling laws is investigated in the critical and pre-critical regime and the results are compared to numerical simulations. Furthermore, we show that our critical Casimir scaling function is deeply related to the universal bulk properties of the critical fluid, giving a simple prescription for the theoretical evaluation of the critical and off-critical Casimir scaling function.
The main results of this Chapter have been published in Ref. [4].

[1] For a thorough discussion of fluctuation-induced forces see [115] and references therein.

2.1 FLUCTUATION-INDUCED INTERACTIONS

Casimir-like forces

In order to understand more deeply the physical mechanisms which originate fluctuation-induced interactions we recall the original argument put forward by Casimir in 1948 [31]. Obviously, it could be possible to describe more accurately this phenomenon (see e.g. [110]): However here, for the sake of simplicity and to keep the focus on the physical mechanism, we impose that the field outside the plates is vanishing and we neglect corrections due to the finite size of the plates.

Let us consider two perfectly conducting plates in vacuum, at $z = 0$ and $z = L$, in the hypothesis $L \ll \sqrt{L_x L_y}$[2], that in principle allows to disregard edge effects. The quantized electromagnetic field is described by the Hamiltonian

$$\hat{H} = \sum_{\boldsymbol{k},\lambda} \hbar\omega(\boldsymbol{k},\lambda) \left[\frac{1}{2} + \hat{a}^\dagger(\boldsymbol{k},\lambda)\hat{a}(\boldsymbol{k},\lambda)\right],$$

where $\hat{a}^\dagger(\boldsymbol{k},\lambda)$ is the operator that creates a photon of momentum $\boldsymbol{k}$ and polarisation λ. The dispersion relation for photons in vacuum is linear $\omega(\boldsymbol{k},\lambda) = \omega(\boldsymbol{k}) = c\,|\boldsymbol{k}|$ and does not depend on the polarisation of the photon. The zero point energy of the electromagnetic field reads

$$E = \sum_{\boldsymbol{k}} g_s(\boldsymbol{k}) \frac{\hbar\omega(\boldsymbol{k})}{2},$$

where the factor $g_s(\boldsymbol{k})$ accounts for the degeneracy of the mode $\boldsymbol{k}$. Now we impose, as usual, periodic boundary conditions in the directions orthogonal to z, while, along z, we require that the tangential electric field and the normal magnetic field vanish on the plates. This conditions can be fulfilled, for $k_z \neq 0$, by a vector potential in the Coulomb gauge given by

$$\boldsymbol{A}(\boldsymbol{r},t) = \boldsymbol{\epsilon}\, \mathrm{e}^{\mathrm{i}(k_x x + k_y y)} \sin(k_z z) \mathrm{e}^{-\mathrm{i}\omega(\boldsymbol{k})t}, \tag{2.2}$$

where $\boldsymbol{\epsilon}$ is the polarisation of the electromagnetic field and

$$k_\alpha = \frac{2\pi}{L_\alpha} \quad \alpha = x, y \qquad n_\alpha \in \mathbb{Z}; \qquad\qquad k_z = \frac{\pi}{L} n_z, \qquad n_z \in \mathbb{N}^0. \tag{2.3}$$

Furthermore, the polarisation $\boldsymbol{\epsilon}$ and the wavevector $\boldsymbol{k}$ are mutually orthogonal ($\boldsymbol{\epsilon} \cdot \boldsymbol{k} = 0$) because $\boldsymbol{\nabla} \cdot \boldsymbol{E}(\boldsymbol{r},t) = 0$, where $\boldsymbol{E}(\boldsymbol{r},t)$ is the electric field.
For $k_z \neq 0$ there always exist two possible polarisations ($g_s(\boldsymbol{k}) = 2$) such that

[2]Here L_x and L_y represent the linear dimensions of the plates in the direction orthogonal to z.

the normal magnetic field and the tangential electric field vanish on the plates. When $k_z = 0$ the vector potential (2.2) identically vanishes, and must be replaced by

$$\boldsymbol{A}(\boldsymbol{r},t) = \boldsymbol{\epsilon}\, \mathrm{e}^{\mathrm{i}(k_x x + k_y y)} \mathrm{e}^{-\mathrm{i}\omega(\boldsymbol{k})t}.$$

It is possible to show that the unique polarisation ($g_s(\boldsymbol{k})|_{k_z=0} = 1$) which fulfils the boundary conditions on the fields is $\boldsymbol{\epsilon} = \hat{\boldsymbol{e}}_z$, where $\hat{\boldsymbol{e}}_z$ is the unit vector along z.
Due to (2.3) the ground state energy of the electromagnetic field between the plates depends on the separation L between them. The contribution arising from the modes with $k_z \neq 0$ reads

$$\begin{aligned} E_0'(L) &= \hbar c {\sum_{\boldsymbol{k}}}' |\boldsymbol{k}| = \hbar c \sum_{n_x,n_y=-\infty}^{+\infty} \sum_{n_z=1}^{+\infty} \sqrt{\left(\frac{2\pi n_x}{L_x}\right)^2 + \left(\frac{2\pi n_y}{L_y}\right)^2 + \left(\frac{\pi n_z}{L}\right)^2} \\ &= \hbar c \int_{-\infty}^{+\infty} \mathrm{d}n_x \int_{-\infty}^{+\infty} \mathrm{d}n_y \sum_{n_z=1}^{+\infty} \sqrt{\left(\frac{2\pi n_x}{L_x}\right)^2 + \left(\frac{2\pi n_y}{L_y}\right)^2 + \left(\frac{\pi n_z}{L}\right)^2} \\ &= \Sigma \frac{\pi^2 \hbar c}{4L^3} \sum_{n_z=1}^{+\infty} \int_0^{+\infty} \mathrm{d}t\, \sqrt{t + {n_z}^2}, \end{aligned}$$

where the prime only reminds that the summation is extended over $k_z \neq 0$. In the second line we replaced with the corresponding integrals the summations over n_x and n_y, limiting the accuracy of our analysis to the case of infinite plates; The last line has been obtained defining a straightforward change of variables.
The contribution to ground state energy E_0 from the modes with $k_z = 0$ follows from the same algebra and reads

$$E_0|_{k_z=0}(L) = \Sigma \frac{\pi^2 \hbar c}{8L^3} \int_0^{+\infty} \mathrm{d}t\, \sqrt{t}.$$

Summing up, the total ground state energy (per unit surface) of the electromagnetic field is

$$\frac{E_0(L)}{\Sigma} = \frac{\pi^2 \hbar c}{4L^3} \left[\frac{1}{2} \int_0^{+\infty} \mathrm{d}t\, \sqrt{t} + \sum_{m=1}^{+\infty} \int_0^{+\infty} \mathrm{d}t\, \sqrt{t + m^2} \right].$$

This quantity is clearly unbounded. However, the potential energy between the walls is given by

$$U(L) = E_0(L) - E_0(L \to \infty). \tag{2.4}$$

Therefore, in order to obtain the real finite potential $U(L)$ we first have to evaluate and subtract the constant unbounded quantity $E_0(L \to \infty)$, that is

the zero-point energy of the electromagnetic field when the two plates are far away. The same algebra shown above allows to evaluate the (diverging) ground state energy in the limit of free electromagnetic field

$$\frac{E_0(L\to\infty)}{\Sigma}=\frac{\pi^2\hbar c}{4L^3}\int_0^{+\infty}\mathrm{d}s\int_0^{+\infty}\mathrm{d}t\,\sqrt{t+s^2}$$

and the potential energy (2.4) per unit surface between the plates reads

$$\begin{aligned}\frac{U(L)}{\Sigma}&=\frac{\pi^2\hbar c}{4L^3}\left[\frac{1}{2}\int_0^{+\infty}\mathrm{d}t\,\sqrt{t}+\sum_{m=1}^{+\infty}\int_0^{+\infty}\mathrm{d}t\,\sqrt{t+m^2}-\int_0^{+\infty}\mathrm{d}s\int_0^{+\infty}\mathrm{d}t\,\sqrt{t+s^2}\right]\\&=\frac{\pi^2\hbar c}{4L^3}\left[\frac{1}{2}\int_0^{+\infty}\mathrm{d}t\,\sqrt{t}+\sum_{m=1}^{+\infty}\int_{m^2}^{+\infty}\mathrm{d}t\,\sqrt{t}-\int_0^{+\infty}\mathrm{d}s\int_{s^2}^{+\infty}\mathrm{d}t\,\sqrt{t}\right].\end{aligned}\tag{2.5}$$

The sum and the integrals in Eq. (2.5) are still diverging. However, if we come back to the physical problem, we realise that conductors are indeed transparent for the electromagnetic radiation at high wave vectors: It is therefore natural to insert in the integrals a cut-off for short wavelengths, which ensure convergence. This procedure is referred to as regularisation. Once the cutoff has been inserted, the sum and the integrals converge and the difference in (2.5) can be estimated applying the Euler-Maclaurin identity [1]

$$\begin{aligned}\sum_{i=m+1}^{n}f(i)-\int_m^n\mathrm{d}x\,f(x)=&\frac{f(n)-f(m)}{2}\\&+\sum_{k=1}^{\lfloor p/2\rfloor}\frac{B_{2k}}{(2k)!}\left[f^{(2k-1)}(n)-f^{(2k-1)}(m)\right]+R_p,\end{aligned}\tag{2.6}$$

where $f(x)=\int_{x^2}^{+\infty}\mathrm{d}t\,\sqrt{t}$, $f^{(l)}$ is the l^{th} order derivative of f, B_{2k} are the Bernoulli coefficients of even index and R_p is an error which is normally small for suitable values of p. The zero-order term in (2.6) cancels out with the $k_z=0$ contribution, whereas the first non vanishing contribution is for $k=2$ and $f^{(3)}(x)=-4$.
Finally, the attractive force per unit surface acting on the plates is minus the derivative w.r.t. L of the potential energy between the plates

$$\frac{U(L)}{\Sigma}=\hbar c\frac{\pi^2}{720}\frac{1}{L^3},$$

and coincides with Eq. (2.1).

This fundamental result follows from the quantization of the electromagnetic field and can be considered as the proof of the reality of the zero point energy. Furthermore, even if this phenomenon is an electromagnetic effect, the charge of the electron does not appear in (2.1), which seems to be a universal result. Strictly speaking, the plates interact due to an imbalance of the normal

modes of the (quantized) electromagnetic field: In the region between the plates only the normal modes with wavevector greater equal π/L (that is wavelength $\lambda \geq 2L$) are allowed (see Eq. (2.3)), whereas in the two half spaces there is not such restriction[3]. The physical mechanism underlying all the Casimir-like forces is exactly this unbalance in the allowed modes of fluctuations.

If we retrace this simple calculation, we can single out the basic ingredients this kind of fluctuation-induced phenomena: The fluctuations and the interfaces able to interact with them.
Fluctuations can be quantum in origin, such as in Casimir's set up where zero point fluctuations at $T = 0$ were considered, or classical, as shown by Lifshitz [138], who extended the idea put forward by Casimir at $T \neq 0$ in a dielectric medium with an arbitrary dielectric constant. Thermal fluctuations of a correlated fluid near a critical point[4] lead to the so called critical Casimir interaction. This phenomenon was predicted in the context of binary mixtures by Fisher and de Gennes in 1978 [72], who probably formulated the first generalisation of Casimir effect in a field different from QED. Furthermore, any system characterised by long-range correlations can display Casimir-like forces: In superfluids and in liquid crystals these interactions arise from the confinement of long-wavelength Goldstone modes of the order parameter[5]. Also fluctuations of charge density close to macroions dispersed in charged solutions lead to Casimir-like corrections to the Poisson-Boltzmann interaction [158].

However, it has become evident that fluctuations alone are not enough to observe an effect: Some kind of constraint on their oscillation modes is also necessary. The *confinement* is microscopically realised by an external field, which couples to the fluctuations and somehow introduces a disturbance. As regard fluids, the external field usually correspond to an interface, which can be or a purely repulsive wall or a hard wall plus an attractive tail. Within Casimir's original setup the interface is a perfectly conducting wall. However the confinement is not always obtained through real, macroscopic objects. In the case of wetting films, two different boundaries confine the fluctuations: The wall-liquid and the liquid-gas interface [79]. The most singular example of confinement is related to the Casimir-Polder interaction: In this case single atoms or molecules interact with vacuum fluctuations.
However, also the *geometry* of the confinement proves to be relevant. In the beginning, the interest was focused on simple geometries, like parallel plates, until it was shown in 1968 that an isolated, conducting sphere in vacuum

[3]The difference between the integral and the sum in Eq. (2.5) precisely accounts for this unbalance of the fluctuations.

[4]In superfluids this effect is observed measuring film thickness when the system is near a critical endpoint.

[5]The thickness of ^{4}He thin films is determined by Van der Waals attraction plus a contribution due to critical fluctuations (when the system is near the critical endpoint) or due to Goldstone modes (when the fluid is in the superfluid phase) [79].

should expand due to repulsive Casimir interaction [21]. This example shows how the geometry is able to influence also the direction of the Casimir force. Also random surface roughness, which mimics real surfaces, can introduce a relevant contribution to the Casimir forces [136].

We conclude this overview about Casimir-like forces spending a few words about the strength and the range of the interaction.
In fluctuation-induced phenomena the *strength* of the interaction is proportional to the amplitude of fluctuations, namely $\hbar$ and $k_{\mathrm{B}}T$ for quantum and thermal fluctuations respectively. Here we report the behaviour of the Casimir potential per unit surface when two infinite parallel planar walls are in vacuum, in a Bose liquid at low temperatures and in a fluid at the critical point:

$$\frac{U_{\mathrm{QED}}(L)}{\Sigma} \sim \frac{\hbar c}{L^3}, \qquad \frac{U_{\mathrm{Bose}}(L)}{\Sigma} \sim \frac{\hbar c_s}{L^3}, \qquad \frac{U_{\mathrm{critical}}(L)}{\Sigma} \sim \frac{k_{\mathrm{B}}T}{L^2}.$$

Here c is the speed of light in vacuum, c_s is the speed of sound in the Bose liquid and T is the critical temperature. Readily the peculiar dependence on L in U_{critical} stands out: It is due to the fact that $\hbar c$ is an energy per length, whereas $k_{\mathrm{B}}T$ has dimensions of energy, and the interaction energy must be proportional to Σ.
The *range* of the fluctuation-induced forces is limited by the range of fluctuations: The Casimir force in QED has an infinite range while, away from the critical point, the critical Casimir interaction has a finite range determined by the correlation length of the order parameter fluctuations.

Critical fluctuations

The onset of Casimir forces in critical systems was theoretically predicted in 1978 by Fisher and de Gennes in a three-page letter to the academy of the sciences of Paris [72][6]. Their work takes inspiration from the observation that the concentration profiles in a critical mixture near a wall are perturbed over a distance of the order of the correlation length. Then, making use of the finite-size scaling approach, they argue that two planar walls, immersed in the same mixture at a distance smaller than the correlation length, will attract each other with a potential proportional to $k_{\mathrm{B}}T$ and decreasing as the second inverse power of the distance. The letter concludes with a remark about colloidal suspensions: An enhanced rate of aggregation is to be expected as a result of critical Casimir forces, and indeed this consequence has been recently observed [28]. Furthermore, forty years later the hint provided by Fisher and die Gennes, experiments on a binary mixture of water and Lutidine led to the first direct measurement of critical Casimir forces [104].
The peculiar interaction predicted by Fisher and de Gennes strongly depends on

[6]The manuscript can also be found in the book [39], with some additional remarks by de Gennes.

the finite size of the system: Indeed, in critical conditions the distance between the walls can be comparable with the bulk correlation length. Finite-size effects can drastically influence the behaviour of the observables and a new form of scaling, the so called *finite-size scaling*, was put forward by Fisher himself in 1970 [71] in order to account for these effects. This form of scaling allows to express the universal contribution to the critical Casimir forces in terms of universal scaling functions, which only depend on the boundary conditions applied and on the universality class of the system in the thermodynamic limit. In the following we present the main concepts of finite-size scaling in order to obtain the universal scaling form of the critical Casimir force.

Finite-size scaling

The principle of thermodynamic additivity, which has its roots in the homogeneity of the free energy with respect to the extensive variables, can be considered the simplest finite-size scaling law: The free energy and the other extensive quantities scale with the volume. If additivity holds, the description of the system can be conveniently formulated in the so called *thermodynamic limit*[7], and reduces to determining the free energy density $f_b(\rho, T)$, which only depends on intensive variables, and, possibly, the correlations. The thermodynamic limit ensures that descriptions based on different ensembles are equivalent and, under general conditions of regularity, that the free energy looses any dependence on the boundaries. Furthermore, the singularities characterising second order phase transitions appear only in this limit [133], and the singular behaviour of the system is fully contained in the bulk free energy density $f_b(T, \rho)$.
Unfortunately, for a finite-size system[8] in near-critical conditions the description introduced above, based on the thermodynamic limit, is no longer valid. This point can be made more explicit if we expand the free energy of a system with finite size L, at fixed (T, ρ), in terms of free energy densities as[9]

$$\frac{\mathcal{F}(T,V,N)}{V} = f_b(T,\rho) + \frac{f_s(T,\rho)}{L} + \frac{f_e(T,\rho)}{L^2} + \dots + \dots + \frac{f_c(T,\rho)}{L^d} + o\left(e^{-L/\xi(T,\rho)}\right), \quad (2.7)$$

where ξ is the bulk correlation length and the surface energy density $f_s(T, \rho)$, the edge contribution $f_e(T, \rho)$ and the corner contribution $f_c(T, \rho)$ have been evaluated in the thermodynamic limit too. Such expansion is meaningful only far from the critical point[10], i.e. when the correlation length is smaller than

[7] That is the limit for $N, V \to \infty$, taken at fixed density.
[8] Namely, any system which has finite size in at least one space dimension.
[9] This expression is valid under free boundary conditions and for systems interacting with short-range potentials.
[10] However, near the critical point the non-singular contribution to the free energy is still given by (2.7).

the size of the system L. Indeed, it is well known that any critical finite-size system shows strong deviations with respect to the corresponding bulk system: In many cases the bulk singularities are smoothened and there can be a shift in the critical point. Equation (2.7) does not hold for a finite-size system in critical conditions because such deviations from the bulk behaviour are not included and it becomes necessary a correct formulation of scaling for finite-size systems.
In what follows we summarise the finite-size scaling theory, starting from the finite-size hypothesis originally put forward by Fisher [71]. For a complete and formal introductions to this fascinating argument see e.g. [14, 180].

Let us consider a system near the critical point where all the relevant parameters determining the thermodynamic state, except the temperature, are fixed at their critical value. The correlation length will diverge approaching the critical temperature T_c from above[11] as

$$\xi = \xi_0 \, t^{-\nu}, \qquad \text{with} \qquad t = \frac{T - T_c}{T_c}, \tag{2.8}$$

where t is the reduced temperature, ξ_0 is a non-universal constant and $\nu > 0$ is the bulk critical exponent, which only depends on the universality class of the system. The singular behaviour of the susceptibility χ in bulk systems is governed by the exponent γ:

$$\chi \sim t^{-\gamma}.$$

Note that the divergence of this quantity near the critical point can be also expressed in terms of the diverging correlation length through Eq. (2.8):

$$\chi \sim \xi^{\gamma/\nu}. \tag{2.9}$$

When the fluid is not confined, the susceptibility will diverge approaching the critical point according (2.9), because also the correlation length diverges. However, if the system has a finite size L, the correlation length will be cut off at L, and the divergence of the susceptibility χ is no more possible. In particular, the susceptibility will assume its bulk value until $L \gg \xi$, whereas for $L \sim \xi$ it will be cut off at a value which depends on the geometry of the system.
The *finite-size scaling hypothesis*, as formulated by Fisher [71], states that the relevant quantity accounting for the properties of finite-size systems near the critical point is the ratio between the size of the system L and the bulk correlation length ξ

$$L/\xi \sim L \, t^{\nu}.$$

[11] Here we limit to super-critical thermodynamic states.

This hypothesis, as well as the considerations presented above, can be implemented for the susceptibility by writing

$$\chi \sim \xi^{\gamma/\nu} \mathcal{X}\left(\frac{L}{\xi}\right), \tag{2.10}$$

where $\mathcal{X}$ is a dimensionless function such that

$$\lim_{x\to 0} \mathcal{X}(x) \sim x^{\gamma/\nu} \qquad \text{and} \qquad \mathcal{X}(x)\big|_{x\gg 1} = \text{const}$$

in order to reproduce the correct scaling behaviour in the different limits. The function $\mathcal{X}(x)$, which has no other arguments except from x, is the so called *finite-size scaling function* for the susceptibility. If the bulk correlation length is unknown, it could be useful to replace its dependence in (2.10) with the reduced temperature t. Therefore we can define another scaling function $\tilde{\mathcal{X}}(x)$ such that

$$\chi \sim L^{\gamma/\nu}\, \tilde{\mathcal{X}}\left(a\, L^{1/\nu}\, t\right),$$

where a is a system dependent metric factor, $\tilde{\mathcal{X}}(x)$ is constant at the critical point ($x = 0$) and there is not a hidden dependence on the variable L.
The finite-size scaling hypothesis can be extended with the same arguments to negative reduced temperatures (the scaling function will be in general different) and to the singular contribution of other diverging quantities, both intensive, as the susceptibility, and extensive, as the free energy. Moreover, within this pedagogical example we supposed that the temperature was the only free parameter: Analogous laws can be formulated when other scaling fields, such as the density or the magnetic field, can vary.

Within finite-size scaling, the scaling functions only depend on the bulk universality class, on the geometry of the problem and on the imposed boundary conditions. This general property is shared by fluctuation-induced interactions, which are categorised depending on the kind of fluctuation, i.e. the *bulk universality class*, and by the confinement, i.e. the *geometry* and the *boundary conditions*.
The geometry has a strong effect on the confinement of fluctuations: As mentioned above, also in the electromagnetic framework confining shapes giving rise to opposite Casimir interactions can be easily identified [21]. There are many possible geometries of interest, but in this work we focus on the so called 1-dimensional layer, that is a system confined in only one dimension. For this geometry, as regards system belonging to the 3d Ising universality class, a genuine phase transitions (i.e. with true singularities) can appear, because the number of unconstrained dimensions is higher than the lower critical dimension [23].
The role of the boundary conditions can be easily understood if we consider a statistical system. Far away from the critical point the perturbation induced by the surface can penetrate into the system only up to distances of the order

of the correlation length, which is comparable with interaction range. If the critical point is approached, the correlation length grows larger and larger, and the same happens for the perturbation due to the surface which can penetrate deeper and deeper inside the system. In addition, for each bulk critical point, more than one surface critical transition can appear, and the critical point turns into a multicritical point [49]. The surface critical behaviour can be classified in surface universality classes, as in the case of bulk universality classes [49]. The universality classes are responsible for the different boundary conditions imposed on the fluctuations. The surface transition can enhance, suppress or leave unchanged[12] the bulk phase transition and the corresponding universality classes are referred to as extraordinary (E), ordinary (O) and special (S). In some situations the surface phase transition may take place (spontaneously or guided by an external field) at higher temperatures than the bulk transition, and the surface transition is referred to as normal transition. This is the typical situation occurring in binary mixtures [123], where the preferential absorption of the surface for one of the two components of the mixture resembles an external (symmetry breaking) field which guarantees order on the surface. However, up to corrections to scaling, the normal transition can not be distinguished from the extraordinary transition (E). The boundary condition is referred to as *symmetry breaking* or *fixed* boundary condition.
Periodic, Dirichlet and free boundary conditions belong to the ordinary (O) surface universality class[13]. Confined binary mixtures belong to the normal/extraordinary (E) [80, 123] surface universality class.
Most of the theoretical predictions available for the finite-size critical Casimir scaling functions have been obtained through Monte Carlo simulations of the Ising model. A magnetic field applied to the surface, if sufficiently large, is able to fix the orientation of the the surface spins. Therefore Ising systems with surface fields belong to the same surface universality class of the binary mixtures. The notation commonly adopted for a film geometry with symmetry breaking boundary conditions is $(+,+)$, $(+,-)$, $(-,+)$ and $(-,-)$, where $+$ and $-$ represent the spin orientation on the surface. The same notation is adopted in confined binary mixtures and the symbols $+$ and $-$ stand for a positive or negative order parameter [80].

[12]The ordering of the bulk and of the surface is simultaneous.

[13]Dirichlet boundary condition: The order parameter is forced to vanish on the surface of the system. Free boundary conditions: Vanishing external field outside the system.
In spin systems free boundary conditions are usually adopted instead of Dirichlet boundary conditions [53], whereas periodic boundary conditions are preferred in Monte Carlo simulations.

Scaling behaviour of the critical Casimir force

The free energy density of a confined system[14] can be split in a regular and in a singular part [179] as

$$\frac{\mathcal{F}_L(T,h)}{k_{\rm B}TV} = f_{L,\rm reg}(T,h) + f_{L,\rm sing}(T,h). \tag{2.11}$$

The non-singular contribution is given, at least for periodic boundary conditions, by Eq. (2.7), whereas the singular contribution obeys the universal scaling law [181]

$$f_{L,\rm sing}(T,h) = \frac{1}{L^d}\mathcal{Y}\left(atL^{\frac{1}{\nu}}, bhL^{\frac{\beta\delta}{\nu}}\right). \tag{2.12}$$

Here ν, β and δ are universal critical exponents[15]; the metric factors s and b are the only non-universal parameters and are system dependent. The scaling function $\mathcal{Y}$ will be determined, as shown before, by the bulk and surface universality classes and by the geometry.

In order to obtain the universal scaling function of the critical Casimir force between two planar walls in a critical fluid, let us move to the so called film geometry. The free energy per unit surface of the *confined* fluid can be written as

$$\begin{aligned}\frac{\mathcal{F}_L(T,h)}{k_{\rm B}TA} &= L\Big[f_{L,\rm reg}(T,h) + f_{L,\rm sing}(T,h)\Big] \\ &= Lf_b(T,h) + f_s(T,h) + \frac{1}{L^{d-1}}\mathcal{Y}\left(atL^{\frac{1}{\nu}}, bhL^{\frac{\beta\delta}{\nu}}\right),\end{aligned} \tag{2.13}$$

where the surface term reads

$$f_s(T,h) = f_s^{(1)}(T,h) + f_s^{(2)}(T,h)$$

with $f_s^{(1)}$ and $f_s^{(2)}$ the contributions to the non-singular free energy arising from the two distinct confining surfaces. The higher order terms in Eq. (2.7) vanish in planar symmetry[16].
The free energy (2.13) varies with the distance L between the walls and the critical Casimir force per unit surface is

$$\begin{aligned}\frac{1}{A}\frac{F_{\rm C}(T,h;L)}{k_{\rm B}T} &= -\frac{\partial}{\partial L}\left(\frac{\mathcal{F}_L(T,h)}{k_{\rm B}TA}\right) \\ &= f_b(T,h) + \frac{1}{L^d}\Theta\left(atL^{1/\nu}, bhL^{\beta\delta/\nu}\right),\end{aligned} \tag{2.14}$$

[14] Here we adopt the magnetic notation.
[15] We assume that the hyperscaling relations hold.
[16] We are assuming that there is no contribution to the free energy arising from the confinement of the fluctuations of the electromagnetic field in the (dielectric) fluid.

where $\Theta(y_1, y_2)$ is the critical Casimir force scaling function

$$\Theta(y_1, y_2) = (d-1)\,\mathcal{Y}(y_1, y_2) - \frac{1}{\nu} y_1 \frac{\partial \mathcal{Y}}{\partial y_1} - \frac{\beta\delta}{\nu} y_2 \frac{\partial \mathcal{Y}}{\partial y_2}.$$

A nice cancellation occurs if the walls are immersed in the fluid: The L-independent bulk term in Eq. (2.14) is counterbalanced by the same contribution originated by the fluid in the outer region. In this configuration, the force between the two walls is only due to the confinement of fluctuations.

Main results on the critical Casimir force

The analysis of the critical Casimir force and of the related universal scaling function Θ is a rather difficult task both experimentally, for the small forces involved, and theoretically, for the lack of an accurate description of critical fluids in confined geometries. In what follows we limit to report the most significant results about the critical Casimir interaction in connection to our work. Further details, in particular as regards the role of the critical Casimir forces on colloidal aggregation, can be found in the recent reviews [160, 144]. Most of the results present in the literature deal with the temperature dependence of the Casimir fluctuation induced interaction at zero magnetic field. An indirect estimate of the scaling function for the film geometry and the 3D Ising universality class, at $h = 0$ under $(+,-)$ and $(+,+)$ boundary conditions was given in Ref. [76, 182] monitoring the thickness of a binary liquid film at different temperatures near T_c. The first direct evaluation of the critical Casimir force was performed in 2008 [104] for a system consisting of a colloidal particle close to a wall (sphere-plate geometry) immersed in a binary mixture of water and Lutidine. The experiments were carried on at different compositions and for both the relevant boundary conditions. This system, however, allowed to probe only the exponential tail of the scaling function. A MC study of the solvent-mediated potential between two spherical particles in a simple fluid along the critical isochore has been performed in Refs. [86, 85] with different boundary conditions. However, the determination of the full Casimir scaling function could not be obtained in the temperature range examined in the simulations. Along the symmetry line ($h = 0$), more precise estimates of the universal Casimir scaling functions for the 3D Ising universality class and film geometry have been obtained via MC simulations of the Ising model [229, 230, 231]. Few theoretical approaches were devised to address this problem: In addition to the mean-field results [122], its is worthwhile mentioning the extended de Gennes-Fisher local functional method [20, 225] and a long-wavelength analysis of density functional theory [28, 174]. The latter investigations have been also extended away from the symmetry line ($h \neq 0$) providing predictions on the shape of the critical Casimir scaling function in the off-critical case [204, 154, 174]. Monte Carlo simulations at $h \neq 0$ were recently performed in Ref. [232].

2.2 DENSITY FUNCTIONAL THEORY

The physical properties of homogeneous fluids at equilibrium do not depend on the position where they are measured. The translational invariance endowed with such systems led to the formulation of simple theories accounting with excellent accuracy for the bulk properties of fluids. However, finite systems we handle in the laboratory are always inhomogeneous: Ubiquitous interfaces break translational invariance and unexpected implications come into play. The portion of fluid in contact with a wall can not be considered homogeneous: The confining potential generated by the wall induces strong oscillations in the density profile. Another illuminating example is the flat interface between a liquid and a vapour that forms in the presence of the gravitational field: Across this interface, if the system is far enough from the critical point, the average density varies abruptly from the bulk to the vapour value. The same happens for wetting films and many other interfacial phenomena.

However, the thermodynamic (or statistical mechanics) description of inhomogeneous fluids at equilibrium brings with it some difficulties. To give an example, it is well known that it is not possible to uniquely define all the local thermodynamic functions in regions where the scale of the inhomogeneities is of the order of the microscopic correlation length. This is the case of a fluid against a hard wall or of the liquid-gas interface in a gravitational field. The local density turns out to be well defined for all kind of inhomogeneities, together with the chemical potential and the temperature, which are constant throughout the system, whereas the pressure tensor lacks of a unique definition (we deal with this problem in Section 4.2).

The goal of this Chapter is to give a microscopic prediction for the solvent-mediated interaction between two planar walls immersed in a classical fluid at different thermodynamic conditions, including the critical region. As we will show below, the force between the walls induced by the confined fluid is strictly related to its density profile. Therefore, in order to achieve the goal we have set ourselves, we need an accurate description of the properties of a confined fluid.
Up to now, the most successful theoretical approach devised to study inhomogeneous systems is Density Functional Theory (DFT) [142]. Although alternative techniques, like integral equations or scaled particle theory, have been proposed [101], DFT is generally considered to be the most accurate and versatile tool for dealing with inhomogeneous systems and has been applied in several frameworks: From the study of fluids in nanopores, to the structure of the liquid-vapour interface, to the theory of freezing (see e.g. [98]).

Density functional theory was born in the late nineteenth century, when Maxwell, Poisson and Lord Rayleigh turned their attention to another interface driven phenomena: The capillarity action [198]. The mechanical approach inspired by Laplace and then proposed again by Maxwell [148] in order to treat the problem was too crude because it assumed that the density profile across the gas-liquid interface was a step function. Poisson and Rayleigh [183] recognised

the weakness in Maxwell's approach, but it was van der Waals in 1893 [226] who first succeeded in fixing some defects: He considered space dependent density profiles and provided a description of the problem within a thermodynamical framework. This work[17] can be considered a milestone and is the first attempt, however crude, to develop a thermodynamic analysis of non-uniform systems. Van der Waals recognised that the local free energy density of an inhomogeneous equilibrium system at a given point $\boldsymbol{r}$ is determined not only by the value of the density at $\boldsymbol{r}$, but also by the density at the neighbouring points. This circumstance is somewhat related to the impossibility of a unique definition of many local thermodynamic functions inhomogeneous systems: Van der Waals (together with Rayleigh) was aware that a local expression of thermodynamic functions can be regarded only as an approximation [197].
Furthermore, Van der Waals introduced in Section 6 of Ref [196] the paradigm at the basis of the density functional theory. He expressed the free energy density in terms of its local value $\rho(\boldsymbol{r})$ and a correction proportional to its second order derivative and he stated that the equilibrium density profile should come from the minimisation of the functional

$$\mathcal{F}[\rho(\boldsymbol{r})] = \int \mathrm{d}\boldsymbol{r}' \Big[f_b\big(\rho(\boldsymbol{r}')\big) + a\,\nabla^2\rho(\boldsymbol{r}') \Big], \tag{2.15}$$

where a is a suitable constant and f_b the homogeneous free energy density.

These works were largely forgotten since the early days of quantum mechanics. At that time no one was able to solve the Schrodinger equation for the wave function in order to obtain the ground state density and energy of many electron atoms. In 1927 Thomas [221] and Fermi [70] independently understood that a way to circumvent the difficulties related to the knowledge of the full wave function was to shift attention to the density. They developed an approximation method which consists in expressing the ground state energy as a function of the electron density, with suitable approximations for the kinetic and the interaction term. They postulated that the equilibrium density is simply obtained by minimisation of the energy functional, taking the number of particles constant. This theory can be considered the first example of DFT applied to quantum systems.
Thirty-seven years had to pass for Hohenberg and Kohn to prove [106] that the variational principle postulated by Thomas and Fermi really holds for the ground state energy of quantum mechanical electrons. The following year Mermin [153] generalised the Hohenberg-Kohn theorem to system at any temperature, paving the way for the application of DFT also in classical systems described by statistical mechanics. The only difference is that within classical systems the functional that has to be minimised with respect to the particle density is the grand canonical functional. The functional techniques were introduced in statistical physics by Bogoliubov [19] and the functional language became familiar in the field of classical fluids in the early sixties thanks to

[17] An English version has been provided by Sir J. S. Rowlinson [196].

the applications given by by Percus and Stell [73]. The use of the results by Hohenberg-Kohn-Mermin became routine after the works by Ebner et al. [60, 201] and by Yang et al. [249].

The variational principle

The density profile[18] of an inhomogeneous fluid at equilibrium at a given temperature T and chemical potential μ, whose particles interact with the potential $U(\{\boldsymbol{r}_i\})$ and are subject to an external field $\phi(\boldsymbol{r})$, depends on position and is defined as [98]

$$\rho\left(\boldsymbol{r}_1\right)=\frac{1}{\mathcal{Q}}\sum_{N=1}^{\infty}\frac{N}{N!}\int \mathrm{d}\boldsymbol{r}_2\ldots\mathrm{d}\boldsymbol{r}_N\,\mathrm{e}^{-\beta U_N(\{\boldsymbol{r}_i\})}\prod_{i=1}^{N}\mathrm{e}^{\beta\Psi(\boldsymbol{r}_i)}. \tag{2.16}$$

In this expression $\mathcal{Q}$ is the grand canonical partition function and we have introduced the intrinsic chemical potential

$$\Psi(\boldsymbol{r})=\mu-\phi(\boldsymbol{r}), \tag{2.17}$$

with $\Lambda=\sqrt{2\pi\beta\hbar^2/m}$ the de Broglie wavelength and m the mass of the particles. If approached on the basis of Eq. (2.16), the evaluation of the density profile turns out to be an impossible task for real systems. The difficulties enclosed in Eq. (2.16) can be overcome by the density functional formalism, which, in a nutshell, shifts the problem of calculating the grand partition function in minimising an appropriate functional of the one-particle density, with the temperature and the chemical potential acting as parameters. Equation (2.16) could lead to believe that, for a system specified by a given inter-particle interaction, the one particle density is a functional of the external field ϕ. Also the grand canonical potential

$$\Omega\left(T,V,\mu\right)=-\frac{1}{\beta}\log\Big[\mathcal{Q}\left(T,V,\mu\right)\Big] \tag{2.18}$$

could seem to be a functional, at fixed temperature, of the intrinsic chemical potential (and therefore of the external potential).
The density functional theory for classical systems overturns this way of thinking stating[19] that, at fixed the temperature T, chemical potential μ and kind of particles (i.e. the interaction potential U_N), there is a one-to-one correspondence between the density profile, the external potential and the

[18]Sometimes referred to as the one-particle density distribution, in order to show the relationship with n-particle density distributions (see e.g. [98]).

[19]For the proof of the theorem in classical formalism see standard textbooks e.g. [98] or the accurate, even if dated, review by Robert Evans [64].

gran canonical probability density F_0[20]:

$$\phi(\boldsymbol{r}) \Longleftrightarrow F_0 \Longleftrightarrow \rho(\boldsymbol{r}). \tag{2.19}$$

This means that if we consider a given equilibrium density profile $\rho(\boldsymbol{r})$, at fixed T, μ and U_N, there exists a unique[21] external potential that gives rise to that profile (modulo additive constants).

Equation (2.19) implies [98] that the equilibrium density profile $\rho(\boldsymbol{r})$ of a system subject to an external potential can be found by minimising a suitably defined density functional $\Omega[n(\boldsymbol{r})]$ at fixed chemical potential μ and temperature T. The grand potential functional can be conveniently expressed in terms of the external potential $\phi(\boldsymbol{r})$ and the intrinsic free energy functional $\mathcal{F}[n(\boldsymbol{r})]$ as

$$\Omega[n(\boldsymbol{r})] = \mathcal{F}[n(\boldsymbol{r})] - \int \mathrm{d}\boldsymbol{r}\, n(\boldsymbol{r})\big(\mu - \phi(\boldsymbol{r})\big). \tag{2.20}$$

When evaluated at the equilibrium density profile, $\Omega[n(\boldsymbol{r})]$ and $\mathcal{F}[n(\boldsymbol{r})]$ actually reduce to the system's gran potential and free energy:

$$\Omega[\rho(\boldsymbol{r})] = \Omega(T, V, \mu), \qquad \mathcal{F}[\rho(\boldsymbol{r})] = \mathcal{F}(T, V, \mu), \tag{2.21}$$

defined in (2.18).

As stated by the Hohenberg-Kohn theorem, the *equilibrium* density profile $\rho(\boldsymbol{r})$ minimises the grand potential functional. In formulae:

$$\left.\frac{\delta\Omega[n]}{\delta n(\boldsymbol{r})}\right|_{\rho(\boldsymbol{r})} = \left.\frac{\delta\mathcal{F}[n]}{\delta n(\boldsymbol{r})}\right|_{\rho(\boldsymbol{r})} + \phi(\boldsymbol{r}) - \mu = 0. \tag{2.22}$$

The explicit knowledge of the intrinsic free energy functional would lead, through a straightforward minimisation, to the equilibrium density profile and to the corresponding value of the gran canonical potential. Unfortunately, the analytical form of $\mathcal{F}[n]$, a unique functional of the density profile, is not exactly known yet. The exact expression of the intrinsic free energy is available only for the ideal gas

$$\beta\mathcal{F}^{\mathrm{id}}[n(\boldsymbol{r})] = \int \mathrm{d}\boldsymbol{r}\, n(\boldsymbol{r})\Big[\log\big(\Lambda^3 n(\boldsymbol{r})\big) - 1\Big] \tag{2.23}$$

and the minimisation of the gran potential functional (2.22) gives the well known *barometric law* for the density profile:

$$\rho(\boldsymbol{r}) = \Lambda^{-3} e^{\beta\Psi(\boldsymbol{r})}. \tag{2.24}$$

[20] Within the quantum formalism the many electron wave function replaces the distribution function.

[21] Modulo an additive constant. For a basic discussion about the issues of non-uniqueness and v-representability in DFT see [30].

In an interacting system, it is customary to separate the ideal contribution, splitting $\mathcal{F}[n(\boldsymbol{r})]$ as the sum of the ideal and the excess term $\mathcal{F}^{\mathrm{ex}}[n(\boldsymbol{r})]$:

$$\mathcal{F}[n(\boldsymbol{r})] = \mathcal{F}^{\mathrm{id}}[n(\boldsymbol{r})] + \mathcal{F}^{\mathrm{ex}}[n(\boldsymbol{r})]. \tag{2.25}$$

Through this decomposition we can express the formal solution of the minimisation (2.22) for an interacting system as the generalisation of the barometric law:

$$\rho(\boldsymbol{r}) = \Lambda^{-3} \exp\left\{\beta\left[\Psi(\boldsymbol{r}) - \left.\frac{\delta\mathcal{F}^{\mathrm{ex}}[n]}{\delta n(\boldsymbol{r})}\right|_{\rho(\boldsymbol{r})}\right]\right\}. \tag{2.26}$$

Looking at Eq. (2.26) we can note that the effects of the inter-particle interactions on the density profile are fully enclosed in the functional derivative of the excess free energy (defined as the one-particle direct correlation function), which acts on the system like an external effective one body potential. Obviously, this reformulation does not solve the problem because the $\rho(\boldsymbol{r})$ appears also in the r.h.s., but it is useful because it offers a self consistent route to perform the minimisation.

Approximated density functionals

The solution of the many-particle problem requires an (approximated) excess free energy functional able to capture the physics of the system[22]. There is not a unique strategy to obtain it and the success of the approximation can be only judged checking the reliability of the results produced by the minimisation and analysing the behaviour of the functional in appropriate limits, where exact solutions are known.
Several approximations for the excess part have been proposed over the years for dealing with specific problems. Hard sphere fluids are successfully described by Rosenfeld's Fundamental Measure Theory (FMT) [190, 192], also at bulk densities close to the solid transition. Even if the FMT is widely used and it its implementation is straightforward, at least for the planar geometry, Rosenfeld's approximation for the excess free energy holds in principle only for fluids of purely hard particles of any shape. We implemented also this version of DFT approximation (see Fig.s 2.3 and 2.6) in order to validate the predictions of our approximated functional in the high-temperature (i.e. when $\beta U_N(\{\boldsymbol{r}_i\}) \to 0$). Without going into further details, which go beyond the purpose of this presentation, we refer to the recent review about FMT [192].
The impact of the attractive contributions in the inter-particle potential on the structure of inhomogeneous fluids have been deeply analysed. In the following we will review the most popular approximations of the free energy functional in

[22] However, strictly speaking, the variational principle is valid only for the *exact* free energy functional, but not in general for an approximated one.

the presence of attractive potentials, trying to show why they are inadequate to account for the behaviour of inhomogeneous fluids in wide regions of the phase diagram, including the critical region. Then we will introduce our original approximation.

Local density approximation

The simplest approximation for the free energy functional can be obtained retaining only local informations. Such, sometimes crude, approximation is in principle even less accurate than the one proposed by van der Waals (2.15). Nonetheless, it is justified when the density profile varies very slowly over the range of molecular interactions. Under this hypothesis, the excess free energy density of the inhomogeneous fluid is locally similar to the excess free energy of the same fluid in bulk and at a density equal to the local density. The so called Local Density Approximation (LDA) is usually expressed as

$$\mathcal{F}[n(\boldsymbol{r})] = \int \mathrm{d}\boldsymbol{r}\, f\big([n(\boldsymbol{r})], \boldsymbol{r}\big) \simeq \int \mathrm{d}\boldsymbol{r}\, f_b\big(n(\boldsymbol{r})\big), \tag{2.27}$$

where $f_b(\rho)$ is the excess free energy density of the homogeneous bulk fluid at density ρ, which can be considered as a known result of liquid state theories. Note that the ideal contribution to the free energy (2.23), which is exactly known, can be written without approximation in the form (2.27), i.e. is local.

Long-wavelength approximation

A refinement of the local density approximation can be obtained by expanding of $f\big([n(\boldsymbol{r})], \boldsymbol{r}\big)$ as a series of density gradients $\partial_\alpha n(\boldsymbol{r})$:

$$\begin{aligned} f\big([n(\boldsymbol{r})]\big) = c^{(0)}\big(n(\boldsymbol{r})\big) + c^{(1)}_\alpha\big(n(\boldsymbol{r})\big)\,\partial_\alpha n(\boldsymbol{r}) + c^{(2,a)}_{\alpha\beta}\big(n(\boldsymbol{r})\big)\,\partial_\alpha n(\boldsymbol{r})\,\partial_\beta n(\boldsymbol{r}) \\ + c^{(2,b)}_{\alpha\beta}\big(n(\boldsymbol{r})\big)\,\partial_\alpha\partial_\beta n(\boldsymbol{r}), \end{aligned} \tag{2.28}$$

where the coefficients $c^{(0)}(\rho)$, $c^{(1)}_\alpha(\rho)$, $c^{(2,a)}_{\alpha\beta}(\rho)$ and $c^{(2,b)}_{\alpha\beta}(\rho)$ are only functions of the local value of the density profile and the sum over repeated indexes is understood. In this expansion, the density gradients include non-local corrections to the LDA functional and account for slowly varying density profiles. The (exact) intrinsic free energy functional $\mathcal{F}\big[\rho(\boldsymbol{r})\big]$ is a unique functional of the equilibrium density profile [64], and also $f\big([n(\boldsymbol{r})], \boldsymbol{r}\big)$ shares this property. Therefore $f\big([n(\boldsymbol{r})], \boldsymbol{r}\big)$ can not depend on the external potential $\phi(\boldsymbol{r})$ and must be invariant under rotations. The coefficients are invariant under rotations because their argument is a scalar function, so that

$$c^{(2,a)}_{\alpha\beta}(n) = \delta_{\alpha\beta}\, c^{(2,a)}(n), \qquad\qquad c^{(2,b)}_{\alpha\beta}(n) = \delta_{\alpha\beta}\, c^{(2,b)}(n).$$

As regards the derivatives of the density profile, only the scalar contributions $\partial^2_\alpha n(\boldsymbol{r})$ and $\partial_\alpha n(\boldsymbol{r})\,\partial_\alpha n(\boldsymbol{r})$ are invariant under rotations. Furthermore simple

algebra gives

$$c^{(2,b)}\big(n(\boldsymbol{r})\big)\partial_\alpha^2 n(\boldsymbol{r}) = \partial_\alpha\left[c^{(2,b)}\big(n(\boldsymbol{r})\big)\partial_\alpha n(\boldsymbol{r})\right] - \left.\frac{\mathrm{d}c^{(2,b)}}{\mathrm{d}n}\right|_{n(\boldsymbol{r})}\partial_\alpha n(\boldsymbol{r})\partial_\alpha n(\boldsymbol{r}),$$

where the first term in this equation vanishes when integrated over the whole system. Summing up, (2.28) reads

$$f\big([n(\boldsymbol{r})],\boldsymbol{r}\big) = f_b\big(n(\boldsymbol{r})\big) + \frac{1}{2}b\big(n(\boldsymbol{r})\big)\big|\boldsymbol{\nabla}n(\boldsymbol{r})\big|^2 + o\big|\boldsymbol{\nabla}n(\boldsymbol{r})\big|^4,$$

where the function $c^{(0)}(\rho)$ equals the homogeneous free energy density, in order to recover the correct bulk description, whereas $b(\rho)$ has not been fixed yet.

Different prescriptions have been devised in order to obtain an estimate for this coefficient. A feasible route is to make the problem easier, imposing that the variation of the density profile with respect to the bulk density ρ_b is also small, as well as slow. According to this hypothesis we can expand the density profile about the bulk density ρ_b and the free energy functional reads

$$\mathcal{F}[n(\boldsymbol{r})] \simeq \mathcal{F}[\rho_b] + \int \mathrm{d}\boldsymbol{r}\left[\mu\Delta n(\boldsymbol{r}) + \frac{1}{2}\left.\frac{\mathrm{d}^2 f_b}{\mathrm{d}\rho^2}\right|_{\rho_b}\big(\Delta n(\boldsymbol{r})\big)^2 + \frac{b(\rho_b)}{2}\big|\boldsymbol{\nabla}n(\boldsymbol{r})\big|^2\right], \quad (2.29)$$

where $\Delta n(\boldsymbol{r}) = \rho(\boldsymbol{r}) - \rho_b$ and the first order derivative of the free energy density is the chemical potential of the bulk system. The only unknown in (2.29) is the constant $b(\rho_b)$, which can be related, as we will show in the following, to the second moment of the correlation function. This link arises from the comparison of (2.29) with the perturbative expansion of the free energy density, which is introduced in the next paragraph.

Let us focus on a system where only small variations of the equilibrium density profile appear, that is $|\Delta\rho(\boldsymbol{r})| \ll \rho_b$. Expanding the free energy functional about the bulk density

$$\mathcal{F}[n(\boldsymbol{r})] \simeq \mathcal{F}[\rho_b] + \int \mathrm{d}\boldsymbol{r}\left.\frac{\delta\mathcal{F}}{\delta n(\boldsymbol{r})}\right|_{\rho_b}\Delta n(\boldsymbol{r}) + \frac{1}{2}\int \mathrm{d}\boldsymbol{r}\int \mathrm{d}\boldsymbol{r}'\left.\frac{\delta^2\mathcal{F}}{\delta n(\boldsymbol{r})\delta n(\boldsymbol{r}')}\right|_{\rho_b}\Delta n(\boldsymbol{r})\Delta n(\boldsymbol{r}')$$

and recalling some definitions we obtain the so called perturbative expansion of the free energy functional

$$\begin{aligned}\mathcal{F}[n(\boldsymbol{r})] \simeq{}& \mathcal{F}[\rho_b] + \mu\int \mathrm{d}\boldsymbol{r}\,\Delta n(\boldsymbol{r}) \\ &+ \frac{1}{2\beta}\int \mathrm{d}\boldsymbol{r}\int \mathrm{d}\boldsymbol{r}'\left[\frac{\delta(\boldsymbol{r}-\boldsymbol{r}')}{\rho_b} - c(|\boldsymbol{r}-\boldsymbol{r}'|,\rho_b)\right]\Delta n(\boldsymbol{r})\Delta n(\boldsymbol{r}'). \quad (2.30)\end{aligned}$$

In this expression the first order functional derivative of the free energy at constant density has been rewritten by means of Eq. (2.22). As regards the second order derivative, the ideal contribution directly follows from (2.23),

whereas the excess contribution, when evaluated at bulk density, is related to the bulk direct correlation function [98]:

$$-\beta \frac{\delta^2 \mathcal{F}^{\mathrm{ex}}\big[n(\boldsymbol{r})\big]}{\delta n(\boldsymbol{r}) \delta n(\boldsymbol{r}')}\bigg|_{n(\boldsymbol{r})=\rho_b} = c(|\boldsymbol{r}-\boldsymbol{r}'|, \rho_b). \tag{2.31}$$

It can be useful to express $\Delta n(\boldsymbol{r})$ and $\Delta n(\boldsymbol{r}')$ in (2.30) by means of their Fourier transforms we readily obtain

$$\mathcal{F}[n(\boldsymbol{r})] \simeq \mathcal{F}[\rho_b] + \mu \int \mathrm{d}\boldsymbol{r}\, \Delta n(\boldsymbol{r}) + \frac{1}{2\beta} \frac{V}{(2\pi)^3} \int \mathrm{d}\boldsymbol{q} \left[\frac{1}{\rho_b} - c(q, \rho_b)\right] \widetilde{\Delta n}(\boldsymbol{q}) \widetilde{\Delta n}(-\boldsymbol{q}), \tag{2.32}$$

where $c(q, \rho_b)$ and $\widetilde{\Delta n}(\boldsymbol{q})$ are the Fourier transform of $c(|\boldsymbol{r}|, \rho_b)$ and $\Delta n(\boldsymbol{r})$ respectively, and we exploited the translational invariance of the expression between squared parenthesis.
Before the invention of the fundamental measure theory by Rosenfeld [190], the structure of fluids with repulsive inter particle potentials was studied through the expansion (2.30). This functional provides quite accurate density profiles for hard spheres confined by hard walls, but is less successful in the description of fluids with attractive or repulsive tails.

After this digression, let us come back to our original problem. The coefficient $b(\rho)$ can be obtained through the comparison of (2.29) with the perturbative expansion of the free energy (2.32), obtained for density profiles showing small deviations from the bulk density, if we impose the additional requirement of long-wavelength variations of $\rho(\boldsymbol{r})$. In this limit an expansion for small wavevector of $c(q, \rho_b)$ is allowed:

$$c(q, \rho) = d_0(\rho) + d_2(\rho)\, q^2 + \ldots, \tag{2.33}$$

where $d_0(\rho) = c(q = 0, \rho)$. Substituting this expression in (2.32) and Fourier transforming back in the real space we obtain:

$$\mathcal{F}[n(\boldsymbol{r})] \simeq \mathcal{F}[\rho_b] + \mu \int \mathrm{d}\boldsymbol{r}\, \Delta n(\boldsymbol{r}) + \frac{1}{2\beta} \left[\frac{1}{\rho_b} - d_0(\rho_b)\right] \int \mathrm{d}\boldsymbol{r} \left(\Delta n(\boldsymbol{r})\right)^2 - \frac{d_2(\rho_b)}{2\beta} \int \mathrm{d}\boldsymbol{r} \left|\boldsymbol{\nabla} n(\boldsymbol{r})\right|^2. \tag{2.34}$$

Finally, the consistency between this expression and the perturbative result allows to fix $b(\rho)$:

$$b(\rho) = -\frac{1}{\beta} d_2(\rho) = \frac{1}{6\beta} \int \mathrm{d}\boldsymbol{r}\, r^2 c(r, \rho) \tag{2.35}$$

because the coefficient of the quadratic term in (2.33) is determined by the so called compressibility sum rule. The parameter $b(\rho)$ is also referred to as

the *stiffness coefficient* and is related to the range of the direct correlation function. This long-wavelength approximation, referred to as *square-gradient approximation* corresponds to the ϕ^4 coarse-grained theory, ubiquitous within statistical field theory. It has been shown recently [20, 225, 28, 174] that square-gradient approximations are suitable for the study of the long-range tails of the interaction between two walls mediated by a correlated fluid.

The detailed presentation of the square-gradient approximation given above is justified by the following circumstance: In the long-wavelength limit (i.e. when the density profile changes slowly *and* by small amounts) *any* DFT approximation fulfilling the condition (2.31) reduces to the square-gradient approximation (2.29), with the coefficient $b(\rho)$ given by (2.35). Therefore, when only the long-wavelength properties of the system are relevant, it is possible to replace an accurate functional, which probably requires heavy calculations for the numerical minimisation, with the minimal approximation given by Eq. (2.29) without any loss of information.
This idea has been recently implemented in Ref. [28, 174], where it has been shown that the square-gradient approximation is suitable for the study of the long-range tails critical Casimir interaction. Furthermore, in Section 2.5 we prove that the scaling functions of the critical Casimir force obtained within our full microscopic DFT approximation overlap with the coarse-grained predictions from Eq. (2.29) (see Fig. 2.17).

Perturbation theory

The perturbative approaches are the most common (and less expensive) way to deal with the attractive contribution to the inter-particle interaction. This kind of approximation starts from a known reference functional, which accounts for the repulsive contribution to the excess free energy functional, to which a small (usually mean-field) perturbation is added in order to describe the effects due to attraction. For a system with a pair-wise interaction potential we have:

$$\mathcal{F}^{\mathrm{ex}}[n(\boldsymbol{r})] = \mathcal{F}^{\mathrm{ex}}_{\mathrm{R}}[n(\boldsymbol{r})] + \frac{1}{2}\int \mathrm{d}\boldsymbol{r} \int \mathrm{d}\boldsymbol{r}'\, n(\boldsymbol{r}) u_{att}(\boldsymbol{r},\boldsymbol{r}') n(\boldsymbol{r}'), \tag{2.36}$$

where $u_{att}(\boldsymbol{r},\boldsymbol{r}')$ is the attractive contribution to the interaction potential. The mean-field contribution in (2.36) is usually referred to as the *Hartree term* [100] and it was introduced in the beginning of the study of many electron problems. Such an approach is quite simple to implement, but it gives only qualitative predictions, particularly in the critical region, because it does not take into account correlations arising from the attractive tail of the potential.

Dealing with correlations

During the seventies the ground state of the many electron problem in atomic, molecular and solid state systems was described within the density

functional formalism by means of the local density approximation. Even if this approach provided quite successful and unexpected results for a large number of properties it soon became evident that the exchange and correlation energy is characterised by a marked non-local character, neglected by simple choices of the energy functional.
A new era began in 1979, when Gunnardson, Jonson and Lundqvist [94] proposed the so called averaged-density approximation, which includes the exchange and correlation contribution to the ground state energy as

$$E^{\mathrm{xc}}[n(\boldsymbol{r})] = \int \mathrm{d}\boldsymbol{r}\, n(\boldsymbol{r}) \epsilon^{\mathrm{xc}}\big(\bar{n}(\boldsymbol{r})\big), \tag{2.37}$$

where $\epsilon^{\mathrm{xc}}(\rho)$ is the exchange-correlation energy density and $\bar{n}(\boldsymbol{r})$ is the density profile averaged in the neighbourhood of the point $\boldsymbol{r}$, thus introducing non-local informations. Within liquid state theories this approximation is known as the Weighted Density Approximation (WDA) and was applied for the first time by Nordholm et al. [162] the following year. The WDA brought about several improvement in the description of inhomogeneous fluids and certainly has been as a source of inspiration for Rosenfeld's fundamental measure theory. Accurate oscillating density profiles were published and soon it was realised that this approximation can also describe wetting because it fulfils the the hard wall sum rule

$$\beta p = \rho_w$$

which links the contact density at a hard wall ρ_w to the bulk pressure of the fluid[23].

In its most general formulation, the WDA consists of expressing the excess part of the free energy functional as

$$\mathcal{F}^{\mathrm{ex}}[n(\boldsymbol{r})] = \int \mathrm{d}\boldsymbol{r}\, n(\boldsymbol{r}) \psi^{\mathrm{ex}}\big(\bar{n}(\boldsymbol{r})\big), \tag{2.38}$$

where $\psi^{\mathrm{ex}}(\rho)$ is the excess free energy per particle of the homogeneous fluid and the *weighted density* $\bar{n}(\boldsymbol{r})$ can be written as a local average of the density profile, in terms of an isotropic weight function $w(r;\hat{n})$:

$$\bar{n}(\boldsymbol{r}) = \int \mathrm{d}\boldsymbol{r}' n(\boldsymbol{r}') w\big(|\boldsymbol{r}-\boldsymbol{r}'|;\hat{n}(\boldsymbol{r})\big). \tag{2.39}$$

The weight function is not fixed *a priori* and can be dependent on the local value of an auxiliary reference density $\hat{n}(\boldsymbol{r})$[24]. It must satisfy the normalisation requirement

$$\int \mathrm{d}\boldsymbol{r}'\, w\big(|\boldsymbol{r}-\boldsymbol{r}'|;\hat{n}(\boldsymbol{r})\big) = 1 \qquad\qquad \forall\, \boldsymbol{r} \tag{2.40}$$

[23] Many approaches to the problem based on integral equations fail.

[24] The definition of this function is not yet specified at this point. We only impose that the only functional dependence of $\hat{n}(\boldsymbol{r})$ is on the weight function $w(r)$.

to ensure that in the homogeneous limit the weighted density coincides with the actual density of the fluid.
The perturbative approach, briefly outlined above, provides a formally exact expression of the excess free energy functional useful to justify the WDA assumption (2.38) and to obtain some hints on how non-local effects enter the problem. It is possible to show [64] that the *exact* excess free energy can be written as

$$\mathcal{F}^{\mathrm{ex}}[n(\boldsymbol{r})] = \int \mathrm{d}\boldsymbol{r}' n(\boldsymbol{r}') \Psi\big([n(\boldsymbol{r})]; \boldsymbol{r}'\big). \tag{2.41}$$

The non-local functional Ψ is given by

$$\Psi\big([n(\boldsymbol{r})]; \boldsymbol{r}'\big) = \int \mathrm{d}\boldsymbol{r}' n(\boldsymbol{r}') u(\boldsymbol{r} - \boldsymbol{r}') \int_0^1 \mathrm{d}\alpha \, g^{(2)}\big(\alpha u(\boldsymbol{r}); \boldsymbol{r}, \boldsymbol{r}'\big)$$

and all the complexity of the problem have been included into the two-particle radial distribution function $g^{(2)}\big(\alpha u(\boldsymbol{r}); \boldsymbol{r}, \boldsymbol{r}'\big)$ of the *inhomogeneous* fluid[25], which is not exactly known. Looking at (2.41) it is clear that the most natural approximation, based only on the knowledge of the properties of bulk fluids, is that adopted in Eq. (2.38), where the homogeneous excess free energy density ψ^{ex} evaluated at the smoothed density $\bar{n}$ takes the place of the product between the functional Ψ and the potential.

As anticipated above, there is some freedom in the choice of the weight function, which is one of the key elements in this approximation, and both the LDA and the mean-field approximations correspond to special choices of the weight function[26]. Nordholm [162] obtained qualitatively good results for hard sphere systems by means of a weight function proportional to the step function:

$$w\big(|\boldsymbol{r}|; \hat{n}(\boldsymbol{r})\big) = \frac{3}{4\pi\sigma^3} \Theta(\sigma - |\boldsymbol{r}|), \tag{2.42}$$

where σ is the diameter of the hard sphere.
Tarazona [216] refined Nordholm's density profiles making use of the Carnahan-Starling expression for the free energy of the bulk fluid. A key remark was subsequently put forward by Tarazona and Evans [219], who noticed that the homogeneous correlation function resulting from (2.42) is characterised by an overestimated range and by values three times bigger respect to that predicted by the PY approximation at short distances. This was a remarkable step in the development of the WDAs, because thereafter the efforts have been focused on devising weight functions able to reproduce correctly the two-particle correlation function in the homogeneous limit. Operationally, the desired bulk correlation $c(|\boldsymbol{r}|, \rho)$ can be obtained by enforcing for each density

[25] Interacting with potential $\alpha u(\boldsymbol{r})$.
[26] E.g. the LDA follows from the choice $w\big(|\boldsymbol{r}|; \hat{n}(\boldsymbol{r})\big) = \delta(\boldsymbol{r})$.

ρ the relation

$$-\beta\frac{\delta^2\mathcal{F}^{\rm ex}[n]}{\delta n(\boldsymbol{r})\delta n(\boldsymbol{r}')}\bigg|_{n(\boldsymbol{r})=\rho} = c^{(2)}(\boldsymbol{r},\boldsymbol{r}')\Big|_{\rho} = c(|\boldsymbol{r}-\boldsymbol{r}'|,\rho), \tag{2.43}$$

where $c^{(2)}(\boldsymbol{r},\boldsymbol{r}')$ is the two-particle direct correlation function for an inhomogeneous system[27] whereas the bulk correlation function $c(|\boldsymbol{r}|,\rho)$ is considered as an input from liquid state theories or simulations. Equation (2.43), once the excess free energy has been expressed in the form (2.38), is a non-linear integro-differential equation for the weight function. If the solution exists, the selected approximation is consistent with a bulk liquid state theory and it is possible to proceed with the (numerical) minimisation of the functional.

Many weighted density approximations

Assuming that we are able to enforce a given direct correlation function in the homogeneous limit through the condition (2.43), only two elements can distinguish between different weighted density approximations. The first one is the underlying bulk liquid state theory, which fixes the free energy densities and the correlations. We will discuss this point in more detail in the next section. The second one is the auxiliary function $\hat{n}(\boldsymbol{r})$.

The easiest way to proceed is to neglect the position dependence of $\hat{n}(\boldsymbol{r})$ and set

$$\hat{n}[n(\boldsymbol{r})] = \rho_b, \tag{2.44}$$

where ρ_b is the bulk density of the system in the homogeneous limit. This choice guarantees a great simplification in Eq. (2.43), because $\hat{n}(\boldsymbol{r})$ looses its functional dependence on the density profile $n(\boldsymbol{r})$

$$\frac{\delta\hat{n}[n(\boldsymbol{r})]}{\delta n(\boldsymbol{r}')} = 0$$

and it straightforwardly follows[28] that Eq. (2.43) takes the form:

$$c(|\boldsymbol{r}-\boldsymbol{r}'|,\rho_b) = -\beta\rho_b\,\frac{\partial^2\psi}{\partial\rho^2}\bigg|_{\rho_b}\int \mathrm{d}\boldsymbol{r}_1\, w\big(|\boldsymbol{r}-\boldsymbol{r}_1|;\rho_b\big)w\big(|\boldsymbol{r}'-\boldsymbol{r}_1|;\rho_b\big) - 2\beta\,\frac{\partial\psi}{\partial\rho}\bigg|_{\rho_b} w\big(|\boldsymbol{r}'-\boldsymbol{r}|;\rho_b\big). \tag{2.45}$$

[27] Here we are assuming that a given auxiliary function $\hat{n}(\boldsymbol{r})$ has been fixed.

[28] This choice implies that the second order functional derivative of the weighted density vanishes.

Leidl and Wagner [134] proposed the so called Hybrid-WDA, based on the following prescription for the auxiliary density:

$$\hat{n}[n(\boldsymbol{r})] = \frac{1}{N}\int \mathrm{d}\boldsymbol{r} \int \mathrm{d}\boldsymbol{r}'\, n(\boldsymbol{r})\, w\big(|\boldsymbol{r}-\boldsymbol{r}'|;\hat{n}\big)\, n(\boldsymbol{r}'), \tag{2.46}$$

where N is the total number of particles in the fluid. The predictions for hard sphere systems provided by the HWDA are accurate up to reduced densities of the order of 0.8. The peaks due to the layering of the fluid are located in the correct positions and the overall density profile is nearly indistinguishable from that obtained with the more complicated WDA by Curtin and Ashcroft [37]. However, in most cases the definition (2.46) introduces several difficulties without real advantages. Computing the functional derivative of the auxiliary function w.r.t. the density profile we get

$$\frac{\delta\hat{n}[n(\boldsymbol{r})]}{\delta n(\boldsymbol{r}')} = \frac{N^{-2}\int \mathrm{d}\boldsymbol{r}_1\mathrm{d}\boldsymbol{r}_2 n(\boldsymbol{r}_1)n(\boldsymbol{r}_2)w\big(|\boldsymbol{r}_1-\boldsymbol{r}_2|;\hat{n}\big) - 2N^{-1}\int \mathrm{d}\boldsymbol{r}_1 n(\boldsymbol{r}_1) w\big(|\boldsymbol{r}'-\boldsymbol{r}_1|;\hat{n}\big)}{N^{-2}\int \mathrm{d}\boldsymbol{r}_1\mathrm{d}\boldsymbol{r}_2 n(\boldsymbol{r}_1)n(\boldsymbol{r}_2)\,\frac{\partial}{\partial\rho}\big[w\big(|\boldsymbol{r}_2-\boldsymbol{r}_1|;\rho\big)\big]\Big|_{n(\boldsymbol{r})} - 1}.$$

If we consider the thermodynamic limit of this expression, the numerator vanishes due to the presence of a multiplicative $1/N$ factor: Therefore also the functional derivative vanishes. It means that the HWDA reduces, for system unbounded at least in one direction, to the WDA resulting from the simpler prescription (2.44). In the following we will deal with unbounded systems and therefore we will adopt a constant auxiliary density. Leidl and Wagner applied the functional resulting from (2.46) only for the repulsive contribution to the excess free energy, whereas the attractive tail of the potential was introduced in the functional as a mean-field correction. Maybe, this was due to the complication in the solution of the equation for the weight function, increased by the presence of an attractive contribution.

The approach suggested by Tarazona [218, 217], and subsequently adopted also by Curtin and Ashcroft [37], identifies the auxiliary density with the weighted density itself

$$\hat{n}[n(\boldsymbol{r})] = \bar{n}(\boldsymbol{r}). \tag{2.47}$$

The non-linear integro-differential equation (resulting from Eq. (2.43)) obeyed by the weight function is hard to solve, even if the direct correlation function is given explicitly as a function of position and density. The problem is therefore shifted to the momentum space by means of a Fourier transform.
Tarazona proposed to solve the differential equation for the weight function in the momentum space through a polynomial expansion of the weight function up to the second order in the density. Skipping all the details [218, 217], the density profiles resulting from this prescription were be better than all the results obtained before using density independent weight functions. However, such an expansion can not be justified at all[29] and it is not possible to guarantee that it holds also for systems other than hard spheres.

[29] Robert Evans, in his review about DFT [101], tells that the approximation by Tarazona

Curtin and Ashcroft [37] made a formally consistent use of the Percus-Yevick approximation, both for the correlation function and for the energy density, without any further approximation. They solved the resulting non-linear differential equation for w at fixed wave vector and density via an iterative procedure, starting from a guess for w appropriately selected. They claimed that the iteration can be stopped after 5/10 iterations with a precision of 1 part in 10^4. Kroll and Laird [124] solved the same equation addressed by Curtin and Ashcroft without reporting details or difficulties. We also tried to reproduce the results, following the same procedure suggested in [37], however we noted that going further in the iteration led to complex solutions for the second order equation used to produce the guess. After a careful analytical analysis, it is possible to show that the equation for the weight function is an Abel differential equation of the second kind [253], which, in a range of densities, has no solutions satisfying the physical boundary conditions.

Many other auxiliary densities have been proposed (among them see [93, 152]), but in the presence of interactions none of them shows better consistency and better predictions than that obtained with the choice in Eq. (2.44). Therefore we decided to proceed selecting this simple, and powerful, prescription. In the next Section we present our WDA approach, which is characterised by an original strategy introduced in order to include the non-mean-field effects arising from the attractive tails of the interparticle potentials.

2.3 A WEIGHTED DENSITY APPROXIMATION FOR CRITICAL FLUIDS

The goal of this Chapter is to provide a microscopic theory of solvent-mediated forces in the whole phase diagram of the fluid, including the liquid-vapour transition. As already stressed, the density functional formalism seems to be a powerful tool to achieve our purpose but we need an approximation of the excess free energy functional which, in the uniform limit, is accurate both in the dense and in the critical regime. As we have tried to review before, such an implementation of DFT has not been devised yet.

In the previous Section we have shown that a good starting point is provided by the weighted density approximation. The accuracy of such DFT implementation strongly relies on the two key ingredients which characterise our WDA ansatz, namely the homogeneous free energy $\psi^{\rm ex}$ and the weight function $w(r;\hat{n}[n(\boldsymbol{r})])$. In addition, as regards $\hat{n}[n(\boldsymbol{r})]$, a good compromise between accuracy and computational agility is the simple prescription (2.44).

As regards the the underlying bulk description of the fluid, the only available microscopic liquid state theory able to account both for non-critical and critical fluid properties is the Hierarchical Reference Theory (HRT) [170, 171], which

"was once described, by an eminent theorist, as a chemical engineer's prescription".

will be therefore adopted in this work for the evaluation of the excess free energy $\psi^{\rm ex}(\rho)$ and of the bulk direct correlation function $c(r;\rho)$ of the uniform fluid.
Although the general formalism of HRT can be applied to fluids and mixtures with arbitrary pair interactions, quantitative results for specific models require the closure of the exact HRT equations by introducing some approximation. A closure which proved remarkably accurate has been implemented in the case of a Hard Core Yukawa (HCY) fluid [169], because the resulting HRT equations considerably simplify by use of the known solution of the Ornstein-Zernike equation available for this interaction. The HCY potential is defined as the superposition of a pure hard core term of diameter σ and an attractive Yukawa *tail* of inverse range ζ

$$v_{\rm Y}(r) = -\epsilon\sigma\,\frac{{\rm e}^{-\zeta(r-\sigma)}}{r}\,\Theta(r-\sigma), \tag{2.48}$$

where the parameter ϵ, which defines the energy scale, is positive and $\Theta(r)$ is the Heaviside step function. In the following we will investigate this model taking σ and $\epsilon/{\rm k_B}$ as the units of length and temperature respectively.

Having established the form of our excess functional in the homogeneous limit, we proceed with the explicit definition of $\mathcal{F}^{\rm ex}[n(\boldsymbol{r})]$ for general density profiles. We first focus our attention on the effects of the attractive contribution to the potential. As we reported in Section 2.2, usually the contribution of attractive tails is introduced in the functional through a mean-field approximation (2.36). The description of a near-critical fluid given by (2.36) is only qualitatively correct, because it leads to mean-field critical exponents and scaling functions. Nonetheless, it is well known that the main contribution to the internal energy is given by the Hartree term: This circumstance has been extensively recognised in the previous treatments. We are therefore led to isolate this term in the excess free energy, by writing

$$\mathcal{F}^{\rm ex}[n(\boldsymbol{r})] = \mathcal{F}^{\rm ex}_{\rm R}[n(\boldsymbol{r})] + \mathcal{F}^{\rm ex}_{\rm H}[n(\boldsymbol{r})], \tag{2.49}$$

where the Hartree contribution is given by

$$\mathcal{F}^{\rm ex}_{\rm H}[n(\boldsymbol{r})] = \frac{1}{2}\int {\rm d}\boldsymbol{r}' \int {\rm d}\boldsymbol{r}''\, n(\boldsymbol{r}')\, v_{\rm Y}(|\boldsymbol{r}'-\boldsymbol{r}''|)\, n(\boldsymbol{r}''),$$

whereas the reference term $\mathcal{F}^{\rm ex}_{\rm R}[n(\boldsymbol{r})]$, *defined* by Eq. (2.49), contains both the *entropic contribution* to the free energy, arising from hard core repulsion, and the *correlations*, induced by the attractive interaction. Our choice is then to use the WDA to represent only the entropy-correlation part of the intrinsic free energy functional, retaining the exact description of the Hartree energy:

$$\mathcal{F}^{\rm ex}_{\rm R}[n(\boldsymbol{r})] = \int {\rm d}\boldsymbol{r}\, n(\boldsymbol{r}) \psi^{\rm ex}_{\rm R}\big(\bar{n}(\boldsymbol{r})\big),$$

where

$$\psi^{\rm ex}_{\rm R}(\rho) = \psi^{\rm ex}(\rho) - \frac{\rho}{2}\int {\rm d}\boldsymbol{r}\, v_{\rm Y}(r). \tag{2.50}$$

The form of the weight function can be determined following the strategy put forward by Tarazona [218, 217] and introduced in Section 2.2 (Dealing with correlations), which consists in requiring that the two-particle direct correlation function reduces, in the homogeneous limit, to the known form of the underlying bulk liquid state theory (see Eq. (2.43)). In accordance with the notation of this Section we have

$$-\beta \frac{\delta^2 \mathcal{F}_{\mathrm{R}}^{\mathrm{ex}}[n]}{\delta n(\boldsymbol{r}) \delta n(\boldsymbol{r}')}\bigg|_{n(\boldsymbol{r})=\rho} = c(|\boldsymbol{r}-\boldsymbol{r}'|;\rho) + \beta\, v_{\mathrm{Y}}(|\boldsymbol{r}-\boldsymbol{r}'|) \equiv c_{\mathrm{R}}(|\boldsymbol{r}-\boldsymbol{r}'|;\rho), \tag{2.51}$$

where $c(r;\rho)$ is the direct correlation function predicted by HRT and the last equality is the definition of $c_{\mathrm{R}}(r;\rho)$. It is straightforward to obtain from (2.51) and (2.45) an algebraic equation for the Fourier transform of the weight function $w(q;\rho)$:

$$\beta\rho \frac{\partial^2 \psi_{\mathrm{R}}^{\mathrm{ex}}}{\partial \rho^2}\bigg|_{\rho} w^2(q;\rho) + 2\beta \left.\frac{\partial \psi_{\mathrm{R}}^{\mathrm{ex}}}{\partial \rho}\right|_{\rho} w(q;\rho) + c_{\mathrm{R}}(q;\rho) = 0 \tag{2.52}$$

which, at least in the cases examined in this work, always admits real solutions[30]. The physical root can be determined enforcing the normalisation condition (2.40), recalling that the compressibility sum rule, satisfied by the HRT direct correlation function, requires

$$c_{\mathrm{R}}(0;\rho) = \int \mathrm{d}\boldsymbol{r}\, c_{\mathrm{R}}(r;\rho) = -2\beta \frac{\partial \psi_{\mathrm{R}}^{\mathrm{ex}}}{\partial \rho} - \beta\rho \frac{\partial^2 \psi_{\mathrm{R}}^{\mathrm{ex}}}{\partial \rho^2}. \tag{2.53}$$

As in other implementations of WDA [218], the range of the weight function always remains comparable to the size of the molecules. This feature is preserved also in the critical region, as shown in Fig. 2.1. Indeed, the onset of this remarkable property of the weight function can be justified as follows. Within the mean spherical approximation closure adopted in the smooth-cutoff formulation of HRT, the critical exponent η, which describes the long-wavelength divergence of the structure factor, is equal to zero. This means that the direct correlation function is characterised by a short range, also near the critical point, and the same property must hold for the weight function too.

Once the intrinsic density functional has been determined, the approximate equilibrium properties, such as the density profile $\rho(\boldsymbol{r})$ and the grand canonical potential $\Omega[\rho(\boldsymbol{r})]$, can be obtained minimising the functional (2.20) at fixed temperature and chemical potential. In most of the situations the relevant quantity held fixed is the bulk density, rather than the chemical potential. In

[30] The existence of the solutions for a given $\psi_{\mathrm{R}}(\rho)$ and $c(q;\rho)$ can not be guaranteed *a priori*. See also the discussion of the Curtin-Ashcroft implementation of the WDA in Sec. 2.2 (Many weighted density approximations).

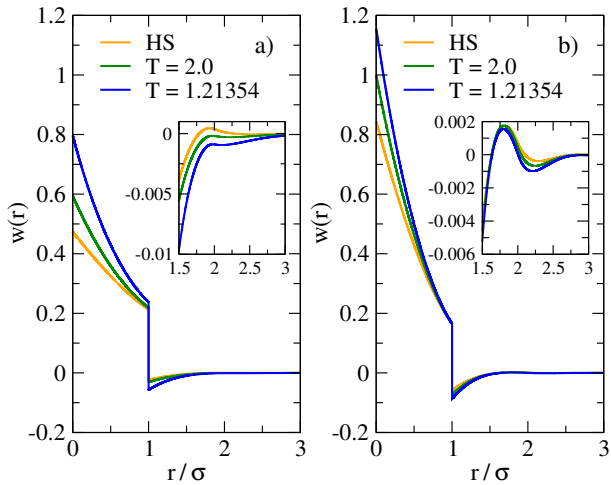

Figure 2.1: Real space weight function at two values of bulk density (panel a): $\rho_b\sigma^3 = 0.3154$; panel b): $\rho_b\sigma^3 = 0.6$) for three values of the temperature. One state shown here ($\rho_b\sigma^3 = 0.3154$, $T = 1.21354$) is very close to the critical point (the correlation length predicted by HRT is about $1.3 \times 10^3\,\sigma$).

a HCY homogeneous fluid, the value of the chemical potential is related to the density by:

$$\mu(\rho) = \frac{1}{\beta}\log\rho + \psi_{\mathrm{R}}^{\mathrm{ex}}(\rho) + \rho\left.\frac{\mathrm{d}\psi_{\mathrm{R}}^{\mathrm{ex}}}{\mathrm{d}\rho}\right|_{\rho} - 4\pi\frac{\zeta+1}{\zeta^2}\rho. \tag{2.54}$$

This expression follows from the bulk limit of Eq. (2.22), with $\phi(\boldsymbol{r}) = 0$, when the excess free energy in the homogeneous limit is given by Eq. (2.50).

Solvent-mediated force

A central quantity for the present investigation is the force acting on two planar hard walls immersed in a HCY fluid. In this geometry, symmetry requires that all the local properties may depend on the single coordinate z, orthogonal to the two plates of surface Σ, placed at $z = 0$ and $z = L$ respectively. Remarkably, if the wall separation L is greater than σ, the force per unit surface f_Σ acting on the plates, sometimes called *solvation force*, can be expressed as a pressure difference (see Appendix 2.8 for an introduction to solvation force and Ref. [103]):

$$f_\Sigma(L;T,\mu) = -\left.\frac{\partial}{\partial L}\left(\frac{\Omega^{(L)}[\rho(z)]}{\Sigma}\right)\right|_{T,\mu} - p(T,\mu), \tag{2.55}$$

where $\Omega^{(L)}[\rho(z)]/\Sigma$ is the grand canonical potential per unit surface of the fluid confined in the region $[0, L]$, determined by the minimisation of the

approximated grand canonical functional at fixed (μ, T) and $p(\mu, T)$ is the bulk pressure of the fluid at the same values of temperature T and chemical potential $\mu = \mu(\rho_b, T)$.
On the other hand, when $L < \sigma$ there are no particles between the walls and the attractive force per unit surface acting on the walls arises uniquely from the presence of the fluid in the regions $z < 0$ and $z > L$: The first term in Eq. (2.55) vanishes and the force is given by

$$f_\Sigma(L; T, \mu) = -p(T, \mu). \tag{2.56}$$

The solvation force f_Σ defined above is a difference of pressures and goes to zero in the limit $L \to \infty$. By means of standard functional identities it is possible to express, without any further approximation, the derivative of the grand potential per unit surface in terms of the contact density (the proof is given in Appendix 2.8)

$$\rho_w^{(L)} \equiv \lim_{\delta \to 0^+} \rho\big(L - \sigma/2 - \delta\big) = \lim_{\delta \to 0^+} \rho\big(\sigma/2 + \delta\big) \tag{2.57}$$

and the solvation force can be finally written as [66]

$$f_\Sigma(L; T, \mu) = k_\mathrm{B} T \, \rho_w^{(L)} - p(T, \mu). \tag{2.58}$$

Furthermore, the chosen WDA exactly satisfies the contact value theorem [227] (the proof and an introduction to the contact theorem can be found in Appendix 2.7)

$$\beta p(T, \mu) = \lim_{L \to \infty} \rho_w^{(L)}, \tag{2.59}$$

leading to the more suggestive identity

$$\beta f \Sigma(L; T, \mu) = \rho_w^{(L)} - \rho_w^{(\infty)}, \tag{2.60}$$

where $\rho_w^{(\infty)}$ is the contact density in the limit of a single wall.

Some (technical) details about the minimisation

The above results show that, in order to obtain the force acting on the walls, we just need to perform the (numerical) minimisation of the functional in the region $[0, L]$, and then to extract the contact density from the equilibrium density profile. The minimisation has been be carried out by a simple iterative *Picard* method, taking advantage of the exact relation obeyed by the equilibrium density profile (see Eq. (2.26))

$$\rho(z) = \mathrm{e}^{-\beta[u(z) - \mu]}, \tag{2.61}$$

where the potential of mean force $u(z)$ is defined as

$$u(z) = \left. \frac{\delta \mathcal{F}_\mathrm{R}^\mathrm{ex}[n]}{\delta n(\boldsymbol{r})} \right|_{\rho(z)} + \int \mathrm{d}\boldsymbol{r}' \rho(z') v_\mathrm{Y}(|\boldsymbol{r} - \boldsymbol{r}'|).$$

Starting from a guess for the density profile, it is possible to evaluate $u(z)$ and then to obtain, by means Eq. (2.61), a new density profile. This density profile gives a new value for the potential of mean force and the iteration can be continued as far as convergence is reached. At moderate densities it is necessary to weight the solution $\rho_i(z)$ at step i with the solution $\rho_{i-1}(z)$ at step $i-1$, because, during the iterative procedure, the peaks in the oscillating density may exceed the physical limit given by the random close packing volume fraction:

$$\rho_i(z) = \alpha\rho_{i-1}(z) + (1-\alpha)\tilde{\rho}(z),$$

where $\tilde{\rho}(z)$ is the density profile evaluated from Eq. (2.61) with $\rho(z) = \rho_{i-1}(z)$ and α is a number between 0 and 1. The particular value of α is chosen in order to obtain the fastest convergence.

The minimisation of the grand canonical functional turns out to be demanding due to the evaluation of the functional derivatives and of the weighted densities for each step of the iteration and for all the points of the mesh. However, the symmetries of the system considerably speed-up the whole minimisation. It can be shown that the 3d-convolution of any function of the single variable z (e.g. $\rho(z)$) with the weight function (see e.g. Eq. (2.39)) can expressed as a 1d-convolution of the same quantity with the cosine Fourier transform of the weight function itself. As regards the density profile, we proceed as follows:

$$\begin{aligned}\bar{n}(z) &= \int_0^h \mathrm{d}z'\, n(z') \int \mathrm{d}\boldsymbol{r}_\perp w\big(|\boldsymbol{r}-\boldsymbol{r}'|;\rho\big) \\ &= 2\pi \int_0^h \mathrm{d}z'\, n(z') \int_{|z-z'|}^\infty \mathrm{d}u\, u\, w(u;\rho). \end{aligned} \tag{2.62}$$

If we express the weight function $w(u;\rho)$, which is directly provided by the analytical solution of Eq. (2.52), in terms of its Fourier transform $w(q;\rho)$ as

$$w(u;\rho) = \frac{2}{(2\pi)^2} \int_0^\infty \mathrm{d}q\, q\, \frac{\sin(uq)}{u}\, w(q;\rho),$$

we obtain from Eq. (2.62)

$$\bar{n}(z) = \int_0^h \mathrm{d}z'\, n(z')\, \mathcal{W}\big(|z-z'|;\rho\big). \tag{2.63}$$

The function $\mathcal{W}(z,\rho)$ is the cosine Fourier transform of the weight function at density ρ:

$$\mathcal{W}(z;\rho) = \frac{1}{2\pi} \int_{-\infty}^\infty \mathrm{d}q\, \cos(qz)\, w(q;\rho),$$

which can be easily evaluated numerically by means of standard routines [178]. Similar arguments lead to the expression of the functional derivative of the

reference excess free energy:

$$\left.\frac{\delta \mathcal{F}_{\mathrm{R}}^{\mathrm{ex}}[n]}{\delta n(\boldsymbol{r})}\right|_{n(z)} = \psi_{\mathrm{R}}^{\mathrm{ex}}\big(\bar{n}(z)\big) + \int_0^h \mathrm{d}z'\, n(z')\, \left.\frac{\partial \psi_{\mathrm{R}}}{\partial \rho}\right|_{\bar{n}(z')} \mathcal{W}\big(|z-z'|;\rho\big). \quad (2.64)$$

We performed minimisations of the functional for values of the temperature T above the critical point ($T > T_c \sim 1.21353$) and bulk reduced densities $\rho_b\sigma^3$ up to 0.85. The free energy and the correlation function of the homogeneous fluid obtained with HRT are given on a mesh of 10300 points for reduced densities between 0 and 1.05. A spatial step-size $\Delta z = 1.5 \times 10^{-2}\sigma$ has been generally used in the numerical minimisation, while for bulk densities $\rho_b\sigma^3 > 0.7$ and close to the critical point Δz has been reduced up to two orders of magnitude. Typically, up to few thousand Picard iterations were necessary to achieve a precision of one part in 10^7 for the density profile and one part in 10^{11} in the grand potential.

Minimisations near the critical point

The solvent-mediated interaction between the walls is characterised by a diverging range if the fluid is set in critical conditions. More precisely, the range of the interaction becomes comparable with the correlation length, which diverges as a power law at the critical point. Therefore, in order to study the onset of the universal properties of the interaction, we need to evaluate the force between the walls at distances at least comparable with the correlation length. The minimisation of the gran potential functional becomes computationally very demanding when the dimension of the system increases. In fact, the number of operations needed to evaluate the weighted densities (2.63) and the derivative of the excess free energy (2.64) does not scale linearly with the dimension of the system. At a first sight, we are lead to believe that the number of operations for each convolution scales as N^2, where N is the number of points of the spatial mesh which discretise the distance between the walls. Actually, the computational complexity of this operation scales as $N \log N$: We will show below that it is possible to exploit the properties of Toeplitz circulant matrices and of the discrete Fourier transform algorithm in order to reduce the complexity of the problem.

The bottleneck in the numerical minimisation of the grand potential functional are integrals of the form

$$g(z) = \int_0^h \mathrm{d}z'\, w(z-z')\, f(z')$$

which, after the discretization of the variables z and z', can be written as

$$g_i = \sum_{j=0}^{h} w_{i-j}\, f_j, \quad (2.65)$$

where i and j are integers in $[0, h]$.
It is useful to interpret the sum in Eq. (2.65) as the product between the (square) matrix W, defined as

$$W = \begin{bmatrix} w_0 & w_{-1} & w_{-2} & \dots & \dots & w_{-h} \\ w_1 & w_0 & w_{-1} & \ddots & & \vdots \\ w_2 & w_1 & \ddots & \ddots & \ddots & \vdots \\ \vdots & \ddots & \ddots & \ddots & w_{-1} & w_{-2} \\ \vdots & & \ddots & w_1 & w_0 & w_{-1} \\ w_h & \dots & \dots & w_2 & w_1 & w_0 \end{bmatrix},$$

and the vector $\boldsymbol{f} = (f_0, \dots, f_h)$. The elements of the matrix are such that

$$W_{i,j} = W_{i+1,j+1} = w_{i-j},$$

and a matrix $W_{i,j}$ with this property is referred to as a *Toeplitz matrix*.
Now, let us define the $(2h+2)$-by-$(2h+2)$ Toeplitz matrix $X_{ij} = x_{i-j}$:

$$X = X_{i-j} = \begin{bmatrix} w_0 & w_{-1} & \dots & w_{-h} & 0 & w_h & w_{h-1} & \dots & w_1 \\ w_1 & w_0 & \ddots & \ddots & w_{-h} & 0 & \ddots & \ddots & \vdots \\ \vdots & \ddots & w_0 & \ddots & \ddots & \ddots & 0 & \ddots & \vdots \\ \vdots & \ddots & \ddots & w_0 & \ddots & \ddots & \ddots & 0 & w_h \\ w_h & \ddots & \ddots & \ddots & w_0 & w_{-1} & \ddots & \ddots & 0 \\ 0 & \ddots & \ddots & \ddots & w_1 & w_0 & \ddots & \ddots & \vdots \\ w_{-h} & 0 & \ddots & \ddots & \ddots & \ddots & w_0 & \ddots & \vdots \\ \vdots & \ddots & 0 & \ddots & \ddots & \ddots & \ddots & w_0 & w_{-1} \\ w_0 & w_{-1} & \ddots & 0 & w_h & \dots & \dots & w_1 & w_0 \end{bmatrix}.$$

This matrix has the additional property

$$x_k = x_{k+2h+2} \tag{2.66}$$

and is referred to as a *circulant matrix*.

The convolution in (2.65) can be written in terms of the circulant matrix X as

$$G_\alpha = \sum_{\beta=0}^{2h+1} X_{\alpha\beta} F_\beta, \tag{2.67}$$

where $\boldsymbol{F}$ is a vector with $2h+2$ elements defined as $\boldsymbol{F} = (f_0, f_1, \dots, f_h, 0, \dots, 0)$. The first $h+1$ components of $\boldsymbol{G}$ correspond to the vector $\boldsymbol{g}$, namely the result

of the convolution. Now we will show that the properties of the matrix X allow to evaluate all the $2h+2$ components of $\boldsymbol{G}$ (and then the $h+1$ of $\boldsymbol{g}$) performing only three discrete Fourier transforms of dimension $2h+2$. From a computational point of view, the complexity of standard Fast Fourier Transform (FFT) algorithms [178] scales, as first recognised by Gauss, as $N \log N$ and the resulting computational complexity of the whole minimisation will be $N \log N$. Eq. (2.67) can be written as

$$G_\alpha = \frac{1}{2h+2} \sum_{l=0}^{2h+1} \tilde{F}_l \sum_{\beta=0}^{2h+1} X_{\alpha-\beta}\, \mathrm{e}^{-2\pi \mathrm{i} \beta l/(2h+2)}, \tag{2.68}$$

where F_β has been expressed by means of its inverse discrete Fourier transform

$$F_\beta = \frac{1}{2h+2} \sum_{n=0}^{2h+1} \tilde{F}_l\, \mathrm{e}^{-2\pi \mathrm{i} \beta l/(2h+2)}. \tag{2.69}$$

The next step is to introduce the transformation $\beta = \alpha - m$ and to separate contributions with positive and negative m:

$$\begin{aligned} G_\alpha &= \frac{1}{2h+2} \sum_{l=0}^{2h+1} \tilde{F}_l \left[\sum_{m=0}^{2h+1-\alpha} X_{-m}\, \mathrm{e}^{-2\pi \mathrm{i}\, l \frac{\alpha+m}{2h+2}} + \sum_{m=0}^{\alpha} X_m\, \mathrm{e}^{-2\pi \mathrm{i}\, l \frac{\alpha-m}{2h+2}} \right] \\ &= \frac{1}{2h+2} \sum_{l=0}^{2h+1} \tilde{F}_l \left[\sum_{m=0}^{2h+1-\alpha} X_{2h+2-m}\, \mathrm{e}^{-2\pi \mathrm{i}\, l \frac{\alpha+m}{2h+2}} + \sum_{m=0}^{\alpha} X_m\, \mathrm{e}^{-2\pi \mathrm{i}\, l \frac{\alpha-m}{2h+2}} \right], \end{aligned}$$

where the second line follows from (2.66). Introducing the transformation $n = 2h+2-m$ in the first summation on r.h.s. we get

$$G_\alpha = \frac{1}{2h+2} \sum_{l=0}^{2h+1} \tilde{F}_l \left[\sum_{n=\alpha+1}^{2h+1} X_n\, \mathrm{e}^{-2\pi l \mathrm{i} \frac{\alpha-n}{2h+2}} + \sum_{m=0}^{\alpha} X_m\, \mathrm{e}^{-2\pi l \mathrm{i} \frac{\alpha-m}{2h+2}} \right],$$

where we made use of the properties of complex exponentials. The final result reads

$$G_\alpha = \frac{1}{2h+2} \sum_{l=0}^{2h+1} \tilde{F}_l \tilde{X}_l\, \mathrm{e}^{-2\pi \mathrm{i} \alpha l/(2h+2)}, \tag{2.70}$$

where $\tilde{F}$ and $\tilde{X}$ are the discrete Fourier transforms of the vectors $\boldsymbol{F}$ and $\boldsymbol{X} = (x_0, x_1, \ldots, x_{2h+1})$[31] respectively, according to the definition (2.69). Equation (2.70) shows that $\boldsymbol{G}$ can be evaluated through the Fourier transform of the vector $\left(\tilde{F}_0 \tilde{X}_0, \ldots, \tilde{F}_{2h+1} \tilde{X}_{2h+1}\right)$.

[31] The elements x_i belong to the circular matrix defined above.

Here we remark that Eq. (2.70) holds exactly and the errors due to the process of zero padding in principle can not arise. This circumstance is relevant because at large distances the forces between the walls are expected to be very small and high accuracy is needed.
The minimisations in the critical region were performed using this method and we obtained the density profiles up to a wall-to-wall distance of about 800σ.

Validation of the method

The minimisation of the previously defined grand canonical functional allows to evaluate the equilibrium properties of the confined fluid. Within this approach, the relevant quantities can be found at every temperature and bulk density of interest, also in the vicinity and below the critical point of the HCY fluid. Most of the calculations refer to a Yukawa fluid with range $\zeta\sigma = 1.8$, where several simulation results are available.

In the high temperature limit[32] our model reduces to a hard sphere fluid, whose properties have been extensively investigated by numerical simulations. As shown by Fig. 2.2, the density profile obtained within our density functional (blue line) is symmetrical with respect to the mid point between the walls. Slight deviations from the old MC data of Ref. [208] can be observed, in particular near the middle point between the walls, probably due to the lack of statistics in the simulation. The density is zero at distances $0 < z/\sigma < 0.5$ and $h/\sigma - 0.5 < z/\sigma < h/\sigma$, due to the infinite repulsion between the wall and the fluid particles.

Figure 2.3 shows the density profiles $\rho(z)$ of a hard sphere fluid near a hard wall at three different values of ρ_b. The agreement of the WDA prediction with the Monte Carlo (MC) data of Ref. [92] is very good up to reduced densities of the order of 0.6, while at higher values the phase of oscillations in the density profile are correctly captured, although a slight underestimation of the peak value is observed. The comparison of our density profiles with those predicted by the "White Bear" version of the FMT [194] shows, as expected, that Rosenfeld's theory gives more accurate estimates of the oscillation peaks, particularly at high density.
When the temperature is decreased, the contribution of the Yukawa tail to the density profile becomes relevant. We compared the density profile obtained within our DFT approximation with the MC simulation data for $\zeta\sigma = 1.8$ at temperature $T = 2$ and for $\zeta\sigma = 3$ at $T = 1.004$. Figure 2.4 shows that the WDA estimate is remarkably accurate at reduced densities 0.4 and 0.5; small deviations from the MC simulation data appear at reduced density 0.7. We note that at $\rho_b\sigma^3 = 0.7$ the contact reduced density is overestimated of about 0.2 with respect to simulation data, even if the contact theorem is verified

[32] All the comparisons with the data of simulations of hard sphere systems are obtained with a reduced temperature equal to 3000.

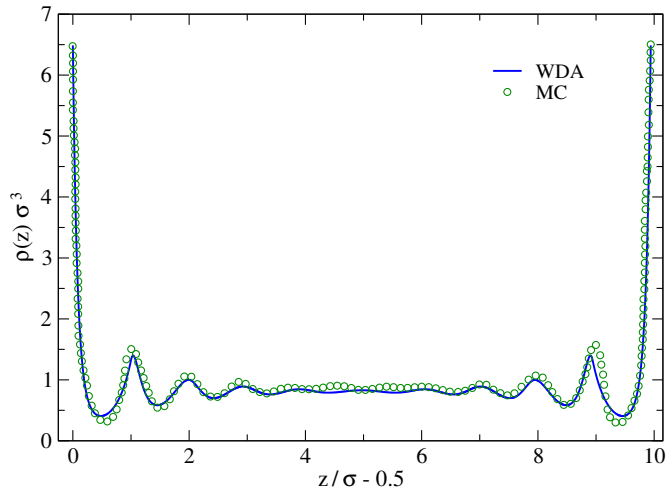

Figure 2.2: Density profile $\rho(z)$ for a hard sphere fluid between two hard walls at distance $h = 10.94\sigma$. The bulk reduced density is $\rho_b\,\sigma^3 = 0.81$. The line correspond to the WDA prediction. Points represent MC data from Ref. [208].

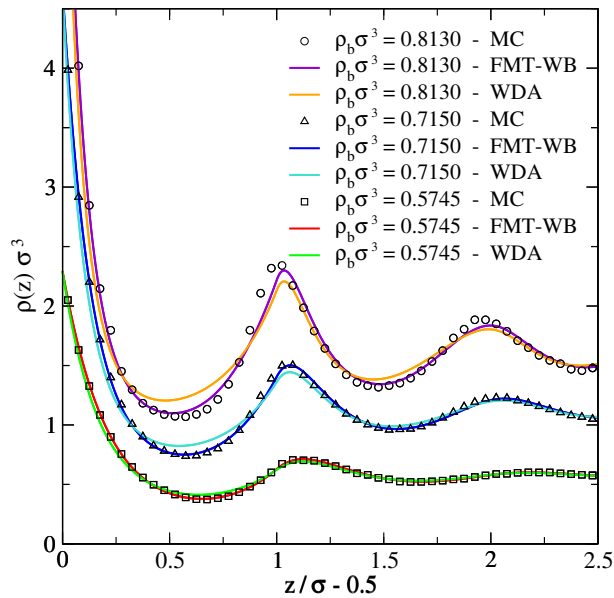

Figure 2.3: Density profiles $\rho(z)$ for a hard sphere fluid between two hard walls (distance $L = 16\,\sigma$) at different values of the bulk reduced density $\rho_b\sigma^3$. MC simulation data (symbols) are taken from Ref. [92]. The FMT data have been obtained through an in-house minimisation of Rosenfeld's functional (White Bear version [194]). To enhance visual clarity the density profiles at $\rho_b\sigma^3 = 0.715$ and $\rho_b\sigma^3 = 0.813$ are shifted upward by 0.4 and 0.8 respectively.

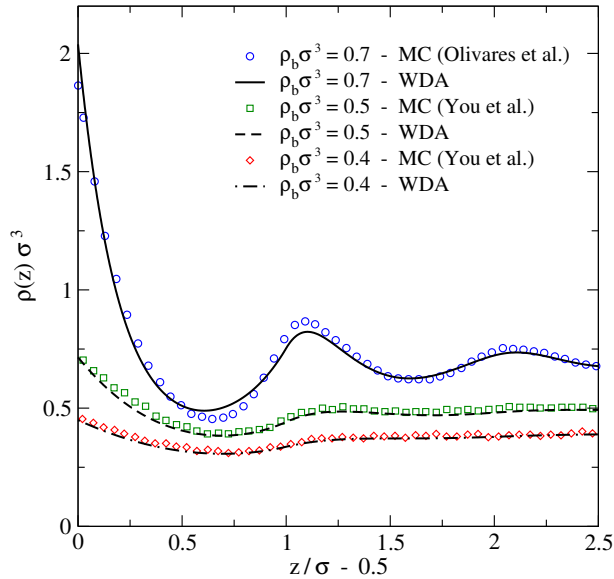

Figure 2.4: Density profile $\rho(z)$ of a Yukawa hard sphere fluid ($\zeta\sigma = 1.8$) at reduced temperature $T = 2$ confined between two hard walls at different values of bulk reduced density $\rho_b\sigma^3$. Lines represent the predictions of the present WDA. Points are MC data from Ref. [165] (reduced density 0.7) and Ref. [251] (reduced density 0.4 and 0.5). The distance between the walls is $10\,\sigma$.

with a relative error of the order of 10^{-5}. This disagreement in the contact value is due to different estimates of the grand canonical potential per unit volume of the homogeneous fluid and it is compatible with the the spread in the values of the bulk pressure obtained within different simulation techniques [84]. In panel a) of Fig. 2.5 we compare our results for the density profile of the HCY fluid characterised by $\zeta\sigma = 3$ with the recent MC simulations from Ref. [114]. This figure shows that at relatively low densities the agreement between our approximation and MC results is remarkable also for attractive potentials of shorter range. In particular we predict accurately the kink in the density profile at $\rho_b\sigma^3 = 0.191$, which is only qualitatively reproduced within mean-field approximation [114].

The minimisation of the grand canonical functional provides both the value of the contact density $\rho_w^{(L)}$ and of the grand canonical potential. It is therefore possible to obtain the depletion force either by calculating the derivative w.r.t. L of the grand potential, as in Eq. (2.55), or by making use of Eq. (2.58). The consistency between the two estimates is a good check for the accuracy of the numerical procedure. To give an example, for a hard sphere fluid, the relative difference between the two results is less than 0.01% if the absolute value of the force per unit surface and $k_B T$ is larger than 10^{-6}. Nonetheless at smaller values of the force the result obtained by differentiation of the grand potential

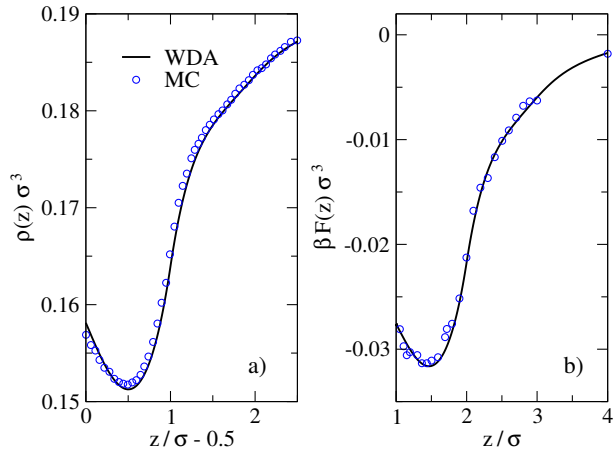

Figure 2.5: Panel a): Density profile $\rho(z)$ of a HCY fluid at a single hard wall ($\zeta\sigma = 3$) for bulk reduced density $\rho_b\sigma^3 = 0.191$ and temperature $T = 1.004$. Lines represent the predictions of the present WDA. Points are MC data from Ref. [114]. Panel b): Force per unit surface acting between two infinite parallel hard walls immersed in a HCY fluid ($\zeta\sigma = 3$) in the same thermodynamic state of panel a). Lines are the predictions of the WDA from Eq. (2.58), whereas points represent the MD simulation of Ref. [114].

is less stable, due to errors introduced by the discretization.
The solvent-mediated force acting on two parallel hard walls immersed in a hard sphere fluid, is compared with the Monte Carlo data of Wertheim et al. [240], as well as the predictions based on FMT, in Fig. 2.6, showing a nice agreement also at relatively high densities. At reduced density 0.2873 the force maximum per unit surface is of the order of $k_B T/\sigma^3$, and the oscillations due to the packing of the hard spheres are damped within two or three diameters. Furthermore, at this value of the reduced density, a small deviation between WDA and FMT is present only at the first minimum. At reduced density 0.6 the force at distances of the order of the hard sphere diameter σ is hundred times larger than at $\rho_b\sigma^3 = 0.2873$. Even this feature is well reproduced by both WDA and FMT, as can be seen in the inset. In order to observe such high values of the force the minimisation of the functional was performed at distances belonging to an equally spaced mesh of step-size 0.00015 and the integrals in the minimisation were estimated on a grid with the same step-size. This panel shows that the strong oscillating behaviour of the MC data is captured by WDA with a correct phase, even if the peak values are a little underestimated, whereas FMT behaves considerably better.
The solvent-mediated force per unit area between two walls in a HCY fluid has not been extensively investigated by numerical simulations. In panel b) of Fig. 2.5 we show a comparison between our results and the Monte Carlo data of Ref. [114] for a HCY fluid of inverse range $\zeta\sigma = 3$ at $T = 1.004$

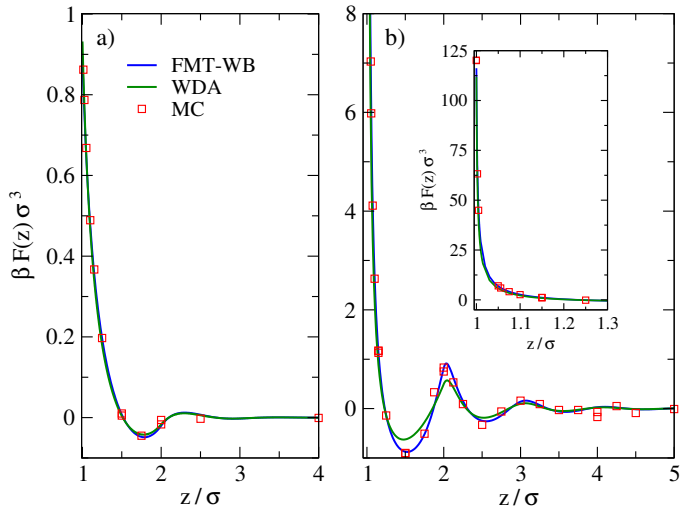

Figure 2.6: Force per unit surface and $k_{\mathrm{B}}T$ between two infinite planar hard walls immersed in a fluid of hard spheres of diameter σ for two values of the bulk reduced density (panel a): $\rho_b\sigma^3 = 0.2873$; panel b): $\rho_b\sigma^3 = 0.6$). The force within the WDA approximation has been obtained via Eq. (2.58). The FMT-WB result comes from the in house implementation of the "White Bear" version of the FMT functional [194] via Eq. (2.58). The MC data is taken from Ref. [240]. The inset highlights the behaviour of the force at $\rho_b\sigma^3 = 0.6$ at small distances.

and $\rho_b\sigma^3 = 0.191$. Even if the net force is quite small, our prediction agrees very well with the numerical simulations at all values of the wall separation. We stress that, particularly at small distances, the WDA force is much more accurate than any mean-field perturbation method (see Ref. [114]).

The detailed comparisons of our novel DFT with both numerical simulations and state-of-the-art theories allow to conclude that in the high temperature limit the present WDA is able to correctly reproduce the density profile and the effective interactions between the hard walls also at high densities, with a very satisfactory accuracy up to reduced densities of about 0.5. It could be possible to further increase the quality of the predictions if the hard sphere contribution in the reference excess free energy functional is described by means of the FMT.
Moreover, this formulation of WDA appears to be the best available DFT for a HCY fluid at finite temperature. In particular this formalism can be adapted in order to treat other systems, provided an accurate underlying bulk liquid state theory is identified instead of the HRT.

2.4 MINIMISATION OF THE FUNCTIONAL THROUGHOUT THE PHASE DIAGRAM

In the last Section we tested our weighted density approximation against a large portion of the available data from numerical simulation. However this comparison is, of necessity, limited: On one side we are obliged to select the works dealing with hard core Yukawa interparticle potentials, on the other side the literature covers limited regions of the bulk phase diagram and seems to be not to much interested into critical behaviour. It follows that a wide portion of the phase diagram remains unexplored and maybe some interesting and unexpected phenomena generated by the presence of an interface can be uncovered. In the following we will show predictions for different densities and for temperatures *above* the critical temperature.
The restriction on the temperature domain deserves some additional considerations. As a result of the action of the external potential (e.g. a hard wall), the density profile oscillates about the bulk density. Even if the thermodynamic state of the bulk fluid lies outside the two phase region, the local peaks of the density profile can reach density values belonging to the coexisting phase, and similar considerations should apply also for the weighted density. Therefore it could be meaningless to evaluate expressions as Eq. (2.64), because the thermodynamic potentials (ψ in our case) are not well defined functions inside the two phase region. Some recent works (see e.g. [68, 250]) address the problem of wetting by means of DFT, also below the critical point. In both contributions the approximated functional is of the form (2.36) whereas the reference term is approximated using FMT in Ref. [68] and LDA in Ref. (2.27) in [250]. They claim that their methods are consistent with simulations, but no mention about the difficulties which can be generated by the coexistence region is found.

Slab geometry

We performed the minimisation of the WDA density functional at several values of temperatures and reduced bulk densities for a HCY fluid of inverse range $\zeta\sigma = 1.8$ confined between two hard walls. At high temperatures the system behaves like a hard sphere fluid, whereas when the temperature is decreased the contribution of the Yukawa tail becomes more and more relevant, and the strongly oscillating character of both the density profiles and the solvent-mediated force is lost.
Figure 2.7 shows the dependence of the density profile on temperature at fixed bulk reduced density $\rho_b\sigma^3 = 0.5$. At reduced temperature $T = 8$ the system behaves like a hard sphere fluid. As the temperature is lowered towards its critical value, the density profile gradually becomes monotonic losing the oscillating features typical of hard spheres and the density at contact assumes values four times lower than the bulk density. The range of the perturbation

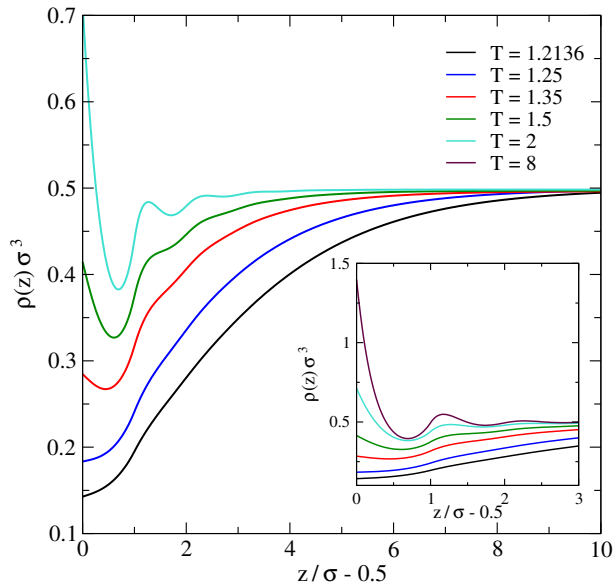

Figure 2.7: Density profile of a HCY fluid ($\zeta\sigma = 1.8$) at a single hard wall at bulk reduced density $\rho_b\sigma^3 = 0.5$ and different values of the temperature. The inset shows the same data, also including the density profile at temperature $T = 8$, using a different scale.

produced by the wall extends at larger and larger distances as the temperature approaches T_c, giving rise to a region where a kind of drying of the wall can be observed.

The attractive tail in the pair interaction of the HCY fluid smoothens the density profile reducing the layering of particles. As a consequence, the effective force between the two walls loses the strongly repulsive peak present at $z \sim \sigma$ when the interaction between the fluid particles is purely hard sphere (see Fig. 2.6). Fig. 2.8 shows the force per unit surface between the walls for different values of the temperature at the critical bulk reduced density $\rho_c\,\sigma^3 = 0.3152$. The repulsive contribution to the interaction force, present at $T = 8$ gradually disappears at lower temperatures and the force becomes purely attractive and monotonic, confirming the findings of the numerical simulations in a different model [86]. By approaching the critical temperature ($T_c \sim 1.21353$) the effective force becomes weaker and weaker at short distance, as can be seen in the right panel of Fig. 2.8: Its amplitude reduces almost by a factor two due to a 10% change in temperature. However, a closer look to the long-distance tail of the solvent-mediated force shows that its range indeed increases close to the critical temperatures, as expected on the basis of scaling arguments. However this occurs at very large separations ($L > 26\sigma$ for the data shown in the figure).

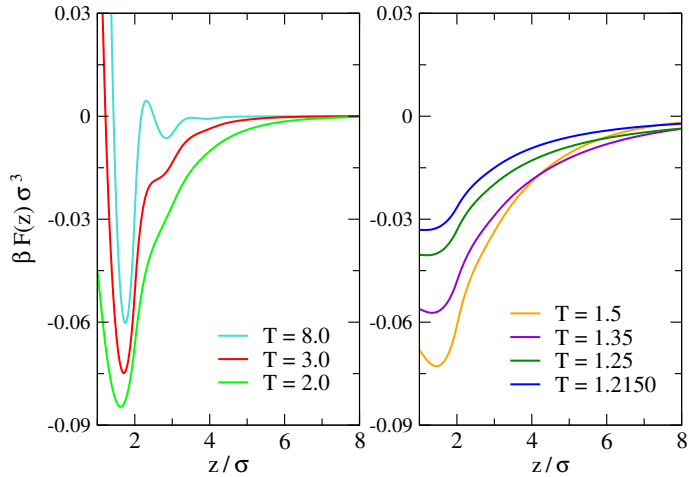

Figure 2.8: Force per unit surface acting between two hard walls immersed in a HCY fluid ($\zeta\sigma = 1.8$) obtained from the minimisation of the WDA functional using Eq. (2.58) at $\rho_b\sigma^3 = 0.3152$ and different values of the temperature.

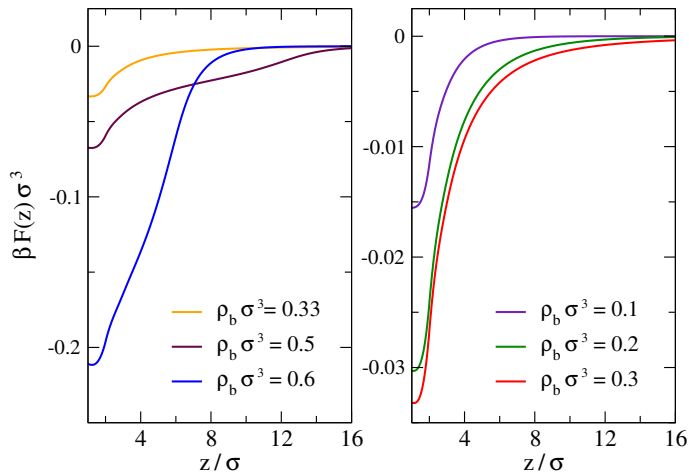

Figure 2.9: Force per unit surface acting between two hard walls immersed in a HCY fluid ($\zeta\sigma = 1.8$) obtained from the minimisation of the WDA functional using Eq. (2.58) at $T = 1.2155$ and different values of the reduced density.

Fig. 2.9 shows the force per unit surface between the walls in different density regimes when the value of the temperature is close to T_c. We note that when the bulk density is higher than ρ_c the force is an order of magnitude larger than for $\rho_b < \rho_c$. The force is monotonic and purely attractive for all values of the reduced density and its range grows near ρ_c, as expected.

In lattice fluid models the coexistence curve is symmetric about the critical

temperature and the critical isochore coincides with the locus $\rho(T)$ of the maxima of the isothermal susceptibility. For such systems, according to the Renormalization Group terminology, the path to the critical point orthogonal to the relevant odd operator coincides with the critical isochore. In a real fluid the coexistence curve is asymmetric about the critical isochore. In this case a good approximation for the same path is given by the line $\tilde{\rho}(T)$ in the phase diagram defined as the locus of the points (ρ, T) such as

$$\tilde{\rho}(T) = \max_{\rho} \{ \rho \, \chi_T \}, \tag{2.71}$$

where χ_T is the isothermal compressibility.
Fig. 2.10 shows the density profile of the HCY fluid at a hard wall along the line $\tilde{\rho}(T)$. Its behaviour at distances larger than the bulk correlation length is well fitted by an exponential of the form

$$\rho(z) = \rho_b + A \, \mathrm{e}^{-z/\xi}, \tag{2.72}$$

where ρ_b is the bulk density of the fluid, A is a negative amplitude factor and ξ is the bulk correlation length. In Appendix 2.9 we prove analytically that any WDA fulfilling (2.43) indeed predicts this exponential decay.
However, the exponential decay of the density profile is observed also if the system is far from the critical region and is probably related to the location in the bulk phase diagram of the point we investigated with respect to the Fisher-Widom line [65, 25].
Following the argument of Ref. [65], we expect that the exponential long-range behaviour of the density profile reflects in an analogous exponential decay of the force between the two walls. Provided we do not cross the Fisher-Widom line, this decay should be present both far from the critical point and in the critical region, where it agrees with the predictions of the theory of the critical Casimir effect [80]:

$$\beta F(z) = f_0 \, \mathrm{e}^{-z/\xi}. \tag{2.73}$$

The exponential decay of the solvation force is indeed confirmed by the exact solution of a two-dimensional [67] Ising slab under symmetry breaking boundary conditions and was observed in Monte Carlo simulations of three dimensional simple fluids [86, 85]. Fig. 2.11 shows the long distance exponential decay of the force per unit surface and $\mathrm{k_B}T$ between two planar hard walls mediated by a HCY fluid along the critical line $\tilde{\rho}(T)$. The force obtained with our approach is very well fitted by Eq. (2.73) at large distances ($z \gg \xi(\rho_b T)$), whereas at short distances, where depletion effects become relevant, the solvent-mediated force, always attractive, displays a plateau (see inset).

Effective interaction between spherical particles

The same WDA formalism previously introduced may be generalised to other interesting geometries, in addition to the planar one. Most importantly,

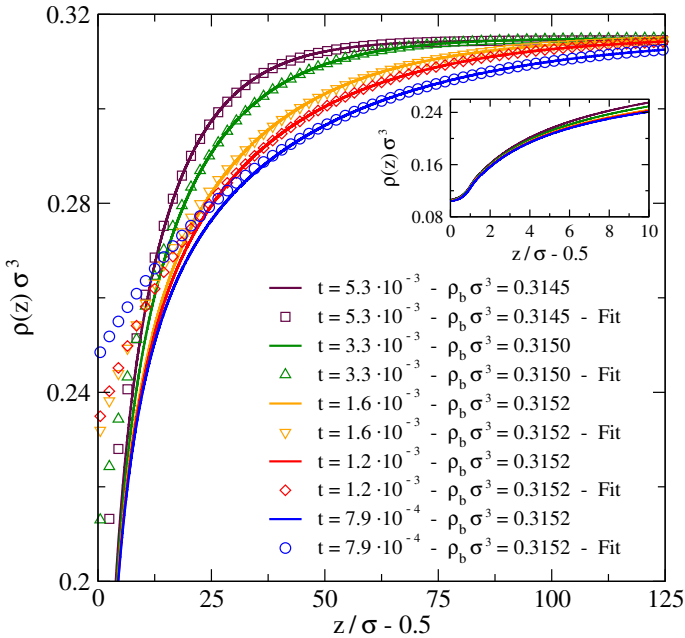

Figure 2.10: Lines: Density profile of a HCY fluid ($\zeta\sigma = 1.8$) at a single hard wall in the critical region. Here $t = (T - T_c)/T_c$. Points: Fits of the density profiles according to Eq. (2.72) performed at distances larger than three times the correlation length of the homogeneous HCY fluid at the same temperature and bulk density. ρ_b, A and ξ are free fitting parameters and the results obtained for ρ_b and ξ agree well with the bulk values of density and correlation length respectively (the accuracy is better than 1% for the bulk density and 5% for the correlation length). The bulk correlation lengths obtained from the fitting procedure are $\xi = 41.1\sigma, 31.8\sigma, 26.5\sigma, 17.3\sigma, 12.9\sigma$, from the lowest to the highest reduced temperature. The inset shows a magnification of the same density profiles at short distances.

it can be used to evaluate the effective interaction between two spherical particles in a solvent, with obvious applications to the study of aggregation in colloidal suspensions.

The force between two spheres of radius R immersed in a solvent is given by the sum of the normal forces over the area of one exclusion sphere as

$$\boldsymbol{F}(L) = \int \mathrm{d}\boldsymbol{r}\, p_{\mathrm{N}}(\boldsymbol{r})\, \delta\left(R + \frac{\sigma}{2} - |\boldsymbol{r}|\right) \frac{\boldsymbol{r}}{|\boldsymbol{r}|}, \tag{2.74}$$

where $L = h - 2R$ with h the center to center distance, $\sigma/2$ is the hard core diameter of the particles belonging to the solvent, $p_{\mathrm{N}}(\boldsymbol{r})$ is the normal pressure on the exclusion sphere (with radius $R+\sigma/2$) and the origin of the coordinates coincides with the center of the sphere. Note that $p_{\mathrm{N}}(\boldsymbol{r})$ implicitly depends on the position of the second sphere. The symmetry of the problem guarantees

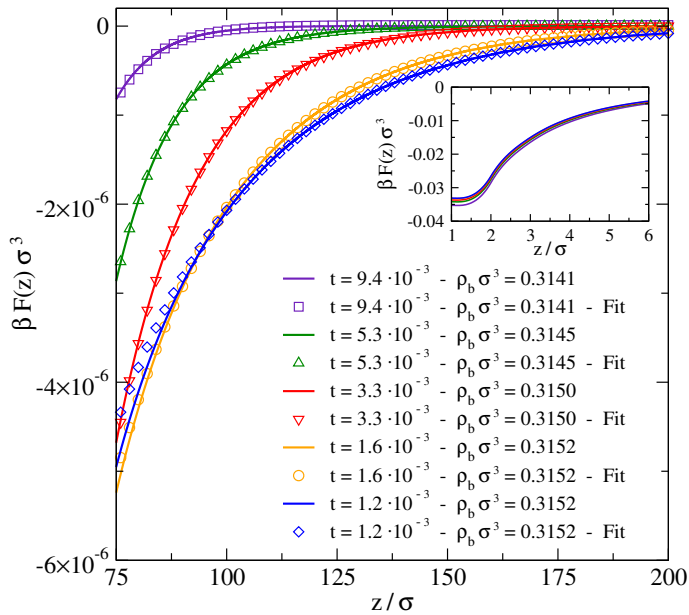

Figure 2.11: Lines: Force per unit surface of a HCY fluid ($\zeta\sigma = 1.8$) at a single hard wall along the line $\tilde{\rho}(T)$. Here $t = (T - T_c)/T_c$. Points: Fits of the force according to Eq. (2.73) performed at distances larger than four times the bulk correlation length of the homogeneous HCY fluid at the same temperature and bulk reduced density. f_0, and ξ are free parameters in the fitting procedure. The result obtained for ξ agrees well with the bulk value of the correlation length (the accuracy of the fit is better than 3%). The bulk correlation lengths obtained from the fitting procedure are $\xi = 31.8\sigma, 26.5\sigma, 17.3\sigma, 12.9\sigma, 9.2\sigma$, from the lowest to the highest reduced temperature. The inset shows the force profile at short distance.

that the resulting force is directed along the line connecting the centres of the spheres. This result can be expressed in a more elegant way exploiting the contact theorem (see Section 2.7) as

$$\beta \boldsymbol{F}(L) = \int \mathrm{d}\boldsymbol{r}\, \rho(\boldsymbol{r})\, \delta\left(R + \frac{\sigma}{2} - |\boldsymbol{r}|\right) \hat{\boldsymbol{n}}.$$

Therefore, once the density profile of the solvent is known, the evaluation of the force is reduced to the computation of a bi-dimensional integral.
Unfortunately, the direct minimisation of the WDA for such a geometry, although numerically feasible, represents a task considerably more complex than in planar geometry. This problem is effectively 2d, and the number of operations for each iteration scales as $N^2 \log N$, where N is the number of points of the mesh. Therefore, in this first application of the formalism, we have chosen to resort to the simple but effective Derjaguin approximation [43], which allows to express the interaction between two convex objects starting

from the knowledge of the force between two planar walls, independently on the physical origin of the force. As regards this system, Derjaguin approximation consists in replacing the local pressure $p_{\mathrm{N}}(\boldsymbol{r})$ on the exclusion surface, by the solvation force per unit surface f_Σ between two walls, identical to the spheres, at distance z. It is straightforward to show, starting from Eq. (2.74), that the force F_{D} between the two spheres can be written as

$$F_{\mathrm{D}}(L) = \pi\left(R + \frac{\sigma}{2}\right)\int_L^{+\infty} \mathrm{d}z\, f_\Sigma(z). \tag{2.75}$$

This approximation gives accurate results provided $L \ll R$ and if the interaction potential between the two walls decays rapidly at large distances.
When the force between the walls is mediated by a hard sphere fluid with particles of diameter σ it is possible to show that Derjaguin's expression is the best approximation of the true depletion interaction without taking in account curvature effects [87] and it is accurate in the limit of $q \ll 1$, where $q = \sigma/2R$ is the size ratio. The range of validity of Derjaguin approximation applied to depletion interactions is a debated issue. Particularly, it is a matter of discussion the size ratio at which Derjaguin's theory starts to fail, and how its accuracy depends on the concentration of depletant. Depletion is actually a global effect, influenced by the arrangement of all the (interacting) depletants around the big objects: It is not possible to guarantee *a priori* that the predictions according to Derjaguin's approximation accurately reproduce experimental data or simulations.

Most of the results present in the literature, both computational and experimental, focus on the depletion potential, more than on the depletion force. Within Derjaguin approximation the depletion potential is given by

$$V_{\mathrm{D}}(L) = \pi\left(R + \frac{\sigma}{2}\right)\int_L^{+\infty} \mathrm{d}z\,(z-h)\, f_\Sigma(z), \tag{2.76}$$

where, as before, f_Σ is the solvation force per unit surface. In most cases the depletant interacts through a hard core potential with the sphere. Under this hypothesis, for $L < \sigma$ the analytical form of the potential following from Derjaguin's approximation (2.76) is a parabola:

$$V_{\mathrm{D}}(L) = \pi\left(R + \frac{\sigma}{2}\right)\left\{\int_0^{+\infty} \mathrm{d}z\, z\, f_\Sigma(z) - L\int_0^{+\infty} \mathrm{d}z\, f_\Sigma(z) - \frac{1}{2}\,p\,L^2\right\},$$

where $-p$ is the solvation force at distances of the walls $L < \sigma$. At large size ratios q the predictions based on Derjaguin approximation become unreliable just at small face to face distances, where the potential is described by this particular analytical expression.

In Fig. 2.12 we compare the predictions for the depletion potential $\beta V(L)$ between two big hard spheres in a fluid of smaller hard spheres obtained both by Derjaguin approximation and MC simulations at two different values of

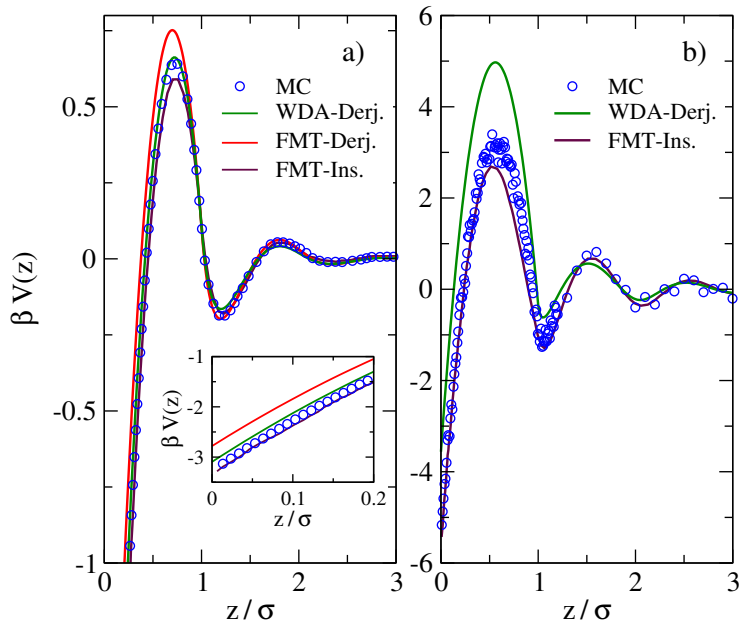

Figure 2.12: Depletion potential per unit $k_{\mathrm{B}}T$ between two hard spheres in a fluid of smaller hard spheres (size ratio $q = 0.1$) at bulk packing fraction $\eta = \frac{\pi}{6}\rho_b\,\sigma^3$ equal to 0.2 (panel a)) and 0.35 (panel b)). MC (points) and FMT predictions obtained with the insertion trick (purple lines) are taken from Ref. [8]. The red line at $\eta = 0.2$ is obtained by use of Derjaguin approximation starting from the solvation force between two planar hard walls evaluated from the FMT-WB [194] approximation implemented in-house. The green lines represent the depletion force obtained within Derjaguin approximation when the solvation force between the walls is given by the present WDA approximation.

the bulk density of the smaller particles. The predictions for the depletion potential obtained by Derjaguin approximation are accurate at $q = 0.1$ only at values of the packing fraction of the small spheres lower than 0.25. At $\eta = 0.35$ Derjaguin approximation overestimates by about $2k_{\mathrm{B}}T$ both the contact value and the first repulsive peak in the potential, while the oscillations at larger values of distance are underestimated when compared to MC data. The rather poor performance of Derjaguin approximation is probably due to the presence of a strong repulsive peak in the solvation force between the two walls at $z \sim \sigma$ (see Fig. 2.6), which appears to be a peculiarity of the slab geometry. We expect that, for smoother inter-wall effective interactions, the agreement would be considerably better.

The results presented above show that Derjaguin approximation can be safely adopted is the size ratio between the depletant and the colloid is sufficiently small and up to moderate densities of depletant (i.e. $q < 0.1$

and $\rho_b\sigma^3 < 0.4$), and we expect that similar considerations apply when the depletant is a Yukawa hard core fluid. Within the limits of validity of the Derjaguin approximation, we can determine the solvent-mediated potential $v_{\rm eff}(r)$ between two hard spheres of radius R immersed in a YHC fluid in order to examine the phase stability of such a colloidal suspension.
According to Noro-Frenkel extended law of corresponding states [163], fluids characterised by short-ranged interaction potentials obey the same equation of state, when expressed in terms of reduced variables[33]. In particular, it was observed that the dimensionless second virial coefficient

$$B_2^*(T) = \frac{B_2(T)}{B_2^{\rm HS}} = 1 + \frac{3}{8R^3}\int_{2R}^{\infty} {\rm d}r\, r^2 \left[1 - {\rm e}^{-\beta v_{\rm eff}(r)}\right], \tag{2.77}$$

where $B_2^{\rm HS}$ is the second virial coefficient of a hard sphere system with particles of radius R, assumes a value of about -1.6 at the critical point independently on the particular form of the interaction and that its value remains constant in a relatively large density range across the coexistence line [236]. It is therefore possible to estimate the the gas-liquid spinodal line for a system of hard sphere colloidal particles dispersed in a HCY fluid, by evaluating their reduced second-virial coefficient. The blue points in Fig. 2.13 identify the phase separation line of a HS fluid induced by the presence of a depletant modeled as a HCY fluid. The size ratio between the depletant and the guest HS particles is $q = 0.1$. At high values of the reduced temperature the phase separation occurs at reduced density of about 0.4, as expected in the limit of HS depletant. When the temperature decreases, the concentration of depletant needed to induce phase separation decreases monotonically. At the depletant critical temperature we observe phase separation at depletant concentrations $\rho_b\sigma^3 \sim 0.15$ much lower than the critical one. This implies that, at this value of the size ratio q, the phase separation is not related to the presence of long-range tails in the effective force, which characterises the critical region of the solvent, but is still mainly due to the short-range attraction generated by the depletion mechanism which is enhanced at lower temperatures.
We note that whenever a direct short-range repulsion is present between the colloidal particles, as for the case of charged systems, the strong attraction due to depletion is severely weakened and particle aggregation takes place at considerably larger solvent densities. Instead, in the critical region, the long-range tails of the solvent mediated (Casimir) force is not effectively contrasted by the additional short-range repulsion. In extreme circumstances (i.e. when the direct repulsion between particles is sufficiently strong), ordinary depletion may be fully screened and phase separation inhibited. However, aggregation is generally expected in a small pocket within the critical region, due to the emergence of long-range Casimir forces. For repulsive wall-solvent interactions, this pocket will be centered at solvent densities larger than the

[33] Namely, the reduced density, the reduced temperature and the reduced second-virial coefficient. For a precise definition of the rescaling see Ref. [163].

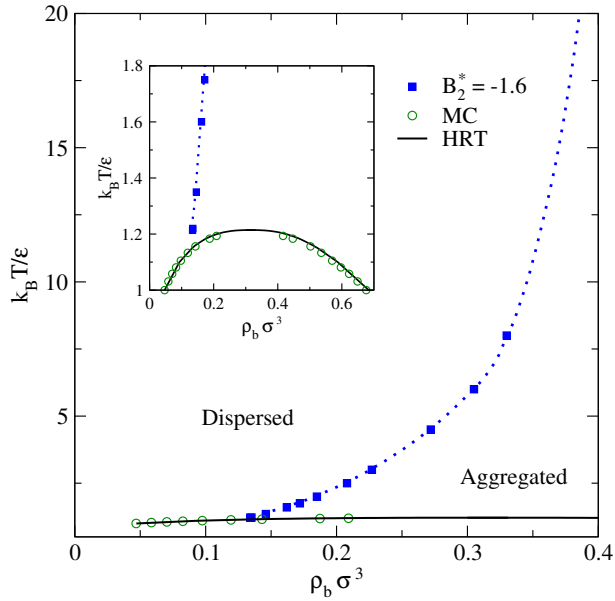

Figure 2.13: Phase diagram of the HCY model ($\zeta\sigma = 1.8$) in the ρ_b - T plane. The HRT results for the coexistence curve [169] are shown by a black line. Green dots represent the MC data from Ref. [176]. Blue points show the aggregation boundary of two big hard spheres (size ratio $q = \sigma/(2R) = 0.1$) predicted on the basis of our WDA plus Derjaguin approximation and Noro-Frenkel criterion. The dashed line connecting the points is a guide to the eye: Aggregation takes place on the right of this boundary. The inset shows the same phase diagram in a wider density interval.

critical one, due to the strong asymmetry of the critical Casimir forces (see e.g. Figs. 2.9 and 2.15).

2.5 CRITICAL CASIMIR EFFECT

The aim of this section is to evaluate the universal properties of the solvent-mediated interaction induced between two walls when the depletant is in the critical regime. As shown in Section 2.1 (Fluctuation-induced interactions), in this regime the effective force between two bodies *immersed* in the critical fluid acquires a universal form and obeys scaling laws, as many physical properties near criticality do.
With a slight change of notation with respect to Section 2.1, we can express the force acting between two walls in a critical fluid as (see Eq. (2.14)):

$$\frac{F_C(t,h;L)}{k_B T \Sigma} = \frac{1}{L^3}\Theta\left(\pm s, \pm y\right), \tag{2.78}$$

where L is the distance between the two walls. The upper sign refers to the super-critical temperature (while the lower to the sub-critical one) and the scaling variables (s, y)

$$s = \frac{L}{\xi}, \qquad y = ah|t|^{-\beta\delta}$$

are defined in terms of the two scaling fields

$$t = \frac{T - T_c}{T_c}, \qquad h = \mu - \mu_c$$

and μ_c is the critical potential of the fluid. Here $\xi \sim \xi_0^{\pm} t^{-\nu}$ is the bulk correlation length at $h = 0$, a is a non-universal metric factor and ν, β and δ are the usual critical exponents. We remark that there is no extra metric factor associated with L/ξ and that there is a dependence on the sign of the field h because boundary conditions at the walls break the bulk symmetry $h \to -h$. According to the theory of finite-size scaling, Eq. (2.78) represents the asymptotic decay of the solvent-mediated force as $t, h \to 0$ and for $L, \xi \to \infty$. The critical Casimir scaling function in planar geometry $\Theta(\cdot, \cdot)$ only depends, as already stressed in Section 2.1 (Fluctuation-induced interactions), on bulk and surface universality classes. The bulk Yukawa fluid under investigation belongs to the 3D Ising universality class and the boundary conditions are determined by the affinity of the wall surfaces with the fluid particles: If the contact density is less than the bulk density the boundary condition is of type $-$, otherwise of type $+$. In this work we only deal with super-critical temperatures ($t > 0$) and with symmetric $(-, -)$ boundary conditions, which arise for purely repulsive interactions between the fluid particles and two identical confining hard walls.

Force profiles

The WDA approach developed in Section 2.3 allows the study of this problem starting from the microscopic HCY fluid model confined between two walls. According to the scaling hypothesis, the effective force per unit surface between the two walls F_C should depend on the physical control parameters T, μ, L only through the combination (2.78), implying the collapse of different data sets onto the same universal curve. Figure 2.14 shows the scaling function obtained from independent calculations at different temperatures along the previously defined critical line $\tilde{\rho}(t)$ (i.e. $y = 0$). Note that, even at reduced temperature $t = (T - T_c)/T_c$ as low as 10^{-3}, our estimates show a marked temperature dependence, and the data along different isotherms do not collapse as we expected. At the lowest temperature we investigated, a significant difference between our prediction and the MC simulations of Ref. [230] suggests the presence of strong corrections to scaling. We also remark that the curves at the lowest temperatures develop a kink at small values of L/ξ, due to the

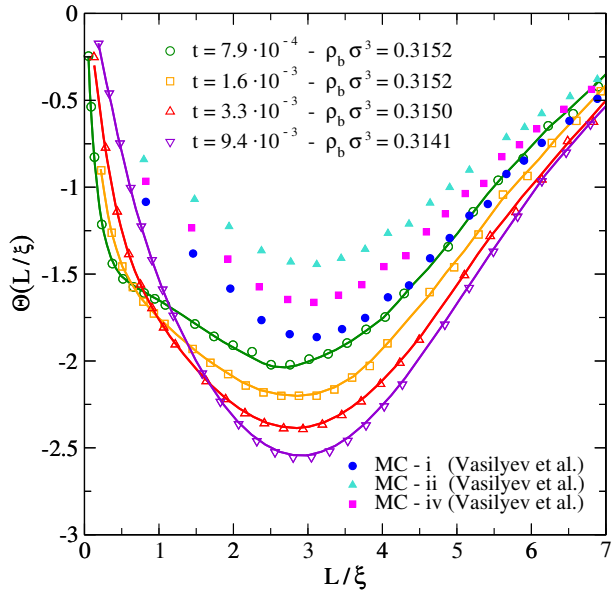

Figure 2.14: Finite-size estimates of the Casimir scaling function at values of temperatures and density along the critical line defined in Eq. (2.71) from the microscopic force obtained within the present WDA approximation. The corresponding bulk correlation lengths are $\xi = 41.1\sigma, 26.5\sigma, 17.3\sigma, 9.2\sigma$, from the lowest to the highest reduced temperature. The lines connecting the points are a guide to the eye. The MC data are taken from Ref. [230] and refer to $(-,-)$ boundary conditions and the different sets correspond to different estimates of the corrections to scaling.

singular behaviour of the scaling function at $L/\xi = 0$. In fact, at any given reduced temperature $t \neq 0$, the quantity $L^3 F_C$ tends to zero as $L/\xi \to 0$, forcing the finite-size estimate of the scaling function to vanish. Figure 2.15 shows the scaling function at fixed temperature near T_c for different values of the scaling variable $y = ah|t|^{-\beta\delta}$, corresponding to different bulk reduced densities. The scaling function is always negative and a strong asymmetry is evident between the curves at density above and below ρ_c. For positive values of the scaling field h (i.e. $\rho > \rho_c$ in our case), the magnitude of the force becomes larger and larger and the peak is shifted towards small values of L/ξ.

Long-wavelength analysis

Although the direct numerical evaluation of the critical Casimir scaling function predicted by this class of DFT is not conclusive, due to severe corrections to scaling, an accurate estimate of the asymptotic behaviour can be obtained by a long-wavelength (LW) analysis of the DFT equations. In fact, following Ref. [174] we note that:

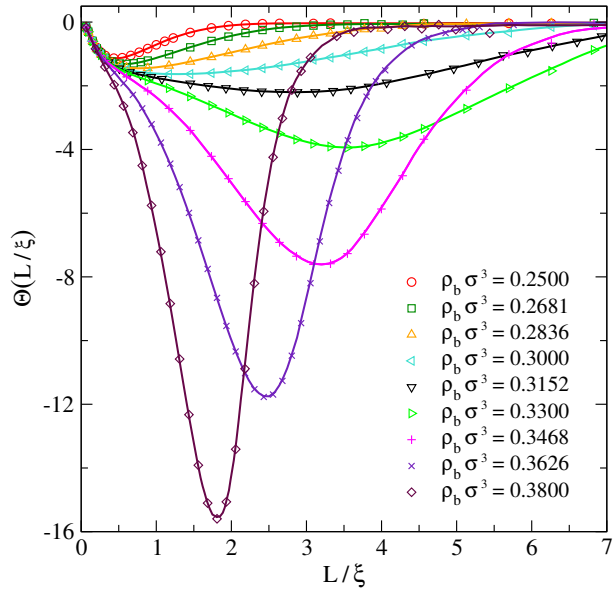

Figure 2.15: Scaling function for the critical Casimir force at $t = 1.6 \cdot 10^{-3}$ and for different values of the scaling variable y. The lines connecting the points are a guide to the eye. The largest correlation length, $\xi = 26.5\sigma$, corresponds to the critical reduced density $\rho_b\sigma^3 = 0.3152$.

1. The density profile $\rho(z)$ displays reflection symmetry about $z = \frac{L}{2}$, limiting the range of interest to $z \in \left[0, \frac{L}{2}\right]$.

2. When the walls are far apart ($L \gg \sigma$) and the system is close to the critical point ($\xi \gg L$), the difference between the density profile corresponding to a wall to wall distance L and its single wall limit, reached for $L = \infty$, is significant only for $z \sim \frac{L}{2}$.

3. As a consequence, the effective force per unit surface F_C (hence the Casimir scaling function) just depends on the long-distance tail of the density profile, which is expected to be a slowly varying function of the coordinate z.

Therefore we can limit ourselves to the study of a free energy functional which retains only the lowest term in a gradient expansion about the bulk density ρ_b (see Eq. (2.34)):

$$\frac{\beta\mathcal{F}\left[\rho_b + \Delta n(z)\right]}{\Sigma} - L\,\varphi(\rho_b) = \\ = \int \mathrm{d}z \left[\frac{b}{2}\left(\frac{\mathrm{d}\Delta n(z)}{\mathrm{d}z}\right)^2 + \varphi\big(\rho_b + \Delta n(z)\big) - \varphi(\rho_b)\right], \qquad (2.79)$$

where $\varphi(\rho)$ is the free energy density in the bulk $f_b(\rho)$, times β. As shown in Section 2.2, this expression coincides with the long-wavelength limit of our WDA functional, the stiffness b being related to the range of the direct correlation function in the homogeneous system $c(r, \rho_b)$:

$$\frac{1}{\rho_b} - \int \mathrm{d}\boldsymbol{r}\, c(r, \rho_b)\, \mathrm{e}^{\mathrm{i}\boldsymbol{q}\cdot\boldsymbol{r}} \longrightarrow \frac{\partial^2 \varphi(\rho_b)}{\partial \rho_b^2} + bq^2 + O\left(q^4\right). \tag{2.80}$$

In the presence of short-range interactions, the direct correlation function is analytic in q^2 away from the critical point, where it displays a $q^{2-\eta}$ singularity. However, within our approximate closure of the HRT equations, the critical exponent $\eta = 0$ and analyticity is preserved also at criticality [169], keeping the stiffness b finite in the whole phase diagram. This implies that the long-wavelength limit of the structure factor of the homogeneous fluid follows the Orstein-Zernike ansatz

$$S(q) \sim \frac{S(0)}{1 + \xi^2 q^2} \tag{2.81}$$

with

$$\rho_b\, S(0) = \left[\frac{\partial^2 \varphi(\rho)}{\partial \rho^2}\right]^{-1}. \tag{2.82}$$

From (2.81) and (2.82) combined with (2.80) it follows that

$$\xi^2 = \rho_b\, S(0)\, b. \tag{2.83}$$

Close to the critical point, the HRT bulk free energy density $\varphi(\rho)$ acquires a scaling form:

$$\varphi(\rho_c + \delta\rho) - \varphi(\rho_c) - \beta\mu(\rho_c)\delta\rho = t^{d\nu}\, a_{11} \Psi\left(b_1\, \delta\rho\, t^{-\beta}\right), \tag{2.84}$$

where ρ_c is the critical density, $\delta\rho = \rho - \rho_c$ and $\mu(\rho)$ is the chemical potential (the temperature dependence of these quantities is understood), while a_{11} and b_1 are non-universal metric factors. In the following it will be convenient to express the universal quantities in terms of the scaling field $x = b_1\, \delta\rho\, t^{-\beta}$ instead of the previously defined variable y. Within our HRT closure, the critical exponents are $\delta = 5$, $\beta = 0.332$, $\nu = 0.664$ in $d = 3$, which agree within 10% with the accepted values. The metric factors appearing in the scaling function are implicitly defined by the requirement that $\Psi(x)$ has the following expansion at small x [173]:

$$\Psi(x) \longrightarrow \frac{x^2}{2!} + \frac{x^4}{4!} + O\left(x^6\right). \tag{2.85}$$

In Fig. 2.16 the asymptotic HRT scaling function $\Psi(x)$ is shown together with a parameterization of the exact result for the 3D Ising universality class.

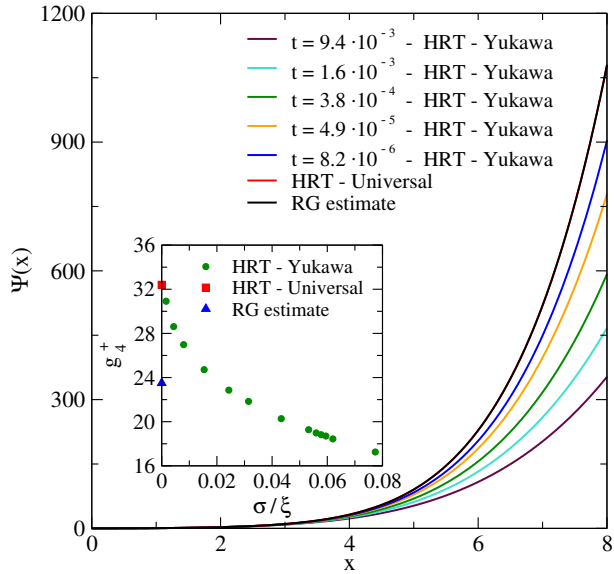

Figure 2.16: Scaling function for the free energy $\Psi(x)$ as predicted by HRT compared with a parameterization of the exact result from Ref. [173] (black curve). The red line, showing the HRT asymptotic result, is identical to the exact result on the scale of the figure. A few rescaled free energies obtained from the integration of the HRT equations at different reduced temperatures are also shown. Inset: Universal amplitude ratio g_4^+ for a HCY fluid at the critical density as a function of the reduced inverse correlation length (green points). The usually accepted value [173] is shown by a blue triangle whereas the red square represents the asymptotic HRT value.

Although the two curves are indistinguishable on this scale, calculations at different reduced temperatures, also shown, suggest the presence of important corrections to scaling.

The minimisation of the long-wavelength functional (2.79) in slab geometry gives rise to a differential equation whose solution allows to evaluate the asymptotic decay of the effective force between two hard walls in a critical fluid. The derivation, already detailed in Ref. [174] and not repeated here, provides a closed form for the critical Casimir scaling function in terms of two universal quantities: The bulk free energy scaling function $\Psi(x)$ and the universal amplitude ratio g_4^+. Defining the auxiliary quantity $\sigma(s,x)$ by the implicit relations:

$$\sigma(s,x) = -\Psi(x+u_0) + \Psi(x) + u_0\,\Psi'(x), \tag{2.86}$$

$$s = \int_{u_0}^{\infty} \frac{\sqrt{2}\,\mathrm{d}u}{\sqrt{\sigma(s,x) + \Psi(x+u) - \Psi(x) - u\,\Psi'(x)}} \tag{2.87}$$

the critical Casimir scaling function in three dimensions is given by

$$\Theta(s,x) = \frac{s^3}{g_4^+}\,\sigma(s,x)\,. \tag{2.88}$$

The universal amplitude ratio g_4^+ is expressed in terms of the non-universal metric factors previously introduced as

$$g_4^+ = b_1^3\,\sqrt{a_{11}b^{-3}}. \tag{2.89}$$

Again, the evaluation of g_4^+ from the HRT equations displays severe corrections to scaling in a HCY fluid, as shown in the inset of Fig. 2.16. More importantly, the usually quoted "exact" value [173] $g_4^+ \sim 23.6$ turns out to differ significantly from the HRT prediction $g_4^+ \sim 32.4$.

The asymptotic study of the DFT equations allows to extract the critical Casimir scaling function just from bulk quantities via Eq.s (2.86 - 2.88). It is then instructive to contrast these predictions with the outcome of the direct minimisation of the HRT functional, already shown in Fig. 2.14. Such a comparison can be found in Fig. 2.17, where the scaling functions obtained from the microscopic DFT at a few reduced temperatures t in the critical region are shown to agree remarkably well with the predictions of the long-wavelength analysis, provided both the scaling function for the free energy $\Psi(x)$ and the universal amplitude ratio g_4^+ are consistently evaluated at the same reduced temperature t.

The presence of strong corrections to scaling in both $\Psi(x)$ and g_4^+, already highlighted, induces strong pre-asymptotic effects in the critical Casimir scaling function which, at reduced temperatures lower than 10^{-3}, is still quite far from its asymptotic limit. The main effect is due to the growth of the amplitude ratio, which, as shown in Fig. 2.16, appears to reach its universal value only extremely close to the critical point, according to the prediction of HRT for the model of critical fluid investigated here. We remark that, due to the already quoted difference between the HRT estimate of the universal amplitude ratio g_4^+ and the value obtained via series expansions, the critical Casimir scaling function predicted by our DFT significantly differs from the one obtained in MC simulations, as can be seen in Fig. 2.17.

2.6 CONCLUSIONS AND PERSPECTIVES

In this Chapter we presented a novel density functional, based on the weighted density paradigm, able to describe classical inhomogeneous fluids in a large portion of their phase diagram, critical point included. This is the first attempt to describe the effects of correlations induced by attractive interactions in confined fluids. The theory is based on the description of the uniform system provided by the hierarchical reference theory, one of the few liquid state approaches able to cope with long-range density fluctuations. This technique,

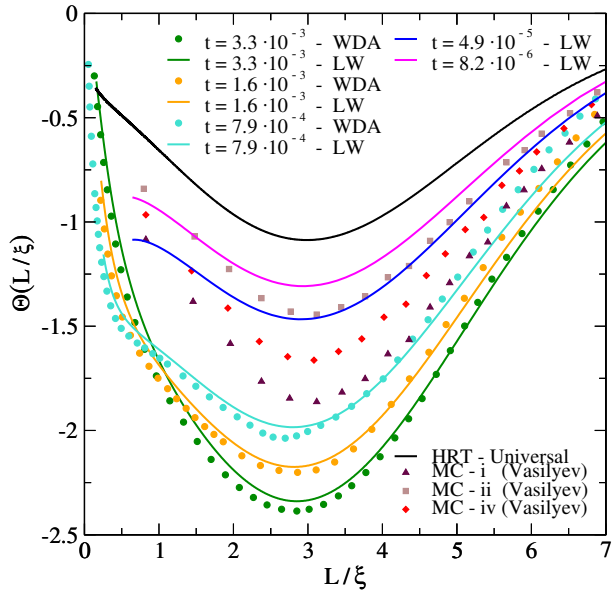

Figure 2.17: Critical Casimir scaling function evaluated at different reduced temperatures. Points: results from the direct minimisation of the microscopic WDA functional. Lines: results from the long-wavelength analysis, starting from the universal quantities $\Psi(x)$ and g_4^+ evaluated at the same reduced temperature as the DFT calculation. Black line: asymptotic limit of the critical Casimir scaling function evaluated via HRT (see the text). Points: prediction of Θ from Monte Carlo simulations [230].

applied to the evaluation of the effective interaction between two hard walls in a fluid, allowed for the investigation of the crossover between a depletion-like mechanism at high temperatures and the critical Casimir effect emerging near the critical point. Our method does not rely on a long-wavelength approximation and provides a complete picture of the solvent-mediated force for any wall separation, displaying the presence of important non-universal contributions in the effective interaction at short distances, even in the critical region. We believe that this DFT will be useful in investigating other correlated systems, when density fluctuations are expected to play an important role.

We showed that, at large separations, the solvent-mediated force per unit surface between the walls decays exponentially on the scale of the correlation length in the whole portion of the phase diagram to the left of the Fisher-Widom line. Such a behaviour cannot be considered as a signature of the onset of critical Casimir effect: only the product between the *amplitude* of the long-range exponential tail and the cube of the correlation length is a genuine universal quantity.

Our microscopic approach allows for the determination of the universal quantities characterising the critical Casimir effect, namely the scaling func-

tion $\Theta(s, y)$, both along the critical isochore ($y = 0$) and in the off-critical regime. Strong corrections to scaling have been observed in the HCY fluid we investigated: The universal features appear to emerge only in a narrow neighbourhood of the critical point, at least in the model we examined. It would be useful to compare this prediction with numerical simulations for the HCY fluid model as well as with theoretical investigations of other systems, like the Ising model, where the corrections to scaling may be weaker. These studies will hopefully clarify the origin of the discrepancy between the HRT estimate of the universal amplitude ratio g_4^+ and the commonly accepted value.

The approach presented in this work allows for further improvements. In our density functional, the ideal gas term and the Hartree contribution to the internal energy have been treated exactly, while the remaining entropy-correlation term has been approximated by use of a weighted density trick. The next step will be to treat the hard sphere term by the fundamental measure theory, known to be very accurate in dealing with excluded volume effects, limiting the weighted density contribution only for the residual correlation term. This adjustment is expected to increase the accuracy of the theory at high density, without however modifying the description of the universal properties of the critical Casimir effect.

In this first application we just considered a planar geometry, whose implications for the phenomenon of colloidal aggregation depend upon further assumptions, namely the Derjaguin approximation, which however turns out to be rather inaccurate when the two external bodies are not very close. A natural further step will be to perform the functional minimisation in cylindrical geometry, appropriate for dealing with two spherical particles thereby avoiding any wall-to-sphere mapping.

2.7 APPENDIX: CONTACT THEOREM

In this Appendix we prove that the WDA introduced in Section 2.3 is consistent with the so called *contact theorem*.

Contact theorem

The mechanical equilibrium condition for a fluid in an external field $\phi(\boldsymbol{r})$ reads [205]

$$\partial_\alpha p^{\alpha\beta}(\boldsymbol{r}) = -\rho(\boldsymbol{r})\partial_\alpha\phi(\boldsymbol{r}), \tag{2.90}$$

where $p^{\alpha\beta}(\boldsymbol{r})$ is the pressure tensor. If we restrict to the planar symmetry[34] the pressure tensor is diagonal and depends only on the direction orthogonal

[34]Within planar symmetry the external potential depends on a single coordinate, e.g. $\phi(\boldsymbol{r}) = \phi(z)$. The same property will hold for the density profile.

to the plane (let us say z):

$$p^{\alpha\beta}(z) = \mathrm{diag}\left\{p_{\mathrm{T}}(z), p_{\mathrm{T}}(z), p_{\mathrm{N}}(z)\right\},$$

where the subscripts T and N denote the tangent and normal components of the pressure. The component $p_{\mathrm{N}}(z)$ of the pressure tensor can be uniquely determined [205] from Eq. (2.90):

$$\frac{\mathrm{d}}{\mathrm{d}z} p_{\mathrm{N}}(z) = -\rho(z) \frac{\mathrm{d}}{\mathrm{d}z} \phi(z). \tag{2.91}$$

The integration of (2.91) across a planar wall-fluid interface up to a value $\tilde{z}$ well beyond the range of the external potential gives an exact *statistical mechanical sum rule* which links the (macroscopic) bulk pressure p[35] to the integral of the (microscopic) density profile:

$$p = -\int_{-\infty}^{\tilde{z}} \mathrm{d}z\, \rho(z) \frac{\mathrm{d}}{\mathrm{d}z} \phi(z) \tag{2.92}$$

$$= \frac{1}{\beta} \int_{-\infty}^{\tilde{z}} \mathrm{d}z\, n(z) \frac{\mathrm{d}}{\mathrm{d}z} \mathrm{e}^{-\beta\phi(z)}, \tag{2.93}$$

where the function $n(z)$, defined by

$$n(z) = \rho(z)\, \mathrm{e}^{\,\beta\phi(z)}, \tag{2.94}$$

is always continuous [98] and allows to extend Eq. (2.92) to discontinuous external potentials (e.g. the hard wall potential). Let us assume that the external potential represents a hard wall located at $z = z_0$:

$$\phi(z) = \phi_{\mathrm{HC}}(z - z_0) = \begin{cases} 0 & z > z_0 \\ +\infty & z < z_0 \end{cases} \tag{2.95}$$

Then, Eq. (2.93) reduces to the well known *contact theorem*:

$$\beta p = \lim_{z \to z_0^+} \rho(z). \tag{2.96}$$

Contact theorem and density functionals

The sum rule (2.92) is an exact identity of a Hamiltonian-based theory, and we can not guarantee *a priori* that approximated density functionals, as the WDA, can exactly satisfy it. This property must be checked for each approximated functional. When the fluid is confined by a hard wall, the proof of the consistence with the contact theorem reduces to show that the given

[35] The pressure tensor becomes isotropic and homogeneous in the bulk when the inter-particle interactions are isotropic.

approximated functional satisfies (2.93).
In the next paragraph we will show that our weighted density approximation satisfies (2.93), and therefore also the contact theorem (2.96). The Percus-Yevick and hypernetted-chain wall-particle closures of the OZ equation do not agree with (2.96).

Here we want to prove that our approximated functional fulfils

$$\begin{aligned} p &= -\int_{-\infty}^{+\infty} \mathrm{d}z\, \rho(z) \frac{\mathrm{d}}{\mathrm{d}z} \phi_{\mathrm{HC}}(z - z_0) \\ &= \int_{-\infty}^{+\infty} \mathrm{d}z\, \rho(z) \frac{\mathrm{d}}{\mathrm{d}z_0} \phi_{\mathrm{HC}}(z - z_0), \end{aligned} \tag{2.97}$$

where $\tilde{z}$ has been replaced, without any approximation, by $+\infty$.
The grand potential functional (2.20) within this simple geometry reads

$$\Omega[n(\boldsymbol{r})] = \mathcal{F}[n(\boldsymbol{r})] + \int \mathrm{d}\boldsymbol{r}' n(\boldsymbol{r}') \big(\phi_{\mathrm{HC}}(z - z_0) - \mu\big) \tag{2.98}$$

and the equilibrium density profile $\rho(z)$ fulfils the following relation:

$$\left.\frac{\delta\Omega[n]}{\delta n(\boldsymbol{r})}\right|_{\rho(z)} = \left.\frac{\delta\mathcal{F}[n]}{\delta n(\boldsymbol{r})}\right|_{\rho(z)} + \phi_{\mathrm{HC}}(z - z_0) - \mu = 0. \tag{2.99}$$

Then, the derivative of the grand potential with respect to z_0 reads

$$\begin{aligned} \frac{\mathrm{d}\Omega}{\mathrm{d}z_0} = \frac{\mathrm{d}}{\mathrm{d}z_0}\Omega[\rho(z)] = \int \mathrm{d}\boldsymbol{r} \Bigg\{ & \left.\frac{\partial n(z - z_0)}{\partial z_0}\right|_{\rho(z)} \Big[\, \phi_{\mathrm{HC}}(z - z_0) - \mu \,\Big] \\ & + \left.\frac{\delta\mathcal{F}[n]}{\delta n(\boldsymbol{r})}\right|_{\rho(z)} \left.\frac{\partial n(z - z_0)}{\partial z_0}\right|_{\rho(z)} + \rho(z) \frac{\mathrm{d}}{\mathrm{d}z_0} \phi_{\mathrm{HC}}(z - z_0) \Bigg\} \end{aligned} \tag{2.100}$$

because the grand potential functional (2.98), evaluated at the equilibrium density, equals the grand potential of the system. Making use of Eq. (2.99) in Eq. (2.100) we obtain

$$\begin{aligned} \frac{\mathrm{d}}{\mathrm{d}z_0}\Omega[\rho(z)] &= \int \mathrm{d}\boldsymbol{r}\, \rho(z) \frac{\mathrm{d}}{\mathrm{d}z_0} \phi_{\mathrm{HC}}(z - z_0) \\ &= \Sigma \int_{-\infty}^{+\infty} \mathrm{d}z\, \rho(z) \frac{\mathrm{d}}{\mathrm{d}z_0} \phi_{\mathrm{HC}}(z - z_0), \end{aligned} \tag{2.101}$$

where Σ is the surface of the wall located at z_0. However

$$\Omega = -p\, V = -p\, \Sigma\, (h - z_0)$$

and the derivative of grand potential w.r.t. z_0 can be written as

$$\frac{\mathrm{d}\Omega}{\mathrm{d}z_0} = p\, \Sigma. \tag{2.102}$$

The final result (2.97) follows comparing (2.101) with (2.102).

2.8 APPENDIX: SOLVATION FORCE

The purpose of this Appendix is to express the force between two walls immersed in a fluid in terms of the contact density at the wall.

Let us consider two parallel[36] planar walls of surface Σ immersed in a classical fluid placed at $z = z_0$ and $z = z_0 + L$. The wall-fluid interaction can be suitably represented by an external potential of the form

$$\phi(z; L) = \phi_{\rm HC}(z) + \phi_{\rm HC}(L - z), \tag{2.103}$$

where $\phi_{\rm HC}(z)$ is defined in Eq. (2.95). A reservoir keeps the system at fixed μ and T. The fluid between the walls exerts a force on the walls whose contribution must be added into the grand potential of the fluid[37]. Following the standard approach in the field [103, 66], we consider the fluid bounded by the two walls with no fluid outside. The variation of the excess grand canonical potential of the confined fluid is

$$\begin{aligned} {\rm d}\Omega^{\rm ex} &= {\rm d}\left[\Omega - \Omega_b\right] = {\rm d}\left[\Omega + p\Sigma L\right] \\ &= -S^{\rm ex}{\rm d}T - N^{\rm ex}{\rm d}\mu + 2\gamma{\rm d}\Sigma - \Sigma f_\Sigma {\rm d}L, \end{aligned}$$

where the excess terms are expressed as *differences w.r.t. the bulk values*[38], the quantity 2γ is the total[39] wall-fluid interfacial tension, and Σf_Σ is the force applied externally against the walls in order to maintain them at a fixed distance L, also known as *solvation force*. The solvation force is an excess quantity expressed by a pressure difference as

$$f_\Sigma = -\frac{1}{\Sigma}\left.\frac{\partial \Omega^{\rm ex}}{\partial L}\right|_{T,\mu} = -\frac{1}{\Sigma}\left.\frac{\partial \Omega}{\partial L}\right|_{T,\mu} - p,$$

where p is the pressure of the bulk fluid. In presence of a wall-wall potential of finite range, f includes both direct interactions between the walls and the solvent-mediated interactions, associated to wall-fluid and fluid-fluid interactions. In this case the term solvation force is referred only to the solvent-mediated contribution to the interaction. According to the contact theorem (2.96) the bulk pressure can be expressed in terms of the contact density against a single wall. The density functional formalism allows to express without approximations the contribution

$$\left.\frac{\partial \Omega}{\partial L}\right|_{T,\mu}$$

[36] Infinite in the thermodynamic limit.

[37] Note that the grand potential outside the walls is constant.

[38] In particular, $N^{\rm ex}$ is the excess number of molecules adsorbed at the surface.

[39] I.e., the relation

$$2\gamma(L \to \infty) = 2\gamma_\infty$$

holds only in the single wall limit.

in terms of the contact density.
The chain rule extended to functionals allows to evaluate the variation of the intrinsic free energy potential as

$$\frac{\mathrm{d}\Omega[n(\boldsymbol{r})]}{\mathrm{d}L} = \int \mathrm{d}\boldsymbol{r}' \frac{\delta\Omega[n]}{\delta\phi(z;L)} \frac{\mathrm{d}\phi(\boldsymbol{r}';L)}{\mathrm{d}L}. \tag{2.104}$$

According to the Hohenberg-Kohn-Mermin theorem (2.19), the grand potential functional depends on the external potential only through the density profile:

$$\frac{\delta\Omega[n]}{\delta\phi(\boldsymbol{r};L)} = \int \mathrm{d}\boldsymbol{r}' \frac{\delta\Omega[n]}{\delta n(\boldsymbol{r}')} \frac{\delta n(\boldsymbol{r}')}{\delta\phi(\boldsymbol{r};L)} + n(\boldsymbol{r}).$$

Evaluating Eq. (2.104) at the equilibrium density $\rho(\boldsymbol{r})$ and exploiting the minimum principle (2.22) it follows that in our simple geometry:

$$\begin{aligned} -\frac{1}{\Sigma}\left.\frac{\mathrm{d}\Omega}{\mathrm{d}L}\right|_{T,\mu} &= -\int \mathrm{d}z\, \rho(z)\, \frac{\mathrm{d}\phi(z;L)}{\mathrm{d}L} \qquad (2.105)\\ &= \frac{1}{\beta}\int \mathrm{d}z\, \rho(z)\, \mathrm{e}^{\beta\phi(z;L)} \frac{\mathrm{d}}{\mathrm{d}L}\, \mathrm{e}^{-\beta\phi(z;L)} \\ &= \frac{1}{\beta}\int \mathrm{d}z\, \rho(z)\, \mathrm{e}^{\beta\phi(z;L)} \frac{\mathrm{d}}{\mathrm{d}L}\Big[\Theta\left(L-z\right) - \Theta\left(z\right)\Big] \\ &= \frac{1}{\beta}\int \mathrm{d}z\, \rho(z)\, \mathrm{e}^{\beta\phi(z;L)} \delta(L-z) \\ &= \frac{1}{\beta}\, \rho(z)\, \mathrm{e}^{\beta\phi(z;L)}\Big|_{z\to L-|\epsilon|}. \qquad (2.106) \end{aligned}$$

The function $\rho(z)\,\mathrm{e}^{\beta\phi(z;L)}$ is everywhere continuous, even if the potential exhibits a discontinuity across the wall surface [98], and Eq. (2.106) can be evaluated in the limit $z \to L-\epsilon$, with $\epsilon \to 0^+$. Finally, the solvation force can be written as

$$\beta f_\Sigma(L;T,\mu) = \rho(L) - \rho(\infty),$$

where $\rho(\infty)$ is the contact density for a single wall.

It is possible to express the solvation force in terms of the local normal pressure. Starting from Eq. (2.105) and together with the definition of the external potential (2.103) it follows that:

$$\begin{aligned} f_\Sigma = -\frac{1}{\Sigma}\left.\frac{\mathrm{d}\Omega}{\mathrm{d}L}\right|_{T,\mu} &= -\int_{-\infty}^{+\infty} \mathrm{d}z\, \rho(z) \frac{\mathrm{d}}{\mathrm{d}z}\phi^\infty(z) \\ &= p_\mathrm{N}(L/2) - 2\int_{L/2}^{+\infty} \mathrm{d}z\, \rho(z) \frac{\mathrm{d}}{\mathrm{d}z}\phi^\infty(z). \end{aligned}$$

The last identity can be obtained integrating from $L/2$ to $+\infty$ the mechanical equilibrium condition (2.90) and taking advantage of the symmetry of the

density profile:

$$p_{\rm N}(+\infty) - p_{\rm N}(L/2) = -\int_{L/2}^{+\infty} {\rm d}z\, \rho(z)\, \frac{{\rm d}}{{\rm d}z}\phi_{\rm HW}(z) + \int_{-\infty}^{L/2} {\rm d}z\, \rho(z)\, \frac{{\rm d}}{{\rm d}z}\phi_{\rm HW}(z)$$
$$= -2\int_{L/2}^{+\infty} {\rm d}z\, \rho(z)\, \frac{{\rm d}}{{\rm d}z}\phi_{\rm HW}(z) + \int_{-\infty}^{+\infty} {\rm d}z\, \rho(z) \frac{{\rm d}}{{\rm d}z}\phi_{\rm HW}(z),$$

where $p_{\rm N}(\infty) = 0$ because there is no fluid outside the walls. If the range of the interaction between the walls is less than $L/2$ (as in the case of hard walls) then the solvation force reduces to

$$f_\Sigma(L; T, \mu) = p_{\rm N}(L/2) - p,$$

which is the same result following from a direct mechanical evaluation of the force.

2.9 APPENDIX: LONG-WAVELENGTH BEHAVIOUR OF THE DENSITY PROFILES

In this Appendix we examine the long-wavelength behaviour of the density profiles of a critical fluid confined by a wall. The analytical form of the density profile far from the wall will be obtained through the DFT formalism. In particular, we will adopt the square-gradient approximation, because all the WDA functionals which provide consistent values of bulk direct correlation function reduce to this form in the long-wavelength limit.

Let us consider a fluid confined by two infinite parallel hard walls at $z = 0$ and $z = h$. The stationarity condition (2.22) applied to a square-gradient functional (here we keep the notation of Eq. (2.79)) reads

$$\frac{b}{2}\left(\frac{{\rm d}\Delta n(z)}{{\rm d}z}\right)^2 - \varphi\big(\rho_b + \Delta n(z)\big) + \varphi(\rho_b) + \frac{\partial\varphi(\rho_b)}{\partial\rho_b}\Delta n(z) = \Gamma(h), \quad (2.107)$$

where $\Gamma(h)$ is an integration constant defined by

$$\left.\frac{{\rm d}\Delta n(z)}{{\rm d}z}\right|_{z=\frac{h}{2}} = 0. \quad (2.108)$$

If we focus our interest on the region between the walls, with the supplementary hypothesis that the walls are far apart with respect to the correlation length, we can safely assume that $\Delta n(z)/\rho_b \ll 1$. If we perform a Taylor expansion of $\varphi(\rho)$ about the bulk density Eq. (2.107) reads

$$\frac{b}{2}\left(\frac{{\rm d}\Delta n(z)}{{\rm d}z}\right)^2 - \frac{1}{2}\frac{\partial^2\varphi(\rho_b)}{\partial^2\rho_b}\Delta n(z) = \Gamma(h). \quad (2.109)$$

It is possible to eliminate the constant term $\Gamma(h)$ in (2.109) through the substitution

$$\Delta n(z) = \Delta n^\star + \delta n(z) \qquad \text{with} \qquad \delta n(h/2) = 0 \tag{2.110}$$

which gives

$$b\left(\frac{\mathrm{d}\delta n(z)}{\mathrm{d}z}\right)^2 = \frac{\partial^2\varphi(\rho_b)}{\partial^2\rho_b}\left[2\Delta n^\star\delta n(z) + \big(\delta n(z)\big)^2\right],$$

where we made use of (2.110) and of the boundary condition (2.108):

$$\Gamma(h) = -\frac{1}{2}\frac{\partial^2\varphi(\rho_b)}{\partial^2\rho_b}\Delta n^{\star 2}.$$

According to Eq. (2.83), the second order derivative of the free energy is equal to b/ξ^2 and we obtain

$$\xi^2\left(\frac{\mathrm{d}\delta n(z)}{\mathrm{d}z}\right)^2 = 2\Delta n^\star\delta n(z) + \big(\delta n(z)\big)^2. \tag{2.111}$$

If we define $z' = \xi\, z$ and $f(z') = \Delta n^\star\delta n(z) > 0$ Eq. (2.111) can be written as

$$\frac{\mathrm{d}f(z')}{\mathrm{d}z'} = -\sqrt{f^2(z') + 2f(z')}.$$

We can solve this differential equation by separation of variables. Integrating between z' and $\xi\, h/2$, where f vanishes, we obtain

$$\frac{h\,\xi}{2} - z' = \log\left[f(z') + 1 + \sqrt{f^2(z') + 2f(z')}\right]$$

and, if we come back to the original variables, the final solution for $\Delta n(z)$ reads

$$\Delta n(z) = \Delta n^\star\,\mathrm{Cosh}\left(\frac{h/2 - z}{\xi}\right).$$

If we take the limit of single wall, that is $h \to \infty$, the density at $h/2$ is asymptotically equal to the bulk density, $\Delta n^\star \to 0$ and the differential equation for the density profile (2.111) reduces to

$$\xi^2\left(\frac{\mathrm{d}\Delta n(z)}{\mathrm{d}z}\right)^2 = \big(\Delta n(z)\big)^2,$$

whose solution is the well known exponential decay

$$\Delta n(z) \sim \mathrm{e}^{-z/\xi}.$$

3

How roughness affects depletion

Interfaces play a crucial role in soft matter physics, from lubrication and bubble formation to the capillary rise of liquids in narrow tubes. Most of the so called surface phenomena can be understood through an idealised picture of the interface, that is usually regarded as an infinitely smooth object. However, in many circumstances natural and artificial interfaces are characterised by chemical heterogeneities, corrugations and roughness which originate new and unexpected phenomena, that are not predictable only relying on too idealised smooth surfaces.

It is well known that wetting in the presence of corrugations significantly differ from that of a smooth surface. In particular it is believed that roughness strongly amplifies the wetting properties of a given interface, making hydrophilic surfaces more hydrophilic and hydrophobic ones more hydrophobic [239]. This peculiar behaviour facilitates the fabrication of nano-hydrophobic devices which mimic plans, where the gain in hydrophobicity due to rough leaves [17, 118, 77] originates the so called the Lotus effect[1]. Furthermore, the spread of liquid drops on rough surfaces is not completely reversible: A hysteresis phenomenon is observed, such that the advancing and the receding contact angles usually differ by ten or more degrees [38].

As regards colloids, it has been shown that surface roughness deeply influences adsorption, motion, interaction and wetting properties of particles confined at liquid-liquid interfaces, with direct implications in the stabilisation of Pickering emulsions provided by colloidal particles [235, 203, 233]. In addition, the

[1] The dust particles present on leaves are adsorbed by water droplets, which roll off these surfaces leaving a clean surface.

deposition of colloids during transport processes in porous media, relevant for both inorganic and biological organisms, is affected by the presence of heterogeneities on colloidal particles: The retention and release rates appear to be strongly altered by surface roughness [207, 22, 223].
Also the amazing behaviour typical of all dense colloidal suspensions (non-Newtonian fluids) is amplified by the particles' surface roughness: If a force is suddenly applied to these systems, the material behaves like a solid, partly because surface roughness hinders the particle motion. Recent rheological studies proved that both shear thickening and Reynolds dilatancy [188] in concentrated suspensions, which are neither predicted by hydrodynamics nor friction, critically depend on particle roughness [107].
From a microscopic point of view, the presence of roughness has a crucial influence on the interaction potential between colloids: Strong deviations appear between the DLVO potentials between rough particles with respect the ones derived assuming ideally smooth surfaces [214, 18, 105]. Recent works [172, 215] show that small amounts of asperities suppress the deep attractive minimum of the DLVO interaction, where the van der Waals contribution dominates.

In this Chapter we will focus on the effects of surface roughness on the depletion potential between two colloidal particles. The pioneering works by Zhao and Mason [254, 255] and by Badaire, Cottin-Bizonne and Stroock [10], have undoubtedly pointed out that asperities on the colloid surface are able to suppress the depletion attraction. In addition, the tunable behaviour of depletion through surface roughness has proven to be suitable in order to control particle aggregation, explore different phases and design novel materials [16, 120, 191, 151, 244, 245]
Notwithstanding the widespread awareness of the effects of roughness on the depletion mechanism only few theoretical works have already dealt with this problem [13, 113], and a simple analytical or semi-analytical approach, able to capture the physics of the problem, is still missing. In particular, it would be interesting to determine how the geometry, the height and the concentration of corrugations can alter the depletion potential.

Here we provide an approximate theory for the evaluation of the depletion interaction between two rough spheres immersed in an ideal depletant. The proposed model is deliberately simple, so to provide analytical expressions for the effective potential without free parameters, both when roughness is fully uncorrelated and in the presence of correlated roughness, e.g. due to strong repulsion between defects on the surface. Within the limits of the theory, we show that this approximation is able to capture the essential features of the effective interaction in a significant range of physical parameters.
The first Section is an introduction to depletion interaction and gives a general argument which allows to obtain the potential between two particles in a mixture. The model is described and analysed in Section 3.2, where the limits of applicability to physical systems are also discussed. The results are compared with the recent simulations [113] in Section 3.3. In the same Section,

the dependence of the effective interaction on the size of the surface roughness and on its geometry are investigated. The implications of the different potential shapes on the efficiency of particle aggregation are also discussed.
The main results of this Chapter have been published in Ref. [5].

3.1 DEPLETION INTERACTION

The study of solvent-mediated interactions in colloids dates back to the seminal works by Asakura and Oosawa (AO) [6, 7]: Two colloidal particles suspended in a polymer solution suffer an effective attraction, referred to as depletion interaction, arising from the depletion of solutes between them. This entropic[2] force is due to the the osmotic pressure arising between the bulk solution, characterised by uniform density, and the polymer-free zone, i.e. the region between the colloids when their surface-to-surface distance is less than the polymer diameter.
In their work [7], Asakura and Oosawa limited to a system where the depletant is a dilute gas of polymers, the colloidal particles are hard spheres much bigger than the polymers and the mutual interaction between colloids and depletant is of the excluded volume type. The AO potential reads [7]

$$\beta v_{\mathrm{AO}}(r)=\begin{cases}+\infty & 0\le r<2R\\ -\rho\,\dfrac{\pi}{12}\left[2(\sigma+2R)^2-3(\sigma+2R)^3\,r+r^3\right] & 2R\le r<2R+\sigma\\ 0 & r\ge 2R+\sigma\end{cases} \tag{3.1}$$

where ρ is the polymer density, $\beta = 1/k_{\mathrm{B}}T$, R is the colloid radius, σ is the polymer diameter and r is the distance between colloid centers. The range of the interaction, referred to as *depletion interaction*, equals the depletant diameter, whereas its strength is linear with polymer density. Even if the original analysis focused the attention on two colloidal spherical particles [7], it has been shown that the AO result is correct for an arbitrary number of colloidal particles when the size ratio

$$q = \frac{\sigma}{2R} \tag{3.2}$$

between the depletant and colloidal diameter is less than 0.155 [50]. In other words, it is possible to map exactly a binary AO mixture into an effective one component system interacting through the AO pair potential.
Some years later, Richmond and Lal [189] considered the depletion interaction between two walls, which was the problem initially tackled by Asakura and Oosawa [6], in the semi-dilute limit. These results were refined by Joanny,

[2]Strictly speaking, a purely entropic interaction arises only if the inter-particle interactions are of excluded volume type.

Leibler and de Gennes [111]: By means of scaling arguments, they showed that the attractive potential between two colloids has a range equal to $\pi\xi$, where ξ is the correlation length of the polymers, and is given by

$$\beta v_{\mathrm{deG}}(h) \sim -\frac{R}{\xi^3}\,(\pi\xi - h)^3, \qquad 0 \le h \le \pi\xi, \tag{3.3}$$

where $h = r - 2R$ is the surface-to-surface distance between the colloids. To complete this historical review about depletion in polymers, a detailed study was presented by Vrij in 1976 [237]: In particular, this work deals with the aggregation of colloidal suspensions in the presence of polymers, discovered by Vester many years before [234].

More realistic hard sphere potentials between depletants introduce strong oscillations in the depletion potential. Many results obtained by means of theoretical and simulation approaches can be found in the literature [193, 8], and some results have been shown in Section 2.4 (Effective interaction between spherical particles).

Asakura-Oosawa potential

The explicit expression of the Asakura-Oosawa potential (3.1) can be obtained following different routes. The most common one relies on the application of the semi-grand canonical formalism, where the colloidal particles are described within the canonical ensemble, while the depletant degrees of freedom are integrated out in the grand canonical ensemble [98].
Here we tackle the problem of depletion interaction through a more general approach with respect to that originally adopted by Asakura and Oosawa. In what follows, a mixture of ν components acts as the depletant, taking the place of the polymeric solvent considered in Ref. [7]. Exploiting the potential distribution theorem, we evaluate the depletion potential between a fixed object of any shape and a *test* particle of a given species, without any constraint on the densities and on the inter-particle potentials [88, 193]. Eq. (3.1) then follows specifying the result to a binary mixture of colloids and ideal polymers and taking the dilute limit for the colloids.

Let us consider a system in equilibrium at temperature T, consisting of a mixture of ν components with chemical potentials $\{\mu_\gamma\} = (\mu_1, \ldots, \mu_\nu)$, in the presence of an external object that we assume fixed in the origin of the coordinate system (without any loss of generality). The particles of species α are subject to an external potential $\phi_\alpha(\boldsymbol{r})$ due to the presence of the fixed object and all the interactions are supposed to be pair-wise additive. The target is to evaluate the potential $v_{t_b}(\boldsymbol{r})$ acting between the fixed object and

a test particle of species b[3] at position $\boldsymbol{r}$, which is given by

$$v_{t_b}(\boldsymbol{r}) = \Omega_{t_b}\big(\boldsymbol{r};\{\mu_\gamma\},T\big) - \Omega_{t_b}\big(\boldsymbol{r};\{\mu_\gamma\},T\big)\Big|_{|\boldsymbol{r}|\to\infty}, \tag{3.4}$$

where

$$\Omega_{t_b}\big(\boldsymbol{r};\{\mu_\gamma\},T\big) = \frac{1}{\beta}\log\Big[\mathcal{Q}_{t_b}\big(\boldsymbol{r};\{\mu_\gamma\},T\big)\Big]$$

is the grand potential of the system when the test particle t_b is located at $\boldsymbol{r}$. The potential distribution theorem allows to express the grand canonical partition function (and therefore the grand potential) of the system after the insertion of the particle in terms of the grand canonical partition function of the mixture $\mathcal{Q}(\{\mu_\gamma\},T)$ without the test particle as [241, 242, 102, 198]:

$$\mathcal{Q}_{t_b}\big(\boldsymbol{r};\{\mu_\gamma\},T\big) = \Lambda_b^3\,\rho_b(\boldsymbol{r})\,\mathcal{Q}\big(\{\mu_\gamma\},T\big)\,\mathrm{e}^{\,\beta\left(\phi_b(\boldsymbol{r})-\mu_b\right)}, \tag{3.5}$$

where Λ_b is the de Broglie wavelength associated to species b and

$$\Omega\big(\{\mu_\gamma\},T\big) = \frac{1}{\beta}\log\Big[\mathcal{Q}\big(\{\mu_\gamma\},T\big)\Big].$$

Here $\rho_b(\boldsymbol{r})$ is the equilibrium density profile of the species b without the test particle, holding the same symmetries of the external field due to the fixed body.

As shown in Section 2.2, it is possible to relate the equilibrium density profile to the one-particle direct correlation function. The generalisation of Eq. (2.26) in mixtures reads

$$\rho_\alpha(\boldsymbol{r}) = \frac{1}{\Lambda_\alpha^3}\,\exp\Big\{\beta\big[\mu_\alpha - \phi_\alpha(\boldsymbol{r})\big] + c_\alpha^{(1)}\big(\boldsymbol{r};\{\mu_\gamma\},T\big)\Big\}, \tag{3.6}$$

where the one-particle direct correlation function $c_\alpha^{(1)}(\boldsymbol{r};\{\mu_\gamma\},T)$ of the species α is given by

$$c_\alpha^{(1)}\big(\boldsymbol{r};\{\mu_\gamma\},T\big) = -\beta\,\frac{\delta\mathcal{F}^{\mathrm{ex}}[\{n_\gamma(\boldsymbol{r}')\}]}{\delta n_\alpha(\boldsymbol{r})}\bigg|_{\{\rho_\gamma(\boldsymbol{r}')\}}, \tag{3.7}$$

$\mathcal{F}^{\mathrm{ex}}$ is the excess free energy functional of the mixture and the functional derivative in Eq. (3.7) is evaluated at the equilibrium density profiles of the species $\{\rho_\gamma(\boldsymbol{r})\}$.

Making use of Eq. (3.6) in Eq. (3.5) we can express the correlation function as

$$c_b^{(1)}\big(\boldsymbol{r};\{\mu_\gamma\},T\big) = \beta\big[\Omega\big(\{\mu_\gamma\},T\big) - \Omega_{t_b}\big(\boldsymbol{r};\{\mu_\gamma\},T\big)\big] \tag{3.8}$$

[3]Without any loss of generality, we assume that the species b belongs to the mixture.

and the interaction potential (3.4) can be finally written as

$$\beta v_{t_b}(\boldsymbol{r}) = c_b^{(1)}\big(\boldsymbol{r};\{\mu_\gamma\},T\big)\Big|_{|\boldsymbol{r}|\to\infty} - c_b^{(1)}\big(\boldsymbol{r};\{\mu_\gamma\},T\big) \tag{3.9}$$

$$= \frac{\delta\beta\mathcal{F}^{\mathrm{ex}}[\{n_\gamma(\boldsymbol{r}')\}]}{\delta n_b(\boldsymbol{r})}\bigg|_{\{\rho_\gamma(\boldsymbol{r})\}} - \frac{\delta\beta\mathcal{F}^{\mathrm{ex}}[\{n_\gamma(\boldsymbol{r}')\}]}{\delta n_b(\boldsymbol{r})}\bigg|_{\{\rho_\gamma(\boldsymbol{r})\},|\boldsymbol{r}|\to\infty} \tag{3.10}$$

This identity is exact and holds for any inter-particle potential and for arbitrary densities of the components of the mixture, because the potential distribution theorem is an exact result and we have not made further assumptions in the derivation. The potential is expressed in terms of one-particle correlation functions, or in terms of the derivatives of the excess free energy functional, of the binary mixture *without* the test particle. Therefore, the symmetry of these quantities coincides with the symmetry of the external object fixed in the origin.

The accuracy of the depletion potential given by Eq. (3.9) critically depends on the reliability of the correlation function of the mixture in the presence of the potential produced by the fixed body. Monte Carlo simulations are good candidates in order to provide correlation functions. Moreover, if the external potential due to the fixed object is characterised by a simple symmetry (e.g. spherical, planar ...), also the density functional approximations prove to be accurate and fast tools for evaluating correlations.

In order to obtain an analytical expression from Eq. (3.9), let us introduce some additional assumptions. We restrict our attention to a binary mixture: The component characterised by the smaller radius is the depletant (d), whereas the other component represents the colloid (c). Furthermore, both the object fixed in the origin and the test particle are colloids.

If the depletant is an ideal gas and the colloids are diluted[4], that is if $\mu_c \to -\infty$, it is possible to show by means of a diagrammatic expansion that the free energy functional can be written *exactly* as

$$\beta\mathcal{F}^{\mathrm{ex}}[\{n_\gamma(\boldsymbol{r}')\}] = -\frac{1}{2}\sum_{\alpha,\gamma=c,d}\int \mathrm{d}\boldsymbol{r}\int \mathrm{d}\boldsymbol{r}' n_\alpha(\boldsymbol{r}) f_{\alpha\gamma}(\boldsymbol{r}-\boldsymbol{r}') n_\gamma(\boldsymbol{r}'), \tag{3.11}$$

where

$$f_{\alpha\gamma}(\boldsymbol{r}) = \mathrm{e}^{-\beta v_{\alpha\gamma}(\boldsymbol{r})} - 1 \tag{3.12}$$

is the Mayer function between species α and γ which interact through a potential $v_{\alpha\gamma}(\boldsymbol{r})$. Under the hypothesis introduced above $f_{dd}(\boldsymbol{r}) = 0$, because the depletant is an ideal gas, and the free energy functional is given by

$$\beta\mathcal{F}^{\mathrm{ex}}[\rho_d(\boldsymbol{r}),\rho_c(\boldsymbol{r})] = -\int \mathrm{d}\boldsymbol{r}\int \mathrm{d}\boldsymbol{r}'\rho_d(\boldsymbol{r}) f_{dc}(|\boldsymbol{r}-\boldsymbol{r}'|)\rho_c(\boldsymbol{r}'), \tag{3.13}$$

[4]Asakura and Oosawa were mainly interested into the effective potential between two colloids.

where the contribution involving $f_{cc}(\boldsymbol{r})$ is quadratic in the density and has not been retained. The direct correlation function of the colloids follows from a straightforward functional derivation of (3.13) with respect to $\rho_c(\boldsymbol{r})$ and the depletion potential between the colloids (3.10) reads

$$\begin{aligned}\beta v_{\mathrm{D}}(\boldsymbol{r}) &= \int \mathrm{d}\boldsymbol{r}' \rho_d(\boldsymbol{r}')\, f_{dc}(|\boldsymbol{r}'' - \boldsymbol{r}'|)\big|_{|\boldsymbol{r}''|\to\infty} - \int \mathrm{d}\boldsymbol{r}' \rho_d(\boldsymbol{r}')\, f_{dc}(|\boldsymbol{r} - \boldsymbol{r}'|) \\ &= \int \mathrm{d}\boldsymbol{r}' \big[\rho_d(|\boldsymbol{r}| \to \infty) - \rho_d(\boldsymbol{r}')\big]\, f_{dc}(|\boldsymbol{r} - \boldsymbol{r}'|), \end{aligned} \tag{3.14}$$

where the second line holds because the Mayer function is different from zero only if $|\boldsymbol{r}'| \simeq |\boldsymbol{r}''| \to \infty$. Furthermore, the density profile of the ideal gas of depletants in the presence of the fixed particle in the origin is given by the well-known barometric law:

$$\rho_d(\boldsymbol{r}) = \rho\, \mathrm{e}^{-\beta v_{dc}(|\boldsymbol{r}|)},$$

where we have defined $\rho_d(|\boldsymbol{r}| \to \infty) \equiv \rho$ and ρ is the polymer density imposed by the reservoir.
The final result under the hypothesis of ideal depletant and dilute colloids can be written as

$$\beta v_{\mathrm{D}}(\boldsymbol{r}) = -\rho \int \mathrm{d}\boldsymbol{r}'\, f_{dc}(|\boldsymbol{r}'|) f_{dc}(|\boldsymbol{r} - \boldsymbol{r}'|) \tag{3.15}$$

and this result is valid for any depletant-colloid potential $v_{dc}(|\boldsymbol{r}|)$.

Following Asakura and Oosawa we assume that the mutual interaction between colloids and depletants is of the excluded volume type. In this case the product of the Mayer functions is non vanishing only when the two depletion layers[5] around the colloids overlap.
The Asakura-Oosawa potential between two hard sphere colloids can be therefore written as

$$\beta v_{\mathrm{AO}}(r) = \begin{cases} +\infty & \text{if the two particles overlap} \\ -\rho\, V^{\mathrm{ov}}(r) & \text{if the two depletion layers overlap} \\ 0 & \text{elsewhere} \end{cases} \tag{3.16}$$

where the potential only depends on the center-to-center distance r between the colloids and $V^{\mathrm{ov}}(r)$ is the overlap volume at a given r.
Eq. (3.16) reduces to Eq. (3.1) if the overlap volume between two spheres of diameter $2R + \sigma$ is evaluated explicitly as a function of the separation r.

Highly size-asymmetric mixtures

A peculiar prediction of the AO model is that the strength of attraction increases with the size of the colloidal particles, at fixed solute volume fraction,

[5] The depletion layer is the region outside the colloid which is not allowed to the depletant due to the core condition.

implying that macroscopic objects should feel extremely large attractive forces at short distances. This paradoxical circumstance becomes evident considering the *contact value* of the AO potential, which diverges as the size ratio (3.2) tends to zero:

$$\beta v_{\mathrm{AO}}^{(c)} = -\eta \left(1 + \frac{3}{2q}\right), \tag{3.17}$$

where η is the polymer reservoir packing fraction. Such a strong, short-ranged, divergence implies that smooth colloidal particles immersed in a molecular solvent would stick together due to depletion interactions. This non-physical behaviour, which contrasts with our daily experience, originates from neglecting the irregularity of any particle surface on molecular scales and in itself calls for a generalisation of the AO approach to include the effects of surface roughness.

It is well known, starting from the studies by Pine and coworkers [52, 51, 147], that surface geometry strongly affects the overlap volumes, leading to the suppression or the enhancement of the depletion interaction [195, 27]. Increasing the overlap volumes reflects in a stronger depletion potential to the point of allowing the realisation of site specific interactions between colloidal particles, as theoretically predicted and experimentally shown in recent works regarding lock-and-key colloids [119, 202]. Furthermore, it has been experimentally shown [10, 254] that depletion attraction between rough colloids can be suppressed when the height of the asperities becomes larger than the depletant because the overlap volume is significantly reduced by a small amount of surface corrugation.

Even if the effects of roughness on depletion have been recognised and exploited in many situations, only a limited number of studies dealing with solvent-mediated interaction between rough objects can be found in the literature.

Zhao and Mason [255] investigated the problem by computing the minimum of the depletion potential between platelets decorated by hemispherical asperities with different height, radius and configurations, and their results corroborate previous experimental findings [254].

More recently, Schweizer and collaborators tackled the question of the role of surface topography on the depletion interaction through a hybrid Monte Carlo plus integral equation theory approach [13]. They consider the interaction between corrugated "raspberry" particles immersed in a hard sphere polymer fluid for different size ratios and packing fractions, finding that the resulting effective interaction is affected by the competition among the standard depletion and the excess entropic contributions arising from the fluid present within the surface interstices. The analysis shows that surface corrugation suppresses the depletion induced aggregation for values of the depletant diameter close to the height of the roughness.

A recent work [113] evaluates, by means of Monte Carlo simulations, the effective potential between two spherical hard colloids, whose surface is decorated with smaller spherical particles, immersed in an ideal depletant, comparing

the results with experiments in a colloidal suspension of silica particles. An interesting outcome of this work is that the best reduction of the depletion potential is obtained for incomplete surface coverings and for a depletant with approximately the same size as the particles attached to the colloidal surface.

Despite the theoretical efforts devoted to this problem, a simple analytical or semi-analytical approach able to capture the physics of the problem is still missing: In particular it would be interesting to determine how the geometry, the height and the concentration of corrugations can alter the depletion potential. Although numerical simulations are a powerful tool to investigate the effects of roughness on the depletion mechanism, they cannot be efficiently performed for the evaluation of the effective interaction in a wide range of parameters characterising the particle corrugation. For instance, Ref. [13] deals only with hemispherical roughness which appears to be strongly correlated, whereas in Ref. [113] a single geometry and a single value of the dimension of the particles which cover the colloidal surface are considered. Furthermore these approaches are not suitable to give a quick estimate of the properties of the potential and of aggregation, which is critical for an experimentalist interested in the behaviour of colloidal suspension in presence of entropic interactions.

3.2 THE MODEL

Let us consider two hard colloidal spheres of radius R, whose surface is divided in patches of area $A \ll R^2$. Each patch can accommodate at most one bump of height ϵ, which represents the roughness. The projection of each bump on the surface of the colloid is a circle of radius a, so the bumps can be viewed as spheres, cylinders, hemispheres and so on. To reduce the number of parameters of the model, we do not allow for a statistical distribution in the dimensions and geometry of the bumps. A relevant parameter of the model is the total number N of bumps on the sphere, which defines the dimensionless coverage c as the fraction of the spherical surface covered by bumps:

$$c = N\frac{a^2}{4R^2}. \tag{3.18}$$

The two colloidal particles are set at a center-to-center distance r and immersed in an ideal gas of particles (typically polymers), modelled as spheres of diameter $\sigma \ll R$, suffering a hard core repulsion with the rough colloidal surface.

Following the classical Asakura-Oosawa approach [7], the solvent-mediated interaction between the two corrugated spheres can be obtained evaluating the overlap volumes for each realisation of the disorder which characterises the roughness of the two spheres. If the patch is small enough so that the colloidal surface can be considered flat on the scale of the patch size, it is possible to reduce the difficulty of the evaluation of the overlap volume resorting to Derjaguin approximation for each patch. For a given realisation of the

roughness and for a center-to-center distance r at which the colloids do not overlap we write:

$$V^{\mathrm{ov}}(r) = \sum_j V_j^{\mathrm{ov}}(r), \tag{3.19}$$

where the sum over j runs over all the patches and $V_j^{ov}(r)$ is the overlap volume generated by the intersection of the excluded volume of the patch j on one sphere with the excluded volume belonging to the corresponding facing patch j on the other sphere.
Due to thermal motion, the rough colloidal particles immersed in the depletant approach from different directions and accordingly the effective interaction results to be the average over all the orientations of the two colloidal particles. Within our formalism, this average process can be mimicked by performing an average over different realisations of the disorder. This amounts to compute

$$\beta v_{\mathrm{eff}}(r) = -\log\left\langle \mathrm{e}^{-\beta v_{\mathrm{AO}}(r)}\right\rangle, \tag{3.20}$$

where angular brackets denote a statistical average over uncorrelated disorder on the two spherical surfaces.

By taking the colloid diameter $2R$ as a length unit, our model is defined by five parameters: The bump dimensions ϵ and a and the coverage c characterising the sphere roughness; the size ratio q and the reservoir density z_p characterising the polymer solution.

Uncorrelated roughness

We begin by considering the case of uncorrelated roughness within each colloidal particle, i.e. when the bumps are located randomly on the colloidal surface. Initially we will focus on the effective potential between two rough spheres without depletant: In this peculiar situation the average can be carried out analytically. The only purpose of this "pedagogical" example is to introduce the reader to the evaluation of averages and to the geometry of the problem. After this simple calculation, we will derive the general expression for the depletion potential at a given non-zero concentration of depletant.

Effective interaction at zero concentration of depletant

Let us consider two colloidal particles randomly corrugated as shown in Fig. 3.1. We divide the colloidal particle surface in circular patches of radius a and area $A = \pi a^2$, which host with probability c at most a single bump of height ϵ. In the absence of depletant the overlap volume (3.19) vanishes, and the Asakura-Oosawa potential (3.16) assumes only two values: It is equal to zero when the corrugated colloidal *particles* do not overlap, whereas it is infinitely repulsive when the the corrugated colloids overlap. Note that the

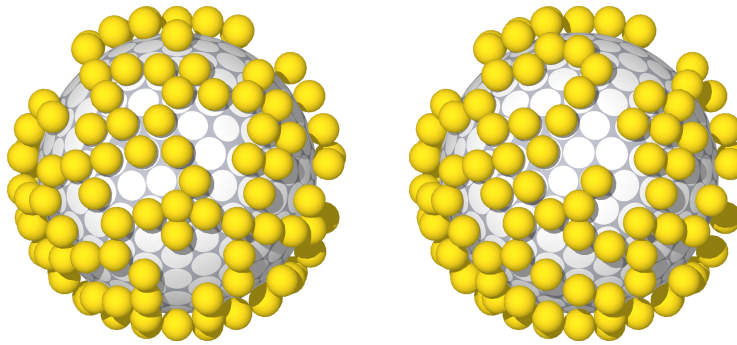

Figure 3.1: Two facing spheres characterised by uncorrelated roughness. At fixed covering c, the patches of radius a are occupied with probability c by spheres of the same radius.

overlap can be originated by two bumps, by an empty patch and a bump and by two empty patches.
The contribution to the average over the disorder (3.20) due to overlapping configurations vanishes, because the associated potential is infinitely repulsive. On the other hand, the contribution to the average arising from non-overlapping configurations equals the probability of the configuration, because the exponential in (3.20) equals one. Therefore, the average over the disorder reduces to

$$\beta v_{\text{eff}}(r) = -\log\left[P_{\text{no}}(r)\right],$$

where $P_{\text{no}}(r)$ is the fraction of non-overlapping (no) random configurations of *bumps* on two facing colloids at center-to-center distance r.
If the two colloidal particles are placed at a center-to-center distance $r < 2R$ the probability of non-overlapping configurations is equal to zero, and the effective potential will be infinitely repulsive $v_{\text{eff}}(r) = \infty$. The opposite circumstance presents when $r < 2R + 2\epsilon$: In this case the probability of a non-overlapping configuration of surface roughness is equal to one, and $v_{\text{eff}}(r) = 0$.
The situation becomes more complex when $2R \leq r \leq 2R + 2\epsilon$. Let us first consider the case shown in Fig.3.2, where the center-to-center distance is $2R + \epsilon < r \leq 2R + 2\epsilon$. Outside the spherical cap determined by the angle θ_1 any roughness configuration is possible. According to Derjaguin approximation, inside the cap the non-vanishing contribution to (3.20) comes from configurations such that any pair of facing patches host at most a single bump (if two facing patches host two bumps, the configuration is overlapping). The fraction of non-overlapping configurations of bumps is given by

$$P_{\text{no}}(r) = \left[2c(1-c) + (1-c)^2\right]^{\nu_c(\theta_1)}, \tag{3.21}$$

where $\nu_c(\theta_1)$ is the number of patches of area πa^2 hosted inside the spherical cap determined by the angle θ_1. If we assume $a, \epsilon \ll R$ elementary geometry

gives

$$\nu(\theta_1) \simeq \frac{R}{a^2}(2R + 2\epsilon - r) \tag{3.22}$$

and the effective potential for $2R + \epsilon \leq r \leq 2R + 2\epsilon$ can be written as

$$\beta v_{\text{eff}}(r) = -\frac{R}{a^2}(2R + 2\epsilon - r)\log(1 - c^2). \tag{3.23}$$

Now let us focus our attention to the configurations at distance $2R \leq r < 2R + \epsilon$ shown in Fig. 3.3. Inside the spherical cap defined by the angle θ_2 the patch-to-patch distance is less than ϵ, and only empty patches do not overlap. Furthermore, the patches belonging to the spherical shell, obtained by subtracting the spherical cap defined by the angle θ_2 from the spherical cap with angle θ_1, are separated more than ϵ but less than 2ϵ. Therefore a pair of facing patches belonging to this spherical shell can accommodate at most a single bump. The probability $P_{\text{no}}(r)$ when $2R \leq r < 2R + \epsilon$ is then given by

$$P_{\text{no}}(r) = \left[2c\,(1 - c) + (1 - c)^2\right]^{\nu_s(\theta_1,\theta_2)} \times \left[(1 - c)^2\right]^{\nu_c(\theta_2)}, \tag{3.24}$$

where $\nu_s(\theta_1, \theta_2)$ is the number of patches of area πa^2 hosted inside the spherical shell defined by the angles θ_1 and θ_2. Also in this case it is straightforward to show that:

$$\nu_s(\theta_1, \theta_2) \simeq \frac{R}{a^2}(2R + \epsilon - r), \qquad \nu_c(\theta_2) \simeq \frac{R}{a^2}\epsilon,$$

and the contribution to the effective potential is

$$\beta v_{\text{eff}}(r) = -\frac{2R}{a^2}(2R + \epsilon - r)\log(1 - c) - \frac{R}{a^2}\epsilon\log(1 - c^2). \tag{3.25}$$

Summing up, the effective potential is purely repulsive and reads

$$\beta v_{\text{eff}}^{(\eta=0)}(r) = \begin{cases} +\infty & r < 2R \\ -\left(\dfrac{2R}{a}\right)^2 \left[\left(1 + \dfrac{\epsilon}{2R} - \dfrac{r}{2R}\right) f(c) + \dfrac{\epsilon}{2R} g(c)\right] & 2R \leq r < 2R + \epsilon \\ -\left(\dfrac{2R}{a}\right)^2 \left(1 + \dfrac{\epsilon}{R} - \dfrac{r}{2R}\right) g(c) & 2R + \epsilon \leq r < 2R + 2\epsilon \\ 0 & r \geq 2R + 2\epsilon \end{cases} \tag{3.26}$$

where $f(c) = \log(1 - c)$ and $g(c) = \log\sqrt{1 - c^2}$. As shown by Fig. 3.4, the potential shows a simple behaviour: It vanishes for $r \geq 2R + 2\epsilon$ while for $2R < r < 2R + 2\epsilon$ it is formed by two straight lines with different slopes, proportional to $f(c)$ and $g(c)$, joined at $r = 2R + \epsilon$.

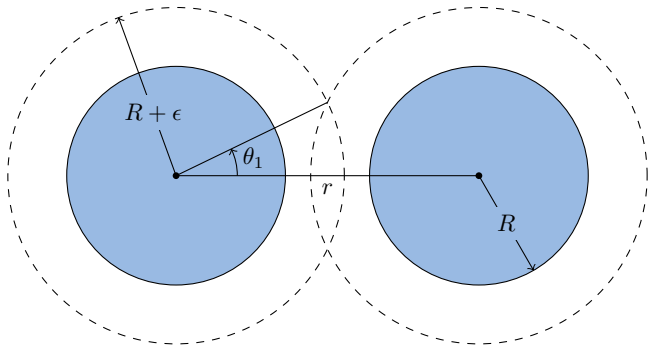

Figure 3.2: Colloidal particles of radius R at a center-to-center distance $2R+\epsilon < r \leq 2R+2\epsilon$. The dashed line represents the local effective radius of the colloid when the patch hosts a bump.

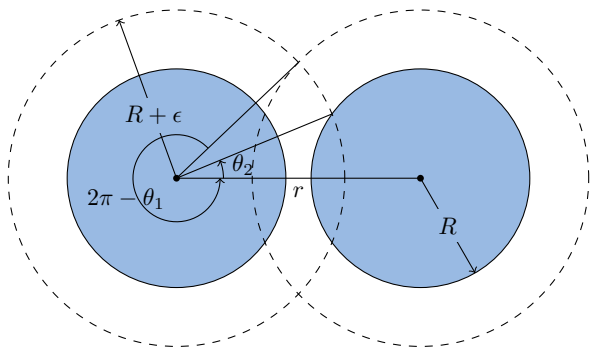

Figure 3.3: Colloidal particles of radius R at a center-to-center distance $2R \leq r < 2R+\epsilon$. The dashed line represents the local effective radius of the colloid when the patch hosts a bump.

Effective interaction at non-zero concentration of depletant

In order to evaluate the average over the disorder when the colloids are immersed in the ideal depletant we follow the same procedure outlined before, dividing the colloidal particle surface in circular patches of radius a, area $A=\pi a^2$ and covered by a bump with probability c.
In this case the evaluation is more complex because we have to account for the overlap volume generated by the depletion layers of the particles and of the bumps. Resorting to Derjaguin approximation, the overlap volume $V^{\rm ov}(r)$ can be written as in Eq. (3.19). Then the average of the Boltzmann weight over different realisations of disorder is given by

$$\left\langle \mathrm{e}^{-\beta v(r)} \right\rangle = \prod_j \left[c^2 \chi_j^{11} \mathrm{e}^{z_p V_j^{11}} + 2c(1-c)\chi_j^{10} \mathrm{e}^{z_p V_j^{10}} + (1-c)^2 \chi_j^{00} \mathrm{e}^{z_p V_j^{00}} \right], \quad (3.27)$$

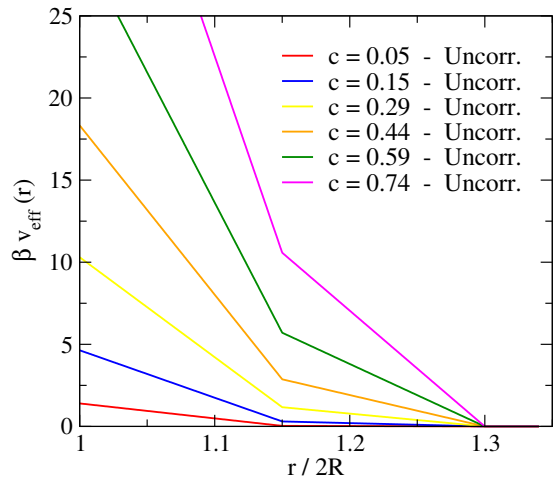

Figure 3.4: Lines: Effective potential between two rough hard spheres (spherical bumps $\epsilon = 2a$) as a function of center-to-center separation at $\eta = 0$. The diameter of a spherical bump is $\epsilon/2R = 0.15$, whereas the covering is varied as shown. The curves are evaluated by means of Eq. (3.26)

where the index j labels the patches on each sphere; the pair of indices (11), (10) and (00) label the three possibilities of having a bump on the facing patches of both spheres, having a bump only on one patch and having no bumps in both patches; $\chi_j^{\mu\nu} = 0, 1$ according whether the configuration $(\mu\nu)$ is possible (i.e. does not violate the hard core constraint) for the patches labelled by j; $V_j^{\mu\nu}$ is just a geometrical quantity, which depends on the shape of the bumps and on the distance between the two facing patches j, defining the overlap volume of the depletion layers for the patch configuration $(\mu\nu)$. Taking the logarithm of Eq. (3.27) and evaluating the sum in terms of an integral over the surface of the colloidal particle, we get

$$\beta v_{\rm eff}(r) = -\frac{2\pi R^2}{A}\int_0^\pi {\rm d}\theta\, \sin\theta\, \log\Big[c^2\chi^{11}{\rm e}^{z_p V^{11}} + 2\,c\,(1-c)\chi^{10}{\rm e}^{z_p V^{10}} + (1-c)^2\chi^{00}{\rm e}^{z_p V^{00}}\Big], \qquad (3.28)$$

where, at fixed center-to-center distance r, the factors $\chi^{\mu\nu}$ and $V^{\mu\nu}$ both depend on the angular coordinate θ. The relation which links, at fixed r, the patch-to-patch distance h_r with θ

$$h_r(\theta) = r - 2\,R\,\cos\theta \qquad (3.29)$$

allows to convert the angular integral in (3.28) into an integral over h, leading to our final expression for the average effective interaction:

$$\beta v_{\text{eff}}(r) = -\frac{R}{a^2}\int_{r-2R}^{2\epsilon+\sigma} \mathrm{d}h\, \log\Big[c^2\Theta(h-2\epsilon)e^{z_p V^{11}} + 2\,c\,(1-c)\Theta(h-\epsilon)e^{z_p V^{10}} + (1-c)^2 e^{z_p V^{00}}\Big], \tag{3.30}$$

where the factors $\chi^{\mu\nu}$ have been defined as

$$\chi^{\mu\nu}(h) = \begin{cases} 1 & \text{if } h > (\mu+\nu)\,\epsilon \\ 0 & \text{elsewhere} \end{cases}$$

and $\Theta(\cdot)$ is the Heaviside step function. The overlap volumes $V^{\mu\nu}(h)$ depend on the shape of the bumps representing the surface roughness, and always vanish for $h > (\mu+\nu)\,\epsilon + \sigma$. If we assume spherical bumps of diameter $\epsilon = 2a$, as in the recent numerical study [113], the explicit expressions are:

$$\begin{aligned} V^{11}(h) &= \frac{\pi}{6}\,(\epsilon + 2\sigma + h)\,(2\epsilon + \sigma - h)^2 && \epsilon+\sigma < h < 2\,\epsilon+\sigma \\ V^{10}(h) &= \frac{\pi}{6}\,(\epsilon + \sigma + 2h)\,(\epsilon + \sigma - h)^2 && \sigma < h < \epsilon+\sigma \\ V^{00}(h) &= \pi\frac{\epsilon^2}{4}(\sigma - h) && 0 < h < \sigma \end{aligned} \tag{3.31}$$

For each geometry of the bumps the effective potential is easily obtained evaluating numerically the integral in Eq. (3.30).

Correlated roughness

In the experimental realisations of surface roughness, bumps are often electrically charged [113]. The occurrence of repulsive interactions can favour a more homogeneous covering of the particle surface: In this situation the bumps are randomly distributed on the colloid, but at the same time long-range fluctuations are inhibited (see Fig. 3.5). This behaviour is expected to be more relevant at high coverings, when the distance of bumps reduces.
In order to model this situation, we require that each patch of area A accommodates exactly one bump, whose projection on the patch surface is $\pi a^2 < A$. The bump is placed randomly within the patch and A is determined by enforcing the surface covering condition $NA = 4\pi R^2$ (in this case N is both the number of patches and of bumps) which leads through Eq. (3.18) to

$$A = \frac{\pi a^2}{c}.$$

Once again for the calculation of the overlap volumes we resort to Derjaguin approximation for each patch and the statistical average in Eq. (3.20) is now

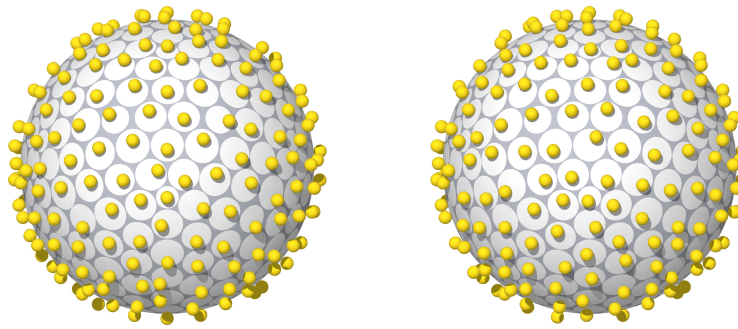

Figure 3.5: Two facing spheres characterised by correlated roughness. At fixed covering c, all the patches of radius $a/\sqrt{c} > a$ are occupied a sphere of radius a located randomly within the patch.

performed over the random location of the bump in the patch. In the case of spherical bumps Eq. (3.27) is replaced by:

$$\left\langle \mathrm{e}^{-\beta v(r)} \right\rangle = \prod_j \left[\frac{1}{A^2} \int \mathrm{d}\boldsymbol{r}_1 \, \mathrm{d}\boldsymbol{r}_2 \, \Theta\left(d_{h_j}(|\boldsymbol{r}_1 - \boldsymbol{r}_2|) - \epsilon \right) \, \mathrm{e}^{z_p V_j(|\boldsymbol{r}_1 - \boldsymbol{r}_2|)} \right],$$

where $\boldsymbol{r}_1$ and $\boldsymbol{r}_2$ are the locations of the two bumps hosted by the facing patches labelled by j, h_j is the distance between the two facing patches (3.29) and the couple of two-dimensional integrals are extended to the surface of a single patch. The surface-to-surface distance between the bumps is

$$d_{h_j}(|\boldsymbol{r}_1 - \boldsymbol{r}_2|) = \sqrt{|\boldsymbol{r}_1 - \boldsymbol{r}_2|^2 + (h_j - \epsilon)^2} \tag{3.32}$$

and V_j is the overlap volume between the depletion layers. Following the same steps which lead to Eq. (3.30) we get

$$\beta v_{\mathrm{eff}}(r) = -\pi \frac{R}{A} \int_{r-2R}^{2\epsilon+\sigma} \mathrm{d}h \, \log \left[\frac{1}{A^2} \int \mathrm{d}\boldsymbol{r}_1 \, \mathrm{d}\boldsymbol{r}_2 \right.$$
$$\left. \Theta\big(d_h(|\boldsymbol{r}_1 - \boldsymbol{r}_2|) - \epsilon\big) \, e^{z_p V(|\boldsymbol{r}_1 - \boldsymbol{r}_2|, h)} \right], \tag{3.33}$$

where d_h has been defined above in Eq. (3.32). The overlap volume can be expressed as the sum of two terms:

$$V(|\boldsymbol{r}_1 - \boldsymbol{r}_2|, h) = 2\, V^{10}(h) + V^{11}\big(d_h(|\boldsymbol{r}_1 - \boldsymbol{r}_2|)\big), \tag{3.34}$$

where V^{10} does not depend on the difference $\boldsymbol{r}_1 - \boldsymbol{r}_2$ and coincides with Eq. (3.31), whereas

$$V^{11}(d) = \frac{\pi}{12} \, (2\epsilon + 2\sigma + d) \, (\epsilon + \sigma - d)^2 \qquad\qquad \epsilon < d < \epsilon + \sigma$$

Substituting the expression for the overlap volume of Eq. (3.34) in Eq. (3.33), we obtain our final result for the effective potential in the case of short-range correlated roughness:

$$\beta v_{\text{eff}}(r) = -\frac{R}{s^2}\left[2\,\rho \int_{r-2R}^{\epsilon+\sigma} \mathrm{d}h\, V^{10}(h) + \int_{r-2R-\epsilon}^{\epsilon+\sigma} \mathrm{d}\xi\, \log \mathcal{K}(\xi)\right], \tag{3.35}$$

where in the second integral on the r.h.s. the change of variable $\xi = h - \epsilon$ has been performed. The function $\mathcal{K}(\xi)$ is defined:

$$\mathcal{K}(\xi) = \frac{1}{\left(\pi s^2\right)^2} \int_{|\boldsymbol{r}_1|<s} \mathrm{d}\boldsymbol{r}_1 \int_{|\boldsymbol{r}_2|<s} \mathrm{d}\boldsymbol{r}_2\, f\left(|\boldsymbol{r}_1 - \boldsymbol{r}_2|; \xi\right), \tag{3.36}$$

where

$$f(r;\xi) = \Theta\left(\sqrt{r^2+\xi^2} - \epsilon\right)\, \mathrm{e}^{z_p\, V^{11}\left(\sqrt{r^2+\xi^2}\right)} \tag{3.37}$$

and $s = a/\sqrt{c}$ is the radius of the patch. The numerical evaluation of the integrals (see the Appendix for details) provides the effective potential.

Approximations and range of parameters

The expressions for the effective potential obtained above within the AO framework (i.e. ideal depletant) mainly rely on the patch-to-patch evaluation of the overlap volume coupled with Derjaguin approximation. In addition, we assume that the size and the geometry of the bumps are the same for each bump and we do not allow for multiple occupancy of the patches.

Regarding the geometry of the roughness, our approach does not allow to model the bumps as objects with a substantial curvature: Due to the patch-to-patch approximation only a small fraction of the possible overlap volume would be taken into account.

The application of Derjaguin approximation requires some care. First of all the bump size must be much smaller than the colloidal particle size ($a \ll R$), because the effective potential is evaluated by decomposing the spherical surface into small patches whose curvature is neglected. We also remark that the condition $a \ll R$ guarantees, in the case of uncorrelated roughness, that the spherical surface is covered by a large number of patches. We expect that our model for correlated roughness works well only at intermediate and high coverings, because at small coverings the patch surface becomes large with respect to the spherical surface and Derjaguin approximation becomes inaccurate.

Furthermore, Derjaguin approximation neglects the occurrence of the interstices between two facing bumps induced by the curvature of the colloidal particle. Figure 3.6 shows two colloidal particles, covered by bumps of height ϵ. The arc l, subtending the angle α, is the projection of a circular patch of

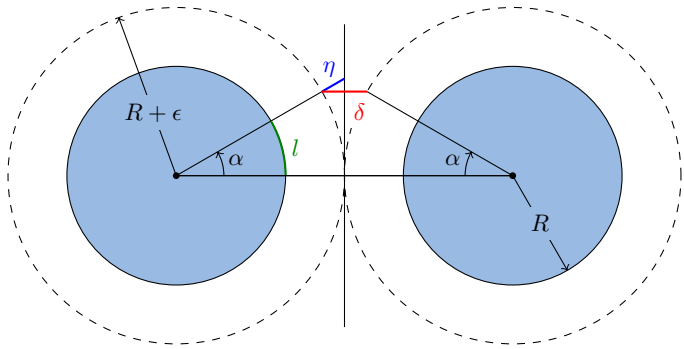

Figure 3.6: Colloidal particles of radius R, eventually covered by bumps of height ϵ. The arc l represents the projection of a patch of radius a. δ is the error induced by Derjaguin approximation. The dimension of the patch has been deliberately magnified.

radius a. The segment δ is the error introduced by Derjaguin approximation: We can assume that our approach works well when the parameters of the system are such that δ is smaller than the depletant diameter ($\delta < \sigma$). Within our approximations α is small (i.e. the patches have a small surface) implying $\delta \simeq 2\eta$, and simple geometry gives

$$R + \epsilon + \eta \simeq \frac{R+\epsilon}{1-\alpha^2/2} \simeq (R+\epsilon)\left(1+\frac{\alpha^2}{2r^2}\right).$$

If we express the angle α in terms of the radius of the patch we obtain

$$\eta \simeq \frac{2\,a^2}{R}$$

and the condition $\delta < \sigma$ reads

$$\sigma > \frac{4\,a^2}{R}.$$

Finally we introduce a condition which relates the parameters a and ϵ. The present approach neglects the overlap between the excluded volumes belonging to non-facing patches of the two colloids. It is possible to give a rough estimate showing that the effect of the neglected volume is not relevant if the height of the bump ϵ is of the same order of magnitude or smaller than the radius a of the projection of the bump on the surface of the colloid.

Summarising, we expect that, in the case of spherical bumps ($\epsilon = 2a$), our model provides reliable results when the parameters fulfil the following conditions:

$$\frac{\epsilon}{2R} \ll 1 \qquad \sigma < \epsilon \qquad \sigma > \frac{\epsilon^2}{2R}$$

3.3 EFFECTIVE POTENTIAL BETWEEN ROUGH COLLOIDS

The numerical evaluation of the integrals in Equations (3.30) and (3.35) provides the solvent-mediated potential between two spheres whose surface roughness is characterised by the geometry of the bumps and the five parameters introduced above. Since the space of the parameters is relatively large, we decided to investigate the behaviour of the potential by varying one parameter at a time. Furthermore, within the AO framework adopted in this work, the polymer packing fraction appears only as a multiplicative factor of the overlap volume (see Eq. (3.16)). Therefore the dependence of the effective potential on η is monotonic: The larger is the density of depletant, the more attractive is the potential.

Figure 3.7 shows the effective potential between two hard spheres whose surface is decorated by spherical bumps for different values of the covering c and the same parameters adopted in the recent simulation [113]. We first used the uncorrelated model of roughness as defined by Eq. (3.30) for covering $c \leq 0.59$. In this case, the minimum distance between the two colloidal particles is $2R$ and the potential vanishes for $r > 2R + 2\epsilon + \sigma$. Figure 3.7 highlights that the presence of surface roughness decreases the depth of the AO attractive minimum of the potential already at small surface coverings. By increasing the covering, the potential becomes more and more repulsive except at distances $r \simeq 2R + 2\epsilon$, where an attractive minimum develops due to the presence of a depletion layer around the bumps. The potential resembles the superposition of an attractive depletion contribution, arising from the overlap between 00, 10 and 11 configurations present at center-to-center distances $r \simeq 2R$, $r \simeq 2R + \epsilon$ and $r \simeq 2R + 2\epsilon$, and the repulsive contribution in Eq. (3.26), already shown in Fig. 3.4, present at all distances.
By comparing our analytical expression (3.30) with recent numerical simulations [113], also shown in Fig. 3.7, it appears that the model of random roughness we developed in Section 3.2 (Uncorrelated roughness) captures the overall shape of the effective interaction and the agreement is quantitative up to a covering $c = 0.44$. For higher values of c a qualitative change in the simulation results occurs, suggesting that some other effect becomes relevant in the regime of high coverings: The interaction is much more repulsive at short distances and becomes attractive at $r \simeq 2R + 2\epsilon$. The numerical results at intermediate/high coverings (i.e. for $c > 0.5$) can be well reproduced by the the approach developed in Section 3.2 (Correlated roughness), where bumps are assumed to be distributed in a more uniform way on the surface of the colloidal particle. In this case, the range of the potential is the same as for the uncorrelated model, but the distance of closest approach is increased to $2R + \epsilon$. The potential is monotonic in the repulsive region until a minimum is reached at distances $r \simeq 2R + 2\epsilon$ due to the presence of the depletion layer on two facing bumps belonging to the two colloidal particles. The good agreement with the numerical data in Fig. 3.7 shows that the model of correlated bumps

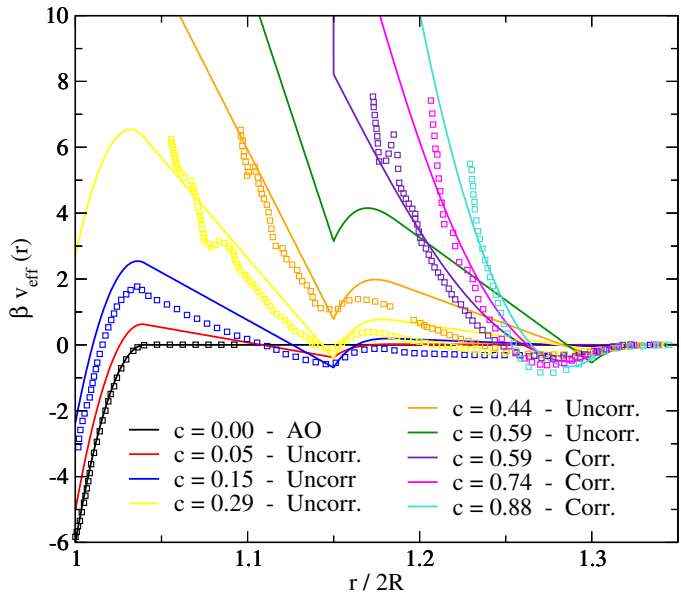

Figure 3.7: Lines: Effective potential between two rough hard spheres (spherical bumps $\epsilon = 2a$) as a function of center-to-center separation. The packing fraction and the diameter of the depletant are $\eta = 0.16$ and $\sigma/2R = 0.04$ respectively. The diameter of a spherical bump is $\epsilon/2R = 0.15$, whereas the covering is varied as shown. The curves are evaluated by means of Eq. (3.30) in the case of uncorrelated covering ($c \leq 0.59$) and by means of Eq. (3.35) in the case of correlated covering ($c \geq 0.59$). Points: Data from the MC simulation of Ref. [113].

provides a faithful representation of the simulation results, suggesting that the procedure adopted in Ref. [113] for modelling the surface roughness induces repulsive correlations among bumps already at intermediate coverage.
Having determined the form of the effective interaction, we can discuss the implications of surface roughness on the tendency towards aggregation of the two colloidal particles by evaluating the reduced second virial coefficient B_2^* (see Eq. (2.77)). In the case of bumps placed at random on the surface, B_2^* changes from -3.5 for smooth spheres to -0.7 for $c = 0.05$, where aggregation is inhibited by the roughness. Clearly, by increasing the coverage, the colloidal particles behave almost as hard spheres, at least for the choice of parameters investigated here.

Figure 3.8 compares the behaviour of the effective potential between two hard spheres decorated by spherical bumps at different values of the ratio σ/ϵ between the depletant diameter and the height of the bumps. In panel a) the value of ϵ is hold fixed whereas σ varies. When σ is small ($q = \sigma/2R = 0.03$) a deep short-ranged minimum of the potential develops at contact and the reduced second virial coefficient is negative ($B_2^* \simeq -8$). The increase of σ reflects in an increase of B_2^*, becoming positive at $q \simeq 0.04$ (see the inset).

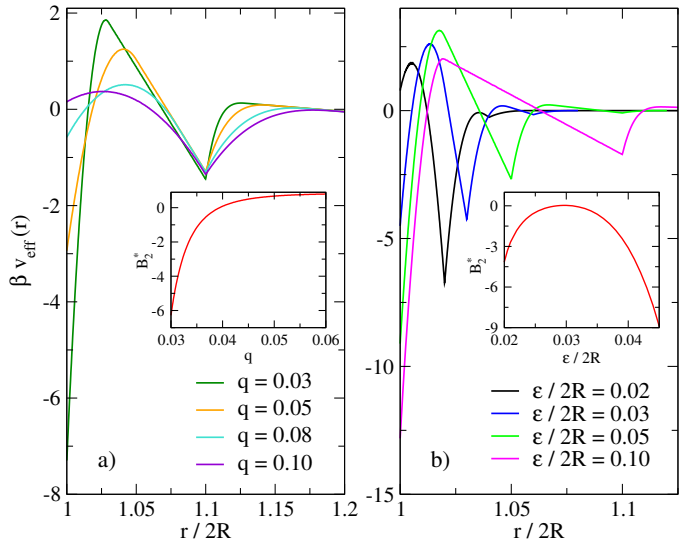

Figure 3.8: Effective pair potential potential as a function of the center-to-center separation between two rough spheres (spherical bumps) evaluated by means of Eq. (3.30). In both panels $\eta = 0.21$ and $c = 0.11$. Panel a): $\epsilon/2R = 0.1$, q ranges from 0.03 to 0.1 as shown. The inset shows the reduced second virial coefficient B_2^* as a function of q. Panel b): $q = 0.02$, $\epsilon/2R$ ranges from 0.02 to 0.1 as shown. The inset shows the reduced second virial coefficient B_2^* as a function of ϵ.

This result depends on the fact that the depletion potential becomes weaker at larger size ratio q, as in the case of smooth spheres (3.17), while the repulsive contribution to the interaction does not change. In panel b) the comparison is carried out at fixed σ. When $\epsilon = \sigma$ the potential is repulsive at contact, but a second attractive minimum of the order of $7k_BT$ appears at $r = 2R + \epsilon$ and $B_2^* \simeq -4$. This minimum becomes less pronounced for larger ϵ while the AO attraction at contact develops. For this choice of the parameters B_2^* shows a peculiar non-monotonic behaviour illustrated in the inset: At $\epsilon/2R \simeq 0.03$ the reduced second virial coefficient is close to zero, whereas at $\epsilon/2R \simeq 0.05$ it becomes strongly negative again. This unexpected behaviour can be attributed to the fact that, in the case of spherical bumps, by increasing ϵ also the bump radius $a = \epsilon/2$ increases and, at fixed coverage, the number of corrugations reduces, exposing larger available portions of the underlying particle surface to the depletion mechanism.

The geometry of the bumps significantly affects the shape of the depletion potential. Our model allows to investigate this effect: Spherical bumps constrain the height of the surface roughness (defined by the parameter ϵ) and the section of each bump (related to the parameter a) by the relation $\epsilon = 2a$. This limitation is lifted in the case of cylindrical bumps with radius a and height ϵ, thereby representing a simple model of roughness allowing to study the effects

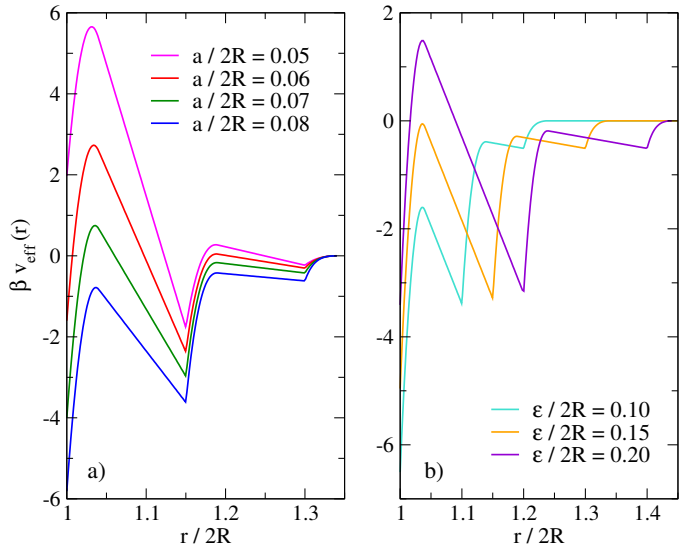

Figure 3.9: Effective potential between two rough spheres as a function of the center-to-center separation evaluated using Eq. (3.30). The spherical surface is decorated with cylinders with basis of radius a and height ϵ. In both panels $\eta = 0.16$, $q = 0.04$ and $c = 0.11$. Panel a): $\epsilon/2R = 0.15$, $a/2R$ ranges from 0.05 to 0.08 as shown. Panel b): $a/2R = 0.075$, $\epsilon/2R$ ranges from 0.1 to 0.2 as shown.

of these two parameters separately. In Fig. 3.9 we display some representative result for such a choice. Panel a) shows that, at constant covering c and height ϵ, the roughness is more effective when the surface is covered by a large amount of small bumps than a small number of corrugations with a large surface. Instead, when the number of bumps is constant, the potential is more repulsive in the case of larger ϵ, as can be seen in panel b).

Figure 3.10 compares the potential obtained with bumps characterised by different geometries in the case of uncorrelated roughness for two values of covering. The spheres and the cylinders have the same height, while the hemispheres are obtained dividing the spheres into two equal parts. The spherical and hemispherical geometry proves to be more effective in suppressing the depletion interaction with respect to the cylindrical geometry at the same covering. This happens because the curvature of spherical bumps reduces the overlap volume with respect to the flat surface of cylinders. It is interesting to note that, in the case of cylindrical bumps, the potential develops a quite deep attractive minimum at $r = 2R + \epsilon$ caused by the large overlap volume arising when a bump on one sphere faces a portion of smooth surface on the other particle.

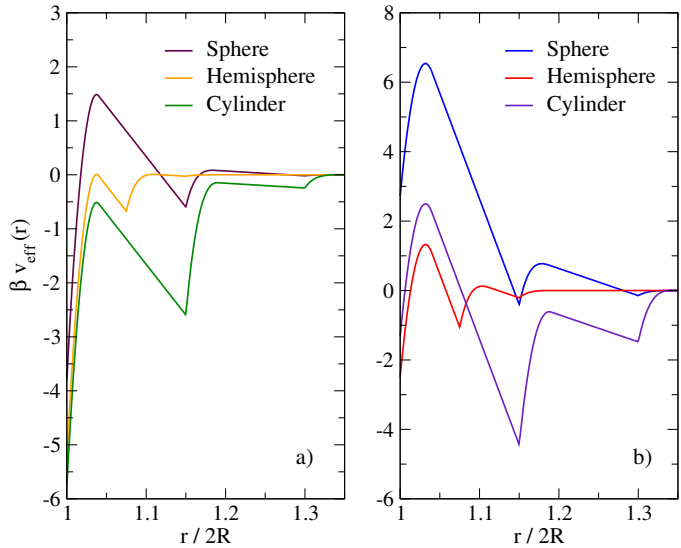

Figure 3.10: Effective potential between two rough spheres as a function of the center-to-center separation evaluated using Eq. (3.30). The spherical surface is decorated with spheres ($\epsilon/2R = a/R = 0.15$), cylinders ($\epsilon/2R = 0.15$, $a/2R = 0.075$) and hemispheres ($\epsilon/2R = a/2R = 0.075$). In both panels $\eta = 0.16$, $q = 0.04$. Panel a): $c = 0.10$. Panel b): $c = 0.29$.

3.4 CONCLUSIONS AND PERSPECTIVES

We introduced an analytical model able to capture the effects of surface roughness on the depletion mechanism. Comparison with available simulations shows that this, admittedly very schematic, parameter-free model allows to quantitatively reproduce the main features of the effective interaction between two spherical colloids in the presence of random surface corrugation. In order to reduce the problem to an analytically tractable model, we introduced several approximations. The two most relevant assumptions are:

- The ideal character of the depletant.
- The uncorrelated character of the corrugations. The surface of the particle has been divided in patches of the same size of the corrugation and a sort of "Ising variable" has been defined on each patch, representing the occupancy of each patch. This procedure neglects the correlations between the presence of bumps on different patches, and is therefore appropriate in the limit of small coverage. We also introduced an alternative model, where surface corrugation is strongly correlated at short distances, as expected when a repulsive interaction between bumps is present. This model has been shown to accurately describe the case of high coverage in the presence of charged adsorbed particles.

- Another important approximation we introduced refers to the calculation of the overlap volume between facing patches on the two particles. In the spirit of mean field theories, we disregarded the effects induced by the presence of two nearby bumps on the overlap volume, thereby neglecting correlations between nearest-neighbour corrugations.

We found that, as expected, surface roughness deeply inhibits the depletion effects, strongly reducing the tendency towards aggregation of the colloidal particles. These findings confirm that irregularities in the particle surface play a key role in the properties of colloidal suspensions. As a general rule, the effects induced by surface roughness appear to be more relevant when the height of the corrugations is of the same order of the size of the depletant. Several parameters are necessary to describe, even approximately, the extent of surface roughness: The height, width, number and shape of the bumps on each particle often induce competing effects on the depletion potential.
The availability of an analytical model may be extremely useful to estimate the effects of a specific surface roughness on the overall features of the effective interaction, even at a semi-quantitative level, without resorting to numerical simulations.

3.5 APPENDIX: ANALYTICAL EVALUATION OF $\mathcal{K}(\xi)$

Exploiting the symmetry of the problem it is possible to reduce the expression in Eq. (3.36) in order to perform a numerical evaluation.
The first step is to perform the change of variables $\boldsymbol{r}_2 = \boldsymbol{r}_1 - \boldsymbol{r}$, obtaining

$$\mathcal{K}(\xi) = \frac{2}{\pi s^4} \int_0^{2s} \mathrm{d}r\, r\, f(r;\xi) \int_{\mathcal{D}} \mathrm{d}\boldsymbol{r}_1,$$

where the domain of the integral is $\mathcal{D} = \{\boldsymbol{r}_1 : |\boldsymbol{r}_1| < s \wedge |\boldsymbol{r}_1 - \boldsymbol{r}| < s\}$ and we have taken advantage of the central symmetry of the integral over $\boldsymbol{r}$. The integral over $\boldsymbol{r}_1$ represents the surface of intersection between two disks of radius s at distance $\boldsymbol{r}$. The straightforward analytical solution allows to write

$$\mathcal{K}(\xi) = \frac{4}{s^2} \int_0^{2s} \mathrm{d}r\, r\, \Theta\left(\sqrt{r^2+\xi^2} - \epsilon\right) \mathrm{e}^{z_p\, V^{11}\left(\sqrt{r^2+\xi^2}\right)} \mathcal{I}\left(\frac{r}{2s}\right),$$

where we used the definition of $f(r;\xi)$ in Eq. (3.37) and

$$\mathcal{I}(x) = \frac{1}{\pi}\left[\arccos(x) - x\sqrt{1-x^2}\right]$$

is a function which is non-zero for $x \in [0,1]$. If we replace the variable of integration r with $t = \sqrt{\xi^2 + r^2}$ we obtain an expression which can be easily integrated numerically:

$$\mathcal{K}(\xi) = \frac{4}{s^2} \int_{\mathrm{Max}[\epsilon,\xi]}^{+\infty} \mathrm{d}t\, t\, \mathrm{e}^{z_p\, V^{11}(t)}\, \mathcal{I}\left(\frac{1}{2s}\sqrt{t^2-\xi^2}\right).$$

4

Thermal forces: A statistical approach

The influence of a non-uniform temperature profile on the motion of fluids in the absence of external fields has been discovered apparently for the first time by Ludwig [143] in 1856 and independently by Soret in 1879 [211, 212, 213]. They observed the so called Ludwig-Soret effect, which consists in an unbalanced thermal migration of the two species in a binary mixture caused by a temperature gradient. The first observation of this phenomenon was performed by Ludwig, who filled with a homogeneous sodium sulphate solution a U-tube, whose extremities were maintained in contact respectively with boiling water and ice, and noticed that the solute crystallised near the cooled limb. However, the contribution of the Swiss physicist and chemist Soret has been essential to characterise this effect: He performed several experiments for many electrolyte solutions and gave more quantitative predictions with respect to Ludwig.
The reciprocal effect, that is a temperature difference induced by a gradient in particle concentration, was observed by Dufour [55, 56] for a mixture of air and Hydrogen. Feddersen, who first named this phenomenon *thermodiffusion* [69], performed similar experiments and understood that the thermal diffusion and the Doufour effect are two sides of the same coin. He clearly realised that the observable effects related to thermodiffusion are frequently small, but, at the same time, that the occurrence of such phenomena is widespread. Quoting Feddersen's last paragraph of Ref. [69]: *"If the forces set free by thermodiffusion appear mostly to be trifling, yet it cannot be forthwith maintained that this phenomenon plays only a quite subordinate part in the economy of nature; for the conditions of its occurrence may at least be widely spread."*

During the same years of Soret's experiments, Tyndall [224], compelled to

remove the dust during his his studies on the decomposition of vapours by light, realised that (dust) particles suspended in a gas (in that case the air of the Royal institution) tend to be repelled by hot surfaces. This phenomenon is related to the Ludwig-Soret effect, at least when the particles are suspended in a very rarefied gas, and it is called particle thermophoresis, or simply *thermophoresis*.
It is believed that interfaces play a key role in phoretic effects: The motion of the particles is indeed driven by the simultaneous presence of an interface, i.e. the particle surface, and a temperature gradient along that surface. The idea is actually pretty simple: When a particle lies in a gas (or a liquid) where a temperature gradient has been imposed, the particle surface induces the motion of the fluid alongside. Due to this flow the particle is subject to a net force (a "tangential stress") and, if the particle is left free in the gas, it drifts because of this *"thermal" force*.

Particle thermophoresis in gases is well understood and many predictions are available at the moment [256]. A key parameter for the microscopic interpretation of this phenomenon is the Knudsen number, defined as the ratio between the mean free path λ and the particle size. In the rarefied limit ($\mathrm{Kn} \geq 1$) both the approaches based on kinetic theories, starting from the seminal works due to Enskog [61] and Chapman [33], and the direct numerical solutions of the Boltzmann equations [209] prove to be very accurate. The particle motion is towards the cold side, provided that the mass of the suspended particles is larger than the gas particle masses.
Within the quasi-hydrodynamic regime, that is for gases at moderate pressures ($\mathrm{Kn} \ll 1$), continuum theories, suitably generalised to account for slip flow, give quite accurate results. By means of these techniques, Epstein [62] evaluated the thermophoretic force on a single spherical particle in a stagnant gas in a thermal gradient. Subsequent works improved Epstein's result, which can be considered as a first-order approximation: These investigations show that the drift velocity of the particle is generally directed towards the cold region of the gas.

As the density of the underlying fluid increases, the situation becomes more complex. First of all, in liquids the effect turns out to be be smaller than in gases and particles can move either towards the cold or the hot region. The drift velocity strongly depends on the surface properties of the particles: The magnitude and even the direction of the drift velocity can change if external parameters, such as temperature, are varied. The various aspects connected to the behaviour of colloidal suspensions in temperature gradients have been deeply described in the recent reviews by Piazza and Parola [175] and Wurger [248].
From a theoretical point of view, different models have been put forward in order to describe thermophoresis in liquids. The basic strategy adopted is to look for an effective force $\boldsymbol{f}$, directly coupled to the particles, leading to the same steady-state situation as that induced by the thermal gradient. In stationary conditions, the net force $\boldsymbol{f}$ is balanced by a frictional force and the

total force acting on the colloidal particle vanishes. Two different routes are generally pursued to evaluate $\boldsymbol{f}$: An energetic approach or a hydrodynamic one. The former consists in writing the net force as the gradient of some thermodynamic potential [57, 47, 48, 247] or of the surface tension [199]. This kind of approach is questionable for two reasons: The minimum condition for a thermodynamic potential used to obtain equilibrium properties does not hold in stationary (nonequilibrium) states and, moreover, it would give information on the total force only, which has to be zero, not on the net force $\boldsymbol{f}$. The hydrodynamic way of proceeding [45, 3, 168] is to explicitly solve the Navier-Stokes equations for the fluid in the particle frame of reference with appropriate boundary conditions, to find the velocity field and then to obtain $\boldsymbol{f}$ by an integration over the whole surface of the momentum flux transferred to the colloid. Obviously, different choices of boundary conditions lead to different trends in the net force.

In spite of a plethora of attempts during the last three decades, a microscopic and universal description of particle thermophoresis is still lacking. Different approaches often fail to predict correctly the magnitude and the direction of the drift when applied to different systems. In most cases the theoretical efforts are addressed to the quantitative interpretation of the experimental data from systems characterised by high degree of complication and several competing effects. Furthermore, continuum theories based on local nonequilibrium thermodynamics necessarily abstain from an accurate (microscopic) description of the fluid in the vicinity of the particle surface [81]. Indeed, close to the surface, in a region of the order of the interaction range, the properties of the fluid are expected to vary considerably and the phenomenon of thermophoresis follows from this microscopic structural modification [97].
In order to understand more deeply the nature of the phenomenon, aiming at the formulation of a microscopic theory of thermophoresis, we revert to the study of thermo-osmosis, which is believed to be the driving mechanism for thermophoresis. The term *thermo-osmosis*[1] refers to the onset of a stationary flow of matter in a one-component gaseous or liquid system[2] induced by temperature gradients. The flow is due to the presence of a confining surface parallel to the thermal gradient and in the absence of the surface no flow is observed. Indeed, when a uniform (bulk) fluid is placed in a thermal gradient, mechanical equilibrium sets in via the force balance condition, implying constant pressure throughout the system. In the absence of external forces, the steady-state is characterised by a space dependent density profile and a constant heat flux not associated to mass current.
The link between thermal osmosis and thermophoresis turns out to be particularly clear if we consider the limiting case of a mesoscopic particle immersed

[1] Also called *thermal osmosis*. Up to our knowledge, this name was coined by Lippman [139] for liquids. In gases [116] the same phenomenon is referred to as *thermal creep* or *thermal transpiration* (after Osborne Reynolds).

[2] In the absence of symmetry-breaking forces like gravity, when convection dominates.

in a microscopic fluid, whose surface can be locally approximated by a planar wall.

This Chapter provides a microscopic description of thermo-osmosis on the basis of statistical physics: linear response theory generalised to inhomogeneous and anisotropic environments. In the case of an imposed uniform thermal gradient, the use of microscopic conservation laws allows to evaluate the velocity profile of the fluid and the thermo-osmotic slip in terms of two physically different equilibrium properties of the fluid near the surface: The pressure tensor and a specific dynamical correlation function. Close similarities to both the kinetic theory and nonequilibrium thermodynamics result are recovered by retaining each of these terms, showing that the gas and liquid regimes are indeed governed by different physical mechanisms.
The first Section critically reviews the main results on thermo-osmosis available in the literature. In Section 4.2 we introduce a convenient formalism for the description of nonequilibrium systems, we derive the microscopic continuity equations for the relevant quantities and we discuss some subtle implications about the definition of the fluxes. Section 4.3 deals with linear response theory and the Kubo formalism applied to mechanical perturbations. Thermal perturbations and the generalisation of Mori's approach to inhomogeneous systems are discussed in Section 4.4. In Section 4.5 we specialise our results to a slit geometry, showing that the velocity profile obeys a simple integro-differential equation. Finally, some limiting results valid for liquids and gases are derived in Section 4.6.

4.1 THERMO OSMOTIC PHENOMENA

The first observation of thermo-osmosis has been reported by Feddersen in 1872 [69]. He measured the temperature induced motion of different gases through a tube fitted with porous plugs of gypsum or spongy platinum. The gas drift was directed towards the warmer side as long as a temperature difference between the sides of the porous partition was present. As Feddersen reported in Ref. [69]: *"It is a universal property of porous bodies, when in the form of diaphragms, to draw gases through them in the direction from the cold to the hot side. We have thus a phenomenon of diffusion which, contrary to ordinary diffusion, occurs even when the same gas under the same pressure is found on both sides of the diaphragm. This is a singular, hitherto unknown phenomenon; and we are therefore justified in giving it the name of Thermodiffusion."*
Even if thermo-osmosis was discovered in gases, the same effect has been observed later also in liquids. However, in liquids the magnitude of the flow turns out to be much smaller than in gases, and probably this is the reason why the first investigations were focused on gases. In the following we critically review the main results on thermo-osmosis in gases and in liquids. It appears that the theoretical approaches adopted in gases and liquids are markedly different. Furthermore, as regards thermo-osmosis in liquids, a full understanding of

the phenomenon is still lacking, both experimentally and theoretically. Many similarities with the development of the study of thermophoresis can be noted.

Thermo-osmosis in gases

The first investigations of thermo-osmosis in gases have been spurred by the invention of the radiometer by Crookes [35, 246][3]. The radiometer (or light mill) consists of a small glass bulb, partially evacuated, inside of which a set of vanes is accommodated on a spike. Each vane is shiny on one side and blackened on the other because, according to Crookes, the purpose of the radiometer was to detect the pressure of light. Unfortunately, when the radiometer is placed in sunlight the vanes spin around the wrong way, that is the black vanes are pushed away by the light. Crookes submitted a work to the Royal Society [35] in which he argued, making a mistake, that the motion of the light mill was a direct consequence of the light impinging on the vanes. Maxwell was the referee of Crookes' paper and substantially agreed with his interpretation of the phenomenon. Only after the experiments performed by Schuster [206], and suggested by Osborne Reynolds, it became clear that the cause of the motion could not be the transfer of momentum on the vanes due to the incident light: The rotation was due to an unbalance of pressure of the residual gas near the two differently heated sides of each vane. The reason of this pressure difference was not clear, and different hypotheses were put forward. The latest chapter of the story is usually ascribed to Maxwell[4], who showed that the thermal creep, and consequently the motion of the radiometer, is originated by the tangential stress of the gas which develops near the confining surfaces to which a temperature gradient is applied [149]. Surprisingly, in the case of the radiometer the tangential stress arises just at the *edges* of the vanes and accurate predictions are hard to obtain [116, 209]. Recently, the phenomenon of thermal creep has been demonstrated through a simple revealing experiment by Sone and Yoshimoto [210].

The thermal creep flow in rarefied gases, that is when the mean free path is larger than the range of the interparticle potentials, is to date accurately predicted by kinetic theories [209]. The expression for the thermo-osmotic velocity has been obtained for the first time by Maxwell in 1789, by means of a calculation able to take into account the effects of the surface on the motion of the gas. The simple model proposed by Maxwell *"treats the surface as something intermediate between a perfectly reflecting and a perfectly absorbing surface, and, in particular, supposes that of every unit of area a portion f absorbs all the incident molecules, and afterwards allows them to evaporate with velocities corresponding to those in still gas at the temperature of the solid, while a portion $1 - f$ perfectly reflects all the molecules incident upon*

[3]However, objects similar to Crookes radiometer were already known in Germany.
[4]But it should also be ascribed to Reynolds [187] and Thomson. For details see Ref. [26].

it" [161, Pag. 706]. Maxwell's expression for the creep velocity in the absence of pressure gradients has been reported also in the classic book by Kennard [116] and reads

$$v_\infty = \frac{3}{4}\frac{\eta}{\rho}\frac{\nabla T}{T}, \tag{4.1}$$

where ρ and η are the bulk mass density and the viscosity of the gas and the temperature gradient ∇T is directed along the wall. The same result can be expressed in terms of the mean free path λ of the particles through the standard relation valid for a hard sphere gas

$$\lambda = \frac{\eta}{p}\sqrt{\frac{\pi k_\mathrm{B} T}{2m}}, \tag{4.2}$$

where p is the gas pressure. Equation (4.2) together with the ideal gas law $p = \rho k_\mathrm{B} T/m$ gives

$$v_\infty = \lambda \frac{3}{2\sqrt{2\pi}}\sqrt{\frac{k_\mathrm{B} T}{m}}\frac{\nabla T}{T}.$$

The mechanism which originates thermo-osmosis in gases can be qualitatively understood as follows [116, 209]. Let us consider a gas at rest over a planar wall with a temperature gradient along it. The molecules bouncing on a given element of surface $\mathrm{d}\Sigma$ come from various directions without collisions over a distance of the order of the mean free path. This means that they preserve the memory of the thermodynamic state of the gas at the point where the last collision took place. The molecules belonging to the hotter region carry an higher average momentum than those from the colder region and therefore they will transfer (on average) more momentum to $\mathrm{d}\Sigma$ during the impact. After the impact, the molecules are kicked back from the wall. If the reflection is specular, then the net transfer of momentum to the wall will be vanishing. However, if the momentum is not conserved during the collision (i.e. if the particles release a fraction of their momentum to the wall) the result is a net momentum transfer from the gas to the wall in the direction opposite to the thermal gradient As a result, the gas will be set in motion in the direction of the gradient, until a steady flow is reached[5]. Here we remark that the onset of the thermal creep is deeply rooted in the specificity of molecule-surface interaction. In particular, a flow is established only if particles loose momentum to the wall during the collision. This idea was first put forward for the first time by Maxwell [26] in a referee report to a work by Reynolds.
To conclude this review of thermal creep in gases we note that in free molecular

[5]A gas in motion is characterised by an average momentum, which will be on average transferred to the wall. The steady state is reached when the transferred momentum in the direction opposite to the motion (i.e. opposite to the gradient) and the transferred momentum in the direction of the motion are equal.

gases (very high gas rarefaction) the flows induced by temperature gradients vanish [209]. The argument introduced above in order to qualitatively justify the onset of the slip velocity is no longer valid: In this limit the molecules can reach the opposite sides of the system without colliding with other molecules and with the walls. It is straightforward to show that two gas reservoirs connected by pipes of any shape and kept at different temperatures T_a and T_b will reach a stationary state without any flow and their pressures will obey the relation [116]

$$\frac{p_a}{p_b} = \sqrt{\frac{T_a}{T_b}}.$$

This phenomenon is called *thermal effusion* and the ratio between pressures does not depend on the specific properties of gas.

Thermo-osmosis in liquids

Thermo-osmosis in liquids was first observed and named in 1907 by Lippman [139]. In his seminal paper Lippman studied the flow of water through a membrane of gelatin separating two volumes held at different temperatures. A few years later Aubert [9] addressed the problem more systematically and found that in the presence of a temperature difference some membranes (e.g. gelatin and pig's bladder) originate a water flow from the cold to the hot whereas other (e.g. parchment paper and viscose) in the opposite direction. Furthermore he noticed that for porous plugs of mineral origin (e.g.. glass) no flow was detectable. He concluded was that thermo-osmosis was due to the presence of electrolytes in the membrane and therefore, according to these pioneering observations, the phenomenon seemed to be a manifestation of electro-osmosis.

The works by Lippman and Aubert were little known in 1941 when Derjaguin and Sidorenko [46] performed similar experiments and reported a remarkable effect for porous plugs of sintered-glass in water and other liquids. Four years later, Reekie and Aird [185] were carrying on some experiments on the flow of water through micro-metric channels. Maybe stimulated by Landau, who remarked in his work on the superfluidity of He^2 that *"the presence of the thermomechanical effect is not in itself peculiar only to helium, anomalous is only the large value of the effect"* [129, 220], they tried to observe this effect within their setup, but they obtained a negative result. Reekie and Aird were not aware of the works by Lippman, Aubert and of the measurements of Derjaguin and Sidorenko. On the other hand, also Derjaguin was not aware of the works published by Lippman and Aubert. However, as later shown by Hutchinson, Nixon and Denbigh [108], Derjaguin's results were strongly influenced by the presence of free charges in the membrane. However thermo-osmosis shows up also in neutral porous membranes, and the first indisputable observation of the flow has been reported by Haase and Steinert [95].

Currently thermal osmosis in liquids, both neutral and charged, is an accepted phenomenon and a renewed interest is stimulated in relation to possible applications to fuel cells, water management [132] and water recovery. Furthermore, thermal osmosis is relevant in desalination of seawater and in power generation from the salinity difference with river water [140]. As regards nano systems, thermo-osmosis could be relevant, together with thermophoresis, for particle motion and manipulation through hot nanostructures [36]. Also in living systems, such as eukaryotic cells, thermo-osmotic driven effects could appear due to the occurrence of large temperature gradients, as recently pointed out in Ref. [34]. The increasing attention on these topics is confirmed by a recent review on thermo-osmosis in membranes by Barragán and Kjelstrup [15].
Although several experimental measurements have been performed up to now, the apparently simple phenomenon of thermal osmosis is not yet fully characterised and understood at a microscopic level. The experimental results often disagree about the direction and the magnitude of thermo-osmotic fluxes. In hydrophobic membranes the flow is always directed from the hot to the cold, whereas in hydrophilic membranes the direction of the flux is strongly influenced by the nature of the liquid, possible solutes and the average temperature of the system. New and refined experiments are necessary to clarify the loose ends.
A recent work [24] claiming the first microscale observation of the velocity field imposed by thermo-osmosis goes towards this direction. The experimental setup consists of a glass slit of about $5\,\mu$m thickness filled with water. The temperature gradient is imposed heating a gold nanoparticle of 125 nm radius immobilised at the upper surface of the slit. The thermo-osmotic flow has been monitored tracking a smaller gold nanoparticle, which was supposed not to be influenced by the temperature gradient. The flow was directed towards the hot region, and the extrapolated velocity of about $40\,\mu$m/s. Here we remark that the results obtained in this work are strongly affected by the presence of surface charge (see e.g. the results reported in Ref. [200]).

The growing interest on thermo-osmosis in liquids has been recently confirmed by the new nonequilibrium MD simulations performed by the groups based in Cambridge [81, 82] and Lyon [74, 75]. Before discussing their results, we introduce the unique, to the best of our knowledge, theoretical approach devised in order to describe thermal osmosis.
The phenomenon of thermo-osmosis is characterised by the presence of energy and matter fluxes, on account of a temperature difference: The system is out of equilibrium and classical thermodynamics is of little help to describe this process. The first attempts in order to account for nonequilibrium phenomena involving heat and matter fluxes[6] dates back to 1854 [222], when Thomson provided a theoretical description of the thermo-electric effect based on the

[6]Heat fluxes in crystals have been studied by Dhuamel and Stokes starting from the beginning of the nineteenth century.

new hypothesis of entropy creation[7]. By means of similar arguments, in the twenties Eastman [58, 59] predicted the existence of thermo-osmosis and interpreted the Ludwig-Soret effect as a nonequilibrium process. As he states in his work [58]: In the presence of a non-uniform temperature profile the *"substances constituting the system are able to move independently from one region of temperature to another, they will in general do so until a condition of equilibrium, accompanied by no further net transfer of material, is reached"*. The theories developed by Thomson and Eastman were then refined and formulated more rigorously by de Groot, Prigogine, Denbigh and other authors. All these approaches are deeply rooted in the works by Onsager [166, 167], whose contribution has been essential in the development of nonequilibrium thermodynamics. In what follows we introduce some elements of the formalism of linear nonequilibrium thermodynamics, in order to understand how these results can be applied to the problem of thermo-osmosis.

Let us consider a planar wall, which may be considered as a simplified model for the surface of a pore in a membrane. A fixed temperature difference ΔT and a fixed pressure difference Δp are imposed at the ends of the wall along the same direction, let us call it x. The inhomogeneities in temperature and pressure give rise to heat J_q and matter J_ρ fluxes along x[8]. The rate of entropy production σ across a surface perpendicular to the direction x can be written as

$$\sigma = J_\rho \, \Delta p + J_q \, \frac{\Delta T}{T}. \tag{4.3}$$

The two quantities coupled to the fluxes in Eq. (4.3) are referred to as the thermodynamic forces:

$$X_\rho = \Delta p, \qquad X_q = \frac{\Delta T}{T}.$$

The fundamental assumption of (linear) nonequilibrium thermodynamics is that the fluxes are linear functions of the forces and we can write:

$$J_\rho = L_{\rho\rho} \, X_\rho + L_{\rho q} \, X_q = L_{\rho\rho} \, \Delta p + L_{\rho q} \, \frac{\Delta T}{T}, \tag{4.4}$$

$$J_q = L_{q\rho} \, X_\rho + L_{qq} \, X_q = L_{q\rho} \, \Delta p + L_{qq} \, \frac{\Delta T}{T}, \tag{4.5}$$

where L_{ij} are phenomenological coefficients. L_{qq} is the coefficient related to the thermal conductivity: Taken alone it describes the heat conduction at constant pressure. On the other hand, $L_{\rho\rho}$ accounts for the flow of liquid at constant temperature. The cross terms, $L_{q\rho}$ and $L_{\rho q}$, act as a coupling between the heat

[7] In this work [222] appears for the first time the term *thermo-dynamics*, page 123.

[8] Here we follow, with some changes, the notations in [45]. Most of the references (see e.g. Ref. [42, 41]) introduce the energy flux instead of the heat flux, because it is a less ambiguous quantity.

and the mass fluxes: The so called *mechanocaloric coefficient* $L_{q\rho}$ represents the mechanical contribution to the heat flux, whereas $L_{\rho q}$ has the inverse meaning. Onsager showed that the cross coefficients are equal: This result is referred to as the Onsager reciprocal relations and is rooted into the microscopic reversibility of the system [166, 167]. Note that the cross-coefficients $L_{q\rho}$ and $L_{\rho q}$ vanish in a homogeneous fluid due to the independence of heat and mass current fluctuations[9].

Derjaguin and Sidorenko [46] applied the formalism introduced above to describe thermo-osmosis. Their strategy consists in two steps: First they express the mechanocaloric coefficient in terms of the local excess enthalpy of the fluid, then they make use of the Onsager reciprocal relations in order to obtain the expression for the mass flow at $\Delta p = 0$, that is the flow in the case of an open system. The fluid velocity far from the wall can be written as[10]

$$v_\infty = \frac{1}{\eta} \int_0^{\tilde{l}} \mathrm{d}z \, \Delta h(z) \, \frac{\nabla T}{T}, \tag{4.6}$$

where η is the bulk viscosity, $\Delta h(z)$ is the excess local enthalpy at a given height z and $\tilde{l}$ is the (microscopic) length after which the excess local enthalpy vanishes. This result is valid under two hypothesis. The first one is that we can approximate the local viscosity with the bulk viscosity also near the surface. The second one is that we can define a local enthalpy in the fluid layers in front of the surface. Here some difficulties arise. First of all the effect of a non-uniform viscosity on the motion of the fluid is not clear. Furthermore, as shown in [81] and as expected from the local behaviour of the pressure tensor, the local enthalpy is not a slowly varying function[11] and a local equilibrium definition is in principle not valid [197]. The inconsistency of the definition of a local enthalpy is somewhat related to the local equilibrium interpretation of the Gibbs-Duhem equation [81].

Coming back to simulations, the recent work published by Fu, Merabia and Joly [74] focuses on the flow in a carbon nanotube generated both by pressure and temperature differences applied to the extremities of the channel. They assert that within their setup the Onsager reciprocity relations are satisfied and that the mechanocaloric coefficient obtained through Derjaguin's approach accurately predicts the observed values. Furthermore, they show that in order to observe consistency with theoretical prediction based on nonequilibrium thermodynamics when the wall-particle interactions are weak it is necessary to apply a hydrodynamic correction to account for the presence of slippage. The group belonging to the University of Cambridge presented two very

[9] See e.g. Ref. [130], Sec. 49 or Ref. [11], Sec. 12.5.

[10] As recently noted by Ganti et al. [81], and some years before by Anderson [3], the result reported in [45] has an extra multiplicative factor 2. The mistake is in the expression of the Poiseuille flow.

[11] We remark, anticipating the content of the next Section, that it is not possible to define the local enthalpy in an inhomogeneous system without ambiguities.

different works. In the first work [81], they test the consistency between the the slip velocity of a LJ fluid in a slit obtained by three different routes. The *mechanical route* consists in two steps. First they run equilibrium simulations at several temperatures in order to obtain the pressure tensor as a function of T for different microscopic definition of the tangential pressure[12]. Then they evaluate the force exerted on the fluid by taking the temperature derivative of the tangential pressure (i.e. by use of the local equilibrium prescription). Finally they run a nonequilibrium (but isothermal) simulation of the flow generated by that force. The *thermodynamic route* consists in the evaluation of the slip velocity by Eq. (4.6), where the local enthalpy is defined as

$$h(z) = u(z) + \frac{p(z)}{\rho(z)}, \tag{4.7}$$

where $u(z)$ is the local energy density, $p(z) = p_{\mathrm{T}}(z)$ the virial expression for the local tangential pressure and $\rho(z)$ the local density profile. However, as already mentioned above, the definition (4.7) is only valid in the bulk. The last method relies on Onsager reciprocal relations: The mechanocaloric cross coefficient is evaluated applying to the system a pressure gradient and the slip velocity follows from (4.4) at $\Delta p = 0$. The conclusion of this paper is that the three routes provide consistent results, showing the presence of a strong space dependence of the viscosity of the fluid.

Reference [82], published the following year, makes use of a clever trick in order to directly evaluate the force on the fluid particles through a *steady-state* nonequilibrium simulation. The result is surprising: The force obtained following the mechanical route of Ref. [81] differs from that evaluated directly from the most recent nonequilibrium simulation [82]. Furthermore, they report that the force predicted by means of the thermodynamic route turns out to be more accurate than that obtained using the other methods proposed in [81]. In this second work there is no mention of the definition of the pressure tensor adopted for the evaluation of the local enthalpy (4.7). However, we can imagine that the virial expression has been chosen, as in [81], even if this definition of pressure tensor does not satisfy the hydrostatic equilibrium condition.

In our opinion the force on the particles evaluated through the nonequilibrium steady-state simulation in [82] is, at least in principle, correct, but we think that any preference among the three methods (and among the definitions of the pressure tensor) put forward in [81] is risky, because, as we tried to show above, some quantities are not well defined (see also the discussion in the next Section).

To close this parenthesis about numerical results, we think that nonequilibrium steady-state MD simulations of systems characterised by a small number of control parameters and simple interfaces are desirable. The problem of

[12] It has been shown that the tangential pressure can not be uniquely defined. See Ref. [205] and the discussion in Section 4.2.

thermo-osmosis of binary mixtures in pores has been studied through simulations more than ten years ago [243, 96, 78], but analogous results for one-component fluids are still missing.

4.2 DYNAMICAL SYSTEMS AND MICROSCOPIC CONSERVATIONS

In this Section we will introduce some notation about dynamical systems, oriented to the statement of microscopic conservation laws. We will obtain the local expressions for the relevant fluxes arising in an out-of-equilibrium system and we will discuss some subtle aspects related to their definition.

Preliminaries on dynamical systems

Let us consider a dynamical system, whose state is characterised at a given instant of time by a set of N generalised coordinates q_i and N conjugated momenta p_i. Any physical observable (dynamical function) can be considered as a real function of the $2N$ variables $(q,p) = (q_1, \ldots, q_N, p_1, \ldots, p_N)$.
The time evolution of the system is completely determined once a privileged dynamical function, the Hamiltonian $H(q,p)$, is fixed. The trajectories in the phase space are represented by set of $2N$ functions of time $(q(t), p(t)) = (q_1(t), \ldots, q_N(t), p_1(t), \ldots, p_N(t))$, which are the unique solutions of the Hamilton's equations

$$\begin{cases} \dot{q}_i = \dfrac{\partial H}{\partial p_i} \\ \dot{p}_i = -\dfrac{\partial H}{\partial q_i} \end{cases} \tag{4.8}$$

once the initial values $q_i(0)$ and $p_i(0)$ are given.
As a result of the motion, the dynamical functions change their value in time. The rate of change of a physical observable $A(q,p)$ is given by

$$\begin{aligned} \frac{\mathrm{d}A}{\mathrm{d}t} &= \sum_i^N \left[\frac{\partial A}{\partial q_i}\dot{q}_i + \frac{\partial A}{\partial p_i}\dot{p}_i \right] \\ &= \sum_i^N \left[\frac{\partial A}{\partial q_i}\frac{\partial H}{\partial p_i} - \frac{\partial A}{\partial p_i}\frac{\partial H}{\partial q_i} \right] \equiv \{A, H\}\,. \end{aligned}$$

The second line follows by means of Hamilton's equations (4.8), whereas the last identity is the definition of the Poisson brackets. The time evolution of the dynamical functions can be expressed more formally introducing the Liouville operator $\mathscr{L}$:

$$\frac{\mathrm{d}A}{\mathrm{d}t} = -\mathscr{L}A, \tag{4.9}$$

where

$$\mathscr{L}\cdot \equiv \{H,\cdot\} = \sum_i^N \left[\frac{\partial H}{\partial q_i}\frac{\partial}{\partial p_i} - \frac{\partial H}{\partial p_i}\frac{\partial}{\partial q_i}\right]\cdot$$

The formal solution to Eq. (4.9) can be written as

$$A(t) = \exp\{-t\mathscr{L}\}A(0). \tag{4.10}$$

Now let us focus our interest on a system of point particles of equal masses m, interacting with a central pair-wise additive potential $v(|\boldsymbol{r}|)$, in the presence of an external potential $V(\boldsymbol{r})$. The generalised coordinates q_i and the conjugated momenta p_i can be taken as the components of the positions q_i^α and of the momenta p_i^α of the particles[13]. The Hamiltonian of the system has the form:

$$\begin{aligned} H\big(\{q_i^\alpha\},\{p_i^\alpha\}\big) &= H_K\big(\{p_i^\alpha\}\big) + H_v\big(\{q_i^\alpha\}\big) + H_V\big(\{q_i^\alpha\}\big) \\ &= \sum_i \frac{|\boldsymbol{p}_i|^2}{2m} + \frac{1}{2}\sum_{i\neq j} v\big(|\boldsymbol{q}_i - \boldsymbol{q}_j|\big) + \sum_i V(\boldsymbol{q}_i), \end{aligned} \tag{4.11}$$

where the sum is extended over the particles.
As stated above, the Hamiltonian induces a dynamics ruled by the Liouvillian $\mathscr{L}$. This operator can be written as the sum of three contributions arising from the kinetic, the internal potential and the external potential contribution in the Hamiltonian:

$$\begin{aligned} \mathscr{L} &= \mathscr{L}_K + \mathscr{L}_v + \mathscr{L}_V \\ &= -\sum_i \frac{\boldsymbol{p}_i}{m}\cdot\frac{\partial}{\partial \boldsymbol{q}_i} + \frac{1}{2}\sum_{i\neq j}\frac{\partial v_{ij}}{\partial \boldsymbol{q}_i}\cdot\left(\frac{\partial}{\partial \boldsymbol{p}_i} - \frac{\partial}{\partial \boldsymbol{p}_j}\right) + \sum_i \frac{\partial V(\boldsymbol{q}_i)}{\partial \boldsymbol{q}_i}\cdot\frac{\partial}{\partial \boldsymbol{p}_i}, \end{aligned} \tag{4.12}$$

where v_{ij} is the shorthand notation for $v(|\boldsymbol{q}_i - \boldsymbol{q}_j|)$.

Statistical mechanics provides the link between the microscopic observables introduced above and macroscopic physical quantities. This link is provided by the so called phase-space distribution functions $F(q,p)$, which belong to the subset of the dynamical functions such that their integral over the phase space is normalised. The distribution $F(q,p)$ specifies the state of the system and the observable value of any dynamical function $A(q,p)$ is given by

$$\langle A\rangle = \iint \mathrm{d}q\,\mathrm{d}p\, A(q,p)\, F(q,p).$$

The time evolution of the distribution $F(q,p)$ is regulated by the Liouville equation

$$\partial_t F(t) = \mathscr{L} F(t) \tag{4.13}$$

[13]Here and in the following Greek indices refer to vector components, whereas Latin indices refer to particles.

which must be supplemented with the initial condition $F(t=0)=F_0$. The formal solution of (4.13) reads

$$F(t)=\mathscr{U}(t)F(0), \tag{4.14}$$

where $\mathscr{U}(t)=\exp\{t\mathscr{L}\}$ is the so called Green propagator (or time evolution operator). This operator can be alternatively defined as the solution of the equation

$$\partial_t\mathscr{U}(t)=\mathscr{L}\mathscr{U}(t) \tag{4.15}$$

with the initial condition $\mathscr{U}(0)=\mathscr{I}$, where $\mathscr{I}$ is the identity operator. Finally, the time evolution of the observables can be written according to Eq. (4.10) as

$$A(t)=\exp\{-t\mathscr{L}\}A(0)=\mathscr{U}(-t)A(0). \tag{4.16}$$

The set of all the transformations $\mathscr{U}(t)$, which has the structure of a Lie Group, is the so called group of the *canonical transformations*. The laws of mechanics are invariant under the actions of the elements belonging to it.

Microscopic continuity equations

In order to obtain the microscopic counterpart of the macroscopic conservation laws of mass, momentum and energy let us adopt the usual definition for the local mass density and the local momentum density "operators"

$$\hat{\rho}(\boldsymbol{r})=m\sum_i\delta(\boldsymbol{q}_i-\boldsymbol{r}), \tag{4.17}$$

$$\hat{j}^\alpha(\boldsymbol{r})=\sum_i\delta(\boldsymbol{q}_i-\boldsymbol{r})\,p_i^\alpha, \tag{4.18}$$

whereas the local energy density operator can be written as

$$\begin{aligned}\hat{\mathcal{H}}(\boldsymbol{r})&=\sum_i\delta(\boldsymbol{q}_i-\boldsymbol{r})\,\hat{h}_i\\&=\sum_i\delta(\boldsymbol{q}_i-\boldsymbol{r})\left[\frac{p_i^2}{2m}+\frac{1}{2}\sum_{j(\neq i)}v(|\boldsymbol{q}_i-\boldsymbol{q}_j|)+V(\boldsymbol{q}_i)\right].\end{aligned} \tag{4.19}$$

Here we point out that according to the *definition* (4.19), the interaction energy v_{ij} between two particles i and j (located at $\boldsymbol{q}_i$ and $\boldsymbol{q}_j$) is ascribed (without justification) half to particle i and half to particle j. To give an example, another admissible definition of the local energy density could ascribe the whole interaction energy v_{ij} to the point $(\boldsymbol{q}_i+\boldsymbol{q}_j)/2$. The apparent[14]

[14]Indeed, integrating over the volume of the system the ambiguity disappears and the Hamiltonian reduces to (4.11).

ambiguity in (4.19) is related to the non-local nature of the interparticle interaction potential $v(\boldsymbol{r})$, which should appear also in the definition of local quantities such as the local thermodynamic potentials (e.g. enthalpy, entropy, free energies ...) and in the corresponding fluxes [197, 63].

Mass conservation

The microscopic continuity equation for $\hat{\rho}(\boldsymbol{r})$ straightforwardly follows from Eq. (4.9):

$$\begin{aligned}\frac{\mathrm{d}\hat{\rho}(\boldsymbol{r})}{\mathrm{d}t} &= -\mathscr{L}\,\hat{\rho}(\boldsymbol{r}) = -\mathscr{L}_K\,\hat{\rho}(\boldsymbol{r}) = \sum_i \frac{\partial}{\partial \boldsymbol{q}_i}\delta(\boldsymbol{q}_i - \boldsymbol{r})\cdot\boldsymbol{p}_i \\ &= -\partial_\alpha\,\hat{j}^\alpha(\boldsymbol{r}),\end{aligned} \tag{4.20}$$

where $\hat{j}^\alpha(\boldsymbol{r})$ is defined in Eq. (4.18). Equation (4.20) has the form of a continuity equation expressing the conservation of mass at the microscopic level. However, we point out that any microscopic mass current operator $\hat{j}^\alpha_\rho(\boldsymbol{r})$ defined as

$$\hat{j}^\alpha_\rho(\boldsymbol{r}) = \hat{j}^\alpha(\boldsymbol{r}) + \Gamma^\alpha(\boldsymbol{r}), \tag{4.21}$$

where $\Gamma^\alpha(\boldsymbol{r})$ is any vector field characterised by a vanishing divergence

$$\partial_\alpha\Gamma^\alpha(\boldsymbol{r}) = 0,$$

fulfils of the continuity equation (4.20). The "generalised" mass current (4.21) shows how continuity equations of the form

$$\frac{\mathrm{d}\hat{A}(\boldsymbol{r})}{\mathrm{d}t} + \partial_\alpha\hat{J}^\alpha_A(\boldsymbol{r}) = 0,$$

where $\hat{A}(\boldsymbol{r})$ is the microscopic conserved observable and $J^\alpha_A(\boldsymbol{r})$ is the corresponding current operator, define fluxes of conserved quantities only up to zero-divergence vector fields.

Momentum conservation

Analogously, the rate of change of $\hat{j}^\alpha(\boldsymbol{r})$ according to (4.9) provides a local conservation law corresponding to the macroscopic momentum balance equation:

$$\begin{aligned}\frac{\mathrm{d}\hat{j}^\alpha(\boldsymbol{r})}{\mathrm{d}t} &= -\mathscr{L}\,\hat{j}^\alpha(\boldsymbol{r}) \\ &= -\partial_\beta\left[\sum_i \frac{p_i^\alpha p_i^\beta}{m}\delta(\boldsymbol{q}_i - \boldsymbol{r})\right] - \frac{\hat{\rho}(\boldsymbol{r})}{m}\partial_\alpha V(\boldsymbol{r}) \\ &\qquad - \frac{1}{2}\sum_{i\neq l}\frac{\partial v_{il}}{\partial q_i^\alpha}\big[\delta(\boldsymbol{q}_i - \boldsymbol{r}) - \delta(\boldsymbol{q}_l - \boldsymbol{r})\big].\end{aligned} \tag{4.22}$$

The last term in Eq. (4.22) can be written as the divergence of a second-rank tensor by means of the distributional identity [205]

$$\delta(\boldsymbol{q}_j - \boldsymbol{r}) - \delta(\boldsymbol{q}_i - \boldsymbol{r}) = \oint_{C_{i\to j}} \mathrm{d}y^\gamma \frac{\partial}{\partial y^\gamma} \delta(\boldsymbol{y} - \boldsymbol{r}) = -\partial_\gamma \oint_{C_{i\to j}} \mathrm{d}y^\gamma \delta(\boldsymbol{y} - \boldsymbol{r}), \tag{4.23}$$

where the integral is along *any* contour $C_{i\to j}$ from $\boldsymbol{q}_i$ to $\boldsymbol{q}_j$. Making use of this result in Eq. (4.22) we obtain the microscopic continuity equation for the momentum density $\hat{j}^\alpha(\boldsymbol{r})$

$$\frac{\mathrm{d}\hat{j}^\alpha(\boldsymbol{r})}{\mathrm{d}t} = -\partial_\beta \hat{J}_j^{\alpha\beta}(\boldsymbol{r}) - \frac{\hat{\rho}(\boldsymbol{r})}{m}\partial_\alpha V(\boldsymbol{r}), \tag{4.24}$$

where we have defined the microscopic momentum current operator $\hat{J}_j^{\alpha\beta}(\boldsymbol{r})$[15] as

$$\hat{J}_j^{\alpha\beta}(\boldsymbol{r}) = \sum_i \frac{p_i^\alpha p_i^\beta}{m}\delta(\boldsymbol{q}_i - \boldsymbol{r}) + \frac{1}{2}\sum_{i\neq l} \frac{\partial v_{il}}{\partial q_i^\alpha} \oint_{C_{i\to l}} \mathrm{d}y^\beta \delta(\boldsymbol{y} - \boldsymbol{r}). \tag{4.25}$$

Finally, as regards system where particles interact through central pair-wise potentials, the momentum flux $\hat{J}_j^{\alpha\beta}(\boldsymbol{r})$ can be more conveniently written as

$$\hat{J}_j^{\alpha\beta}(\boldsymbol{r}) = \sum_i \frac{p_i^\alpha p_i^\beta}{m}\delta(\boldsymbol{q}_i - \boldsymbol{r}) - \frac{1}{2}\sum_{i\neq l} \frac{q_{il}^\alpha}{|\boldsymbol{q}_{il}|} \left.\frac{\mathrm{d}v(q)}{\mathrm{d}q}\right|_{q=|\boldsymbol{q}_{il}|} \oint_{C_{i\to l}} \mathrm{d}y^\beta \delta(\boldsymbol{y} - \boldsymbol{r}), \tag{4.26}$$

with $\boldsymbol{q}_{ij} = \boldsymbol{q}_j - \boldsymbol{q}_i$. Note that the last term in Eq. (4.24) acts as a source contribution when a space dependent external field $V(\boldsymbol{r})$ is present. The average value of the operator $\hat{J}_j^{\alpha\beta}(\boldsymbol{r})$ is the so called (local) *pressure tensor*

$$p^{\alpha\beta}(\boldsymbol{r}) = \left\langle \hat{J}_j^{\alpha\beta}(\boldsymbol{r}) \right\rangle. \tag{4.27}$$

Equation (4.25) explicitly shows that the local momentum current, which enters the continuity equation for the momentum density (4.24), can not be defined without ambiguity because different contours in (4.25) lead to different expressions for $\hat{J}_j^{\alpha\beta}(\boldsymbol{r})$ and also for the pressure tensor. This arbitrariness in the definition of the momentum flux has the same origin as the arbitrariness in the definition of the mass flux. Also the continuity equation for the momentum

[15] Some references adopt a slightly different notation, introducing the *stress tensor* $\hat{\sigma}^{\alpha\beta}$, defined as $\hat{\sigma}^{\alpha\beta}(\boldsymbol{r}) = -\hat{J}_j^{\alpha\beta}(\boldsymbol{r})$.

uniquely defines only the gradient of the momentum momentum flux. As before, any other tensor which differs from $\hat{J}_j^{\alpha\beta}(\boldsymbol{r})$ by a quantity $\Gamma^{\alpha\beta}(\boldsymbol{r})$ such that

$$\partial_\beta \Gamma^{\alpha\beta}(\boldsymbol{r}) = 0 \tag{4.28}$$

fulfils the continuity equation. The arbitrariness with respect to the choice of the contour in the definition (4.25) is just a different statement of this fact. A remarkable consequence of the arbitrariness in the choice of the contour is that both symmetric and anti-symmetric definitions of the pressure tensor are legitimate and a privileged choice can not be justified. However, it has been shown [150] that it is always possible to construct a symmetric momentum flux tensor. Furthermore, the symmetries of the system restrain the range of admissible definitions of the tensor, but in general an infinite number of possibilities can be available.

For a system of particles interacting through central pair-wise additive potentials the pressure tensor reads[16]

$$\begin{aligned} p^{\alpha\beta}(\boldsymbol{r}) = & \frac{\rho(\boldsymbol{r})\, k_{\mathrm{B}} T}{m}\, \delta^{\alpha\beta} \\ & - \frac{1}{2} \int \mathrm{d}\boldsymbol{y}\, \frac{y^\alpha}{|\boldsymbol{y}|} \frac{\mathrm{d}v(|\boldsymbol{y}|)}{\mathrm{d}|\boldsymbol{y}|} \oint_{C_{\mathbf{0}\to\boldsymbol{y}}} \mathrm{d}s^\beta \rho^{(2)}(\boldsymbol{r}-\boldsymbol{s}, \boldsymbol{r}-\boldsymbol{s}+\boldsymbol{y}), \end{aligned} \tag{4.29}$$

where $\rho^{(2)}(\boldsymbol{r}, \boldsymbol{r}')$ is the two-particle density [98] and the line integral is extended, without any loss in generality [205], from the origin $\mathbf{0}$ to a given point $\boldsymbol{y}$. Making use of this result it is straightforward to show that in the homogeneous and isotropic limit the ambiguity in the definition of the pressure tensor disappears. Indeed the two-particle distribution function can be expressed in terms of the radial distribution function

$$\rho^{(2)}(\boldsymbol{r}, \boldsymbol{r}') = \left(\frac{\rho}{m}\right)^2 g(|\boldsymbol{r}-\boldsymbol{r}'|)$$

and (4.29) reduces to

$$p^{\alpha\beta}(\boldsymbol{r}) = p\, \delta^{\alpha\beta} = \frac{\rho\, k_{\mathrm{B}} T}{m}\, \delta^{\alpha\beta} - \frac{1}{2}\frac{\rho^2}{m^2} \int \mathrm{d}\boldsymbol{r}\, \frac{r^\alpha r^\beta}{|\boldsymbol{r}|} \frac{\mathrm{d}v(|\boldsymbol{r}|)}{\mathrm{d}|\boldsymbol{r}|}\, g(|\boldsymbol{r}|), \tag{4.30}$$

which is the well known *virial* (or pressure) equation for a homogeneous and isotropic fluid at density ρ [98].

[16] Note that (4.25) can be written as

$$\hat{J}_j^{\alpha\beta}(\boldsymbol{r}) = \sum_i \frac{p_i^\alpha p_i^\beta}{m} \delta(\boldsymbol{q}_i - \boldsymbol{r}) - \frac{1}{2} \sum_{i\neq l} \frac{q_{il}^\alpha}{|\boldsymbol{q}_{il}|} \left.\frac{\mathrm{d}v(q)}{\mathrm{d}q}\right|_{q=|\boldsymbol{q}_{il}|} \oint_{C_{i\to l}} \mathrm{d}y^\beta \delta(\boldsymbol{y} - \boldsymbol{r}),$$

with $\boldsymbol{q}_{ij} = \boldsymbol{q}_j - \boldsymbol{q}_i$, and after a proper change of variables (see [205], Eq. (3.2)) we obtain (4.29).

The non-uniqueness of the local pressure tensor has been first recognised by Kirkwood in the fifties. He provided an expression for the configurational contribution to the stress tensor in a paper with Buff [117] and a different one in another work with Irving [109][17]. The first explicit description of the ambiguity can be found in the paper by Harasima [99] whereas a rigorous and exhaustive study of the problem was given in the eighties by Schofield and Henderson [205].

This lack of uniqueness in the definition of the pressure tensor has been recently recovered in two papers [81, 82] dealing with thermo-osmosis. The authors try to discriminate between different expressions of the pressure tensor estimating the value of the thermo-osmotic flow resulting from (approximate) predictions, which involve the knowledge of the pressure tensor itself. In the most recent paper [82] they compare these predictions with the (exact) results obtained through a clever nonequilibrium molecular dynamics simulation and they conclude that both the virial and the Irving-Kirkwood expression do not accurately predict surface forces due to temperature gradients.

However, we remark that the infinite possible definitions of the the pressure tensor are indeed equivalent, i.e. all the *physical observables* must be invariant with respect to different choices of the path $C_{i\to j}$ [205]. As regards an inhomogeneous fluid, the pressure tensor is not a well defined observable on a length scale shorter than the correlation length or the range of the interparticle potential [197]. Qualitatively, we can try to understand this circumstance reflecting on the fact that it is not possible to identify the surface where the pressure is acting. Analogously, it is not possible to define without ambiguities the surface which separates two different phases of the same fluid. On the other hand, the force exerted on a given region of fluid and the surface tension of an interface are well defined quantities and do not depend on the particular definition of the pressure tensor[18]. To give a more concrete example, it is straightforward to check that the force $\boldsymbol{F}_V$ exerted by the particles on a sub-volume V of the system, which is a legitimate physical quantity, is unambiguously defined. Indeed, making use of the microscopic continuity equation for the momentum we obtain

$$F_V^\alpha = \frac{\mathrm{d}}{\mathrm{d}t}\int_V \mathrm{d}\boldsymbol{r}\,\hat{j}^\alpha(\boldsymbol{r}) = -\int_V \mathrm{d}\boldsymbol{r}\,\left[\partial_\beta \hat{J}_j^{\alpha\beta}(\boldsymbol{r}) + \frac{\hat{\rho}(\boldsymbol{r})}{m}\partial_\alpha V(\boldsymbol{r})\right]$$

and we readily realise that the force is not altered by divergence-free fields (4.28) added to the momentum flux.

As regards approximate theories, such as the local equilibrium assumption or the approach originally put forward by Derjaguin and recently adopted in [81, 82], the invariance of the observables with respect different definitions of

[17] The so called Irving-Kirkwood definition of the stress tensor is reported in the Appendix of [109].

[18] The virial expression is an allowed choice for the pressure tensor only for homogeneous and isotropic fluids.

the pressure tensor can not be guaranteed. However, the slip velocity of a fluid subject to a temperature gradient is a genuine physical quantity, also from the microscopic viewpoint. Therefore an *exact* prediction of the thermo-osmotic slip must be invariant on the choice of the trajectory in (4.25): We conclude that both the local thermal equilibrium and the Derjaguin approach include some errors, because their expression are not endowed by this invariance.
Finally, we stress that the virial pressure tensor (4.30), used in [81, 82] to obtain the thermo-osmotic velocity of the fluid, does not correspond to any path in Eq. (4.25) and does not fulfil the hydrostatic balance condition for inhomogeneous fluids. This expression is commonly adopted within continuum hydrodynamics, where the relevant quantities are assumed to be varying on a length scale larger than the correlation length, i.e. when the definition of local thermodynamic quantities is legitimate[19].

Energy conservation

The microscopic conservation law for the energy density $\hat{\mathcal{H}}(\boldsymbol{r})$ can be obtained through the same steps followed before in the case of the mass current:

$$\begin{aligned}\frac{\mathrm{d}\hat{\mathcal{H}}(\boldsymbol{r})}{\mathrm{d}t} &= -\mathscr{L}\,\hat{\mathcal{H}}(\boldsymbol{r}) \\ &= -\mathscr{L}_K\hat{\mathcal{H}}(\boldsymbol{r}) - \sum_i \delta(\boldsymbol{q}_i-\boldsymbol{r})\Big[\mathscr{L}_v+\mathscr{L}_V\Big]\frac{p_i^2}{2m}\end{aligned} \tag{4.31}$$

After some algebra, the action of the Liouvillians on the Hamiltonian gives

$$\mathscr{L}_K\hat{\mathcal{H}}(\boldsymbol{r}) = \sum_i \frac{p_i^\alpha}{m}\left[h_i\partial_\alpha\delta(\boldsymbol{q}_i-\boldsymbol{r}) - \frac{\partial V(\boldsymbol{q}_i)}{\partial q_i^\alpha}\right] - \frac{1}{2m}\sum_{i\neq j}\delta(\boldsymbol{q}_i-\boldsymbol{r})\frac{\partial v_{ij}}{\partial q_i^\alpha}\left(p_i^\alpha - p_j^\alpha\right),$$

$$\Big[\mathscr{L}_v+\mathscr{L}_V\Big]\frac{p_i^2}{2m} = \frac{p_i^\alpha}{m}\left[\sum_{j(\neq i)}\frac{\partial v_{ij}}{\partial q_i^\alpha} + \frac{\partial V(\boldsymbol{q}_i)}{\partial q_i^\alpha}\right].$$

Making use of these results in Eq. (4.31), we get

$$\frac{\mathrm{d}\hat{\mathcal{H}}(\boldsymbol{r})}{\mathrm{d}t} = -\partial_\alpha\left[\sum_i \delta(\boldsymbol{q}_i-\boldsymbol{r})\frac{p_i^\alpha}{m}h_i\right] - \frac{1}{2m}\sum_{i\neq j}p_i^\alpha\frac{\partial v_{ij}}{\partial q_i^\alpha}\left[\delta(\boldsymbol{q}_i-\boldsymbol{r}) - \delta(\boldsymbol{q}_j-\boldsymbol{r})\right].$$

The identity (4.23) allows to rewrite the last Equation in the form of a microscopic conservation law

$$\frac{\mathrm{d}\hat{\mathcal{H}}(\boldsymbol{r})}{\mathrm{d}t} = -\partial_\alpha\hat{J}^\alpha_{\mathcal{H}}(\boldsymbol{r}), \tag{4.32}$$

[19] Unless the pathological case where the system is in near critical conditions.

where we have defined the energy current $\hat{J}^{\alpha}_{\mathcal{H}}(\boldsymbol{r})$ as

$$\hat{J}^{\alpha}_{\mathcal{H}}(\boldsymbol{r}) = \sum_i \frac{p_i^{\alpha}}{m}\delta(\boldsymbol{q}_i - \boldsymbol{r})\hat{h}_i - \frac{1}{2}\sum_i \frac{p_i^{\delta}}{m}\sum_{j(\neq i)} \frac{\partial v_{ij}}{\partial q_i^{\delta}} \oint_{C_{i\to j}} \mathrm{d}y^{\alpha}\delta\left(\boldsymbol{y} - \boldsymbol{r}\right) \quad (4.33)$$

and the integral is along any contour $C_{i\to j}$ from $\boldsymbol{q}_i$ to $\boldsymbol{q}_j$.
Here we stress that Eq. (4.33) is the microscopic energy flux according to the definition of the local energy density given in Eq. (4.19). Different microscopic choices for the local energy result in different expressions of $\hat{J}^{\alpha}_{\mathcal{H}}(\boldsymbol{r})$. In addition to this, the same considerations stated above in the case of the momentum current apply: The ambiguity in the definition of the heat flux is recovered in the freedom connected to the choice of the path. However, the thermal transport coefficients turn out to be independent on the particular choice in Eq.s (4.33) and (4.19) (see Ref. [63]).

4.3 LINEAR RESPONSE THEORY

A common way to obtain information from an equilibrium system is to perturb it and to study the associated response. The *perturbation* can be achieved by applying an external field, which couples to an observable of the system and therefore an additional term appears in the Hamiltonian. Besides the so called mechanical perturbations, it is possible to bring a system out of equilibrium by imposing a temperature gradient. The main difference between mechanical and thermal perturbations is that it is not possible to represent a thermal disturbance as an additional term in the Hamiltonian, because thermal perturbations carry a statistical nature.
The *response* of the system to the perturbation is characterised by the presence of fluxes (or currents) and can always be expressed in terms of time-dependent correlation functions of the unperturbed system. Furthermore, if we restrict to *small* perturbations[20], the response of the system turns out to be linear in the perturbation and can be expressed through the equilibrium average of an appropriate product of two space and time-dependent operators [112].

Linear nonequilibrium thermodynamics [41] assumes linear relations between the external fields and the corresponding fluxes (see e.g. Eq. (4.4) and (4.5)): The proportionality constants of these phenomenological relations are collectively called *transport coefficients*. Linear response theory provides a microscopic expression for these coefficients in terms of dynamical correlations at equilibrium and, in the continuum limit, the description it based on this

[20]Some objections were raised by van Kampen, based on the fact that the trajectory of a charged particle in the presence of an electric field deviates drastically with respect to the unperturbed case. The replies to these objections are rooted on the fact that statistical mechanical calculations are based on the behaviour of a large number of independent particles. See e.g. [54] and references therein.

formalism reduces to the hydrodynamic Navier-Stokes equations. The relations linking transport coefficients to time correlation functions are referred to as Kubo (or Green-Kubo) formulas, even if much of the work on them dates back to Nyquist [164], Kirkwood, Callen and Welton [29] and finally Green [89, 90, 91].

The approaches based on linear response theory prove to be a powerful tool towards a general theory of nonequilibrium statistical mechanics, at least for slight deviations from equilibrium. Indeed, as stated by Zwanzig [257], in equilibrium statistical mechanics all the thermodynamic properties follow, at least in principle, from the evaluation of the partition function of the system whereas the dynamical correlation functions play the same role in the description of systems out of equilibrium. The analogy is somehow broken by the fact that the partition function gives all the thermodynamic properties whereas a correlation function describes a single transport process.

Kubo's formalism for mechanical perturbations

The method proposed by Kubo [125, 126] is attractive because of its simplicity and its marked operational character. In order to clarify this point, let us consider the measurement of the conductivity of a metal. The experiment consists of three stages. The first one is the initial preparation of the system, in which the metal is set in a condition of thermal equilibrium. The experimentalist "samples" from the equilibrium ensemble imposing a fixed temperature to the wire and repeating the measurement for different portions of the same wire. Then the perturbation, in this case the external electric field, is switched on. There are different ways to turn on the perturbation, but here we will not discuss the possible prescriptions. The last step is the measurement of the current induced in the sample by the field and the average of the results. The approach by Kubo is the formal (mathematical) translation of this operational procedure.

To make things more quantitative, let us consider a system consisting of several species of charged particles with total charge equal to zero. Particle i is characterised by a charge $z_i e$, where e is the charge of the electron. The quantity we want to measure is the charge current, which can be locally defined as

$$\hat{j}_q^\alpha(\boldsymbol{r}) = \sum_i \frac{z_i e}{m} \delta(\boldsymbol{q}_i - \boldsymbol{r})\, p_i^\alpha. \tag{4.34}$$

The system is prepared in thermal equilibrium and its state is specified by the canonical distribution function $F_0(q,p) = \exp\{-\beta H_0(q,p)\}/Z$, where $\beta = 1/k_{\mathrm{B}}T$, $H_0(q,p) = H_K(q,p) + H_v(q,p)$ is the free Hamiltonian and Z is the canonical partition function. From the dynamical point of view, the unperturbed system can be described through the solutions of the Hamilton's equations induced by the Hamiltonian H_0, to which a Liouvillian $\mathscr{L}_0 =$

$\mathscr{L}_K + \mathscr{L}_v$ is associated (see Eq. (4.12)).
Following Kubo's approach, at a given time (let us say $t = 0$) we switch on an electric field $\boldsymbol{E}(t)$, constant in space. Due to the presence of the external field, the additional term

$$H_V(t) = -e \sum_i z_i E^\alpha(t) q_i^\alpha$$

adds to the unperturbed Hamiltonian. The Liouvillian $\mathscr{L}_V(t)$ associated to this term has the form (see Eq. (4.12))

$$\mathscr{L}_V(t) = -e \sum_i z_i E^\alpha(t) \frac{\partial}{\partial p_i^\alpha}. \tag{4.35}$$

After the switch-on of the electric field, the state of the system is described by a time-dependent distribution function which evolves according the Liouville equation (4.13)

$$\partial_t F(t) = \big[\mathscr{L}_0 + \mathscr{L}_V(t)\big] F(0), \tag{4.36}$$

where the initial condition is $F(0) = F_0$.

The next step is to obtain the distribution $F(t)$ of the perturbed system in order to evaluate the average of the current (4.34), i.e. the response of the system, at a given time $t > 0$. Here we wish to solve the evolution equation (4.36) under the hypothesis that the perturbation due to $\mathscr{L}_V(t)$ is small, because we are interested in the linear response of the system to external fields. Let us begin assuming that the time evolution operator (see Eq. (4.14)) of the unperturbed system $\mathscr{U}_0$ is known. Then, in the spirit of perturbative approaches, we express the evolution operator $\mathscr{U}$ associated to the perturbed Hamiltonian as

$$\begin{aligned}\mathscr{U}(t) &= \mathscr{U}_0(t) + \int_0^t \mathrm{d}t'\, \mathscr{U}_0(t-t')\, \mathscr{L}_V(t') \mathscr{U}(t') \\ &= \mathscr{U}_0(t) + \int_0^t \mathrm{d}t'\, \mathscr{U}_0(t')\, \mathscr{L}_V(t-t') \mathscr{U}(t-t'),\end{aligned}$$

where the second line follows from a straightforward change of variables. This equation can be solved iteratively and gives rise to an infinite series of terms. Here we are interested into linear responses and, at linear order in the perturbation, we get

$$\mathscr{U}(t) = \mathscr{U}_0(t) + \int_0^t \mathrm{d}t'\, \mathscr{U}_0(t')\, \mathscr{L}_V(t-t') \mathscr{U}_0(t-t').$$

The probability distribution at time t reads

$$\begin{aligned}F(t) = \mathscr{U}(t) F_0 &= F_0 + \int_0^t \mathrm{d}t'\, \mathscr{U}_0(t') \mathscr{L}_V(t-t') F_0 \\ &= F_0 + \beta \int_0^t \mathrm{d}t'\, E^\alpha(t-t') \int \mathrm{d}\boldsymbol{r}'\, \mathscr{U}_0(t') \left\{ \hat{j}_q^\alpha(\boldsymbol{r}') F_0 \right\}\end{aligned} \tag{4.37}$$

because the equilibrium distribution F_0 is a stationary solution to the Liouville equation and Eq. (4.37) follows from the identity

$$\begin{aligned}\mathscr{L}_V(t)F_0 &= -e\sum_i z_i E^\alpha(t)\frac{\partial F_0}{\partial p_i^\alpha} = F_0\beta\sum_i \frac{z_i e}{m}E^\alpha(t)p_i^\alpha \\ &= F_0\beta E^\alpha(t)\int \mathrm{d}\boldsymbol{r}'\sum_i \frac{z_i e}{m}\delta(\boldsymbol{q}_i-\boldsymbol{r}')p_i^\alpha \\ &= F_0\beta E^\alpha(t)\int \mathrm{d}\boldsymbol{r}'\,\hat{j}_q^\alpha(\boldsymbol{r}').\end{aligned}$$

The last step of Kubo's method is the evaluation of the average charge current at time t, which, according to Eq. (4.37), is given by

$$\begin{aligned}\left\langle \hat{j}_q^\alpha(\boldsymbol{r})\right\rangle_t &= \beta\int_0^t \mathrm{d}t'\,E^\delta(t-t')\int \mathrm{d}\boldsymbol{r}'\iint \mathrm{d}q\,\mathrm{d}p\,\hat{j}_q^\alpha(\boldsymbol{r})\,\mathscr{U}_0(t')\left[\hat{j}_q^\delta(\boldsymbol{r}')F_0\right] \\ &= \beta\int_0^t \mathrm{d}t'\,E^\delta(t-t')\int \mathrm{d}\boldsymbol{r}'\iint \mathrm{d}q\,\mathrm{d}p\,\mathscr{U}_0(-t')\left[\hat{j}_q^\alpha(\boldsymbol{r})\right]\,\hat{j}_q^\delta(\boldsymbol{r}')\,F_0 \\ &= \beta\int_0^t \mathrm{d}t'\,E^\delta(t-t')\int \mathrm{d}\boldsymbol{r}'\left\langle \hat{j}_q^\alpha(\boldsymbol{r},t')\hat{j}_q^\delta(\boldsymbol{r}')\right\rangle_0. \qquad (4.38)\end{aligned}$$

In the first line the average of $\hat{j}_q^\alpha(\boldsymbol{r})$, evaluated with respect to F_0, is vanishing because $\hat{j}_q^\alpha(\boldsymbol{r})$ is an odd function of the momenta; in the second equality we have exploited the invariance of the dynamics with respect to the canonical transformation $\mathscr{U}_0(t)$ and $\langle\ldots\rangle_0$ indicates the average evaluated with the distribution F_0.

Equation (4.38) expresses the response to a disturbance in terms of an unperturbed correlation function of two space and time-dependent operators. This result is general and can be extended to all kind of mechanical perturbations because in our derivation the only assumption is the particular form of the perturbing field.

In the case of a homogeneous system the average current density does not depend on position and, performing a straightforward change of variables, Eq. (4.38) can be written in a more evocative form as

$$\left\langle \hat{j}_q^\alpha\right\rangle_t = \int_{-\infty}^t \mathrm{d}t'\,E^\delta(t')\,\chi^{\alpha\delta}(t-t'), \qquad (4.39)$$

where the integrated kernel, defined

$$\chi^{\alpha\delta}(t) = \beta\int \mathrm{d}\boldsymbol{r}'\left\langle \hat{j}_q^\alpha(\boldsymbol{r},t)\hat{j}_q^\delta(\boldsymbol{r}')\right\rangle_0,$$

is usually referred to as the (tensorial) *response function*, or the admittance. Equation (4.39) is the most general relationship which describes the response of a system to a perturbation with the properties of causality, linearity and

stationarity.
If we limit to a time-independent perturbing field $\boldsymbol{E}(t) = \boldsymbol{E}$, the evolution of the measured current is the following. For $t < 0$ the system is at equilibrium with $\boldsymbol{E} = \boldsymbol{0}$ and $\langle \hat{j}_q^\alpha \rangle_t = 0$. As soon as the field is switched-on, the system reacts to the perturbation and a current appears: The current varies in time until a steady state is reached. The current is proportional to the field $\boldsymbol{E}$ and the constant of proportionality is, by definition, the electrical conductivity tensor $\sigma^{\alpha\delta}$. If this steady state exists, it will be reached by our system at $t \to \infty$ and (4.38) becomes

$$\langle \hat{j}_q^\alpha \rangle_{t\to\infty} = \sigma^{\alpha\delta} E^\delta,$$

where the conductivity has the form

$$\sigma^{\alpha\delta} = \beta \int_0^{+\infty} \mathrm{d}t' \int \mathrm{d}\boldsymbol{r}' \, \langle \hat{j}_q^\alpha(\boldsymbol{r}, t') \hat{j}_q^\delta(\boldsymbol{r}') \rangle_0.$$

This result for the static conductivity is an example of *Green-Kubo relation*, and was first obtained in this form by Kubo [125]. In the spirit of Eq. (4.39), the transport coefficients are therefore nothing but an example of response functions.

We add some remarks before concluding. The derivation of the Green-Kubo relations is a particular consequence of a class of relations collected under the name of the fluctuation-dissipation theorem [126]. According to this theorem the (linear) response to an external perturbation, which brings the system out of equilibrium, is linked to the fluctuation properties of the equilibrium system. Roughly speaking, this connection is rooted in the fact that the system cannot distinguish between a relaxation towards equilibrium as a result of a random thermal fluctuation and a relaxation towards equilibrium as a result of the perturbation due to an external field [166, 167].
Furthermore, we mention that the explicit evaluation of the transport coefficients by means of the Green-Kubo relations is a hard task, because the solution of the complete (N-body) problem is required. Finally, special care must be paid when dealing with correlation functions involving currents of conserved quantities. Indeed, it is well known since the work by Adler and Wainwright [2] that the velocity autocorrelation function for a hard sphere gas decays as a power law for large times. This long tail behaviour has been confirmed by means of kinetic equations [12].

4.4 MORI'S LINEAR RESPONSE APPROACH TO THERMAL PERTURBATIONS

The formalism outlined in the previous Section provides a general framework linking transport coefficients to dynamical correlation functions. These arguments can be applied only in the case of mechanical perturbations, that is

when the presence of disturbance results in an additional term in the Hamiltonian of the system.
However, we are familiar with another class of transport coefficients, introduced in the context of (macroscopic) hydrodynamics in order to close the set of mass, energy and momentum continuity equations. The bulk η and shear ζ viscosity link the dissipative contribution to the pressure tensor (momentum flux) to the velocity gradients, whereas the thermal conductivity κ is the proportionality coefficient between the heat flux and the temperature gradient. Furthermore in a diffusive process the mass current is linked to the concentration gradient by the diffusion coefficient D. One common feature shared by these transport coefficients is that the corresponding fluxes arise due to a perturbation not represented by an additional term in the Hamiltonian. For example, it has not been devised yet a convincing (and natural) way to represent the effects of a temperature gradient by means of a perturbation to the Hamiltonian [257, 11]. Similar considerations apply whenever the fluxes are the response to *spatial inhomogeneities* of the system, e.g. temperature and chemical potential gradients.

Even if Kubo's method can not be applied to perturbations due to spatial inhomogeneities, several approaches [257] have been developed in order to express the so called thermal transport coefficients in terms of time integrals of dynamical correlation functions. All the predictions obtained agree with each other[21] [257] and there is no reason to prefer one formalism from the others. Furthermore the results of the aforementioned approaches, where transport coefficients are interpreted as generalised susceptibilities, have been corroborated within kinetic theory. At the lowest order, for dilute systems, kinetic theories express the transport coefficients as integrals of time correlation functions, analogously to what happens in the case of the correlation function approaches [12]. It was formally shown by Rèsibois [186] that this equivalence indeed holds to all orders, because it is possible to prove that in both cases the transport coefficients follow from the solution of an identical (up to an exact transformation) inhomogeneous integral equation. Here we point out that this equivalence is not a justification of the correlation function methods through kinetic theories, but only a proof of their internal consistence despite the severe assumptions taken.

The method proposed by Hazime Mori [155, 156] handles the disturbances due to spatial inhomogeneities through the concept of local equilibrium. His second work, published in 1958, describes the relaxation towards equilibrium of a liquid in a nonequilibrium state in contact with heat and mass reservoirs. Mori's fundamental assumption is that the initial state of the liquid (which is assumed to be known) can be described through a local equilibrium distribution. Recalling Kubo's method outlined in the previous Section, this assumption is

[21] Up to the harmless discrepancies in the time correlation functions generated by the different ensembles adopted.

equivalent to replace the (global) canonical distribution function $F(0) = F_0$ in Eq. (4.36) with a given local equilibrium distribution. Once we have done this substitution, the derivation of the transport coefficients follows along the same line outlined before. Mori's approach can therefore be considered as a generalisation of Kubo's linear response method to treat inhomogeneities not arising from external potentials.
The local equilibrium distribution, as we shall see below, accommodates all the inhomogeneities of the system via two scalar and one vector field: The scalar fields are linked to the local temperature and chemical potential, whereas the vector field is linked to the fluid velocity profile. The limits of validity of Mori's approach are naturally related to those of the local equilibrium distribution. In particular, Mori's assumption is an extension of local equilibrium concept to the full distribution function: Single particle local equilibrium distributions arise naturally in the context of kinetic theories, but the generalisation to many particle distribution in principle can be an hazard.

Mori's local equilibrium theory has been certainly an important step in order to carry out Kirkwood's program on statistical physics. According to the American physicist, the main objectives of statistical mechanics of transport processes were to obtain a microscopic derivation of the hydrodynamics equations, to investigate the limits of validity of the phenomenological constitutive relations between forces and fluxes (such as Fick and Fourier's laws) and to give a microscopic expression for the transport coefficients. Mori's theory of transport processes goes towards this direction because gives a microscopic basis for the phenomenological equations and provides explicit expressions for the kinetic coefficients involved in such equations. The resulting expressions for the thermal transport coefficients are completely analogous to the Kubo formula for the electrical conductivity and involve integrals of time correlation function evaluated at equilibrium (i.e. without perturbation).
To give an example, the isotropic thermal conductivity turns out to be proportional to the time integral of the two-point correlation function of the heat current[22]

$$\kappa = \frac{1}{k_{\mathrm{B}} T^2 V} \int_0^\infty \mathrm{d}t' \left\langle \hat{J}_Q^x(t') \, \hat{J}_Q^x \right\rangle_0,$$

where $\hat{J}_Q^\alpha = \hat{J}_H^\alpha - h_m \sum_{i=1}^N p_i^\alpha$ is the (total) heat flux operator[23], $\hat{J}_H^x$ is the (total) energy current operator and h_m is the hentalpy per unit mass.

The goal of this Chapter is the description of an inhomogeneous system in a stationary state slightly off-equilibrium. To achieve our purpose we will adopt Mori's theory, generalised to inhomogeneous and anisotropic fluids. Within our system space inhomogeneities are generated by a temperature gradient and an external potential. Even if the original work was formulated within

[22] Mori's paper adopts a quantum mechanics description, here we give the classical limit.
[23] We will define this operator more formally below. In particular we will give a local definition of this vector.

quantum statistical mechanics, we will adopt classical statistical mechanics and the grand canonical formalism. Furthermore, Mori was interested in the relaxation behaviour of a system, starting from an out-of-equilibrium state towards full equilibrium. Instead here we keep the system in a nonequilibrium condition imposing a fixed temperature difference at some boundaries.
In the first Subsection we will introduce Mori's formalism and then we will apply the results to an infinite channel.

Mori's formalism for inhomogeneous systems

Let us consider a system of interacting particles in the presence of an external potential, described by the Hamiltonian defined in Eq. (4.11) and kept at a non-uniform temperature. Following the approach developed by Mori, we define a Local Thermal Equilibrium (LE) distribution function which resembles a local generalisation of the Boltzmann weight:

$$F^{LE} = \mathcal{Q}^{-1}\, \mathrm{e}^{-\int \mathrm{d}\boldsymbol{r}\, \beta(\boldsymbol{r})\, \hat{\mathcal{E}}(\boldsymbol{r})}, \tag{4.40}$$

where $\beta(\boldsymbol{r})$ is a scalar field related to the local temperature, $\hat{\mathcal{E}}(\boldsymbol{r})$ is the local internal energy operator and $\mathcal{Q} = \mathrm{Tr}\{F^{LE}\}$ is the partition function. The presence of a non-uniform temperature induces in the system a non-uniform chemical potential and a local velocity profile. Therefore the internal energy must include the contributions arising from these two local fields:

$$\hat{\mathcal{E}}(\boldsymbol{r}) = \hat{\mathcal{H}}(\boldsymbol{r}) - \hat{\boldsymbol{j}}(\boldsymbol{r}) \cdot \boldsymbol{u}(\boldsymbol{r}) - \mu(\boldsymbol{r})\hat{\rho}(\boldsymbol{r}).$$

The local Hamiltonian, momentum and particle densities have been defined in Eq.s (4.19), (4.18) and (4.17) respectively. Here $\boldsymbol{u}(\boldsymbol{r})$ and $\mu(\boldsymbol{r})$ are the vector and scalar fields linked to the local velocity profile and chemical potential (per unit mass) of the fluid respectively. The three fields just introduced couple locally to the conserved quantities: $\mu(\boldsymbol{r})$ couples to the local mass, $\boldsymbol{u}(\boldsymbol{r})$ to the local momentum and $\beta(\boldsymbol{r})$ to the local energy. These fields define the LE state and are considered as *external known parameters*: We will discuss later how to fix them. In order to justify the linear response formalism, we require that they are smooth functions and that their gradients $\partial_\alpha \beta(\boldsymbol{r})$, $\partial_\alpha u^\beta(\boldsymbol{r})$ and $\partial_\alpha \mu(\boldsymbol{r})$ are small. Furthermore we limit to the study of systems where it is possible to find a Galileo transformation such that the field $\boldsymbol{u}(\boldsymbol{r})$ is small[24].

Local Equilibrium averages

The averages according to the LE distribution (4.40) can be evaluated within linear response theory as follows. The essential hypothesis is that the

[24]For this reason we can neglect the quadratic terms in the expression of the local energy density $\hat{\mathcal{E}}(\boldsymbol{r})$ given in [156, 11].

nonequilibrium state defined by the LE distribution is very close, or analogously is a small perturbation, of an equilibrium state. First of all we introduce the underlying (zero order) equilibrium distribution function

$$F^{eq} = \mathcal{Q}_0^{-1} \mathrm{e}^{-\beta(H-\mu m N)} \tag{4.41}$$

defined by uniform temperature β and chemical potential (per unit mass) μ and vanishing velocity field $\boldsymbol{u}(\boldsymbol{r}) = 0$. Here $\mathcal{Q}_0$ is the equilibrium grand canonical partition function. The fields characterising the out-of-equilibrium state can then be written in terms of small deviations from the constant values of the temperature, the chemical potential and the vanishing velocity profile:

$$\beta(\boldsymbol{r}) = \beta + \delta\beta(\boldsymbol{r}), \qquad \mu(\boldsymbol{r}) = \mu + \delta\mu(\boldsymbol{r}), \qquad \boldsymbol{u}(\boldsymbol{r}) = \boldsymbol{0} + \delta\boldsymbol{u}(\boldsymbol{r}).$$

Following the method inspired by linear response theory, we expand the LE distribution (4.40) about the equilibrium distribution (4.41) to the first order in the deviations $\delta\beta(\boldsymbol{r})$, $\delta\mu(\boldsymbol{r})$ and $\delta\boldsymbol{u}(\boldsymbol{r})$. Noticing that the deviations from the equilibrium underlying distribution arise both in the exponential and in the partition function of F^{LE} we get

$$F^{LE} \simeq \frac{\mathrm{e}^{-\int \mathrm{d}\boldsymbol{r}\, \beta(\boldsymbol{r})\, \hat{\mathcal{E}}(\boldsymbol{r})}}{\mathcal{Q}} = \frac{\mathcal{Q}_0\, F^{eq}\, (1 - \hat{C}_e)}{\mathcal{Q}_0\, (1 - C_{\mathcal{Q}})} \simeq F^{eq}(1 - \hat{C}_e + C_{\mathcal{Q}}),$$

where the linear corrections to the exponential and the partition function are:

$$\begin{aligned} \hat{C}_e &= \int \mathrm{d}\boldsymbol{r} \Big\{ \delta\beta(\boldsymbol{r}) \Big[\hat{\mathcal{H}}(\boldsymbol{r}) + \mu\hat{\rho}(\boldsymbol{r}) \Big] - \beta \Big[\hat{\boldsymbol{j}}(\boldsymbol{r}) \cdot \delta\boldsymbol{u}(\boldsymbol{r}) - \delta\mu(\boldsymbol{r})\hat{\rho}(\boldsymbol{r}) \Big] \Big\}, \\ C_{\mathcal{Q}} &= \int \mathrm{d}\boldsymbol{r} \left\{ \delta\beta(\boldsymbol{r}) \Big[\big\langle \hat{\mathcal{H}}(\boldsymbol{r}) \big\rangle_0 - \mu \big\langle \hat{\rho}(\boldsymbol{r}) \big\rangle_0 \Big] + \beta\delta\mu(\boldsymbol{r}) \big\langle \hat{\rho}(\boldsymbol{r}) \big\rangle_0 \right\}. \end{aligned} \tag{4.42}$$

The averages $\langle \dots \rangle_0$ are evaluated using the equilibrium distribution (4.41) and the difference in the notation underlines that $\hat{C}_e$ still depends on the phase space coordinates. Within the linear approximation the LE distribution reads

$$\begin{aligned} F^{LE} = F^{eq} \Bigg\{ 1 - \int \mathrm{d}\boldsymbol{r} \Big\{ & \delta\beta(\boldsymbol{r}) \Big[\hat{\mathcal{H}}(\boldsymbol{r}) - \mu\hat{\rho}(\boldsymbol{r}) \Big] \\ & - \beta \Big[\hat{\boldsymbol{j}}(\boldsymbol{r}) \cdot \delta\boldsymbol{u}(\boldsymbol{r}) + \delta\mu(\boldsymbol{r})\hat{\rho}(\boldsymbol{r}) \Big] \Big\} + C_{\mathcal{Q}} \Bigg\}. \end{aligned} \tag{4.43}$$

Finally, the local equilibrium average of an observable $\hat{A}(\boldsymbol{r})$ is given by

$$\begin{aligned} \big\langle \hat{A}(\boldsymbol{r}) \big\rangle_{LE} = \big\langle \hat{A}(\boldsymbol{r}) \big\rangle_0 - \int \mathrm{d}\boldsymbol{r}' \Big\{ & \delta\beta(\boldsymbol{r}') \Big[\big\langle \hat{A}(\boldsymbol{r})\, \hat{\mathcal{H}}(\boldsymbol{r}') \big\rangle_0 - \mu \big\langle \hat{A}(\boldsymbol{r})\, \hat{\rho}(\boldsymbol{r}') \big\rangle_0 \Big] \\ & - \beta \Big[\big\langle \hat{A}(\boldsymbol{r})\, \hat{j}^{\alpha}(\boldsymbol{r}') \big\rangle_0 \delta u^{\alpha}(\boldsymbol{r}) + \delta\mu(\boldsymbol{r}') \big\langle \hat{A}(\boldsymbol{r}) \hat{\rho}(\boldsymbol{r}') \big\rangle_0 \Big] \Big\} + C_{\mathcal{Q}} \big\langle \hat{A}(\boldsymbol{r}) \big\rangle_0. \end{aligned}$$

In some circumstances the resulting expressions for $\langle \hat{A}(\boldsymbol{r}) \rangle_{LE}$ loose some terms because the equilibrium averages $\langle \dots \rangle_0$ of any odd operator in the momentum coordinates $\hat{O}_{odd}$ (e.g. the momentum density $\hat{j}^\alpha(\boldsymbol{r}) \sim p^\alpha$) vanish:

$$\langle \hat{O}_{odd} \rangle_0 = 0. \tag{4.44}$$

Indeed, it is possible to factorise the momentum and the configurational equilibrium averages and the momentum average reduces to an integral of a odd function on the whole momentum space. Eq. (4.44) holds as well if $\hat{O}_{odd} = \hat{O}_1 \cdot \hat{O}_2 \cdot \dots$, provided that the operators are evaluated at the same time. In the following we report the expectation values for the most relevant observables.

The local equilibrium average of the momentum density is

$$\begin{aligned} \langle \hat{j}^\alpha(\boldsymbol{r}) \rangle_{LE} &= \beta \int \mathrm{d}\boldsymbol{r}' \, \langle \hat{j}^\alpha(\boldsymbol{r}) \hat{j}^\gamma(\boldsymbol{r}') \rangle_0 u^\gamma(\boldsymbol{r}') \\ &= \langle \hat{\rho}(\boldsymbol{r}) \rangle_0 \, u^\alpha(\boldsymbol{r}). \end{aligned}$$

The local equilibrium average of the energy current can be written as

$$\langle \hat{J}^\alpha_{\mathcal{H}}(\boldsymbol{r}) \rangle_{LE} = \beta \int \mathrm{d}\boldsymbol{r}' \, \langle \hat{J}^\alpha_{\mathcal{H}}(\boldsymbol{r}) \, \hat{j}^\gamma(\boldsymbol{r}') \rangle_0 \, u^\gamma(\boldsymbol{r}')$$

The local equilibrium average of the mass density is

$$\begin{aligned} \langle \hat{\rho}(\boldsymbol{r}) \rangle_{LE} = \langle \hat{\rho}(\boldsymbol{r}) \rangle_0 + C_{\mathcal{Q}} \, \langle \hat{\rho}(\boldsymbol{r}) \rangle_0 + \int \mathrm{d}\boldsymbol{r}' \Big\{ \beta \, \delta\mu(\boldsymbol{r}') \, \langle \hat{\rho}(\boldsymbol{r}) \, \hat{\rho}(\boldsymbol{r}') \rangle_0 \\ - \delta\beta(\boldsymbol{r}') \Big[\langle \hat{\rho}(\boldsymbol{r}) \, \hat{\mathcal{H}}(\boldsymbol{r}') \rangle_0 - \mu \, \langle \hat{\rho}(\boldsymbol{r}) \, \hat{\rho}(\boldsymbol{r}') \rangle_0 \Big] \Big\}, \end{aligned} \tag{4.45}$$

where the constant $C_{\mathcal{Q}}$ has been defined in Eq. (4.42). This result can be written as

$$\langle \hat{\rho}(\boldsymbol{r}) \rangle_{LE} = \langle \hat{\rho}(\boldsymbol{r}) \rangle_0 \Big|_{\beta(\boldsymbol{r}), \mu(\boldsymbol{r})}, \tag{4.46}$$

showing that the local equilibrium average of the density can be evaluated in the same way as the equilibrium average (4.41), provided that the temperature and the chemical potential are fixed on their local value in $\boldsymbol{r}$, that is $\beta = \beta(\boldsymbol{r})$ and $\mu = \mu(\boldsymbol{r})$.

The local equilibrium average of the momentum current reads

$$\begin{aligned} \langle \hat{J}^{\alpha\beta}_j(\boldsymbol{r}) \rangle_{LE} = \langle \hat{J}^{\alpha\beta}_j(\boldsymbol{r}) \rangle_0 + C_{\mathcal{Q}} \langle \hat{J}^{\alpha\beta}_j(\boldsymbol{r}) \rangle_0 + \int \mathrm{d}\boldsymbol{r}' \Big\{ \Big[\mu \, \langle \hat{J}^{\alpha\beta}_j(\boldsymbol{r}) \, \hat{\rho}(\boldsymbol{r}') \rangle_0 \\ - \langle \hat{J}^{\alpha\beta}_j(\boldsymbol{r}) \, \hat{\mathcal{H}}(\boldsymbol{r}') \rangle_0 \Big] \delta\beta(\boldsymbol{r}') + \beta \, \delta\mu(\boldsymbol{r}') \langle \hat{J}^{\alpha\beta}_j(\boldsymbol{r}) \, \hat{\rho}(\boldsymbol{r}') \rangle_0 \Big\}. \end{aligned} \tag{4.47}$$

Note that the equilibrium averages $\langle \dots \rangle$ in Eq. (4.47) are different from zero *also* if $\alpha \neq \beta$, because, due to the configurational contribution in (4.25),

$\hat{J}_j^{\alpha\beta}(\boldsymbol{r})$ is not an odd operator with respect to the momenta. It follows that the pressure tensor, which is diagonal in *equilibrium* systems, can acquire off diagonal components when the state of the system is described by a LE distribution as (4.40). Anyway, the *diagonal* components of this tensor can be written making use of the shorthand notation introduced in Eq. (4.45) as

$$\left\langle \hat{J}_j^{\alpha\alpha}(\boldsymbol{r}) \right\rangle_{LE} = \left\langle \hat{J}_j^{\alpha\alpha}(\boldsymbol{r}) \right\rangle_0 \Big|_{\beta(\boldsymbol{r}),\mu(\boldsymbol{r})} = p^{\alpha\alpha}(\boldsymbol{r}) \Big|_{\beta(\boldsymbol{r}),\mu(\boldsymbol{r})}.$$

Time-evolution of the distribution function

The equilibrium distribution F^{eq} defined above is to be a stationary solution of the Liouville equation (4.13) because it just depends on the five global constants of motion. On the other hand, the LE distribution function (4.40) is not stationary under the action of the Liouvillian: It can be shown that $\mathscr{L}F^{LE} \neq 0$. Then, the LE distribution will depend on time due to the dynamics and the evolution will be conditioned by the particular constraints to which the system is subject. The system considered by Mori in Ref. [155] is a liquid in a nonequilibrium state *and* in contact to heat and mass reservoirs, described at an initial time by a LE distribution analogous to (4.40). He showed that, if the system is free to evolve, at large times it will reach the equilibrium state imposed by reservoirs. Here we are not interested into a relaxation process towards equilibrium, but rather in the description of a time-independent thermo-osmotic flow, which is an out-of-equilibrium *stationary* state. Therefore we will adopt a strategy which in some points slightly differs from the one proposed in [155].

Following Mori, we assume that the system is described at $t = 0$ by a non-stationary LE state $F(t = 0) = F^{LE}$ and that for $t > 0$ the distribution $F(t)$ evolves spontaneously according to (4.13). The main difference in comparison to Mori's derivation is that here we keep the system out of equilibrium imposing fixed (i.e. time-independent) external parameters $\rho(\boldsymbol{r})$, $\boldsymbol{u}(\boldsymbol{r})$ and $\mu(\boldsymbol{r})$. The formal solution (4.14) of Eq. the Liouville equation (4.13) can be written in an integral form as

$$\begin{aligned} F(t) &= F(0) + \int_0^t \mathrm{d}t' \, \frac{\mathrm{d}}{\mathrm{d}t'} F(t') \\ &= F(0) + \int_0^t \mathrm{d}t' \, \mathscr{L} F(t') \\ &= F(0) + \int_0^t \mathrm{d}t' \, \mathscr{L}\, \mathscr{U}(t') F(0), \end{aligned}$$

where we made use of the Liouville equation and of its formal solution. Noticing that the initial state is F^{LE} and that within classical statistical mechanics the Liouvillian commutes with the evolution operator, the time evoluted

distribution reads

$$F(t) = F^{LE} + \int_0^t \mathrm{d}t'\, \mathscr{U}(t') \Big[\mathscr{L} F^{LE} \Big]. \tag{4.48}$$

At late times we expect that the system will relax to the stationary state determined by the fixed external fields $\beta(\boldsymbol{r}), \mu(\boldsymbol{r}), \boldsymbol{u}(\boldsymbol{r})$. We will take the limit $t \to \infty$ at the end of the computation with some care, due to the long tails of the time correlation functions involving conserved quantities (see the last paragraph of Section 4.3).
The explicit evaluation of the right hand side of (4.48) is straightforward. The Liouvillian $\mathscr{L}$ acts on the LE distribution as a partial derivative with respect to the phase space coordinates and we get

$$\begin{aligned} F(t) &= F^{LE} - \int_0^t \mathrm{d}t' \int \mathrm{d}\boldsymbol{r}\, \mathscr{U}(t') \Big[F^{LE}\, \beta(\boldsymbol{r})\, \mathscr{L} \hat{\mathcal{E}}(\boldsymbol{r}) \Big] \\ &= F^{LE} - \int_0^t \mathrm{d}t' \int \mathrm{d}\boldsymbol{r}\, \mathscr{U}(t') \Big\{ F^{LE}\, \beta(\boldsymbol{r}) \Big[\partial_\alpha \hat{J}^\alpha_{\mathcal{H}}(\boldsymbol{r}) - \partial_\gamma \hat{J}^{\alpha\gamma}_j(\boldsymbol{r}) u^\alpha(\boldsymbol{r}) \\ &\qquad - \mu(\boldsymbol{r}) \partial_\alpha \hat{j}^\alpha_\rho(\boldsymbol{r}) - \hat{\rho}(\boldsymbol{r}) \partial_\alpha V(\boldsymbol{r}) u^\alpha(\boldsymbol{r})/m \Big] \Big\}, \end{aligned}$$

where the action of the Liouvillian on the local energy, mass and momentum operators has already been evaluated in Section 4.2 and corresponds to the local conservation of energy, momentum and mass respectively (see Eq.s (4.32), (4.24) and (4.20) and the definition of the fluxes given therein).
If we assume that the perturbation on the system due to the fields $\beta(\boldsymbol{r})$, $\boldsymbol{u}(\boldsymbol{r})$ and $\mu(\boldsymbol{r})$ is small, it is possible to evaluate the response of the system within linear response theory. Within this approximation the (time-dependent) average of a local observable $\hat{A}(\boldsymbol{r})$ reads

$$\begin{aligned} \big\langle \hat{A}(\boldsymbol{r}) \big\rangle_t = \big\langle \hat{A}(\boldsymbol{r}) \big\rangle_{LE} - \int_0^t \mathrm{d}t' \int \mathrm{d}\boldsymbol{r}'\, \mathrm{Tr} \Big\{ \hat{A}(\boldsymbol{r})\, \mathscr{U}(t') \Big[F^{LE}\, \beta(\boldsymbol{r}') \Big(\partial'_\alpha \hat{J}^\alpha_{\mathcal{H}}(\boldsymbol{r}') \\ - \partial'_\gamma \hat{J}^{\alpha\gamma}_j(\boldsymbol{r}') u^\alpha(\boldsymbol{r}') - \mu(\boldsymbol{r}') \partial'_\alpha \hat{j}^\alpha_\rho(\boldsymbol{r}') - \hat{\rho}(\boldsymbol{r}') \partial'_\alpha V(\boldsymbol{r}') u^\alpha(\boldsymbol{r}')/m \Big) \Big] \Big\}, \end{aligned}$$

where $\mathrm{Tr}\{\dots\}$ is the trace over all the degrees of freedom and the symbol ∂' represents the derivative w.r.t. $\boldsymbol{r}'$. Integrating by parts and neglecting the contributions at the boundaries, we obtain

$$\begin{aligned} \big\langle \hat{A}(\boldsymbol{r}) \big\rangle_t = \big\langle \hat{A}(\boldsymbol{r}) \big\rangle_{LE} + \int_0^t \mathrm{d}t' \int \mathrm{d}\boldsymbol{r}'\, \mathrm{Tr} \Big\{ \hat{A}(\boldsymbol{r}, t')\, F^{LE} \Big[\hat{J}^\alpha_{\mathcal{H}}(\boldsymbol{r}') \partial'_\alpha \beta(\boldsymbol{r}') \\ - \hat{J}^{\alpha\gamma}_j(\boldsymbol{r}')\, \partial'_\gamma \big[\beta u^\alpha\big](\boldsymbol{r}') - \hat{j}^\alpha_\rho(\boldsymbol{r}') \partial'_\alpha \big[\beta\mu\big](\boldsymbol{r}') \\ + \hat{\rho}(\boldsymbol{r}') \partial'_\alpha V(\boldsymbol{r}') u^\alpha(\boldsymbol{r}')/m \Big] \Big\}, \end{aligned} \tag{4.49}$$

where have shifted the time dependence on the observable $A(\boldsymbol{r})$ performing the canonical transformation $\mathscr{U}(-t')$ and recalling the time evolution equation for the observables (4.16).
The product between F^{LE} and the terms between round brackets still retains quadratic terms in the gradients of the fields and in the velocity profile, as can be noted in (4.43). Therefore we approximate F^{LE} with the underlying equilibrium distribution and we retain only the *linear* contributions in (4.49) obtaining

$$\begin{aligned}\big\langle \hat{A}(\boldsymbol{r})\big\rangle_t = \big\langle \hat{A}(\boldsymbol{r})\big\rangle_{LE} + \int_0^t \mathrm{d}t' \int \mathrm{d}\boldsymbol{r}' \Big[&\big\langle \hat{A}(\boldsymbol{r},t')\, \hat{J}^{\alpha}_{\mathcal{H}}(\boldsymbol{r}')\big\rangle_0 \,\partial'_\alpha \beta(\boldsymbol{r}') \\ &- \beta \big\langle \hat{A}(\boldsymbol{r},t')\, \hat{J}^{\alpha\gamma}_{j}(\boldsymbol{r}')\big\rangle_0 \,\partial'_\gamma u^\alpha(\boldsymbol{r}') - \big\langle \hat{A}(\boldsymbol{r},t')\, \hat{j}^{\alpha}_{\rho}(\boldsymbol{r}')\big\rangle_0 \,\partial'_\alpha \big[\beta\mu\big](\boldsymbol{r}') \\ &+ \partial'_\alpha V(\boldsymbol{r}') \big\langle \hat{A}(\boldsymbol{r},t')\, \hat{\rho}(\boldsymbol{r}')\big\rangle_0 \, u^\alpha(\boldsymbol{r}')/m \Big].\end{aligned}$$

This expression shows how the dynamics induces corrections to the LE average through terms involving the gradients in the external fields and a term depending on the external potential linear in the velocity.

The distribution function (4.40), together with the definitions of the fluxes, allows to calculate the averages of any microscopic observable in terms of the parameters $\beta(\boldsymbol{r})$, $\boldsymbol{u}(\boldsymbol{r})$ and $\mu(\boldsymbol{r})$. Here we provide the explicit expressions of the most important quantities.
The formal expression of the average flux of fluid molecules is

$$\begin{aligned}\big\langle \hat{j}^{\sigma}(\boldsymbol{r})\big\rangle_t = \big\langle \hat{j}^{\sigma}(\boldsymbol{r})\big\rangle_{LE} + \int_0^t \mathrm{d}t' \int \mathrm{d}\boldsymbol{r}' \Big[&\big\langle \hat{j}^{\sigma}(\boldsymbol{r},t')\, \hat{J}^{\alpha}_{\mathcal{H}}(\boldsymbol{r}')\big\rangle_0 \,\partial'_\alpha \beta(\boldsymbol{r}') \\ &- \beta \big\langle \hat{j}^{\sigma}(\boldsymbol{r},t')\, \hat{J}^{\alpha\gamma}_{j}(\boldsymbol{r}')\big\rangle_0 \,\partial'_\gamma u^\alpha(\boldsymbol{r}') - \big\langle \hat{j}^{\sigma}(\boldsymbol{r},t')\, \hat{j}^{\alpha}_{\rho}(\boldsymbol{r}')\big\rangle_0 \,\partial'_\alpha \big[\beta\mu\big](\boldsymbol{r}') \\ &+ \partial'_\alpha V(\boldsymbol{r}') \big\langle \hat{j}^{\sigma}(\boldsymbol{r},t')\, \hat{\rho}(\boldsymbol{r}')\big\rangle_0 \, u^\alpha(\boldsymbol{r}')/m \Big].\end{aligned} \tag{4.50}$$

The average heat flux is

$$\begin{aligned}\big\langle \hat{J}^{\sigma}_{\mathcal{H}}(\boldsymbol{r})\big\rangle_t = \big\langle \hat{J}^{\sigma}_{\mathcal{H}}(\boldsymbol{r})\big\rangle_{LE} + \int_0^t \mathrm{d}t' \int \mathrm{d}\boldsymbol{r}' \Big[&\big\langle \hat{J}^{\sigma}_{\mathcal{H}}(\boldsymbol{r},t')\, \hat{J}^{\alpha}_{\mathcal{H}}(\boldsymbol{r}')\big\rangle_0 \,\partial'_\alpha \beta(\boldsymbol{r}') \\ &- \beta \big\langle \hat{J}^{\sigma}_{\mathcal{H}}(\boldsymbol{r},t')\, \hat{J}^{\alpha\gamma}_{j}(\boldsymbol{r}')\big\rangle_0 \,\partial'_\gamma u^\alpha(\boldsymbol{r}') - \big\langle \hat{J}^{\sigma}_{\mathcal{H}}(\boldsymbol{r},t')\, \hat{j}^{\alpha}_{\rho}(\boldsymbol{r}')\big\rangle_0 \,\partial'_\alpha \big[\beta\mu\big](\boldsymbol{r}') \\ &+ \partial'_\alpha V(\boldsymbol{r}') \big\langle \hat{J}^{\sigma}_{\mathcal{H}}(\boldsymbol{r},t')\, \hat{\rho}(\boldsymbol{r}')\big\rangle_0 \, u^\alpha(\boldsymbol{r}')/m \Big]\end{aligned} \tag{4.51}$$

and the average momentum flux is

$$\begin{aligned}\big\langle \hat{J}^{\sigma\delta}_{j}(\boldsymbol{r})\big\rangle_t = \big\langle \hat{J}^{\sigma\delta}_{j}(\boldsymbol{r})\big\rangle_{LE} + \int_0^t \mathrm{d}t' \int \mathrm{d}\boldsymbol{r}' \Big[&\big\langle \hat{J}^{\sigma\delta}_{j}(\boldsymbol{r},t')\, \hat{J}^{\alpha}_{\mathcal{H}}(\boldsymbol{r}')\big\rangle_0 \,\partial'_\alpha \beta(\boldsymbol{r}') \\ &- \beta \big\langle \hat{J}^{\sigma\delta}_{j}(\boldsymbol{r},t')\, \hat{J}^{\alpha\gamma}_{j}(\boldsymbol{r}')\big\rangle_0 \,\partial'_\gamma u^\alpha(\boldsymbol{r}') - \big\langle \hat{J}^{\sigma\delta}_{j}(\boldsymbol{r},t')\, \hat{j}^{\alpha}_{\rho}(\boldsymbol{r}')\big\rangle_0 \,\partial'_\alpha \big[\beta\mu\big](\boldsymbol{r}') \\ &+ \partial'_\alpha V(\boldsymbol{r}') \big\langle \hat{J}^{\sigma\delta}_{j}(\boldsymbol{r},t')\, \hat{\rho}(\boldsymbol{r}')\big\rangle_0 \, u^\alpha(\boldsymbol{r}')/m \Big].\end{aligned} \tag{4.52}$$

It is also useful to evaluate the average mass density

$$\begin{aligned}\big\langle\hat\rho(\boldsymbol{r})\big\rangle_t = \big\langle\hat\rho(\boldsymbol{r})\big\rangle_{LE} + \int_0^t \mathrm{d}t' \int \mathrm{d}\boldsymbol{r}' \Big[&\big\langle\hat\rho(\boldsymbol{r},t')\,\hat J^\alpha_{\mathcal{H}}(\boldsymbol{r}')\big\rangle_0\,\partial'_\alpha\beta(\boldsymbol{r}') \\ &- \beta\big\langle\hat\rho(\boldsymbol{r},t')\,\hat J^{\alpha\gamma}_j(\boldsymbol{r}')\big\rangle_0\,\partial'_\gamma u^\alpha(\boldsymbol{r}') - \big\langle\hat\rho(\boldsymbol{r},t')\,\hat j^\alpha_\rho(\boldsymbol{r}')\big\rangle_0\,\partial'_\alpha\big[\beta\mu\big](\boldsymbol{r}') \\ &+ \partial'_\alpha V(\boldsymbol{r}')\big\langle\hat\rho(\boldsymbol{r},t')\,\hat\rho(\boldsymbol{r}')\big\rangle_0\,u^\alpha(\boldsymbol{r}')/m\Big]. \end{aligned} \tag{4.53}$$

Constraints for the external fields

As already pointed out, the expressions given above allow to evaluate the average of the relevant observables for a system out of equilibrium. However, the time-independent fields $\beta(\boldsymbol{r})$, $\mu(\boldsymbol{r})$ and $\boldsymbol{u}(\boldsymbol{r})$, which enter these expressions, have not been fixed yet, and in addition they can not be determined *a priori*. In order to understand why, let us consider a fluid in an channel with two thermostats at its ends, set at different temperatures. The actual temperature profile along the channel can not be fixed from the outset. On the contrary, it will be self-consistently determined by the fluid, as well as the local chemical potential and, possibly[25], the velocity field. Just to stress the point, within this setup it is only possible to control the value of the temperature of the thermostats.

These considerations also apply to the fields $\beta(\boldsymbol{r})$, $\mu(\boldsymbol{r})$ and $\boldsymbol{u}(\boldsymbol{r})$. In order to obtain their value, we will impose the physical constraints characterising a stationary state, that is the continuity equations satisfied by the average local energy density $\big\langle\hat{\mathcal{H}}(\boldsymbol{r})\big\rangle$, by the average local momentum density $\big\langle\hat j^\gamma(\boldsymbol{r})\big\rangle$ and by the average local particle density $\langle\hat\rho(\boldsymbol{r})\rangle$. In formulae:

$$\partial_\gamma\big\langle\hat j^\gamma(\boldsymbol{r})\big\rangle = 0, \tag{4.54}$$

$$\partial_\gamma\big\langle\hat J^\gamma_{\mathcal{H}}(\boldsymbol{r})\big\rangle = 0, \tag{4.55}$$

$$\partial_\gamma\big\langle\hat J^{\alpha\gamma}_j(\boldsymbol{r})\big\rangle = -\frac{\langle\hat\rho(\boldsymbol{r})\rangle}{m}\,\partial_\alpha V(\boldsymbol{r}), \tag{4.56}$$

where $\big\langle\hat j^\gamma(\boldsymbol{r})\big\rangle$, $\big\langle\hat J^\gamma_{\mathcal{H}}(\boldsymbol{r})\big\rangle$, $\big\langle\hat J^{\alpha\gamma}_j(\boldsymbol{r})\big\rangle$ and $\langle\hat\rho(\boldsymbol{r})\rangle$ correspond to the $t\to\infty$ limit of Eq.s (4.50), (4.51), (4.52) and (4.53) respectively. The solution of this set of five independent differential equations formally provides the values of the gradients of the fields $\partial_\alpha\beta(\boldsymbol{r})$, $\partial_\alpha\mu(\boldsymbol{r})$ and $\partial_\alpha u^\gamma(\boldsymbol{r})$.

Unfortunately, without further approximations the general solution of this system can not be obtained in closed form. On the other hand, when the equations are specialised to some simple geometry, symmetry considerations

[25] If we consider a homogeneous fluid and we apply a temperature gradient we do not observe a mass flow.

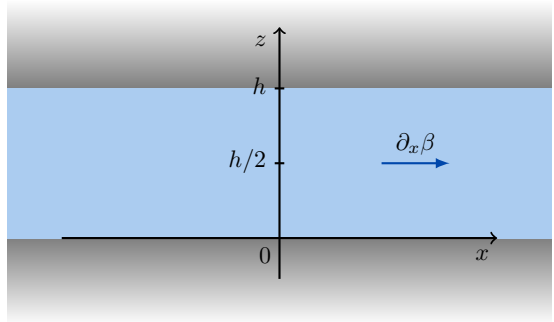

Figure 4.1: Schematic representation of the slab geometry. The y direction is perpendicular to the plane of the sheet.

allow to considerably simplify the problem, leading to analytical expressions easier to handle.

4.5 FLOW IN A SLIT

Let us consider a *gedanken* experiment realised in order to observe the phenomenon of thermo osmosis. The system (see Fig. 4.1) consists of a fluid which fills the region between two infinite parallel planar walls (slit), placed at a fixed distance h. Within this simple geometry the external potential just depends on the z coordinate. To further simplify the problem we impose that the walls behave as hard objects with respect to the fluid. In addition we keep the fluid out of equilibrium applying a temperature difference in the x direction. The temperature difference is set at infinity and is such that the gradient is small and finite.

The planar symmetry of the problem will reduce, as we will show below, the complexity of the problem. In the following Subsection we present the symmetry properties related to the planar geometry, whereas the next one applies the results obtained to the continuity equations.

Symmetries in planar systems

Under the hypotheses introduced above, the system is invariant along the x and y-directions, when held at a constant temperature. Therefore the equilibrium averages evaluated by means of the underlying equilibrium distribution F^{eq} do not depend on that coordinates. To give an example, the average equilibrium density profile $\langle \hat{\rho}(\boldsymbol{r}) \rangle$ depends only on the coordinate orthogonal to the walls z. Obviously, the thermal gradient along the x direction introduces an additional dependence of the averages on x.

Furthermore, any second-rank tensor representing a physical quantity and

belonging to systems characterised by a broken symmetry along a single direction, let us say z as in our case, reads

$$T^{\alpha\beta} = a\,\delta^{\alpha\beta} + b\,\hat{\boldsymbol{z}}^{\alpha}\hat{\boldsymbol{z}}^{\beta}, \tag{4.57}$$

because it has to preserve the symmetry of the system. In Eq. (4.57) a and b are constants, possibly position dependent if the tensor is a tensor field, and $\hat{\boldsymbol{z}}$ is the unit vector along the z-direction. This peculiar expression is motivated by the symmetry properties of its terms: The identity tensor has no intrinsic symmetry whereas the product between the unit versors $\hat{\boldsymbol{z}}\hat{\boldsymbol{z}}$ owns the symmetry of the problem. Equation (4.57) is the most general expression for a second-rank tensor that we can obtain combining the delta function and the unit versor $\hat{\boldsymbol{z}}$, which are the unique tensors preserving the symmetries of the system.
It follows that in planar symmetry the equilibrium momentum flux tensor is diagonal and is determined by two different non-vanishing components:

$$\overline{\overline{p}}(z) = \begin{bmatrix} p_{\mathrm{T}}(z) & 0 & 0 \\ 0 & p_{\mathrm{T}}(z) & 0 \\ 0 & 0 & p_{\mathrm{N}}(z) \end{bmatrix},$$

where p_{T} and p_{N} are referred to as the tangential and the normal pressure respectively. According to the notation introduced in Eq. (4.57), $a = p_{\mathrm{T}}(z)$ and $b = p_{\mathrm{N}}(z) - p_{\mathrm{T}}(z)$.

In the following we will deal with expressions as

$$I^{\alpha\gamma} = \int \mathrm{d}\boldsymbol{r}'\, T^{\alpha\gamma}(\boldsymbol{r}'), \tag{4.58}$$

where $T^{\alpha\gamma}(\boldsymbol{r})$ is second-rank tensor. Now let us impose that the tensor $T^{\alpha\gamma}(\boldsymbol{r})$ is invariant under a given coordinate transformation $\mathcal{R}$, represented by a matrix matrix belonging to the orthogonal group $\mathscr{O}(3)$

$$T^{\alpha\gamma}(R\boldsymbol{r}) = R^{\alpha\sigma}R^{\gamma\delta}T^{\sigma\delta}(\boldsymbol{r}).$$

It follows that the integral must obey the following property

$$I^{\alpha\gamma} = R^{\alpha\sigma}R^{\gamma\delta}I^{\gamma\delta}, \tag{4.59}$$

because the Jacobian of the transformation is equal to 1. Then, if T is invariant under all the rotations belonging to $\mathscr{O}(3)$ it follows, due to Schur's lemma, that the tensor $I^{\alpha\gamma} = a\delta^{\alpha,\gamma}$. However, if T is invariant under a subset of $\mathscr{O}(3)$, e.g. the rotations about the z-axis, Eq. (4.59) is fulfilled only if the $I^{\alpha\gamma}$ has the form (4.57).

Following the same argument adopted in the construction of the second-rank tensor, it is possible to show that a third-rank tensor endowed with the same symmetries reads

$$T^{\alpha\beta\gamma} = a_1\,\delta^{\alpha\beta}\hat{\boldsymbol{z}}^{\gamma} + a_2\,\delta^{\alpha\gamma}\hat{\boldsymbol{z}}^{\beta} + a_3\,\delta^{\gamma\beta}\hat{\boldsymbol{z}}^{\alpha} + b\,\hat{\boldsymbol{z}}^{\alpha}\hat{\boldsymbol{z}}^{\beta}\hat{\boldsymbol{z}}^{\gamma}. \tag{4.60}$$

Continuity equations

On the basis of the simple geometry of the problem, we *expect* that the *solutions* of the system of continuity equations (4.54), (4.55) and (4.56) will show some additional properties. Here we will assume these properties and then we will show that such a solution exist. The assumptions on the solutions are the following:

1. The gradient of the field $\beta(\boldsymbol{r})$ is uniform throughout the fluid and is set in the x-direction

   $$\boldsymbol{\nabla}\beta(\boldsymbol{r}) = \big(\partial_x\beta\,,0\,,0\,\big),$$

   where $\partial_x\beta$ is a constant.

2. The gradient of the field $\mu(\boldsymbol{r})$ is uniform throughout the fluid and is set in the x-direction

   $$\boldsymbol{\nabla}\mu(\boldsymbol{r}) = \big(\partial_x\mu\,,0\,,0\,\big).$$

   Within linear response theory the combination this assumption with the first one implies that $\partial_x(\beta\mu)$ is a constant[26] and, at linear order in the derivatives of the fields, we can write

   $$\boldsymbol{\nabla}\left[\beta\mu\right](\boldsymbol{r}) = \big(\partial_x(\beta\mu)\,,0\,,0\,\big). \tag{4.61}$$

3. The only non-vanishing component of the velocity field is along the x-axis and is dependent only on the coordinate z normal to the wall

   $$\boldsymbol{u}(\boldsymbol{r}) = \big(u^x(z)\,,0\,,0\,\big). \tag{4.62}$$

In what follows we apply these assumptions to the conservation laws (4.54), (4.55) and (4.56).

Mass and energy conservation laws

Due to the symmetries of the system, it turns out that the steady-state conservation law for the mass density (4.54) and for the momentum density (4.55) are identically satisfied.

The average value of the momentum density is

$$\big\langle\hat{j}^\alpha(\boldsymbol{r})\big\rangle = \langle\hat{\rho}(z)\rangle_0\,u^x(z)\delta^{\alpha x} + \int_0^\infty \mathrm{d}t' \int \mathrm{d}\boldsymbol{r}' \Big[\big\langle\hat{j}^\alpha(\boldsymbol{r},t')\,\hat{J}^x_{\mathcal{H}}(\boldsymbol{r}')\big\rangle_0\,\partial_x\beta$$
$$- \beta\big\langle\hat{j}^\alpha(\boldsymbol{r},t')\,\hat{J}^{xz}_j(\boldsymbol{r}')\big\rangle_0\,\partial'_z u^x(z') - \big\langle\hat{j}^\alpha(\boldsymbol{r},t')\,\hat{j}^x_\rho(\boldsymbol{r}')\big\rangle_0\,\partial_x\big(\beta\mu\big)\Big],$$

[26] The term $\partial_x\beta\partial_x\mu$ is of the second order.

where we only made use of the three assumptions introduced above. Here we remark that the linear correction to the LE averages arising from the external potential $V(z)$ is vanishing: The potential enters the expressions multiplied to the velocity profile in the form

$$\partial_\alpha V(\boldsymbol{r})\, u^\alpha(\boldsymbol{r})$$

and, thanks to (4.62), this combination is zero. Furthermore, due to the symmetry properties recalled above, only the x-component of the average momentum density is non-vanishing ($\langle j^y(\boldsymbol{r})\rangle = \langle j^z(\boldsymbol{r})\rangle = 0$, similar considerations apply to both terms):

$$\begin{aligned}\big\langle \hat{j}^x(\boldsymbol{q})\big\rangle = \langle \hat{\rho}(z)\rangle_0\, u^x(z) + \int_0^\infty \mathrm{d}t' \int \mathrm{d}\boldsymbol{r}' \Big[\big\langle \hat{j}^x(\boldsymbol{r},t')\, \hat{J}^x_{\mathcal{H}}(\boldsymbol{r}')\big\rangle_0\, \partial_x\beta \\ - \beta \big\langle \hat{j}^x(\boldsymbol{r},t')\, \hat{J}^{xz}_j(\boldsymbol{r}')\big\rangle_0\, \partial'_z u^x(z') - \big\langle \hat{j}^x(\boldsymbol{r},t')\, \hat{j}^x_\rho(\boldsymbol{r}')\big\rangle_0\, \partial_x\big(\beta\mu\big)\Big]. \quad (4.63)\end{aligned}$$

Therefore the stationarity condition for the mass density reads

$$\begin{aligned}0 = \partial_\alpha \big\langle \hat{j}^\alpha(\boldsymbol{q})\big\rangle = \partial_x \int_0^\infty \mathrm{d}t' \int \mathrm{d}\boldsymbol{r}' \Big[\big\langle \hat{j}^x(\boldsymbol{r},t')\, \hat{J}^x_{\mathcal{H}}(\boldsymbol{r}')\big\rangle_0\, \partial_x\beta \\ - \beta \big\langle \hat{j}^x(\boldsymbol{r},t')\, \hat{J}^{xz}_j(\boldsymbol{r}')\big\rangle_0\, \partial'_z u^x(z') - \big\langle \hat{j}^x(\boldsymbol{r},t')\, \hat{j}^x_\rho(\boldsymbol{r}')\big\rangle_0\, \partial_x\big(\beta\mu\big)\Big].\end{aligned}$$

The two-point correlation functions depend only on the difference $x - x'$ because the averages are evaluated at equilibrium and the system is homogeneous along the coordinate x. Therefore their integral over $\boldsymbol{r}'$ will be independent on x and its derivative vanishes.

Analogous considerations apply for the continuity equation for $\big\langle \hat{\mathcal{H}}(\boldsymbol{r})\big\rangle$. Only the component of the flux along x is different from zero:

$$\begin{aligned}\big\langle \hat{J}^x_{\mathcal{H}}(\boldsymbol{r})\big\rangle = \beta \int \mathrm{d}\boldsymbol{r}' \big\langle \hat{J}^x_{\mathcal{H}}(\boldsymbol{r})\, \hat{j}^x(\boldsymbol{r}')\big\rangle_0\, u^x(z') \\ - \int_0^\infty \mathrm{d}t' \int \mathrm{d}\boldsymbol{r}' \Big[\beta \big\langle \hat{J}^x_{\mathcal{H}}(\boldsymbol{r},t')\, \hat{J}^{xz}_j(\boldsymbol{r}')\big\rangle_0\, \partial'_z u^x(z') \\ - \big\langle \hat{J}^x_{\mathcal{H}}(\boldsymbol{r},t')\, \hat{J}^x_{\mathcal{H}}(\boldsymbol{r}')\big\rangle_0\, \partial_x\beta + \big\langle \hat{J}^x_{\mathcal{H}}(\boldsymbol{r},t')\, \hat{j}^x_\rho(\boldsymbol{r}')\big\rangle_0\, \partial_x\big(\beta\mu\big)\Big].\end{aligned}$$

As before, the continuity equation, which in the stationary limit reduces to the derivative w.r.t. x of $\big\langle \hat{J}^x_{\mathcal{H}}(\boldsymbol{r})\big\rangle$, is identically satisfied because the integral of the correlation functions does not depend on x.

Momentum conservation law

The third stationarity condition (4.56) gives origin to three independent equations. Two of them are identically satisfied whereas the last one defines

the gradient of the velocity profile.
Let us start with the conservation law for $\langle \hat{j}^z(\boldsymbol{r})\rangle$. The terms involved in this relation are of the form

$$\langle \hat{J}_j^{\alpha z}(\boldsymbol{r})\rangle = \langle \hat{J}_j^{\alpha z}(\boldsymbol{r})\rangle_{LE} + \int_0^\infty \mathrm{d}t' \int \mathrm{d}\boldsymbol{r}' \Big[\langle \hat{J}_j^{\alpha z}(\boldsymbol{r},t')\, \hat{J}_{\mathcal{H}}^{x}(\boldsymbol{r}')\rangle_0\, \partial_x\beta$$
$$-\beta \langle \hat{J}_j^{\alpha z}(\boldsymbol{r},t')\, \hat{J}_j^{xz}(\boldsymbol{r}')\rangle_0\, \partial_z' u^x(z') - \langle \hat{J}_j^{\alpha z}(\boldsymbol{r},t')\, \hat{j}_\rho^{x}(\boldsymbol{r}')\rangle_0\, \partial_x\big(\beta\mu\big)\Big]$$

and making use of the usual symmetry properties we obtain

$$\langle \hat{J}_j^{\alpha z}(\boldsymbol{r})\rangle = \langle \hat{J}_j^{\alpha z}(\boldsymbol{r})\rangle_{LE} + \delta^{\alpha x} \int_0^\infty \mathrm{d}t' \int \mathrm{d}\boldsymbol{r}' \Big[\langle \hat{J}_j^{xz}(\boldsymbol{r},t')\, \hat{J}_{\mathcal{H}}^{x}(\boldsymbol{r}')\rangle_0\, \partial_x\beta$$
$$-\beta \langle \hat{J}_j^{xz}(\boldsymbol{r},t')\, \hat{J}_j^{xz}(\boldsymbol{r}')\rangle_0\, \partial_z' u^x(z') - \langle \hat{J}_j^{xz}(\boldsymbol{r},t')\, \hat{j}_\rho^{x}(\boldsymbol{r}')\rangle_0\, \partial_x\big(\beta\mu\big)\Big], \quad (4.64)$$

where the second equality follows from the usual symmetry properties. The term proportional to the delta function does not depend on x, because the correlation functions only depend on $x - x'$, and a suitable change of variable in the integral makes it independent on x.
The local equilibrium contribution in (4.64) for planar symmetry has not been specified yet. Introducing the assumptions detailed in Section 4.5 in the general expression (4.47) we obtain

$$\langle \hat{J}_j^{\alpha z}(\boldsymbol{r})\rangle_{LE} = \langle \hat{J}_j^{\alpha z}(z)\rangle_0 + \beta\, \partial_x\mu \int \mathrm{d}\boldsymbol{r}' x' \langle \hat{J}_j^{\alpha z}(\boldsymbol{r})\, \hat{\rho}(\boldsymbol{r}')\rangle_0 + C_{\mathcal{Q}} \langle \hat{J}_j^{\alpha z}(z)\rangle_0$$
$$-\partial_x\beta \int \mathrm{d}\boldsymbol{r}'\, x' \Big[\langle \hat{J}_j^{\alpha z}(\boldsymbol{r})\, \hat{\mathcal{H}}(\boldsymbol{r}')\rangle_0 - \mu \langle \hat{J}_j^{\alpha z}(\boldsymbol{r})\, \hat{\rho}(\boldsymbol{r}')\rangle_0 \Big]. \quad (4.65)$$

The quantity $\langle \hat{J}_j^{yz}(\boldsymbol{r})\rangle_{LE}$ does not depend on y, because on one side the equilibrium pressure tensor is diagonal and on the other side the linear corrections, which are integrated along y', loose their dependence on y.
As already pointed out, $\langle \hat{J}_j^{xz}(\boldsymbol{r})\rangle_{LE}$ is different from zero due to the presence of the linear contributions in the derivatives of the fields in Eq. (4.65). These terms depend on z, but do not depend on x: The integrals in (4.65) can be rearranged as

$$\int \mathrm{d}\boldsymbol{r}'\, x' \langle \hat{J}_j^{\alpha z}(\boldsymbol{r})\, \hat{A}(\boldsymbol{r}')\rangle_0 = \int \mathrm{d}\boldsymbol{r}'\, (x' - x) \langle \hat{J}_j^{\alpha z}(\boldsymbol{r})\, \hat{A}(\boldsymbol{r}')\rangle_0, \quad (4.66)$$

with $\hat{A}(\boldsymbol{r})$ a scalar operator, and the symmetry properties ensure

$$\int \mathrm{d}\boldsymbol{r}'\, \langle \hat{J}_j^{\alpha z}(\boldsymbol{r})\, \hat{A}(\boldsymbol{r}')\rangle_0 = 0.$$

The integral in Eq. (4.66) does not depend on x: The correlation function itself depends only on $x' - x$ and we can perform a change of variable which

removes this dependence (the integration domain is over the whole real axis). Therefore, the xz-component of the LE pressure tensor reads[27]

$$\left\langle \hat{J}_j^{xz}(\boldsymbol{r})\right\rangle_{LE} = \int \mathrm{d}\boldsymbol{r}'\,(x-x')\left[\partial_x\beta\left\langle \hat{J}_j^{xz}(\boldsymbol{r})\,\hat{\mathcal{H}}(\boldsymbol{r}')\right\rangle_0 - \partial_x\big(\beta\mu\big)\left\langle \hat{J}_j^{xz}(\boldsymbol{r})\,\hat{\rho}(\boldsymbol{r}')\right\rangle_0\right]. \quad (4.67)$$

Finally, the continuity equation we are considering involves also the LE average of the zz-component of the momentum flux, which can be written as

$$\left\langle \hat{J}_j^{zz}(\boldsymbol{r})\right\rangle_{LE} = p_{\mathrm{N}}(z)\Big|_{\beta(x),\mu(x)}.$$

Note that $\langle \hat{J}_j^{zz}(\boldsymbol{r})\rangle_{LE}$ depends both on z and on x, because the equilibrium averages are evaluated at a different $\beta(x)$ and $\mu(x)$.
Gathering the results obtained so far, the stationarity condition for the z-component of the momentum density reads

$$\partial_\alpha\left\langle \hat{J}_j^{\alpha z}(\boldsymbol{r})\right\rangle = \partial_z p_{\mathrm{N}}(z)\Big|_{\beta(x),\mu(x)} = -\frac{1}{m}\,\rho(z)\big|_{\beta(x),\mu(x)}\,\partial_z V(z), \quad (4.68)$$

where $\rho(z)$ is the equilibrium density profile evaluated at the local $\beta(x)$ and $\mu(x)$. Equation (4.68), the so called *hydrostatic equilibrium condition*, is always fulfilled by the normal component of the pressure tensor at each value of the coordinate x and is not specific to our problem. For hard walls (4.68) implies that the normal pressure is constant along z and equals the bulk pressure p evaluated at the local $\beta(x)$ and $\mu(x)$:

$$p_{\mathrm{N}}(z)\Big|_{\beta(x),\mu(x)} = p\,\big(\beta(x),\mu(x)\big). \quad (4.69)$$

However, this equation underlines that the normal pressure in general will depend on x.

The stationarity condition for $\left\langle \hat{j}^y(\boldsymbol{r})\right\rangle$ is identically satisfied because the symmetry of the problem implies $\partial_\alpha\left\langle \hat{J}_j^{\alpha y}(\boldsymbol{r})\right\rangle = 0$.

The only non-trivial continuity equation comes from the conservation of the x component of the momentum density:

$$\partial_\alpha\left\langle \hat{J}_j^{\alpha x}(\boldsymbol{r})\right\rangle = \partial_x\left\langle \hat{J}_j^{xx}(\boldsymbol{r})\right\rangle + \partial_z\left\langle \hat{J}_j^{xz}(\boldsymbol{r})\right\rangle = 0.$$

It is straightforward to show that the relevant terms in this relation can be

[27] Keeping in mind that according to linear response approach

$$\partial_x(\beta\mu) = \mu\,\partial_x\beta + \beta\,\partial_x\mu.$$

written as

$$\big\langle \hat{J}_j^{\alpha x}(\boldsymbol{r})\big\rangle = \big\langle \hat{J}_j^{\alpha x}(\boldsymbol{r})\big\rangle_{LE} + \delta^{\alpha z}\int_0^\infty \mathrm{d}t' \int \mathrm{d}\boldsymbol{r}' \Big[\big\langle \hat{J}_j^{xz}(\boldsymbol{r},t')\,\hat{J}^x_{\mathcal{H}}(\boldsymbol{r}')\big\rangle_0\,\partial_x\beta$$
$$-\beta\big\langle \hat{J}_j^{xz}(\boldsymbol{r},t')\,\hat{J}_j^{xz}(\boldsymbol{r}')\big\rangle_0\,\partial'_z u^x(z') - \big\langle \hat{J}_j^{xz}(\boldsymbol{r},t')\,\hat{j}^x_\rho(\boldsymbol{r}')\big\rangle_0\,\partial_x\big(\beta\mu\big)\Big], \quad (4.70)$$

where

$$\big\langle \hat{J}_j^{xx}(\boldsymbol{r})\big\rangle_{LE} = p_{\mathrm{T}}(z)\Big|_{\beta(x),\mu(x)}$$

and $\big\langle \hat{J}_j^{zx}(\boldsymbol{r})\big\rangle_{LE}$ has been evaluated in Eq. (4.67). Note, as remarked before for the normal pressure, that also the tangential pressure acquires a dependence on x because the equilibrium averages are evaluated at the local $\beta(x)$ and $\mu(x)$.
Finally, the stationarity condition for the x-component of the momentum density reads

$$0 = \partial_x p_{\mathrm{T}}(z)\Big|_{\beta(x),\mu(x)} + \partial_z\int_0^\infty \mathrm{d}t' \int \mathrm{d}\boldsymbol{r}' \Big[\big\langle \hat{J}_j^{xz}(\boldsymbol{r},t')\,\hat{J}^x_{\mathcal{H}}(\boldsymbol{r}')\big\rangle_0\,\partial_x\beta$$
$$-\big\langle \hat{J}_j^{x}(\boldsymbol{r},t')\,\hat{j}^x_\rho(\boldsymbol{r}')\big\rangle_0\,\partial_x\big(\beta\mu\big) - \beta\big\langle \hat{J}_j^{xz}(\boldsymbol{r},t')\,\hat{J}_j^{xz}(\boldsymbol{r}')\big\rangle_0\,\partial'_z u^x(z')\Big]$$
$$+\partial_z\int \mathrm{d}\boldsymbol{r}'\,(x-x')\Big[\partial_x\beta\,\big\langle \hat{J}_j^{xz}(\boldsymbol{r})\,\hat{\mathcal{H}}(\boldsymbol{r}')\big\rangle_0$$
$$-\partial_x\big(\beta\mu\big)\big\langle \hat{J}_j^{xz}(\boldsymbol{r})\,\hat{\rho}(\boldsymbol{r}')\big\rangle_0\Big]. \quad (4.71)$$

This condition is an integro-differential equation for the velocity profile $u^x(z)$. In order to make further progress we have to specify the appropriate boundary conditions. The free flow of fluid in an open channel imposes equal normal pressure at the left and the right boundaries. If the fluid cannot flow through the slit, that is in the case of a closed system, a normal pressure gradient forms such that the integrated mass flow vanishes.

Open channel

The continuity equation for the momentum density along the x-direction (4.71) can be integrated provided we restrict to the free flow in a *infinitely long channel* (see Fig. 4.1), large enough to guarantee that in the central region the perturbation due to the walls is absent. In this region the fluid can be considered homogeneous and isotropic: The normal and tangential components of the pressure tensor coincide and reduce to the bulk pressure p of the fluid evaluated at the given value of the fields $\beta(x)$ and $\mu(x)$

$$p_{\mathrm{N}}(z\sim h/2)\Big|_{\beta(x),\mu(x)} = p_{\mathrm{T}}(z\sim h/2)\Big|_{\beta(x),\mu(x)} = p\,\big|_{\beta(x),\mu(x)}.$$

We remark again that when temperature gradient is applied to the system the *bulk* pressure itself acquires a dependence on the x-coordinate.

The flow in an *open* channel imposes equal bulk pressure at the left and the right boundaries. It follows that the temperature and the chemical potential gradients will adapt in order to guarantee that

$$0 = \partial_x p\,\big|_{\beta(x),\mu(x)} = \partial_x \beta\,\left[\partial_\beta p + \frac{\partial_x \mu}{\partial_x \beta}\,\partial_\mu p\right].$$

This equation determines the ratio between the temperature and the chemical potential gradients, which can be expressed in terms of thermodynamic densities as

$$\frac{\partial_x \mu}{\partial_x \beta} = -\frac{\partial_\beta p}{\partial_\mu p} = k_{\rm B}\,T^2\,\frac{s}{\rho},$$

where s is the entropy density and we made use of the thermodynamic relations:

$$\partial_T p\,\big|_\mu = -\partial_T(\Omega/V)\big|_\mu = s, \qquad \partial_\mu p\,\big|_T = -\partial_\mu(\Omega/V)\big|_T = \rho.$$

Here the derivatives of the grand potential Ω have always been evaluated at constant volume V. The condition obtained above allows to express $\partial_x(\beta\mu)$ more naturally as

$$\partial_x(\beta\mu) = \partial_x\beta\left(\mu + T\,\frac{s}{\rho}\right) = \partial_x\beta\frac{u+p}{\rho} = \partial_x\beta\,h_m, \tag{4.72}$$

where u is the internal energy and h_m is the entropy per unit mass.

Now, the stationarity condition (4.71) can be easily integrated along z from 0 to $h/2$, where h is the distance between the walls. All the integrals derived w.r.t. z in (4.71) are odd functions of z with respect to $h/2$ and, when evaluated at this point, vanish. Therefore, the integro-differential equation for the velocity profile can be written in the compact form

$$\int_0^h {\rm d}z' \mathcal{K}(z,z')\,\partial_z' u^x(z') = \partial_x\beta\,\mathcal{S}(z). \tag{4.73}$$

The kernel $\mathcal{K}(z,z')$ is related to the local viscosity of the fluid

$$\mathcal{K}(z,z') = \beta\int_0^\infty {\rm d}t' \int {\rm d}\boldsymbol{r}'_\perp \big\langle \hat{J}_j^{xz}(\boldsymbol{r},t')\,\hat{J}_j^{xz}(\boldsymbol{r}')\big\rangle_0$$

and the source term $\mathcal{S}(z)$ is written as the sum of two distinct contributions $\mathcal{S}(z) = \mathcal{S}_s(z) + \mathcal{S}_d(z)$ depending on the static and dynamical equilibrium correlations respectively:

$$\mathcal{S}_s(z) = \int_{h/2}^z {\rm d}z'\,\left.\frac{\partial p_{\rm T}(z')}{\partial\beta}\right|_p - \int {\rm d}\boldsymbol{r}'\,(x-x')\,\big\langle \hat{J}_j^{xz}(\boldsymbol{r})\,\hat{\mathcal{P}}(\boldsymbol{r}')\big\rangle_0, \tag{4.74}$$

$$\mathcal{S}_d(z) = \int_0^\infty {\rm d}t' \int {\rm d}\boldsymbol{r}'\big\langle \hat{J}_j^{xz}(\boldsymbol{r},t')\,\hat{J}_Q^{x}(\boldsymbol{r}')\big\rangle_0. \tag{4.75}$$

Here we defined the operator $\hat{\mathcal{P}}(\boldsymbol{r}) = h_m\,\hat{\rho}(\boldsymbol{r}) - \hat{\mathcal{H}}(\boldsymbol{r})$ and the heat flux operator $\hat{J}^\alpha_Q(\boldsymbol{r}) = \hat{J}^\alpha_{\mathcal{H}}(\boldsymbol{r}) - h_m\,\hat{j}^\alpha_\rho(\boldsymbol{r})$. Note that the static contribution has been rewritten regarding the tangential pressure as a function of $\beta(x)$ and of the bulk pressure p. Indeed, at midpoint

$$p_{\mathrm{T}}(h/2)\Big|_{\beta(x),\mu(x)} \sim p$$

for each value of the coordinate x and we can replace the local chemical potential with the bulk pressure obtaining

$$\partial_x p_{\mathrm{T}}\big|_{\beta(x),p} = \partial_\beta p_{\mathrm{T}}\,\partial_x\beta.$$

The solution of this set of equations provides the gradient of the velocity field $\partial_z\,u^x(z)$, which does not have a direct physical meaning: The real flow is related to the average value for the mass current, Eq. (4.63), which we report here:

$$\left\langle \hat{j}^x(z)\right\rangle = \rho(z)\,u^x(z) + \int_0^\infty \mathrm{d}t' \int \mathrm{d}\boldsymbol{r}' \left[\left\langle \hat{j}^x(\boldsymbol{r},t')\,\hat{J}^x_Q(\boldsymbol{r}')\right\rangle_0 \partial_x\beta \right.$$
$$\left. - \beta\left\langle \hat{j}^x(\boldsymbol{r},t')\,\hat{J}^{xz}_j(\boldsymbol{r}')\right\rangle_0 \partial'_z u^x(z')\right] \quad (4.76)$$

Anyway, the mass flux can not be fully determined by Eq. (4.76), because the velocity field (and not only its derivative) appears in the first term. To resolve this ambiguity we have to know the mass flux at a given height z. This further requirement is not a limitation of the theory but rather a consequence of the Galilean invariance of the problem which, in an experimental set-up, is broken by the presence of friction between the fluid and the wall [228]. Instead, in the simplified model considered here, the wall is represented by an external confining potential (a hard wall) which does not modify the tangential (x) component of the particles' momenta[28]. Supplementing this solution by a no-slip boundary condition for the mass flux, i.e.

$$\left\langle \hat{j}^x(0)\right\rangle = \left\langle \hat{j}^x(h)\right\rangle = 0,$$

Eq. (4.76) allows to evaluate the thermo-osmotic flow in slab geometry: We first have to solve Eq. (4.73) for $u^x(z)$ and then substitute the result into Eq. (4.76).

Equation (4.76) is the main result of this Chapter and proves that the mass flow is an interfacial phenomenon: Indeed *all* the contributions in (4.76) vanish in the bulk. In the homogeneous limit Eq. (4.73) admits only a constant solution for $u^x(z)$: The source term is zero because it involves bulk integrals of odd correlation functions and the derivative of the tangential pressure (which

[28] A roughened interface can be modeled considering an x-dependent external potential.

is equal to the constant normal pressure) evaluated at constant bulk pressure. Furthermore the integral of the mass-heat correlation function vanishes because mass and heat fluctuations are decoupled in the bulk[29].

For an arbitrary wall-particle potential $V(z)$ the normal pressure depends on z (see Eq. (4.68)) and a pressure gradient along x arises for any choice of the constant $\partial_\beta p_{\rm T}/\partial_\mu p_{\rm N}$. In this case, even for isotropic fluids (i.e. without surfaces which break homogeneity) where $p_{\rm N} = p_{\rm T}$, a non-vanishing particle flux sets in within the range of the wall-particle interaction. For a large tube it is natural to assume that the normal pressure gradient vanishes far from the wall. Therefore we can evaluate in the bulk the value of the constant ratio $\partial_x\mu/\partial_x\beta$ and we can obtain the velocity profile far from the wall also for a fluid with arbitrary wall-particle interaction.

We conclude this Section with a comment related to the ambiguities on the definition of the fluxes. There are grounds for asking whether the actual value of the mass flow is itself subject to the same pathology suffered by the fluxes, which indeed appear both directly in Eq. (4.76) and indirectly through the velocity profile, which is the solution of (4.73). The answer is no. It is possible to prove that the terms in (4.76) which directly involve the fluxes do not depend on the particular choice for $\hat{J}_Q^\alpha$ and $\hat{J}_j^{\alpha\beta}$. The same considerations apply also to the velocity profile u^α, because this quantity has been determined making only use of the continuity equations (4.54), (4.55) and (4.56), which only involve the gradients of the currents.

4.6 SOME LIMITING APPROXIMATIONS

The above analysis of a model of simple fluid close to a wall is exact, within linear response theory, and shows that two distinct mechanisms give rise to thermo-osmosis, both related to interface physics: The presence of anisotropies in the pressure tensor close to the wall (see Eq. (4.74)) and the dependence of the dynamical correlation functions on the existence of a confining surface (see Eq. (4.75)). We now consider two limiting situations where these terms play a very different role in order to clarify their relevance in providing the required thermal force.

Thermo-osmosis in liquids

To the best of our knowledge, in liquids the theoretical approaches dealing with thermo-osmosis are based on nonequilibrium thermodynamics. For instance, according to Derjaguin's result (4.6), the slip velocity far from the walls arises due to the anisotropy of the local enthalpy density near the surface.

[29] See e.g. Ref. [130], Sec. 49 or Ref. [11], Sec. 12.5.

However, the predictions given by this and similar works can not be completely correct: Indeed, the impact of the surfaces on the system can only be included *a posteriori*. The reason is that continuum theories, as nonequilibrium thermodynamics, can not account for changes in thermodynamic quantities over length scales of the order of the range of the microscopic interactions[30] and approximations must be introduced[31].
Another derivation of Derjaguin's result (4.6) has been recently put forward in Ref. [81] following the same thermodynamics arguments and with a questionable application of the Gibbs-Dhuem relation in regions where strong inhomogeneities on the length scale of the interparticle potential appear[32].
Finally, note that according to Eq. (4.6) no dynamical quantity, apart from the viscosity, influences thermo-osmosis.

Back to Derjaguin's result

Comparing Derjaguin's result (4.6) to Eq.s (4.76) and (4.73) it could seem that, according to "continuum approximations", the contributions to thermo-osmosis arising from the dynamical correlations near the interface are negligible and that the dynamical correlations can be estimated by their bulk values. However, up to now there is no clear evidence that Derjaguin's approach quantitatively predicts the thermo-osmotic slip.
In the following we evaluate Eq.s (4.76) and (4.73), which are exact at least for sufficiently small perturbations, under the hypothesis of the continuum approximations in order to we check if the the slip velocity is consistent with Eq. (4.6). To do this, we evaluate all the dynamical correlation functions in the bulk and we assume that the kernel is a short ranged function

$$\mathcal{K}(z, z') \sim \eta\, \delta(z - z'), \tag{4.77}$$

with η the bulk viscosity. Under these assumptions the dynamic source term (4.75) vanishes, because in bulk the tensors which preserve isotropy and homogeneity are proportional to the identity. For the same reason the static source (4.74) retains only the contribution including the anisotropy of the pressure tensor. The source term within this "Derjaguin" approximation reads

$$\mathcal{S}_{\mathrm{Derj}}(z) = \int_{h/2}^{z} \mathrm{d}z'\, \frac{\partial p_{\mathrm{T}}(z')}{\partial \beta}\bigg|_{p}.$$

[30]Furthermore, in the spirit of continuum approaches, Eq. (4.6) depends on the *bulk* viscosity η, without accounting for modifications due to the surface.
[31]However, as shown in [81], the enthalpy of the fluid strongly oscillates near the surface.
[32]We remind that in these regions the free energy densities can not be defined [197] without ambiguities.

Furthermore the momentum density (4.76) retains only the term linear in the velocity

$$\left\langle \hat{j}^x(z) \right\rangle = \rho(z)\, u^x(z) \tag{4.78}$$

and the differential equation for the velocity profile reads

$$\partial_z u^x(z) = -\frac{\partial_x \beta}{\eta} \int_z^{h/2} \mathrm{d}z' \left. \frac{\partial p_{\mathrm{T}}(z')}{\partial \beta} \right|_p . \tag{4.79}$$

The integration of this first-order differential equation requires a boundary condition and, as we anticipated above, we adopt the no-slip boundary condition $\left\langle \hat{j}^x(0) \right\rangle = 0$, which implies $u^x(0) = 0$. Once this choice is made, the mass flux readily follows integrating Eq. (4.79)[33]

$$\left\langle \hat{j}^x(z) \right\rangle = -\frac{\rho(z)\partial_x \beta}{\eta} \int_0^{h/2} \mathrm{d}z' \, \mathrm{Min}(z, z') \left. \frac{\partial p_{\mathrm{T}}(z')}{\partial \beta} \right|_p .$$

In the asymptotic limit, i.e. when z and the width of the slit are larger than the typical length scale of the correlations ($z \to \infty$ and $h \to \infty$), $\mathrm{Min}(z, z') \sim z'$ and the slip velocity reads

$$v_\infty = \frac{\left\langle \hat{j}^x \right\rangle_\infty}{\rho_b} = -\frac{\partial_x T}{\eta} \left. \frac{\partial}{\partial T} \right|_p \int_0^\infty \mathrm{d}z' \, z \left[p_{\mathrm{T}}(z') - p \right]. \tag{4.80}$$

In accordance with the "Derjaguin" approximation we have assumed $\rho(z) \simeq \rho_b$[34] and the bulk pressure in the integral can be subtracted because the derivative is taken at fixed p.
This expression for the asymptotic slip velocity closely resembles the prediction (4.6) obtained by Derjaguin [45], where the enthalpy difference enters the integral. However, the two expressions (4.80) and (4.6) do not match, even in the bulk, where we can write

$$\begin{aligned} \left. \frac{\partial p}{\partial T} \right|_{\beta\mu} &= \left. \frac{\partial}{\partial T} \Big[p\big(T, \mu\big) \Big] \right|_{\beta\mu} = \left. \frac{\partial}{\partial T} \Big[p\big(T, k_{\mathrm{B}} T\, \beta\mu\big) \Big] \right|_{\beta\mu} \\ &= \left. \frac{\partial p}{\partial T} \right|_{\mu} + \frac{\mu}{T} \left. \frac{\partial p}{\partial T} \right|_{\beta} = s + \frac{\mu\rho}{T} = \frac{h}{T}, \end{aligned} \tag{4.81}$$

with h the enthalpy per unit volume. This identity shows that the enthalpy per unit volume is linked to the temperature derivative of the pressure at

[33] After the straightforward change of variable

$$\int_0^z \mathrm{d}x \int_x^{h/2} \mathrm{d}y \, f(y) = \int_0^{h/2} \mathrm{d}y \, f(y) \int_0^{\mathrm{Min}(y,z)} \mathrm{d}x.$$

fixed $\beta\mu$ times T, whereas our result involves the derivative of the tangential pressure at fixed bulk pressure. Anyway we stress that Eq. (4.81) holds only in the bulk and has been reported here for its *evocative* value. The application of (4.81) for an inhomogeneous system is indeed equivalent to the application of the Gibbs-Duhem equation, and is not correct.

On the other hand, Eq. (4.80) coincides with the solution of the linearised Navier-Stokes equation for an incompressible fluid in the presence of a gradient in the tangential pressure given by the LE expression [81, 175]. The fully macroscopic approach based on the continuum approximation states that the differential equation obeyed by a the stationary velocity field $\boldsymbol{v}(\boldsymbol{r})$ of an incompressible fluid can be written as

$$0 = \partial_t(\rho v^\alpha) = -\partial_\beta \Pi^{\alpha\beta} + F^\alpha.$$

This equation is the (stationary) Navier Stokes equation, where $\boldsymbol{F}$ is the force field acting on the fluid, which may be due either to the presence of the wall or to an external field. The momentum flux tensor $\Pi^{\alpha\beta}$ can be written in terms of the stationary momentum flux $\left\langle \hat{J}_j^{\alpha\beta}(\boldsymbol{r}) \right\rangle = \pi^{\alpha\beta}$ introduced above as

$$\Pi^{\alpha\beta} = \pi^{\alpha\beta} + \rho v^\alpha v^\beta - \eta \left[\frac{\partial v^\alpha}{\partial r^\beta} - \frac{\partial v^\beta}{\partial r^\alpha} \right].$$

In the limit of small velocities and within the adopted planar symmetry, the the x-component of the velocity field fulfils the linearised the Navier-Stokes equation

$$\eta \frac{\mathrm{d}^2 v^x}{\mathrm{d}z^2} = \partial_x p_{\mathrm{T}}$$

if the wall-fluid interaction is modelled as a hard core potential ($\boldsymbol{F}$ is vanishing in the fluid domain). Following the same line of reasoning as above, the last contribution can be written in terms of the temperature derivative of the tangential pressure at fixed bulk pressure:

$$\eta \frac{\mathrm{d}^2 v^x}{\mathrm{d}z^2} = \partial_x T \left. \frac{\partial p_{\mathrm{T}}(z)}{\partial T} \right|_p . \tag{4.82}$$

Imposing no slip boundary conditions at the wall ($v^x(0) = 0$) Eq. (4.82) can be easily integrated as before, and the asymptotic velocity field is[35]

$$v_\infty = -\frac{\partial_x T}{\eta} \left. \frac{\partial}{\partial T} \right|_p \int_0^\infty \mathrm{d}z' \, z \left[p_{\mathrm{T}}(z') - p \right],$$

which coincides with Eq. (4.80).

[35]The first integration is from $h/2$ to 0, and we take advantage of the symmetry of the problem which implies that the derivative of the velocity profile vanishes in the middle point between the walls. Then the second integration proceeds as already described above.

The temperature derivative of the pressure tensor has been recently evaluated by numerical simulations [81] for a Lennard-Jones fluid. Use of these results allows to estimate that the resulting thermo-osmotic velocity is opposite to the thermal gradient and of the order of few micrometer per second.

Thermo-osmosis in gases

In the low-density limit, where kinetic theories provide a quantitative interpretation of the phenomenon (see Section 4.1), our formalism should reproduce the known results, at least for small temperature gradients, because no approximation has been introduced. In the *ideal gas* limit, i.e. ignoring the interparticle interactions, the momentum (4.25) and the energy (4.33) fluxes acquire the simple form

$$\hat{J}_j^{\alpha\beta}(\boldsymbol{r}) = \sum_i \frac{p_i^\alpha p_i^\beta}{m}\delta(\boldsymbol{q}_i - \boldsymbol{r}), \qquad \hat{J}_{\mathcal{H}}^{\alpha}(\boldsymbol{r}) = \sum_i \frac{p_i^2 p_i^\alpha}{m}\delta(\boldsymbol{q}_i - \boldsymbol{r})$$

and the evaluation of the slip velocity can be carried out analytically.

Solution of the equation for $u^x(z)$

The static source term $\mathcal{S}_s(z)$ vanishes because for ideal gases $p_{\mathrm{T}} = p_{\mathrm{N}} = p$ and the equilibrium average in (4.74) is performed on a quantity which is odd in the momenta. Then, the source term reduces to

$$\mathcal{S}(z) = \sum_{i,l} \Big\langle \int_0^\infty dt \int \mathrm{d}\boldsymbol{r}'\, \delta\big(\boldsymbol{r} - \boldsymbol{q}_l(t)\big)\, \delta\big(\boldsymbol{r}' - \boldsymbol{q}_i\big) \cdot \frac{p_l^x(t)\, p_l^z(t)}{m^2}\, p_i^x \left[\frac{p_i^2}{2m} - m h_m\right] \Big\rangle_0 , \quad (4.83)$$

where the equilibrium average is evaluated according to the equilibrium distribution (4.41) and $\boldsymbol{q}_i$ and $\boldsymbol{p}_i$ are the coordinate and the momentum of the particle at $t = 0$ respectively.
Without any kind of interaction between particles the time integral in (4.83) is diverging because the correlations persist at all times. In order to mimic the behaviour of an almost ideal gas, where some collisions appear, we introduce a finite relaxation time τ. This procedure allows to insert the collisions between ideal particles *a posteriori* and τ is the mean time between two collisions of a given particle. In addition, only the contribution arising from the same particle (i.e. $i = l$) is non vanishing and the source term reads

$$\mathcal{S}(z) = \sum_{i} \Big\langle \int_0^\tau dt \int \mathrm{d}\boldsymbol{r}'\, \delta\big(\boldsymbol{r} - \boldsymbol{q}_i(t)\big)\, \delta\big(\boldsymbol{r}' - \boldsymbol{q}_i\big) \cdot \frac{p_i^x(t)\, p_i^z(t)}{m^2}\, p_i^x \left[\frac{p_i^2}{2m} - m h_m\right] \Big\rangle_0 . \quad (4.84)$$

In the case of a perfectly reflecting wall, it is straightforward to show that $\mathcal{S}(z) = 0$. Indeed, specular reflections without energy exchange conserve both the x-component of the momentum and the modulus of the momentum. Then all the integrated quantities in Eq. (4.84) can be evaluated at time t. If we perform the canonical transformation $\mathscr{U}(-t)$ the average over the momenta does not depend on time, and the source term vanishes.

In agreement with the results obtained within kinetic theory [116], the occurrence of thermal creep is possible only assuming that in the particle-surface scattering the momentum is not conserved[36]. In order to mimic this behaviour and to obtain analytical results we assume that, due to the interaction with the surface during the scattering process, the x-component of the particles' momenta before and after the collision are fully uncorrelated. Furthermore, we restrict to the limiting semi-infinite geometry, where only the wall at $h = 0$ in Fig. 4.1 is present, in order to avoid multiple collisions between the surfaces. The averages can be evaluated without any loss in generality within the canonical (N, V, T) ensemble and the source term reads

$$\mathcal{S}(z) = \frac{N}{\tilde{\mathcal{Q}}_{\mathrm{c}}} \int_0^\tau dt \int \mathrm{d}\boldsymbol{r}' \int \mathrm{d}\boldsymbol{q} \int \mathrm{d}\boldsymbol{p}\; \delta\big(\boldsymbol{r} - \boldsymbol{q}(t)\big)\, \delta\big(\boldsymbol{r}' - \boldsymbol{q}\big) \cdot \frac{p^x(t)\, p^z(t)}{m^2}\, p^x \left[\frac{p^2}{2m} - m h_m\right] \mathrm{e}^{-\beta p^2/2m}, \qquad (4.85)$$

where $\tilde{\mathcal{Q}}_{\mathrm{c}} = V(2\pi m k_{\mathrm{B}} T)^{3/2}$ and the factor N takes into account that the contributions in (4.84) arising from different particles are equal.
In order to evaluate the source term, let us briefly examine the behaviour of a particle before a given time t and for a given initial coordinate $\boldsymbol{q}$ as a function of the initial momentum $\boldsymbol{p}$. If $p^z \geq -mq^z/t$ the particle does not bounce on the wall in the time interval $[0, t]$ and we can write

$$\boldsymbol{p}(t) = \boldsymbol{p}, \qquad \boldsymbol{q}(t) = \boldsymbol{q} + \frac{\boldsymbol{p}}{m} t. \qquad (4.86)$$

On the other hand, when $p^z < -mq^z/t$ the particle hits the wall at time t_s, before t. During the scattering the particle has completely lost the memory of the value of p^x before the bounce, therefore its self correlation is equal to 0 and the contribution in (4.85) arising from $p^z < -mq^z/t$ vanishes. Therefore we can restrict the integral over p^z to the set $[-m\,q^z/\,t, +\infty]$ and, according to Eq. (4.86), we can write

$$\mathcal{S}(z) = \frac{N}{\tilde{\mathcal{Q}}_{\mathrm{c}}} \int_0^\tau dt \int \mathrm{d}\boldsymbol{r}' \int \mathrm{d}\boldsymbol{q} \int \mathrm{d}\boldsymbol{p}_\perp \int_{-mq^z/t}^{+\infty} \mathrm{d}p^z\, \delta\left(\boldsymbol{r} - \boldsymbol{q} - \frac{\boldsymbol{p}}{m} t\right) \cdot \delta\big(\boldsymbol{r}' - \boldsymbol{q}\big) \frac{\big(p^x\big)^2 p^z}{m^2} \left[\frac{p^2}{2m} - m h_m\right] \mathrm{e}^{-\beta p^2/2m},$$

[36] The additional contributions in Eq. (4.63) vanish for perfectly reflecting walls. See below.

where the integral over the momentum $\boldsymbol{p}_\perp$ orthogonal to p^z is extended to $\mathbb{R}^2$. The final result for the source term, after a careful evaluation of the remaining integrals, reads

$$\mathcal{S}(z) = -\frac{N\pi m\tau}{\tilde{\mathcal{Q}}_{\rm c}\,\beta^4}\exp\left[-\beta\,\frac{mz^2}{2\tau^2}\right].$$

Similar arguments allow to express the kernel as

$$\mathcal{K}(z,z') = \frac{N2\pi m^2}{\tilde{\mathcal{Q}}_{\rm c}\,\beta^2}\Theta(z)\Theta(z')\,\exp\left[-\beta\,\frac{m\,(z-z')^2}{2\tau^2}\right].$$

Performing an appropriate change of variables, the differential equation (4.73) for $u^x(z)$ can be written as

$$\int_0^{+\infty}\mathrm{d}z'\,\partial'_z u^x(z')\frac{2m}{\tau k_{\rm B}\partial_x T}\mathrm{e}^{-z'^2+2\zeta z'} = 1,$$

where $\zeta = z\sqrt{m\beta/2\tau^2}$. The solution can be determined up to an additive constant C and reads

$$u^x(z) = \frac{k_{\rm B}}{2m}\,\tau\,\partial_x T\,\Theta(z+\delta) + \mathrm{C},$$

where $\delta \to 0^+$ and the constant can be fixed imposing a given boundary condition. The relaxation time introduced above can be related to the *bulk* viscosity η, which appears in most of the results present in the literature [149, 116], and can be defined in terms of τ as

$$\eta = \beta\int_0^\tau \mathrm{d}t\int\mathrm{d}\boldsymbol{r}'\,\left\langle \hat{J}^{xz}_j(\boldsymbol{r},t)\,\hat{J}^{xz}_j(\boldsymbol{r}')\right\rangle_0. \tag{4.87}$$

The integrals in (4.87) can be easily evaluated making use of the same arguments introduced above, and, after simple algebra, we obtain $\eta = p\,\tau$. Finally, far from the wall the field $u^x(z)$ can be written as

$$u^x(z) = \frac{\eta}{p}\frac{k_{\rm B}T}{2m}\frac{\partial_x T}{T} + \mathrm{C} = \frac{\eta}{2\rho}\frac{\partial_x T}{T} + \mathrm{C}. \tag{4.88}$$

Mass current

As already stated, the velocity field does not have a direct physical meaning: The real flow is related to the average value of the x-component of the mass current (Eq. (4.76)), which we report here:

$$\left\langle\hat{j}^x(z)\right\rangle = \rho\,u^x(z) + \int_0^\tau \mathrm{d}t\int\mathrm{d}\boldsymbol{r}'\left\{\left\langle\hat{j}^x(\boldsymbol{r},t)\left[\hat{J}^x_{\mathcal{H}}(\boldsymbol{r}') - h_m\hat{j}^x(\boldsymbol{r}')\right]\right\rangle_0\partial_x\beta\right.$$
$$\left. - \beta\left\langle\hat{j}^x(\boldsymbol{r},t)\,\hat{J}^{xz}_j(\boldsymbol{r}')\right\rangle_0\partial'_z u^x(z'),\right\}$$

where ρ is the density of the ideal fluid and the heat flux $\hat{J}_Q^\alpha$ has been written explicitly. It is straightforward to show that in the case of perfectly reflecting hard walls the mass current vanishes: As shown before, the velocity profile is equal to zero and it is easy to prove that the other two contributions exactly cancel. Therefore, in order to obtain a net thermo-osmotic flow we must impose, as done before, a scattering process which induces an exchange of momentum between the particle and the wall. In doing so, the first contribution is trivial, whereas, after some algebra, the integrals over $\boldsymbol{r}'$ of the dynamical correlation functions read

$$h_m \int \mathrm{d}\boldsymbol{r}' \left\langle \hat{j}^x(\boldsymbol{r},t)\hat{j}^x(\boldsymbol{r}')\right\rangle_0 = \frac{5}{2}\frac{N\pi m^2}{\tilde{\mathcal{Q}}_\mathrm{c}\beta^3}\frac{2\pi}{m\beta}\left[\mathrm{erf}\left(z\sqrt{\frac{\beta m}{2t^2}}\right)+1\right],$$

$$\int \mathrm{d}\boldsymbol{r}' \left\langle \hat{j}^x(\boldsymbol{r},t)\hat{J}^x_{\mathcal{H}}(\boldsymbol{r}')\right\rangle_0 = h_m \int \mathrm{d}\boldsymbol{r}' \left\langle \hat{j}^x(\boldsymbol{r},t)\hat{j}^x(\boldsymbol{r}')\right\rangle_0 - \frac{N\pi m^2}{\tilde{\mathcal{Q}}_\mathrm{c}\beta^3}\frac{z}{t}\mathrm{e}^{-\frac{\beta m z^2}{2t^2}},$$

$$\int \mathrm{d}\boldsymbol{r}' \left\langle \hat{j}^x(\boldsymbol{r},t)\,\hat{J}^{xz}_j(\boldsymbol{r}')\right\rangle_0 \partial'_z u^x(z') = \frac{Nm^2\pi k_\mathrm{B}\,\tau\partial_x T}{\tilde{\mathcal{Q}}_\mathrm{c}\beta\,t}\,z\,\mathrm{e}^{-\frac{\beta m z^2}{2t^2}}.$$

The final result for the mass current, after the time integration, is

$$\left\langle \hat{j}^x(z)\right\rangle = \frac{\eta}{2}\frac{\partial_x T}{T} + \frac{\eta}{4}\left\{\sqrt{\frac{2}{3\pi}}\,\frac{z}{\ell_g}\,\mathrm{Ei}\left[\frac{3}{2}\left(\frac{z}{\ell_g}\right)^2\right] + \mathrm{erf}\left(\sqrt{\frac{3}{2}}\frac{z}{\ell_g}\right)\right\}\frac{\partial_x T}{T},$$

where we have imposed no-slip boundary conditions for the mass current at $z = 0$[37], $\mathrm{Ei}(\cdot)$ is the exponential integral and $\ell_g = \tau\sqrt{2/(m\beta)}$. Far from the walls ($z \gg \ell_g$) the exponential integral rapidly decays to 0 and the slip velocity $v_\infty = \left\langle \hat{j}^x(z)\right\rangle|_{z\gg\ell_g}/\rho$ reduces to

$$v_\infty \sim \frac{3}{4}\,\frac{\eta}{\rho}\,\frac{\partial_x T}{T} = \frac{3}{4}\,k_\mathrm{B}T\,\frac{\eta}{p}\,\frac{\partial_x T}{T}, \tag{4.89}$$

which coincides with kinetic theory results (4.1) [149, 116], showing how the slip velocity grows at low pressure, as experimentally demonstrated [209].

4.7 CONCLUSIONS AND PERSPECTIVES

In this Chapter we have provided a microscopic theory of thermo-osmosis. The linear response theory formalism, applied to systems characterised by thermal disturbances, turned out to be the natural framework for a quantitative

[37] The constant C is equal to $\eta/4$.

description of flows originated by thermal inhomogeneities in the presence of interfaces. The emerging picture turns out to be more complex than expected on the basis of the previously adopted theoretical approaches, making use of kinetic theories and linear irreversible thermodynamics. We have found the general expression which allows to evaluate the thermo-osmotic flow for a simple microscopic model of fluid close to a planar wall subject to a temperature gradient. The resulting velocity profile of the fluid depends on both *static* and *dynamical* equilibrium properties of the system (see Eq.s (4.73) and (4.76)): In particular the transport coefficients near the surface assume a key role. Our approach is exact within the limits of validity of linear response theory, i.e. for small gradients in the fields, and will be useful in the interpretation of future experiments and numerical simulations in the whole phase diagram of a fluid.

Although our result is expressed in terms of quantities, like the tangential pressure near the wall and the heat flux, which are not uniquely defined on microscopic grounds, the *combination* of these terms (see for instance Eq. (4.74)) is indeed *independent* of the adopted choice, thereby solving the problem posed in Ref. [81].

A preliminary comparison with the existing macroscopic approach by Derjaguin shows that it closely resembles one of the two contributions found in our general expression. The other contribution, instead, allows to reproduce the known expressions of the kinetic theory of gases in the appropriate limits and sheds some light on the relevance of the scattering process at the confining surfaces at least in the rarefied limit.

Our approach is general and can be applied also to other simple geometries. The expressions obtained in Section 4.4 applied to a spherical geometry can provide many insights on the driving mechanism which leads to thermophoresis.

Although our result is expressed in terms of quantities, like the tangential pressure near the wall and the heat flux, which are not uniquely defined on microscopic grounds, the *combination* of these terms (see for instance Eq. (4.74)) is indeed *independent* of the adopted choice, thereby solving the problem posed in Ref. [81].

Finally, a quantitative investigation in liquids requires an accurate evaluation of the tangential pressure: We are preforming Monte Carlo simulations and DFT calculations based on the fundamental measure theory.

References

[1] Abramowitz, M., and Stegun, I. *Handbook of Mathematical Functions: With Formulas, Graphs, and Mathematical Tables*. Applied mathematics series. Dover, New York, 1964.

[2] Alder, B. J., and Wainwright, T. E. *Journal of the Physical Society of Japan 26* (1968), 267.

[3] Anderson, J. L. Colloid Transport by Interfacial Forces. *Annual Review of Fluid Mechanics 21* (1989), 61–99.

[4] Anzini, P., and Parola, A. Solvent-mediated forces in critical fluids. *Physical Review E 94* (2016), 052113.

[5] Anzini, P., and Parola, A. How roughness affects the depletion mechanism. *Soft Matter 13* (2017), 5150–5157.

[6] Asakura, S., and Oosawa, F. On Interaction between Two Bodies Immersed in a Solution of Macromolecules. *Journal of Chemical Physics 22* (1954), 1255.

[7] Asakura, S., and Oosawa, F. Interaction between particles suspended in solutions of macromolecules. *Journal of Polymer Science 33* (1958), 183.

[8] Ashton, D. J., Wilding, N. B., Roth, R., and Evans, R. Depletion potentials in highly size-asymmetric binary hard-sphere mixtures: Comparison of simulation results with theory. *Physical Review E 84* (2011), 061136.

[9] Aubert, M. Thermo-osmose. *Annales de chimie et de physique 26* (1912), 145.

[10] Badaire, S., Cottin-Bizonne, C., and Stroock, A. D. Experimental Investigation of Selective Colloidal Interactions Controlled by Shape, Surface Roughness, and Steric Layers. *Langmuir 24* (2008), 11451.

[11] Balescu, R. *Equilibrium and nonequilibrium statistical mechanics*. John Wiley & Sons, 1975.

[12] Balescu, R. *Statistical Dynamics: Matter Out Of Equilibrium*. World Scientific, 1997.

[13] Banerjee, D., Yang, J., and Schweizer, K. S. Entropic depletion in colloidal suspensions and polymer liquids: role of nanoparticle surface topography. *Soft Matter 11* (2015), 9086.

[14] Barber, M. N. Finite-size scaling. In *Phase transitions and critical phenomena*, C. Domb, M. Green, and J. Lebowitz, Eds. Academic Press, 1983, pp. 145–266.

[15] Barragán, V. M., and Kjelstrup, S. Thermo-osmosis in Membrane Systems: A Review. *Journal of Non-Equilibrium Thermodynamics 42* (2017), 217.

[16] Barry, E., and Dogic, Z. Entropy driven self-assembly of nonamphiphilic colloidal membranes. *Proceedings of the National Academy of Sciences of the United States of America 107* (2010), 10348.

[17] Barthlott, W., and Neinhuis, C. Purity of the sacred lotus, or escape from contamination in biological surfaces. *Planta 202* (1997), 1–8.

[18] Bhattacharjee, S., Ko, C.-H., and Elimelech, M. DLVO Interaction between Rough Surfaces. *Langmuir 14* (1998), 3365–3375.

[19] Bogoliubov, N. N. *Journal of Physics URSS 10* (1946), 256.

[20] Borjan, Z., and Upton, P. J. Off-Critical Casimir Effect in Ising Slabs with Symmetric Boundary Conditions in $d = 3$. *Physical Review Letters 101* (2008), 125702.

[21] Boyer, T. H. Quantum Electromagnetic Zero-Point Energy of a Conducting Spherical Shell and the Casimir Model for a Charged Particle. *Physical Review 174* (1968), 1764–1776.

[22] Bradford, S. A., and Torkzaban, S. Determining Parameters and Mechanisms of Colloid Retention and Release in Porous Media. *Langmuir 31* (2015), 12096–12105.

[23] Brankov, J. G., Danchev, D. M., and Tonchev, N. S. *Theory of Critical Phenomena in Finite-Size Systems*, first ed. World Scientific, 2000.

[24] Bregulla, A. P., Würger, A., Günther, K., Mertig, M., and Cichos, F. Thermo-Osmotic Flow in Thin Films. *Physical Review Letters 116* (2016), 188303.

[25] Brown, W. E. RESEARCH NOTE The Fisher-Widom line for a hard core attractive Yukawa fluid. *Molecular Physics 88* (1996), 579–584.

[26] Brush, S. G., and Everitt, C. W. F. Maxwell, Osborne Reynolds, and the Radiometer. *Historical Studies in the Physical Sciences 1* (1969), 105–125.

[27] Bryk, P., Roth, R., Schoen, M., and Dietrich, S. Depletion potentials near geometrically structured substrates. *Europhysics Letters 63* (2003), 233.

[28] Buzzaccaro, S., Colombo, J., Parola, A., and Piazza, R. Critical Depletion. *Physical Review Letters 105* (2010), 198301.

[29] Callen, H. B., and Welton, T. A. Irreversibility and Generalized Noise. *Physical Review 83* (1951), 34–40.

[30] Capelle, K. A bird's-eye view of density-functional theory. *arXiv preprint cond-mat/0211443* (2002).

[31] Casimir, H. B. G. On the Attraction Between Two Perfectly Conducting Plates. *Koninklijke Nederlandse Akademie van Wetenschappen 10* (1948), 261–263.

[32] Casimir, H. B. G., and Polder, D. The Influence of Retardation on the London-van der Waals Forces. *Physical Review 73* (1948), 360–372.

[33] Chapman, S. XII. The kinetic theory of a gas constituted of spherically symmetrical molecules. *Philosophical Transactions of the Royal Society of London A: Mathematical, Physical and Engineering Sciences 211* (1912), 433–483.

[34] Chrétien, D., Bénit, P., Ha, H.-H., Keipert, S., El-Khoury, R., Chang, Y.-T., Jastroch, M., Jacobs, H. T., Rustin, P., and Rak, M. Mitochondria are physiologically maintained at close to 50 C. *PLOS Biology 16* (2018), 1–17.

[35] Crookes, W. XIII. On repulsion resulting from radiation. Parts III. & IV. *Philosophical Transactions of the Royal Society of London 166* (1876), 325–376.

[36] Cuche, A., Canaguier-Durand, A., Devaux, E., Hutchison, J. A., Genet, C., and Ebbesen, T. W. Sorting Nanoparticles with Intertwined Plasmonic and Thermo-Hydrodynamical Forces. *Nano Letters 13* (2013), 4230–4235.

[37] Curtin, W. A., and Ashcroft, N. W. Weighted-density-functional theory of inhomogeneous liquids and the freezing transition. *Physical Review A 32* (1985), 2909.

[38] de Gennes, P. G. Wetting: statics and dynamics. *Reviews of Mododern Physics 57* (1985), 827–863.

[39] de Gennes, P.-G. *Simple Views on Condensed Matter*. World Scientific, 1998.

[40] de Gennes, P.-G., Brochard-Wyart, F., and Quere, D. *Capillarity and Wetting Phenomena: Drops, Bubbles, Pearls, Waves*. Springer, New York, 2004.

[41] de Groot, S., and Mazur, P. *Non-equilibrium Thermodynamics*. Dover Books on Physics. Dover Publications, 1984.

[42] Denbigh, K. G., Raumann, G., and Freeth, F. A. The thermo-osmosis of gases through a membrane I. Theoretical. *Proceedings of the Royal Society of London. Series A. Mathematical and Physical Sciences 210* (1952), 377–387.

[43] Derjaguin, B. Untersuchungen über die Reibung und Adhäsion, IV. *Kolloid-Zeitschrift 69* (1934), 155–164.

[44] Derjaguin, B. V. Some results from 50 years' research on surface forces. *Progress in Surface Science 40* (1992), 240 – 251.

[45] Derjaguin, B. V., Churaev, N. V., and Muller, V. M. *Surface Forces in Transport Phenomena*. Springer, Boston, 1987.

[46] Derjaguin, B. V., and Sidorenkov, G. P. Thermoosmosis at ordinary temperatures and its analogy with the thermomechanical effect in helium II. *Doklady Akademii Nauk SSSR 32* (1941), 622–626.

[47] Dhont, J. K. G. Thermodiffusion of interacting colloids. I. A statistical thermodynamics approach. *The Journal of Chemical Physics 120* (2004), 1632–1641.

[48] Dhont, J. K. G., Wiegand, S., Duhr, S., and Braun, D. Thermodiffusion of Charged Colloids: Single-Particle Diffusion. *Langmuir 23* (2007), 1674–1683.

[49] Diehl, H. W. The Theory of Boundary Critical Phenomena. *International Journal of Modern Physics B 11* (1997), 3503–3523.

[50] Dijkstra, M., Brader, J. M., and Evans, R. Phase behaviour and structure of model colloid-polymer mixtures. *Journal of Physics: Condensed Matter 11* (1999), 10079.

[51] Dinsmore, A. D., and Yodh, A. G. Entropic Confinement of Colloidal Spheres in Corners on Silicon Substrates. *Langmuir 15* (1999), 314.

[52] Dinsmore, A. D., Yodh, A. G., and Pine, D. J. Entropic control of particle motion using passive surface microstructures. *Nature 383* (1996), 239.

[53] Domb, C., Green, M., and Lebowitz, J. *Phase Transitions and Critical Phenomena*. Academic Press, 1986.

[54] Dorfman, J. R. *An Introduction to Chaos in Nonequilibrium Statistical Mechanics*. Cambridge University Press, Cambridge, 1999.

[55] Dufour, L. *Archives des Sciences physiques et naturelles, Genève 45* (1872), 9–12.

[56] Dufour, L. Ueber die Diffusion der Gase durch poröse Wände und die sie begleitenden Temperaturveränderungen. *Annalen der Physik 224* (1873), 490–492.

[57] Duhr, S., and Braun, D. Thermophoretic Depletion Follows Boltzmann Distribution. *Physical Review Letters 96* (2006), 168301.

[58] Eastman, E. D. Thermodynamics of non-isothermal systems. *Journal of the American Chemical Society 48* (1926), 1482–1493.

[59] Eastman, E. D. Theory of the Soret effect. *Journal of the American Chemical Society 50* (1928), 283–291.

[60] Ebner, C., Saam, W. F., and Stroud, D. Density-functional theory of simple classical fluids. I. Surfaces. *Physical Review A 14* (1976), 2264–2273.

[61] Enskog, D. Bemerkungen zu einer Fundamentalgleichung in der kinetischen Gastheorie. *Physikalische Zeitschrift 12* (1911), 533–539.

[62] Epstein, P. S. Zur Theorie des Radiometers. *Zeitschrift für Physik 54* (1929), 537–563.

[63] Ercole, L., Marcolongo, A., Umari, P., and Baroni, S. Gauge Invariance of Thermal Transport Coefficients. *Journal of Low Temperature Physics 185* (Oct 2016), 79–86.

[64] Evans, R. The nature of the liquid-vapour interface and other topics in the statistical mechanics of non-uniform, classical fluids. *Advances in Physics 28* (1979), 143–200.

[65] Evans, R., Henderson, J. R., Hoyle, D., Parry, A., and Sabeur, Z. Asymptotic decay of liquid structure: oscillatory liquid-vapour density profiles and the Fisher-Widom line. *Molecular Physics 80* (1993), 755–775.

[66] Evans, R., and Parry, A. O. Liquids at interfaces: what can a theorist contribute? *Journal of Physics: Condensed Matter 2* (1990), SA15.

[67] Evans, R., and Stecki, J. Solvation force in two-dimensional Ising strips. *Physical Review B 49* (1994), 8842–8851.

[68] Evans, R., Stewart, M. C., and Wilding, N. B. Critical drying of liquids. *Physical Review Letters 117* (2016), 176102.

[69] Feddersen, W. V. On thermodiffusion of gases. *Philosophical Magazine Series 5 46* (1873), 55–62.

[70] Fermi, E. Un metodo statistico per la determinazione di alcune proprietà dell'atomo. *Rendiconti dell'Accademia Nazionale dei Lincei 6* (1927), 602–607.

[71] Fisher, M. E. The theory of critical point singularity. In *Proceedings of the 51st "Enrico Fermi" Summer School*, M. S. Green, Ed. Academic Press, 1971, pp. 1–99.

[72] Fisher, M. E., and de Gennes, P.-G. Phénomenès aux parois dans un mélange binaire critique. *Comptes rendus de l'Académie des sciences, Série B 287* (1978), 207–209.

[73] Frisch, H., and Lebowitz, J. *The Equilibrium Theory of Classical Fluids: A Lecture Note and Reprint Volume*. W.A. Benjamin, 1964.

[74] Fu, L., Merabia, S., and Joly, L. What Controls Thermo-osmosis? Molecular Simulations Show the Critical Role of Interfacial Hydrodynamics. *Physical Review Letters 119* (2017), 214501.

[75] Fu, L., Merabia, S., and Joly, L. Understanding Fast and Robust Thermo-Osmotic Flows through Carbon Nanotube Membranes: Thermodynamics Meets Hydrodynamics. *The Journal of Physical Chemistry Letters 9* (2018), 2086–2092.

[76] Fukuto, M., Yano, Y. F., and Pershan, P. S. Critical Casimir Effect in Three-Dimensional Ising Systems: Measurements on Binary Wetting Films. *Physical Review Letters 94* (2005), 135702.

[77] Fürstner, R., Barthlott, W., Neinhuis, C., and Walzel, P. Wetting and Self-Cleaning Properties of Artificial Superhydrophobic Surfaces. *Langmuir 21* (2005), 956–961.

[78] Galliéro, G., Colombani, J., Duguay, B., Caltagirone, J.-P., and Montel, F. Evaluation de la thermodiffusion en milieu poreux nanométrique intégré par dynamique moléculaire hors équilibre directe. *Entropie* (2002), 98–102.

[79] Gambassi, A. The Casimir effect: From quantum to critical fluctuations. *Journal of Physics: Conference Series 161* (2009), 012037.

[80] Gambassi, A., Maciołek, A., Hertlein, C., Nellen, U., Helden, L., Bechinger, C., and Dietrich, S. Critical casimir effect in classical binary liquid mixtures. *Physical Review E 80* (2009), 061143.

[81] Ganti, R., Liu, Y., and Frenkel, D. Molecular Simulation of Thermo-osmotic Slip. *Physical Review Letters 119* (2017), 038002.

[82] Ganti, R., Liu, Y., and Frenkel, D. Hamiltonian Transformation to Compute Thermo-osmotic Forces. *Physical Review Letters 121* (2018), 068002.

[83] Garcia, R., and Chan, M. H. W. Critical Casimir Effect near the $^3He - ^4He$ Tricritical Point. *Physical Review Letters 88* (2002), 086101.

[84] Garnett, E., Mier-Y-Terán, L., and Río, F. D. On the hard core Yukawa fluid of variable range: Monte Carlo simulations and test of the MSA equation of state. *Molecular Physics 97* (1999), 597–601.

[85] Gnan, N., Zaccarelli, E., and Sciortino, F. Tuning effective interactions close to the critical point in colloidal suspensions. *The Journal of Chemical Physics 137* (2012), 084903.

[86] Gnan, N., Zaccarelli, E., Tartaglia, P., and Sciortino, F. How properties of interacting depletant particles control aggregation of hard-sphere colloids. *Soft Matter 8* (2012), 1991–1996.

[87] Götzelmann, B., Evans, R., and Dietrich, S. Depletion forces in fluids. *Physical Review E 57* (1998), 6785–6800.

[88] Götzelmann, B., Roth, R., Dietrich, S., Dijkstra, M., and Evans, R. Depletion potential in hard-sphere fluids. *Europhysics Letters 47* (1999), 398–404.

[89] Green, M. S. Brownian Motion in a Gas of Noninteracting Molecules. *The Journal of Chemical Physics 19* (1951), 1036–1046.

[90] Green, M. S. Markoff Random Processes and the Statistical Mechanics of Time-Dependent Phenomena. *The Journal of Chemical Physics 20* (1952), 1281–1295.

[91] Green, M. S. Markoff Random Processes and the Statistical Mechanics of Time-Dependent Phenomena. II. Irreversible Processes in Fluids. *The Journal of Chemical Physics 22* (1954), 398–413.

[92] Groot, R., Faber, N., and van der Eerden, J. Hard sphere fluids near a hard wall and a hard cylinder. *Molecular Physics 62* (1987), 861–874.

[93] Groot, R. D., and van der Eerden, J. P. Renormalized density-functional theory for inhomogeneous liquids. *Physical Review A 36* (1987), 4356–4359.

[94] Gunnarsson, O., Jonson, M., and Lundqvist, B. I. Descriptions of exchange and correlation effects in inhomogeneous electron systems. *Physical Review B 20* (1979), 3136–3164.

[95] Haase, R., and Steinert, C. Thermoosmose in Flüssigkeiten. *Zeitschrift für Physikalische Chemie 21* (1959), 570.

[96] Hafskjold, B. Computer Simulations of Thermal Diffusion in Binary Fluid Mixtures. In *Thermal Nonequilibrium Phenomena in Fluid Mixtures*. Springer Berlin Heidelberg, 2002, pp. 3–23.

[97] Han, M. Thermophoresis in liquids: a molecular dynamics simulation study. *Journal of Colloid and Interface Science 284* (2005), 339–348.

[98] Hansen, Jean-Pierre and McDonald, Ian R. *Theory of Simple Liquids*, fourth ed. Academic Press, 2013.

[99] Harasima, A. Molecular Theory of Surface Tension. *Advances in Chemical Physics 1* (1958), 203 – 237.

[100] Hartree, D. R. The Wave Mechanics of an Atom with a Non-Coulomb Central Field. Part I. Theory and Methods. *Mathematical Proceedings of the Cambridge Philosophical Society 24* (1928), 89–110.

[101] Henderson, D. *Fundamentals of Inhomogeneous Fluids*. Taylor & Francis, 1992.

[102] Henderson, J. R. Statistical mechanics of fluids at spherical structureless walls. *Molecular Physics 50* (1983), 741–761.

[103] Henderson, J. R. Compressibility route to solvation structure. *Molecular Physics 59* (1986), 89–96.

[104] Hertlein, C., Helden, L., Gambassi, A., Dietrich, S., and Bechinger, C. Direct measurement of critical Casimir forces. *Nature 451* (2008), 172–175.

[105] Hoek, E. M., and Agarwal, G. K. Extended DLVO interactions between spherical particles and rough surfaces. *Journal of Colloid and Interface Science 298* (2006), 50 – 58.

[106] Hohenberg, P., and Kohn, W. Inhomogeneous Electron Gas. *Physical Review 136* (1964), 864–871.

[107] Hsiao, L. C., Jamali, S., Glynos, E., Green, P. F., Larson, R. G., and Solomon, M. J. Rheological State Diagrams for Rough Colloids in Shear Flow. *Physical Review Letters 119* (2017), 158001.

[108] Hutchison, H. P., Nixon, I. S., and Denbigh, K. G. The thermoosmosis of liquids through porous materials. *Discussions of the Faraday Society 3* (1948), 86–94.

[109] Irving, J. H., and Kirkwood, J. G. The Statistical Mechanical Theory of Transport Processes. IV. The Equations of Hydrodynamics. *The Journal of Chemical Physics 18* (1950), 817–829.

[110] Itzykson, C., and Zuber, J. *Quantum Field Theory*. Dover, 2012.

[111] Joanny, J. F., Leibler, L., and de Gennes, P.-G. Effects of polymer solutions on colloid stability. *Journal of Polymer Science: Polymer Physics Edition 17* (1979), 1073–1084.

[112] Kadanoff, L. P., and Martin, P. C. Hydrodynamic equations and correlation functions. *Annals of Physics 24* (1963), 419 – 469.

[113] Kamp, M., Hermes, M., van Kats, C. M., Kraft, D. J., Kegel, W. K., Dijkstra, M., and van Blaaderen, A. Selective Depletion Interactions in Mixtures of Rough and Smooth Silica Spheres. *Langmuir 32* (2016), 1233.

[114] Karanikas, S., Dzubiella, J., Moncho-Jordá, A., and Louis, A. A. Density profiles and solvation forces for a Yukawa fluid in a slit pore. *The Journal of Chemical Physics 128* (2008), 204704.

[115] Kardar, M., and Golestanian, R. The "friction" of vacuum, and other fluctuation-induced forces. *Reviews of Modern Physics 71* (1999), 1233–1245.

[116] Kennard, E. *Kinetic theory of gases: with an introduction to statistical mechanics*. McGraw-Hill, 1938.

[117] Kirkwood, J. G., and Buff, F. P. The Statistical Mechanical Theory of Surface Tension. *The Journal of Chemical Physics 17* (1949), 338–343.

[118] Koch, K., Bhushan, B., and Barthlott, W. Diversity of structure, morphology and wetting of plant surfaces. *Soft Matter 4* (2008), 1943–1963.

[119] König, P.-M., Roth, R., and Dietrich, S. Lock and key model system. *Europhysics Letters 84* (2008), 68006.

[120] Kraft, D. J., Ni, R., Smallenburg, F., Hermes, M., Yoon, K., Weitz, D. A., van Blaaderen, A., Groenewold, J., Dijkstra, M., and Kegel, W. K. Surface roughness directed self-assembly of patchy particles into colloidal micelles. *Proceedings of the National Academy of Sciences of the United States of America 109* (2012), 10787.

[121] Krech, M. *The Casimir effect in critical systems*. World Scientific, 1994.

[122] Krech, M. Casimir forces in binary liquid mixtures. *Physical Review E 56* (1997), 1642–1659.

[123] Krech, M. Fluctuation-induced forces in critical fluids. *Journal of Physics: Condensed Matter 11* (1999), R391.

[124] Kroll, D. M., and Laird, B. B. Comparison of weighted-density-functional theories for inhomogeneous liquids. *Physical Review A 42* (1990), 4806–4809.

[125] Kubo, R. Statistical-Mechanical Theory of Irreversible Processes. I. General Theory and Simple Applications to Magnetic and Conduction Problems. *Journal of the Physical Society of Japan 12* (1957), 570–586.

[126] Kubo, R. The fluctuation-dissipation theorem. *Reports on Progress in Physics 29* (1966), 255–284.

[127] Lamoreaux, S. K. Demonstration of the Casimir Force in the 0.6 to 6 μm Range. *Physical Review Letters 78* (1997), 5–8.

[128] Lamoreaux, S. K. Erratum: Demonstration of the Casimir Force in the 0.6 to 6 μm Range [Phys. Rev. Lett. 78, 5 (1997)]. *Physical Review Letters 81* (1998), 5475–5476.

[129] Landau, L. The Theory of Superfluidity of Helium II. *Journal of Physics (USSR) 5* (1941), 71.

[130] Landau, L., and Lifshitz, E. *Fluid Mechanics*, second ed. Pergamon, 1987.

[131] Laplace, P. Traité De Mécanique Céleste: Supplément au dixième livre du traité de méchanique céleste sur l'action capillaire. In *Traité De Mécanique Céleste*. Gauthier-Villars, Paris, 1878–1912.

[132] Lee, J., Laoui, T., and Karnik, R. Nanofluidic transport governed by the liquid/vapour interface. *Nature Nanotechnology 9* (2014).

[133] Lee, T. D., and Yang, C. N. Statistical Theory of Equations of State and Phase Transitions. II. Lattice Gas and Ising Model. *Physical Review 87* (1952), 410–419.

[134] Leidl, R., and Wagner, H. Hybrid WDA: A weighted density approximation for inhomogeneous fluids. *The Journal of Chemical Physics 98* (1993), 4142–4148.

[135] Li, H., and Kardar, M. Fluctuation-induced forces between rough surfaces. *Physical Review Letters 67* (1991), 3275–3278.

[136] Li, H., and Kardar, M. Fluctuation-induced forces between manifolds immersed in correlated fluids. *Physical Review A 46* (1992), 6490–6500.

[137] Libri, G. *Histoire des sciences mathématiques en Italie, depuis la renaissance des lettres jusqu'à la fin du dix-septiéme siécle*, vol. 3. Chez Jules Renouard et C^{ie}, Paris, 1840.

[138] Lifshitz, E. The theory of molecular attractive forces between solids. *Soviet Physics - JETP 2* (1956), 73–83.

[139] Lippmann, G. Endosmose entre deux liquides de même composition chimique et de températures différentes. *Comptes rendus de l'Académie des sciences 145* (1907), 104–105.

[140] Logan, Bruce E.; Elimelech, M. Membrane-based processes for sustainable power generation using water. *Nature 488* (2012), 313–319.

[141] London, F. Zur Theorie und Systematik der Molekularkräfte. *Zeitschrift fur Physik 63* (1930), 245–279.

[142] Löwen, H. Density functional theory of inhomogeneous classical fluids: recent developments and new perspectives. *Journal of Physics: Condensed Matter 14* (2002), 11897.

[143] Ludwig, C. *Diffusion zwischen ungleich erwärmten Orten gleich zusammengesetzter Lösung.* 1856.

[144] Maciołek, A., and Dietrich, S. Collective behavior of colloids due to critical casimir interactions. *Reviews of Modern Physics 90* (2018), 045001.

[145] Mahale, N., and Cole, M. Size effect contributions to the chemical potential of a film. *Surface Science 172* (1986), 311 – 318.

[146] Marangoni, C. *Sull'espansione delle goccie d'un liquido galleggianti sulla superfice di altro liquido.* Tipografia dei Fratelli Fusi, Pavia, 1865.

[147] Mason, T. G. Osmotically driven shape-dependent colloidal separations. *Physical Review E 66* (2002), 060402.

[148] Maxwell, J. C. Capillarity Action. In *Encyclopaedia Britannica*, 9 ed. 1876.

[149] Maxwell, J. C. VII. On stresses in rarified gases arising from inequalities of temperature. *Philosophical Transactions of the Royal Society of London 170* (1879), 231–256.

[150] McLennan, J. A. Symmetry of the stress tensor. *Physica 32* (1966), 689 – 692.

[151] Meester, V., and Kraft, D. J. Spherical, Dimpled, and Crumpled Hybrid Colloids with Tunable Surface Morphology. *Langmuir 32* (2016), 10668.

[152] Meister, T. F., and Kroll, D. M. Density-functional theory for inhomogeneous fluids: Application to wetting. *Physical Review A 31* (1985), 4055–4057.

[153] Mermin, N. D. Thermal properties of the inhomogeneous electron gas. *Physical Review 137* (1965), A1441–A1443.

[154] Mohry, T. F., Kondrat, S., Maciolek, A., and Dietrich, S. Critical Casimir interactions around the consolute point of a binary solvent. *Soft Matter 10* (2014), 5510–5522.

[155] Mori, H. A Quantum-statistical Theory of Transport Processes. *Journal of the Physical Society of Japan 11* (1956), 1029–1044.

[156] Mori, H. Statistical-Mechanical Theory of Transport in Fluids. *Physical Review 112* (1958), 1829–1842.

[157] Morris, M. S., Thorne, K. S., and Yurtsever, U. Wormholes, Time Machines, and the Weak Energy Condition. *Physical Review Letters 61* (1988), 1446–1449.

[158] Netz, R., and Orland, H. Beyond Poisson-Boltzmann: Fluctuation effects and correlation functions. *The European Physical Journal E 1* (2000), 203–214.

[159] Newton, I. *Opticks, Or a Treatise of the Reflexions, Refractions, Inflexions and Colours of Light: Also Two Treatises of the Species and Magnitude of Curvilinear Figures.* Printed for Sam. Smith, and Benj. Walford, Printers to the Royal Society, at the Prince's Arms in St. Paul's Church-yard, London, 1704.

[160] Nguyen, V. D., Dang, M. T., Nguyen, T. A., and Schall, P. Critical Casimir forces for colloidal assembly. *Journal of Physics: Condensed Matter 28* (2016), 043001.

[161] Niven, W., Ed. *The Scientific Papers of James Clerk Maxwell*, vol. II. Dover Publications, 2003.

[162] Nordholm, S., Johnson, M., and Freasier, B. Generalized van der Waals theory. III. The prediction of hard sphere structure. *Australian Journal of Chemistry 33* (1980), 2139–2150.

[163] Noro, M. G., and Frenkel, D. Extended corresponding-states behavior for particles with variable range attractions. *Journal of Chemical Physics 113* (2000), 2941.

[164] Nyquist, H. Thermal Agitation of Electric Charge in Conductors. *Physical Review 32* (1928), 110–113.

[165] Olivares-Rivas, W., Degrève, L., Henderson, D., and Quintana, J. Grand canonical Monte Carlo and modified singlet integral equations for the density profile of a Yukawa fluid near a planar wall. *The Journal of Chemical Physics 106* (1997), 8160–8164.

[166] Onsager, L. Reciprocal Relations in Irreversible Processes. I. *Physical Review 37* (1931), 405–426.

[167] Onsager, L. Reciprocal Relations in Irreversible Processes. II. *Physical Review 38* (1931), 2265–2279.

[168] Parola, A., and Piazza, R. Particle thermophoresis in liquids. *The European Physical Journal E 15* (2004), 255–263.

[169] Parola, A., Pini, D., and Reatto, L. The smooth cut-off hierarchical reference theory of fluids. *Molecular Physics 107* (2009), 503–522.

[170] Parola, A., and Reatto, L. Liquid-State Theory for Critical Phenomena. *Physical Review Letters 53* (1984), 2417–2420.

[171] Parola, A., and Reatto, L. Liquid state theories and critical phenomena. *Advances in Physics 44* (1995), 211–298.

[172] Parsons, D. F., Walsh, R. B., and Craig, V. S. J. Surface forces: Surface roughness in theory and experiment. *The Journal of Chemical Physics 140* (2014), 164701.

[173] Pelissetto, A., and Vicari, E. Critical phenomena and renormalization-group theory. *Physics Reports 368* (2002), 549–727.

[174] Piazza, R., Buzzaccaro, S., Parola, A., and Colombo, J. When depletion goes critical. *Journal of Physics: Condensed Matter 23* (2011), 194114.

[175] Piazza, R., and Parola, A. Thermophoresis in colloidal suspensions. *Journal of Physics: Condensed Matter 20* (2008), 153102.

[176] Pini, D., Stell, G., and Wilding, N. B. A liquid-state theory that remains successful in the critical region. *Molecular Physics 95* (1998), 483–494.

[177] Plinius Secundus, G. *Naturalis Historia*, vol. 2. 77.

[178] Press, W., Flannery, B., Teukolsky, S., and Vetterling, W. *Numerical Recipes in FORTRAN*. Cambridge University Press, 1989.

[179] Privman, V. Universal size dependence of the free energy of finite systems near criticality. *Physical Review B 38* (1988), 9261–9263.

[180] Privman, V. *Finite Size Scaling and Numerical Simulation of Statistical Systems*. World Scientific, 1990.

[181] Privman, V., and Fisher, M. E. Universal critical amplitudes in finite-size scaling. *Physical Review B 30* (1984), 322–327.

[182] Rafai, S., Bonn, D., and Meunier, J. Repulsive and attractive critical Casimir forces. *Physica A: Statistical Mechanics and its Applications 386* (2007), 31–35.

[183] Rayleigh, L. XVI. On the instability of a cylinder of viscous liquid under capillary force. *The London, Edinburgh, and Dublin Philosophical Magazine and Journal of Science 34* (1892), 145–154.

[184] Rayleigh, L. XX. On the theory of surface forces. II. Compressible fluids. *The London, Edinburgh, and Dublin Philosophical Magazine and Journal of Science 33* (1892), 209–220.

[185] Reekie, J., and Aird, J. Flow of Water Through Very Narrow Channels and Attempts to Measure Thermomechanical Effects in Water. *Nature 156* (1945), 367–368.

[186] Rèsibois, P. On the Connection between the Kinetic Approach and the Correlation-Function Method for Thermal Transport Coefficients. *The Journal of Chemical Physics 41* (1964), 2979–2992.

[187] Reynolds, O. XVIII. On certain dimensional properties of matter in the gaseous state. - Part I. Experimental researches on thermal transpiration of gases through porous plates and on the laws of transpiration and impulsion, including an experimental proof that gas is not a continuous plenum. - Part II. On an extension of the dynamical theory of gas, which includes the stresses, tangential and normal, caused by a varying condition of gas, and affords an explanation of the phenomena of transpiration and impulsion. *Philosophical Transactions of the Royal Society of London 170* (1879), 727–845.

[188] Reynolds, O. LVII. On the dilatancy of media composed of rigid particles in contact. With experimental illustrations. *The London, Edinburgh, and Dublin Philosophical Magazine and Journal of Science 20* (1885), 469–481.

[189] Richmond, P., and Lal, M. A theoretical treatment of entropic repulsions by polymers. *Chemical Physics Letters 24* (1974), 594–596.

[190] Rosenfeld, Y. Free-energy model for the inhomogeneous hard-sphere fluid mixture and density-functional theory of freezing. *Physical Review Letters 63* (1989), 980–983.

[191] Rossi, L., Soni, V., Ashton, D. J., Pine, D. J., Philipse, A. P., Chaikin, P. M., Dijkstra, M., Sacanna, S., and Irvine, W. T. M. Shape-sensitive crystallization in colloidal superball fluids. *Proceedings of the National Academy of Sciences of the United States of America 112* (2015), 5286.

[192] Roth, R. Fundamental measure theory for hard-sphere mixtures: a review. *Journal of Physics: Condensed Matter 22* (2010), 063102.

[193] Roth, R., Evans, R., and Dietrich, S. Depletion potential in hard-sphere mixtures: Theory and applications. *Physical Review E 62* (2000), 5360–5377.

[194] Roth, R., Evans, R., Lang, A., and Kahl, G. Fundamental measure theory for hard-sphere mixtures revisited: the White Bear version. *Journal of Physics: Condensed Matter 14* (2002), 12063.

[195] Roth, R., Götzelmann, B., and Dietrich, S. Depletion Forces near Curved Surfaces. *Physical Review Letters 83* (1999), 448.

[196] Rowlinson, J. S. Translation of J. D. van der Waals' "The thermodynamik theory of capillarity under the hypothesis of a continuous variation of density". *Journal of Statistical Physics 20* (1979), 197–200.

[197] Rowlinson, J. S. Thermodynamics of inhomogeneous systems. *The Journal of Chemical Thermodynamics 25* (1993), 449 – 461.

[198] Rowlinson, J. S., and Widom, B. *Molecular Theory of Capillarity.* Dover, 2002.

[199] Ruckenstein, E. Can phoretic motions be treated as interfacial tension gradient driven phenomena? *Journal of Colloid and Interface Science 83* (1981), 77–81.

[200] Rusconi, R., Isa, L., and Piazza, R. Thermal-lensing measurement of particle thermophoresis in aqueous dispersions. *Journal of the Optical Society of America B: Optical Physics 21* (2004), 605–616.

[201] Saam, W. F., and Ebner, C. Density-functional theory of classical systems. *Physical Review A 15* (1977), 2566–2568.

[202] Sacanna, S., Irvine, W. T. M., Chaikin, P. M., and Pine, D. J. Lock and key colloids. *Nature 464* (2010), 575.

[203] San-Miguel, A., and Behrens, S. H. Influence of Nanoscale Particle Roughness on the Stability of Pickering Emulsions. *Langmuir 28* (2012), 12038–12043.

[204] Schlesener, F., Hanke, A., and Dietrich, S. Critical Casimir Forces in Colloidal Suspensions. *Journal of Statistical Physics 110* (2003), 981–1013.

[205] Schofield, P., and Henderson, J. R. Statistical Mechanics of Inhomogeneous Fluids. *Proceedings of the Royal Society of London A: Mathematical, Physical and Engineering Sciences 379* (1982), 231–246.

[206] Schuster, A. II. On the nature of the force producing the motion of a body exposed to rays of heat and light. *Proceedings of the Royal Society of London 24* (1876), 391–392.

[207] Shellenberger, K., and Logan, B. E. Effect of Molecular Scale Roughness of Glass Beads on Colloidal and Bacterial Deposition. *Environmental Science & Technology 36* (2002), 184–189.

[208] Snook, I. K., and Henderson, D. Monte Carlo study of a hard sphere fluid near a hard wall. *The Journal of Chemical Physics 68* (1978), 2134–2139.

[209] Sone, Y. Flows Induced by Temperature Fields in a Rarefied Gas and their Ghost Effect on the Behavior of a Gas in the Continuum Limit. *Annual Review of Fluid Mechanics 32* (2000), 779–811.

[210] Sone, Y., and Yoshimoto, M. Demonstration of a rarefied gas flow induced near the edge of a uniformly heated plate. *Physics of Fluids 9* (1997), 3530–3534.

[211] Soret, C. Sur l'état d'équilibre que prend au point de vue de sa concentration une dissolution saline primitivement homohéne dont deux parties sont portées à des températures différentes. *Archives des Sciences physiques et naturelles, Genève 2* (1879), 48–64.

[212] Soret, C. Influence de la température sur la distribution des sels dans leurs solutions. *Comptes Rendus Hebdomadaires des Séances de l'Académie des Sciences 91* (1880), 289–291.

[213] Soret, C. Sur l'état d'équilibre que prend au point de vue de sa concentration une dissolution saline primitivement homohéne dont deux parties sont portées à des températures différentes. *Annales de Chimie et de Physique 22* (1881), 293–297.

[214] Suresh, L., and Walz, J. Y. Effect of Surface Roughness on the Interaction Energy between a Colloidal Sphere and a Flat Plate. *Journal of Colloid and Interface Science 183* (1996), 199 – 213.

[215] Svetovoy, V., and Palasantzas, G. Influence of surface roughness on dispersion forces. *Advances in Colloid and Interface Science 216* (2015), 1–19.

[216] Tarazona, P. A density functional theory of melting. *Molecular Physics 52* (1984), 81–96.

[217] Tarazona, P. Erratum: Free-energy density functional for hard spheres. *Physical Review A 32* (1985), 3148–3148.

[218] Tarazona, P. Free-energy density functional for hard spheres. *Physical Review A 31* (1985), 2672–2679.

[219] Tarazona, P., and Evans, R. A simple density functional theory for inhomogeneous liquids. *Molecular Physics 52* (1984), 847–857.

[220] ter Haar, D. *Men of Physics L. D. Landau*, vol. I. Pergamon Press, 1965.

[221] Thomas, L. H. The calculation of atomic fields. *Mathematical Proceedings of the Cambridge Philosophical Society 23* (1927), 542–548.

[222] Thomson, W. IX.—On the Dynamical Theory of Heat. Part V. Thermoelectric Currents. *Transactions of the Royal Society of Edinburgh 21* (1854), 123–171.

[223] Torkzaban, S., and Bradford, S. A. Critical role of surface roughness on colloid retention and release in porous media. *Water Research 88* (2016), 274 – 284.

[224] Tyndall, J. On Haze and Dust. *Nature 1* (1870).

[225] Upton, P. J., and Borjan, Z. Off-critical Casimir effect in Ising slabs with antisymmetric boundary conditions in $d = 3$. *Physical Review B 88* (2013), 155418.

[226] van der Waals, J. D. Thermodynamische Theorie der Capillariteit in de Onderstelling van Continue Dichtheidsverandering. *Verhandel. Konink. Akad. Weten. Amsterdam 1* (1893).

[227] van Swol, F., and Henderson, J. R. Wetting and drying transitions at a fluid-wall interface: Density-functional theory versus computer simulation. *Physical Review A 40* (1989), 2567–2578.

[228] Vanossi, A., Manini, N., Urbakh, M., Zapperi, S., and Tosatti, E. Colloquium: Modeling friction: From nanoscale to mesoscale. *Review of Modern Physics 85* (Apr 2013), 529–552.

[229] Vasilyev, O., Gambassi, A., Maciolek, A., and Dietrich, S. Monte Carlo simulation results for critical Casimir forces. *Europhysics Letters 80* (2007), 60009.

[230] Vasilyev, O., Gambassi, A., Maciolek, A., and Dietrich, S. Universal scaling functions of critical Casimir forces obtained by Monte Carlo simulations. *Physical Review E 79* (2009), 041142.

[231] Vasilyev, O., Maciołek, A., and Dietrich, S. Critical Casimir forces for Ising films with variable boundary fields. *Physical Review E 84* (2011), 041605.

[232] Vasilyev, O. A., and Dietrich, S. Critical Casimir forces for films with bulk ordering fields. *Europhysics Letters 104* (2013), 60002.

[233] Velikov, K. P., and Velev, O. D. *Stabilization of Thin Films, Foams, Emulsions and Bifluid Gels with Surface-Active Solid Particles.* Wiley-Blackwell, 2011, ch. 9, pp. 277–306.

[234] Vester, C. F. Die Rahmung des Hevea-Latex mittels Kolloiden. *Kolloid-Zeitschrift 84* (1938), 63–74.

[235] Vignati, E., Piazza, R., and Lockhart, T. P. Pickering Emulsions: Interfacial Tension, Colloidal Layer Morphology, and Trapped-Particle Motion. *Langmuir 19* (2003), 6650–6656.

[236] Vliegenthart, G. A., and Lekkerkerker, H. N. W. Predicting the gas-liquid critical point from the second virial coefficient. *The Journal of Chemical Physics 112* (2000), 5364–5369.

[237] Vrij, A. Polymers at Interfaces and the Interactions in Colloidal Dispersions. *Pure and Applied Chemistry 48* (1976), 471.

[238] Weinberg, S. The cosmological constant problem. *Reviews of Modern Physics 61* (1989), 1–23.

[239] Wenzel, R. N. Resistance of solid surfaces to wetting by water. *Industrial & Engineering Chemistry 28* (1936), 988–994.

[240] Wertheim, M., Blum, L., and Bratko, D. Statistical mechanics of confined systems: The solvent-induced force between smooth parallel plates. In *Micellar Solutions and Microemulsions*, S.-H. Chen and R. Rajagopalan, Eds. Springer New York, 1990, pp. 99–110.

[241] Widom, B. Some Topics in the Theory of Fluids. *The Journal of Chemical Physics 39* (1963), 2808–2812.

[242] Widom, B. Potential-distribution theory and the statistical mechanics of fluids. *The Journal of Physical Chemistry 86* (1982), 869–872.

[243] Wold, I., and Hafskjold, B. Nonequilibrium Molecular Dynamics Simulations of Coupled Heat and Mass Transport in Binary Fluid Mixtures in Pores. *International Journal of Thermophysics 20* (1999), 847–856.

[244] Wolters, J. R., Avvisati, G., Hagemans, F., Vissers, T., Kraft, D. J., Dijkstra, M., and Kegel, W. K. Self-assembly of "Mickey Mouse" shaped colloids into tube-like structures: experiments and simulations. *Soft Matter 11* (2015), 1067.

[245] Wolters, J. R., Verweij, J. E., Avvisati, G., Dijkstra, M., and Kegel, W. K. Depletion-Induced Encapsulation by Dumbbell-Shaped Patchy Colloids Stabilize Microspheres against Aggregation. *Langmuir 33* (2017), 3270.

[246] Woodruff, A. E. William Crookes and the Radiometer. *Isis 57* (1966), 188–198.

[247] Würger, A. Capillary attraction of charged particles at a curved liquid interface. *Europhysics Letters 75* (2006), 978–984.

[248] Würger, A. Thermal non-equilibrium transport in colloids. *Reports on Progress in Physics* (2010), 126601.

[249] Yang, A. J. M., Fleming, P. D., and Gibbs, J. H. Molecular theory of surface tension. *The Journal of Chemical Physics 64* (1976), 3732–3747.

[250] Yatsyshin, P., Durán-Olivencia, M.-A., and Kalliadasis, S. Microscopic aspects of wetting using classical density functional theory. *Journal of Physics: Condensed Matter 30* (2018), 274003.

[251] You, F.-Q., Yu, Y.-X., and Gao, G.-H. Structure of Inhomogeneous Attractive and Repulsive Hard-Core Yukawa Fluid: Grand Canonical Monte Carlo Simulation and Density Functional Theory Study. *The Journal of Physical Chemistry B 109* (2005), 3512–3518.

[252] Young, T. III. An essay on the cohesion of fluids. *Philosophical Transactions of the Royal Society of London 95* (1805), 65–87.

[253] Zaitsev, V., and Polyanin, A. *Handbook of Exact Solutions for Ordinary Differential Equations*. CRC Press, 2002.

[254] Zhao, K., and Mason, T. G. Directing Colloidal Self-Assembly through Roughness-Controlled Depletion Attractions. *Physical Review Letters 99* (2007), 268301.

[255] Zhao, K., and Mason, T. G. Suppressing and Enhancing Depletion Attractions between Surfaces Roughened by Asperities. *Physical Review Letters 101* (2008), 148301.

[256] Zheng, F. Thermophoresis of spherical and non-spherical particles: a review of theories and experiments. *Advances in Colloid and Interface Science 97* (2002), 255 – 278.

[257] Zwanzig, R. Time-Correlation Functions and Transport Coefficients in Statistical Mechanics. *Annual Review of Physical Chemistry 16* (1965), 67–102.

Ringraziamenti

Ogni tesi che si rispetti si conclude con la pagina dei ringraziamenti. Per non essere da meno, anche io mi piegherò a questa usanza che, per quanto mi riguarda, è tutto fuor che una formalità. È finalmente arrivato il momento di abbandonare l'inglese, perché qui si passa dal rigore scientifico, se rigore c'è stato[38], alla (ir)razionalità del cuore. E poi, lo ammetto: una buona dose di sano campanilismo italo-lombardo mi appartiene.

Il primo grazie va sicuramente ad Alberto. Come dico sempre, senza la sua pazienza e le sue idee (a volte decisamente troppo brillanti per il sottoscritto) ci sarebbe stato ben poco di ciò che avete letto nelle pagine precedenti. Sono stato contento di avere lavorato con te durante questi tre anni. Ho capito che ti prendi cura di noi e che ci vuoi bene, con discrezione e senza mai sbilanciarti troppo, da vero milanese che non si abbandona facilmente al sentimento. Te ne sono grato, soprattutto perché non mi sono mai sentito abbandonato durante un percorso, il dottorato, in cui delusioni e frustrazioni sono all'ordine del giorno.

Insieme ad Alberto devo ringraziare i miei compagni di ufficio, il Manu e lo Zen. Sono stato bene con voi, siamo un bel team, ci sosteniamo a vicenda, e, da ultimo, il cazzeggio ci riesce veramente bene. Siete due ragazzi sani (però Zeno, smettila di fumare) e la cosa di cui sono più felice è che in verità condividiamo ben più di un (freddo) ufficio.

Poi, non tutti sanno che il nostro è l'ufficio del *buen retiro*, e spesso si gareggia per accaparrarsi una scrivania. Tra gli innumerevoli ospiti non posso non ricordare il Massimo (campione del mondo!), l'Enrico e il Gino. Abbiamo passato poco tempo insieme, ma io me la sono spassata alla grande, soprattutto durante le infinite, profonde e dotte (soprattutto grazie al Gino) chiacchierate.

Una menzione speciale la merita anche un collega speciale, il Roberto Piazza: sappi che contraccambio, con gli interessi, la stima che tu hai per me. E poi, se non avessi insistito così tanto probabilmente l'articolo sulla termo osmosi non sarebbe stato ancora sottomesso.

L'Insubria è come una grande famiglia, dove tutti si conoscono. Non so se sono fortunato, ma qui mi sono affezionato a tante belle persone, e in particolare voglio ricordare l'Artuso, il Chesi, il Gabri, la Gabri e lo Zana.

[38] In ogni caso posso affermare con orgoglio che c'è stato sicuramente più rigore in queste pagine che nei *Nature* in cui si sostiene l'esistenza di materia ed energia oscura.

Grazie agli amici di sempre, per la pazienza e il sostegno, in particolare, al Lezzi, a Rimo, alla Marta, a Lampo, a Claudio, a don Andrea e a don Giorgio. Grazie Puri, la cura semplice e discreta che hai nei miei confronti mi fa bene. Grazie agli amici della Banda, anche in questo caso amici da una vita, che mi sopportano nonostante arrivi sempre con (almeno) mezz'ora di ritardo alle prove, soprattutto a Marco, a Silvia e ai Mariani.

Più passa il tempo, più mi accorgo che una delle più grandi grazie ricevute è la mia famiglia. Se sono qui a scrivere queste righe è soprattutto grazie a voi!

In più, durante questo dottorato ho avuto, come il Manu, la folle idea di sposarmi (occhio Zen!). A parte gli scherzi, sono veramente felice di averlo fatto. Grazie Gaia, semplicemente perché ci sei!